

SHALLOW LANDSLIDES TRIGGERED BY RAINFALL IN
UNSATURATED SOILS

A THESIS SUBMITTED TO
THE GRADUATE SCHOOL OF NATURAL AND APPLIED SCIENCES
OF
MIDDLE EAST TECHNICAL UNIVERSITY

BY

MOHAMMAD AHMADI-ADLI

IN PARTIAL FULFILLMENT OF THE REQUIREMENTS
FOR
THE DEGREE OF DOCTOR OF PHILOSOPHY
IN
CIVIL ENGINEERING

DECEMBER 2014

Approval of the thesis:

**SHALLOW LANDSLIDES TRIGGERED BY RAINFALL IN
UNSATURATED SOILS**

submitted by **MOHAMMAD AHMADI-ADLI** in partial fulfillment of the requirements for the degree of **Doctor of Philosophy in Civil Engineering Department, Middle East Technical University** by,

Prof. Dr. Gülbin Dural Ünver
Dean, Graduate School of **Natural and Applied Sciences**

Prof. Dr. Ahmet Cevdet Yalçiner
Head of Department, **Civil Engineering**

Asst. Prof. Dr. Nejan Huvaj Sarıhan
Supervisor, **Civil Engineering Dept., METU**

Asst. Prof. Dr. Nabi Kartal Toker
Co-Supervisor, **Civil Engineering Dept., METU**

Examining Committee Members:

Prof. Dr. Erdal Çokça
Civil Engineering Dept., METU

Asst. Prof. Dr. Nejan Huvaj Sarıhan
Civil Engineering Dept., METU

Prof. Dr. Tamer Topal
Geological Engineering Dept., METU

Assoc. Prof. Dr. Sami Oğuzhan Akbaş
Civil Engineering Dept., Gazi University

Asst. Prof. Dr. Onur Pekcan
Civil Engineering Dept., METU

Date: 29 December 2014

I hereby declare that all information in this document has been obtained and presented in accordance with academic rules and ethical conduct. I also declare that, as required by these rules and conduct, I have fully cited and referenced all material and results that are not original to this work.

Name, Last name: MOHAMMAD AHMADI-ADLI

Signature:

ABSTRACT

SHALLOW LANDSLIDES TRIGGERED BY RAINFALL IN UNSATURATED SOILS

Ahmadi-Adli, Mohammad

Ph.D., Department of Civil Engineering

Supervisor: Asst. Prof. Dr. Nejan Huvaj Sarihan

Co-Supervisor: Asst. Prof. Dr. Nabi Kartal Toker

December 2014, 301 pages

Rainfall triggered landslides are common natural hazards with significant consequences all over the world, including Turkey. Majority of available methods for predicting rainfall-induced slope instability are based on regional statistical data of past slope failures and rainfall records rather than a physically-based model that takes the mechanism of the problem into account. Current study aims to define a numerical model for typical slopes in the region (Northern Turkey), use unsaturated soil properties and obtain rainfall intensity-duration (I-D) thresholds for later use in early warning systems.

In order to verify the findings from numerical simulation of seepage and slope stability of unsaturated finite slopes (at 44 to 60 degrees) subjected to infiltration (SEEP/W and SLOPE/W), 16 laboratory flume tests on a fine sand soil at three relative densities (34, 48 and 61%) subjected to different rainfall intensities (4 to 67 mm/hr) are carried out. To study infinite slopes subjected to rainfall, a MATLAB code is developed and Laminar Box setup is designed and manufactured to verify the results in future works.

This study achieves several feats for the first time in the literature (to the author's knowledge): (i) Necessity of considering hysteresis effects (using wetting and drying soil water characteristic curves and hydraulic conductivity functions) in numerical

simulation of infiltration and evaporation/drainage through unsaturated slopes is assessed. (ii) Rainfall intensity duration thresholds that would trigger a landslide (I-D plots) are obtained physically in the laboratory and by numerical simulations. The obtained I-D plots are linked to landslide mechanism rather than statistical data. (iii) The shape of the I-D threshold is demonstrated to be a linear relation in log-log plot for the soil used in this study. (iv) Below a certain rainfall intensity (15 mm/hr in this study) landslides are not triggered in unsaturated soil used in this study (i.e. the I-D plot seems to be asymptotic to the rainfall duration axis). (v) The effect of density of the soil on the I-D threshold is demonstrated by physical laboratory tests and numerical simulations, and it is observed that shallow landslides are not triggered by any rainfall in dense soils used in this study. (vi) Sensitivity analyses show that soil particle size seems to be the most influential parameter effecting I-D thresholds.

Keywords: Rainfall triggered landslides, unsaturated soils, soil water characteristic curve, infiltration, slope stability, early warning systems

ÖZ

SUYA DOYGUN OLMAYAN ZEMİNLERDE YAĞMURLA TETİKLENEN SİĞ HEYELANLAR

Ahmadi-Adli, Mohammad

Doktora, İnşaat Mühendisliği Bölümü

Tez Yöneticisi: Yrd. Doç. Dr. Nejan Huvaj Sarihan

Ortak Tez Yöneticisi: Yrd. Doç. Dr. Nabi Kartal Toker

Aralık 2014, 301 sayfa

Yağmurla tetiklenen heyelanlar tüm dünyada olduğu gibi, Türkiye’de de sıkça karşılaşılan ve önemli sonuçları olan bir doğal afettir. Yağmurla oluşan heyelanların tahmininde kullanılan yöntemlerin çoğu, problemin fiziksel mekanizmasını dikkate almak yerine, geçmişte olmuş olan heyelan ve yağış verilerine dayalı istatistikî yöntemlerdir. Bu çalışma, Türkiye’nin kuzey kesimlerindeki tipik şevler için, zeminin suya doygun olmayan malzeme özelliklerini kullanarak, ileride erken uyarı sistemlerine fayda sağlamak üzere, yağış şiddeti-süresi (I-D) eşik grafiği elde etmeye yönelik bir nümerik yöntem tanımlamayı amaçlamaktadır.

Suyun zemine sızması (infiltrasyonu) ve şev stabilitesi nümerik analizlerinin (SEEP/W ve SLOPE/W) doğrulanması amacıyla, suya doygun olmayan ve ince kum malzemede üç farklı görelî sıklık durumundaki (34, 48 ve 61%) sonlu bir şevde (44 ila 60 derece), farklı yağış şiddet ve süreleri altında (4 ila 67 mm/saat), 16 adet laboratuvar model deneyi gerçekleştirilmiştir. Yağmur uygulanan sonsuz şev durumunu çalışmak için bir MATLAB kodu geliştirilmiş ve bunların ileride doğrulanması amacıyla kullanılmak üzere bir laminar kutu düzeneği tasarlanmış ve yapılmıştır.

Bu çalışmada, yazarın bilgisi dahilinde literatürde ilk defa olarak, aşağıdaki sonuçlar elde edilmiştir: (i) ıslanma ve kuruma durumlarında farklı zemin su karakteristik eğrisi

ve hidrolik iletkenlik fonksiyonlarının, bir diğere deyişle histerezis etkisinin, suya doygun olmayan zeminlerde su sızması ve buharlaşma/kuruma modellemesi yapan nümerik analizlerde dikkate alınmasının gerekliliğı tespit edilmiştir. (ii) Heyelan tetikleyen yağış şiddeti ve süresi (I-D) eşik eğrisi laboratuvarda fiziksel olarak ve nümerik simülasyonlarla elde edilmiştir. Elde edilen I-D eğrisi istatistiki verilerle değil heyelan mekanizması ile ilişkilendirilmiştir. (iii) Bu çalışmada kullanılan zemin için, I-D eşik eğrisinin şeklinin log-log grafikte lineer olduğu gösterilmiştir. (iv) Kullanılan suya doygun olmayan zeminde, belli bir yağış şiddetinin altındaki yağışlarda (bu çalışmada 15 mm/saat) heyelan tetiklenmemiştir; bir diğere deyişle I-D eşik eğrisinin yağış süresi eksenine asimptotik olduğu tahmin edilmektedir. (v) Zemin sıklılığının I-D eşik eğrisine olan etkisi laboratuvar deneyleri ve nümerik simülasyonlarla gösterilmiştir. Bu çalışmada kullanılan sıkı zeminlerde hiçbir yağışta sığ heyelan tetiklenmemiştir. (vi) Yapılan hassasiyet analizlerine göre, I-D eşik eğrisini etkileyen en önemli zemin özelliğinin dane boyu olduğu tespit edilmiştir.

Anahtar Kelimeler: Yağmurla tetiklenen heyelanlar, suya doygun olmayan zeminler, zemin su karakteristik eğrisi, infiltrasyon, şev stabilitesi, erken uyarı sistemleri

تقدیم بہ خانوادہ عزیزم

To my beloved family

ACKNOWLEDGEMENT

Following people contributed to this work in various ways. My infinite thanks to;

Dr. Nejan Huvaj, the thesis supervisor, for her brilliant offer at the beginning, never forgotten friendly attitude in accompaniment, even when I had a weak performance and patience at the end of the job,

Dr. Kartal Nabi Toker, for all his brainstormings that saved my research and also for all his clearest and most to-the-point guidances,

PhD research committee members, professors Erdal Çokça, Tamer Topal, Sami Oğuzhan Akbaş and Onur Pekcan for all of their kind, on time and accurate warnings and feedbacks,

My thanks are also directed to the Scientific and Technological Research Council of Turkey (TUBITAK) for supporting research project (issued as 109M635) which was the core of current study. I should also thank project team members, Dr. Huvaj who coordinated the project, Dr. Toker, Dr. İsfendiyar Egeli and Prof. Vedat Doyuran (God bless him) who leaded this project scientifically and former research assistant and M.Sc. student Yavuz Şahin who assisted the job partially. Faculty of engineering and civil engineering laboratory at Izmir Institute of Technology who were one of the host universities of this project are also appreciated.

My sincere thanks belong to the members of geotechnical division and civil engineering and geological departments at METU. All who provided scientific support for current study directly and indirectly. Before all, I have to thank Prof. Ulusay, visiting professor at geological department, for his comprehensive course in slope stability analysis. I also thank Dr. Toker for his impressive course in partially saturated soil mechanics. I respect for both who created much of the scientific back ground in scope of the research for the author. I thank Ulas Nacar, Kanber Ülgen and Gülşah Bilici, technicians of laboratory of

soil mechanics at department of civil engineering at METU for all patience and helpful attitudes at all stages of PhD education especially at the time of thesis research.

“FORE” testing equipment company manufactured pressure plate and infiltration column setups to be used in current research and METU soil mechanic laboratory. “Eylül Lab” material testing also produced some parts for hanging column setup. “ALFA” testing equipment company also was responsible for production of pressure chamber to be used in saturation of miniature tensiometers. “Akdoğan Reklam” was the manufacturer of flume setup (flume box). “Öz-san” industries also accepted to produce different parts of laminar box setup. I appreciate Mr. Cem Yılmaz, Erman Eylül, Mostafa Alyousif, Uğur Mutlutürk and Mustafa Özsan who were responsible from aforementioned companies, respectively, for my job. Merkezcam Glass and Frame Industries and Süsoy companies also provided tempered glasses and rainfalling system employed in the flume experiment tests.

I also thank Mr. Aidin Talefiourz for his support in performance of some index tests. He also has assisted me in initial tests by laminar box. I should appreciate current PhD students Mr. Raza Ahmadi-Naghadeh and Mr. Arash Maghsoudloo for their valuable technical support in different parts of the research as kind research mates. I conduct my special thanks to Dr. Melih Çalamak for his encouragement to focusing on SWCC estimation methods and even more, his supports in availability of some technical softwares. Former M.Sc. student Mrs. Gamze Kürkçü also accompanied me in some limited studies on assessment of SWCC of different soils. As an auxiliary part to my research, I made a separate study with Mr. Kaveh Hassan Zehtab focusing on a new method to assess shear strength of unsaturated soils using SWCC. I need to thank him for all his assists. Some undergraduate students who were doing their summer internship in geotechnical division at CE-METU or voluntarily were available at Huvaj GRG assisted me in some tasks. Thus, I have to appreciate Gökalp Özen, Elif Bilir, Emre Özyürek, Mertcan Geyin, Faruk Tekait and Hüseyin Paksoy for all their contributions.

I direct my special thanks to Toker drilling and construction company for whom I worked unofficially for more than a year as geotechnical engineer in the days after

research assistantship termination. I should thank for special regards from Mr. Mustafa Toker.

I should also thank all of my friends who accompanied me in this milestone. I shall say “thank you” to Ali, Amin, Amir, Ayda, Bora, Burak, Emrah, Mehdi, Marjan, Mehmet, Mehran, Pozhan, Raheleh, Reza, Siamak, Volkan and Yashar (in alphabetic order) for being with me.

I don’t know how I can really compensate their sincere supports and assists. I owe forever to my parents, Habib and Mahin for their unending and unconditional patience and support. I am not afraid to confess that for sure this job could not even be started if I weren’t encouraged with them.

In Ankara, Houman, my brother was the only member of my family. I thank him and his lovely family not only for their being and hospitality but also for their sincere supports and encouragements.

I will never forget supports and all kindnesses from my lovely sister, Mahsa and her family. She was the origin of hope throughout this job like a light at the end of tunnel despite being very far from me.

TABLE OF CONTENTS

ABSTRACT	v
ÖZ.....	vii
ACKNOWLEDGEMENT	x
TABLE OF CONTENTS	xiii
LIST OF TABLES	xx
LIST OF FIGURES.....	xxii
LIST OF ABBREVIATIONS	xxxvii
CHAPTERS	
1. INTRODUCTION.....	1
1.1. Research Motivation	1
1.1.1. Precipitation-triggered landslides.....	1
1.1.2. Impacts on society and economy	5
1.1.3. The mechanism of rainfall-triggered landslides and early warning	5
1.2. Objectives of the current study.....	9
1.3. Research scope	10
1.4. Thesis organization	12
2. LITERATURE REVIEW	13
2.1. Variably saturated soils	13
2.1.1. Basics	13
2.1.1.1. Soil suction.....	13
2.1.1.2. Soil suction measurement	15

2.1.2. Soil Water Retention.....	16
2.1.2.1. Characteristics of SWCC	17
2.1.2.2. Experimental methods to assess SWCC	18
2.1.2.3. SWCC models.....	18
2.1.2.4. Methods for estimation of SWCC.....	21
2.1.3. Soil Water Transition.....	23
2.1.3.1. Water flow through porous media	23
2.1.3.2. Hydraulic conductivity function	25
2.1.3.3. Experimental methods to assess HCF.....	25
2.1.3.4. HCF models	27
2.1.4. Stress and Strengths in unsaturated soils	28
2.1.4.1. The parameter χ	28
2.1.4.2. The parameter ϕb	30
2.1.4.3. The parameter σs	31
2.2. Stability of slopes.....	32
2.3. Studies on Rainfall-Triggered Landslides	33
2.3.1. Statistical studies.....	33
2.3.2. Numerical studies.....	36
2.3.3. Field studies	40
2.3.4. Laboratory Flume studies	44
3. INITIAL STUDIES – A LANDSLIDE PREDICTION ATTEMPT AND A PARAMETRIC STUDY OVER A FLUME CASE.....	53
3.1. Back analyses and predictions for Cervinara field case and flume models.....	53
3.1.1. Summary of prepared data	54

3.1.1.1. Geological/geotechnical characterization of the study site	54
3.1.1.2. Data from infiltration flume experiments.....	55
3.1.1.3. Data from field monitoring	55
3.1.1.4. Blind prediction.....	55
3.1.2. Contribution by METU team in Round Robin test (IWL2013)	57
3.1.2.1. Controlled infiltration flume experiments.....	57
3.1.2.2. Cervinara Field Experiment	61
3.1.2.3. Conclusions and remarks	65
3.2. Effects of SWCC on unsaturated slope stability (A parametric study).....	66
3.2.1. Numerical model	67
3.2.1.1. Geometry and material properties	68
3.2.1.2. Numerical Analyses	70
3.2.2. Parametric study.....	71
3.2.2.1. Hypothetical soils.....	72
3.2.2.2. Seepage and stability analyses	75
3.2.2.3. Rainfall intensity-duration (I-D) thresholds.....	79
3.2.2.4. Conclusions and remarks	82
4. MATERIAL, EQUIPMENT AND PROCEDURES	85
4.1. Material properties and index tests.....	85
4.1.1. Assessment of Soil Water Characteristic Curve (SWCC)	87
4.1.1.1. Hanging Column	87
4.1.1.2. Pressure plate extractor	88
4.1.1.3. Capillary Column.....	90
4.1.2. Hydraulic Conductivity Function Assessment.....	91

4.1.3. Unsaturated shear strength tests	94
4.2. Flume tests	95
4.2.1. Flume Setup	96
4.2.2. Measurement devices	100
4.2.2.1. Tensiometers	100
4.2.2.2. PDCRs.....	101
- Saturation of PDCRs	101
- Calibration of PDCRs.....	103
4.2.3. Inclinometers.....	104
4.2.4. Testing program	105
4.2.5. Sample preparation	107
4.2.5.1. Plotting geometry of the experiment on the glass walls	107
4.2.5.2. Providing and placement of supports and filter barriers	108
4.2.5.3. Placement of inclinometers.....	108
4.2.5.4. Sample placement and compaction.....	109
4.2.5.5. Tensiometers and PDCRs placement.....	111
4.2.5.6. Trimming sample edges.....	111
4.2.5.7. Droplet drain montage and covering flume box	112
4.2.5.8. Positioning (tilting) flume box.....	113
4.2.5.9. Equalization stage	113
4.2.6. Testing.....	114
4.3. Laminar box tests.....	115
4.3.1. Laminar Box Setup	116
4.3.2. Test program	118

4.3.3. Sample preparation.....	119
4.3.3.1. Batching of the laminates.....	119
4.3.3.2. Fixing laminates using clamping system	119
4.3.3.3. Sample placement and compaction	120
4.3.3.4. Tensiometers and PDCRs placement.....	120
4.3.3.5. Positioning laminar box	121
4.3.3.6. Equalization stage	121
4.3.4. Testing.....	121
5. NUMERICAL SIMULATIONS	123
5.1. Seepage and stability analyses in infinite slopes.....	123
5.1.1. Developed spreadsheets and Matlab codes	123
5.1.1.1. 1D seepage analysis	124
5.1.1.2. Slope stability analysis.....	125
5.1.2. Numerical simulation of laminar box tests	127
5.2. 2D seepage and stability analyses in finite slopes.....	129
5.2.1. Model definition.....	130
5.2.1.1. Boundary conditions	131
5.2.1.2. Material properties	133
5.2.2. Analyses	133
5.2.3. Calibration of Hydraulic properties.....	135
6. RESULTS OF TESTS AND NUMERICAL SIMULATIONS	137
6.1. Material index test results	137
6.1.1. SWCCs of QS soil.....	138
6.1.2. Assessment of HCF for QS soil	140

6.1.3. Results of shear strength tests on QS soils.....	143
6.2. Flume Test Results.....	144
6.2.1. Pore water pressure response	144
6.2.2. Wetting front.....	147
6.2.3. Failure surface.....	147
6.2.4. Time to failure.....	148
6.3. Numerical simulations for flume tests	149
6.3.1. Suction response	150
6.3.2. Failure surface.....	152
6.3.3. Time to failure.....	152
6.4. Laminar box tests.....	153
7. DISCUSSION OF RESULTS FROM EXPERIMENTS AND SIMULATIONS.....	155
7.1. Seepage due to rainfall infiltration.....	155
7.1.1. Flume Experiments	155
7.1.1.1. Pore water pressures	155
7.1.1.2. Wetting front.....	158
7.1.2. Laminar box tests.....	160
7.2. Slope stability.....	160
7.2.1. Flume experiments.....	160
7.2.1.1. Factor of safety versus time (FS vs. t)	161
7.2.1.2. Time to failure (t to failure)	162
7.2.1.3. Slip surface.....	163
7.2.2. Laminar box	164
7.3. I-D thresholds.....	164

8. CONCLUSIONS AND RECOMMENDATIONS FOR FUTURE STUDIES.....	167
8.1. Achievements.....	167
8.2. Conclusions.....	169
8.2.1. A Landslide prediction competition.....	169
8.2.2. Parametric study.....	170
8.2.3. Numerical simulations and laboratory experiments.....	171
8.2.4. I-D thresholds.....	173
8.3. Recommendations for future works.....	174
REFERENCES.....	177
APPENDIX A. DETAIL OF EXPERIMENTS IN FLUME AND LAMINAR BOX TESTS.....	193
APPENDIX B. RESULTS OF FLUME EXPERIMENTS.....	243
APPENDIX C. RESULTS OF NUMERICAL SIMULATIONS.....	259
APPENDIX D. COMPARISON OF TEST RESULTS AND NUMERICAL SIMULATIONS.....	269
APPENDIX E. CODE FOR SEEPAGE AND STABILITY OF INFINITE SLOPE ELEMENT.....	279
APPENDIX F. DIRECT SHEAR TEST RESULTS.....	295
CURRICULUM VITAE.....	299

LIST OF TABLES

Table 2.1. Well-known techniques for applying/measuring soil suction (After Toker 2002)	16
Table 2.2. Effective stress and shear strength theories for unsaturated soil mechanics ..	29
Table 2.3. Well-known LEMs showing considered equilibrium types and assumptions (Pockoski and Duncan, 2000)	33
Table 2.4. Landslide triggering experiments on natural field slopes (modified after Askarinejad, 2013)	50
Table 2.5. Landslide triggering experiments in the laboratory (flume and centrifuge tests)	51
Table 3.1. Main physical properties of the investigated volcanic ashes (Bogaard et al., 2014)	54
Table 3.2. Main characteristics of the flume infiltration tests (Bogaard et al., 2014)	55
Table 3.3. Main characteristics of the flume infiltration test to be blindly predicted during the Round Robin contest (Bogaard et al., 2014).....	56
Table 4.1. Flume tests program.....	106
Table 4.2. Laminar box tests program	119
Table 5.1. Inputs for numerical simulation of 1D seepage and stability in a laminar box test	129
Table 5.2. Inputs for material properties.....	129
Table 5.3. Applied rainfall intensity for any of flume tests	134
Table 6.1. Some geotechnical properties of QS.....	138
Table 6.2. Settlement after rainfall, in minimum dry density checkup cubes	138
Table 6.3. Summary of fitting parameters for Fredlund and Xing (1994) SWCC model	140
Table 6.4. Unsaturated hydraulic conductivity calculation procedure	142
Table 6.5. Time to failure in flume experiments	150
Table 6.6. Time to failure (F.S. = 1.0) obtained from numerical simulations.	153

Table 7.1. Recorded time to failure in flume experiments and their numerical simulation
..... 163

LIST OF FIGURES

Fig. 1.1. (a) & (b) Damage due to landslides in Feke-Adana, in December 2010 (left) and March 2009 (right), (c) & (d) Landslide after heavy rainfall in Gündoğdu district in Rize, August 2010.....	2
Fig. 1.2. Map of landslide occurrence distribution in Turkey considering (a) occurrence frequency and (b) volume of moved mass based on recorded landslide data in 1950-2008, (General Directorate of Disaster Affairs, 2008). Legend at the right belongs to (b) in m ³	3
Fig. 1.3. (a) Shallow landslides occur after an intense rainfall in a part of Black Sea Region, (b) threatening and destroying buildings	4
Fig. 1.4. Plasticity index of soils in recent rainfall triggered landslides in the Black Sea Region, Turkey (Huvaj et al. 2013)	4
Fig. 1.5. Schematic illustration of the processes leading to failure in rainfall-triggered landslides in unsaturated soils.....	7
Fig. 2.1. Components of soil water potential (Toker, 2007).....	14
Fig. 2.2. An element of an air water interface (Toker, 2007)	15
Fig. 2.3. (a) Main features of a typical SWCC and (b) Typical SWCCs for different types of soils (Fredlund and Xing, 1994).....	17
Fig. 2.4. Soil properties affecting characteristics of SWCC (Ahmadi-adli et al., 2014) .	18
Fig. 2.5. Relation between χ and degree of saturation (from Öberg and Sällfors ,1995)	30
Fig. 2.6. Shear strength changes for Madrid clayey sand (Escario and Juca, 1989).....	31
Fig. 2.7. Rainfall intensity and duration of shallow instabilities (Caine, 1980)	34
Fig. 2.8. (a) Critical combinations of rainfall intensity and duration needed for saturation of shallower 1.2m of slope as a function of slope and soil properties (e.g. slope angle (for 40° and 43°) and antecedent soil moisture (wet and dry)) by Terlien (1998) and (b) rainfall intensity - duration thresholds with distinction on scale by Guzzetti et al. (2007). (e.g. very thick line, global threshold; thick line, regional threshold; thin line, local threshold. Black lines show thresholds	

determined for regions or areas pertaining to the Central European Adriatic Danubian South-Eastern area).....	35
Fig. 2.9. Geometry of slope (Rahimi et al., 2011).....	38
Fig. 2.10. (a) SWCC and (b) HCF of assigned soils to the model (Rahimi et al., 2011)	38
Fig. 2.11. Rainfall patterns, (a) delayed rainfall pattern, (b) normal rainfall pattern and (c) advanced rainfall pattern (Rahimi et al., 2011).....	39
Fig. 2.12. Normalized factor of safety, F_{sn} , versus time, t , for various rainfall patterns: (a) HC soil type; (b) LC soil type; (c) comparison of HC and LC (from Rahimi et al., 2011)	39
Fig. 2.13. Pore-water pressure distribution caused by antecedent rainfall at crest (x-x) and toe (y-y) cross section for HC soil type: (a) delayed rainfall pattern; (b) normal rainfall pattern; (c) advanced rainfall pattern (from Rahimi et al., 2011).....	40
Fig. 2.14. (a) Geology of study site and (b) soil layer thickness above bedrock (Askarinejad et al., 2012)	41
Fig. 2.15. Normal vs. shear stress at failure for Rudlingen soil case (Askarinejad et al., 2012).....	42
Fig. 2.16. (a) SWCC and (b) HCF of typical study soil obtained from laboratory test data, with van Genuchten curve fit (for SWCC) (Askarinejad et al., 2012) ..	42
Fig. 2.17. Instrumentation plan of the Ruedlingen slope (Askarinejad et al., 2012).	43
Fig. 2.18. Applied rainfall scenarios (a) First experiment and (b) second experiment (Askarinejad et al., 2012)	43
Fig. 2.19. (a) Changes in the volumetric water content profile in cluster 3, (b) changes in the piezometric level at two points on the upper part of the slope (Askarinejad et al., 2012).....	44
Fig. 2.20. (a) Hillslope cross section and (b) detailed cross section and location of instrumentations in a shallow landslide that occurred in 2006, in Edmonds field site near Seattle, USA, (Godt et al., 2009).....	45
Fig. 2.21. (a) Hourly and cumulative rainfall, (b) soil saturation, (c) soil suction, (d) suction stress and (e) factor of safety for the period 24 September 2005 to 14 January 2006 at various depths from the upslope and downslope instrument	

arrays (Fig. 2.20) . Black and red arrows indicate the times (6 and 10 January 2006 and 14 January 2006, respectively) of the occurrence of several landslides along the 15 km stretch of bluffs in the vicinity of the field site and the study site.....	46
Fig. 2.22. Experimental model for suction change monitoring due rainfall in slopes (Schnellmann et al., 2010)	47
Fig. 2.23. (a) SWCC and (b) HCF of used soil.....	48
Fig. 2.24. Pore water pressure response, (Schnellmann et al., 2010)	48
Fig. 3.1. Numerical models for simulation of D3 (a) and D4 (b) infiltration flume tests	58
Fig. 3.2. (a) TDR records in time used to obtain wetting soil water characteristic curve (SWCC) and (b) SWCC at drying and wetting states	59
Fig. 3.3. Drying and wetting hydraulic conductivity function (HCF)	59
Fig. 3.4. Simulated versus measured pore water pressure at location of T3, T4 and T6 tensiometers for flume test D3	60
Fig. 3.5. (a) Defined numerical model for C4 and (b) calculated suction response at T2, T3, T4, T5 and T6 in test C4.....	61
Fig. 3.6. (a) Topography of the study region and (b) selected slope cross section.....	62
Fig. 3.7. (a) Soil composition in location of instrumentation station and (b) buried measurement devices at the instrumentation station.....	63
Fig. 3.8. Suction response in different depths at instrumentation station, rainfall records and calibration periods	63
Fig. 3.9. (a) SWCC & (B) HCF of soils A, B, C and D.....	64
Fig. 3.10. Measured suctions in various depths at instrumentation station versus calculated suctions using calibrated soil materials at three calibration time periods	64
Fig. 3.11. Calculated suctions at required depths due climatic changes between 01/01/2012 and 12/02/2012	65
Fig. 3.12. Drying and wetting soil-water characteristic curve and its characteristic parameters	67
Fig. 3.13. (a) Laboratory flume setup used by Gallage & Uchimura (2010) and (b) grain size distribution of Edosaki sand (data from Gallage & Uchimura, 2010).....	68

Fig. 3.14. (a) Soil-water characteristic curves and (b) hydraulic conductivity function (data from Gallage and Uchimura (2010) and Gallage et al. (2013)) (FX: Fredlund and Xing, 1994)	69
Fig. 3.15. (a) Numerical slope model defined in SEEP/W and SLOPE/W and (b) comparison of suction versus time after start of rainfall, for one of the selected points, P8, in the slope (Ahmadi-adli et al. 2012)	70
Fig. 3.16. Drying (left) / wetting (right) SWCCs for hypothetical soils with different (a) AEV, (b) θ_s , (c) DSR and (d) θ_r values. SWCC of Edosaki sand is shown by the solid bold line	73
Fig. 3.17. Estimated HCFs corresponding to SWCC of hypothetical soils with different (a) AEV, (b) θ_s , (c) DSR and (d) θ_r values. HCF of Edosaki sand is shown by the solid line	74
Fig. 3.18. Pore water pressure distribution and failure mode of slopes composed of hypothetical soils with different AEVs	76
Fig. 3.19. Pore water pressure and failure mode of slopes composed of hypothetical soils with highest and lowest θ_s values	77
Fig. 3.20. Pore water pressure and failure mode of slopes composed of hypothetical soils with highest and lowest DSR values	78
Fig. 3.21. Pore water pressure and failure mode of slopes composed of hypothetical soils with highest and smallest θ_r values	78
Fig. 3.22. Decrease of factor of safety in the slopes with soils of different AEV, θ_s , DSR and θ_r values. Time zero is the time rainfall starts, and rainfall is applied till failure.....	80
Fig. 3.23. Changes in factor of safety of slope made up of Edosaki sand under different rainfall intensities	80
Fig. 3.24. Rainfall intensity-duration plot for slope composed of of Edosaki sand with different factor of safety values	81
Fig. 3.25. I-D thresholds for soils of different AEV, θ_s , DSR and θ_r values.....	82
Fig. 4.1. Microscopic view of the grains in QS soil.....	86

Fig. 4.2. Cubic samples subjected to rainfall to obtain minimum dry density with no volume change under rainfall, (a) & (b) before and (c) & (d) after applying rainfall	86
Fig. 4.3. (a), (b), (c) and (d) Hanging column setup designed, manufactured and mounted in METU geotechnical laboratory.....	88
Fig. 4.4. Specimen preparation for hanging column setup (a) Sampling ring, (b) prepared sample in the ring, (c) placed samples on the pressure plate and (d) submerged samples left for saturation.	89
Fig. 4.5. Pressure plate setup at METU geotechnical laboratory.....	89
Fig. 4.6. Samples in pressure chamber setup, (a) placed and (b) submerged	90
Fig. 4.7. Capillary tube setup	91
Fig. 4.8. Test in Capillary tube (a, b, c & d) specimen placement in the tube segments, (e) mounted tube, (f) moved water in the column due capillarity and (g & h) water content specimens.	91
Fig. 4.9. Infiltration column setup designed, manufactured for METU geotechnical laboratory (a) sketch proposed by ASTM D7664, (b) dispatched parts and (c) montaged infiltration column setup, (d) water drain on pedestal and filter close up and (e) tools for ponding into the sample (water cup + cotton wicks).	92
Fig. 4.10. (a), (b), (c), (d) & (e) Sample placement in infiltration column and (f) equalized suctions.	94
Fig. 4.11. Water content controlled direct shear test procedure, Nylon sealant placement in (a) top and (b) down of the sample.	95
Fig. 4.12. Schematic view of the flume setup designed and manufactured for METU geotechnical laboratory	96
Fig. 4.13. Dimensions of the flume box.....	97
Fig. 4.14. (a) Distribution of openings, (b) sealant of glass walls, (c) an openings and (d) rubber sealants.....	97
Fig. 4.15. Close up of some details in flume box, (a) drainage from the flume, (b) up/down and right/left moveable rainfalling system montage and (c) removable upstream and downstream walls	98

Fig. 4.16. Lifting system (a) holding pedestal, (b) winch and (c) Steel frame.....	98
Fig. 4.17. Rainfalling system in detail (a) control panel, (b) & (c) rainfalling pan	99
Fig. 4.18. (a) Measuring water discharge from each of nozzles and (b) Rainfall intensity measurement over flume bottom.....	100
Fig. 4.19. Rainfall intensity checkup over inclined surface	100
Fig. 4.20. 2100F Soilmoisture Probes.....	101
Fig. 4.21. Druck PDCR-81 probe.....	102
Fig. 4.22. Setup for saturation of PDCR devices	103
Fig. 4.23. (a) Setup for calibration of PDCRs, (b) detail of connections.....	104
Fig. 4.24. Calibration charts for (a) PDCR-1 (yellow) and (b) PDCR-2 (blue).....	104
Fig. 4.25. (a) & (b) Preparation of side and (c) central inclinometers	105
Fig. 4.26. Drawing of layers of sample placement and geometry of specimen	108
Fig. 4.27. Filter material preparation, placement and removing after test.	109
Fig. 4.28. (a) Inclinometer placement (hanging from wooden bars), (b) middle inclinometers and (c) wall inclinometer	110
Fig. 4.29. Bakery blender used to mix misted soil.....	110
Fig. 4.30. Plate and weights used to compact soils sample.....	111
Fig. 4.31. Tensiometer placement with two distances from the flume wall, (a) FLM_03 and (b) FLM_06	112
Fig. 4.32. Sample (a) after deposition (b) after trimming (FLM_04)	112
Fig. 4.33. Drop drain (a) mounted over the box wall and (b) close up	113
Fig. 4.34. (a) Desiccation over sample while equalization, (b) sample cover and (c) box (extra) cover	114
Fig. 4.35. Sample positioning, left for suction equalization	114
Fig. 4.36. Rainfall intensity checkup tares placed over sample surface.....	115
Fig. 4.37. Overview of designed and constructed laminar box setup	116
Fig. 4.38. Detail of laminate dimensions and connections.....	117
Fig. 4.39. (a) Laminate surface smoothening, (b) surface before and (c) after smoothening	117
Fig. 4.40. Setup for assessing friction between laminates	118

Fig. 4.41. (a) Needed shear force to slip laminates and (b) friction angle between laminates	118
Fig. 4.42. Inclined placement of laminates in sample preparation	120
Fig. 4.43. Clamping system to fix laminates beside each other in sample preparation .	120
Fig. 4.44. Positioning laminar box setup within flume box.....	121
Fig. 5.1. Laminar box test setup representing a vertical slice in an infinite slope	123
Fig. 5.2. The main scheme of the code for 1D seepage calculation process	124
Fig. 5.3. Detail of calculations in 1D seepage analysis	126
Fig. 5.4. A vertical slice of infinite slope subjected to rainfall infiltration.....	127
Fig. 5.5. Detail of calculations in stability analysis of a vertical slice of soil element in infinite slope (as represented in laminar box)	128
Fig. 5.6. Geometry and boundary conditions for FLM_04 flume test.....	131
Fig. 5.7. (a) Assessment of rainfall intensity distribution over an inclined slope, (b) normalized rainfalling pattern on the FLM_03 test	132
Fig. 5.8. Calibrated HCF of QS soil ($R_d:34\%$)	136
Fig. 5.9. Simulated pore water pressures using calibrated HCF and measured suction for TNS-06.....	136
Fig. 6.1. Particle size distribution of QS.....	137
Fig. 6.2. Drying and wetting SWCCs of QS soil in (a) suction-gravimetric water content and (b) suction-volumetric water content space.....	139
Fig. 6.3. Fx (Fredlund and Xing, 1994) fit to experimental data of SWCC	140
Fig. 6.4. (a) Sketch of infiltration column test (setup explained in more detail in Chapter 4), (b) used SWCC for assessing volumetric water content using suction values, (c) Matric suction and (d) volumetric water content changes with time	141
Fig. 6.5. Hydraulic conductivity of QS soil obtained from infiltration column test for relative densities of 34% and 61%.....	142
Fig. 6.6. Generated shear force and settlement/swelling in water content controlled direct shear tests (numbers in the legend are normal stresses).....	143
Fig. 6.7. Water content controlled direct shear test results on QS.....	145

Fig. 6.8. (a) Location of instrumentation and (a) pore water pressure response to rainfalling for FLM_04.	146
Fig. 6.9. (a & b) Location of vertical sections for measuring the depth of the wetting front and (c) the location of the wetting front at 1 hour and 1 hour+45 minutes after the start of rainfall in FLM_06 in response to rainfall infiltration (circle symbols show the location of tensiometers and pore pressure transducers)	148
Fig. 6.10. (a) Failure surface projection on monitoring side wall of the flume box, (b, c & d) side and top views of the failed mass (M: middle inclinometers, W: wall inclinometers) for FLM_08 flume test and (e) plot of inclinometers and emerging failure surface	149
Fig. 6.11. (a) Pore pressure distribution in the slope at the time of failure for FLM_04 and (b) pore water pressure response to rainfall infiltration, at different locations in the soil with time.....	151
Fig. 6.12. Failure surface in 2D slope stability analysis for FLM_04.....	152
Fig. 6.13. Factor of safety versus time for FLM_04 flume test	153
Fig. 6.14. Suction response in laminar box test and simulations (LAM_1 test).....	154
Fig. 7.1. (a) Measured and simulated pore water pressure changes in the location of instrumentations for FLM_03	156
Fig. 7.2. Measured and simulated pore water pressure changes in the location of instrumentations for FLM_04	157
Fig. 7.3. Detected (measured) and simulated wetting front for FLM_03	159
Fig. 7.4. Detected (measured) and simulated wetting front for FLM_04	159
Fig. 7.5. Simulated time to failure in flume model FLM_04	161
Fig. 7.6. Simulated time to failure for flume tests with (a) 34% and (b) 48% relative density	162
Fig. 7.7. Rainfall intensity duration pairs assessed experimentally and numerically ...	166
Fig. A.1. Deposition, instrumentation and positioning for FLM_00	194
Fig. A.2. (a) Sample placement in layers with no drain in slope toe, (b) soil layer placement, (c) placement of relative density checkup tares, (d) controlled compaction of soil layers, (e) placed instrumentation (tensiometers) and (f) trimmed soil slope for FLM_00	195

Fig. A.3. (a) positioned flume (slope), (b) rainfall spraying, (c) measurement of wetting front progress, (d) wetting front at the time of failure, (e) accumulation of water at toe of slope, (f) no failure in slope due to raining in FLM_00 ..	196
Fig. A.4. Deposition, instrumentation and positioning for FLM_01	197
Fig. A.5. (a) Constructed 2-sided slope subjected to rainfall for FLM_01, (b) covering flume box to have more controlled intensity for rainfall, (c) wetting front and locations of measurement, (d) instrumentations (pore pressure transducers and PCDR devices and (e) crest of the slope after raining, no failure crack (FLM_01).....	198
Fig. A.6. Deposition, instrumentation and positioning for FLM_02	199
Fig. A.7. (a) & (b) Right slope surface from FLM_01 which is trimmed in FLM_02, (c) & (d) controlled deposition of right and left slopes for FLM_02, (e) slope shape (covered till test date) and (f) slope subjected to rainfall for FLM_02	200
Fig. A.8. Deposition, instrumentation and positioning for FLM_03	201
Fig. A.9. (a) Geonet in the base of flume, (b) filter material and soil layer placement, (c) placement of tensiometers and dry density checkup tares, (d) fully placed sample, (e) trimmed soil sample and (f) tilted flume, covered surface and left for equalization in FLM_03	202
Fig. A.10. (a) & (b) desiccated soil surface, (c) wetting front at the time of failure, (d) slipped soil (top view), (e) slipped soil (side view), (f) & (g) disturbance in slipped mass in vicinity of tensiometers in FLM_03	203
Fig. A.11. Deposition, instrumentation and positioning for FLM_04	204
Fig. A.12. (a) Geonet in the base of flume and filter material boxes, (b) soil layer placement, (c) & (d) placement of tensiometers, (e) trimmed soil sample and (f) tilted flume, covered surface and left for equalization for FLM_04.....	205
Fig. A.13. (a) & (b) placement of intensity checkup tares on soil surface, (c) & (d) wetting front at the time of failure, (e) deformation in slope crest (top view), (f) slipped soil block in FLM_04	206
Fig. A.14. Deposition, instrumentation and positioning for FLM_05	207

Fig. A.15. Geonet in the base of flume, (b) filter material and soil layer placement, (c) placement of tensiometers and dry density checkup tares, (d) fully placed sample, (e) trimmed soil sample and (f) tilted flume, covered surface and left for equalization in FLM_05	208
Fig. A.16. (a) & (b) placement of intensity checkup tares on soil surface, before and after, (c) & (d) wetting front recordings while testing, (e) slipped soil (top view) and (f) deformed soil surface for FLM_05.....	209
Fig. A.17. Deposition, instrumentation and positioning for FLM_06	210
Fig. A.18. (a), (b) & (c) mounted new inclinometers, placement of tensiometers and relative density checkup tares, (d) placed of soil layers, (e) & (f) fully placed sample for FLM_06.....	211
Fig. A.19. (a) placement of intensity checkup tares, (b) & (c) slipped block and deformed inclinometers (d) wetting front at the time of failure at FLM_06	212
Fig. A.20. Deposition, instrumentation and positioning for FLM_07	213
Fig. A.21. (a) wall inclinometers, (b) placement of tensiometers, (c), (d), (e) & (f) placement of soils for FLM_07	214
Fig. A.22. (a) rainfall intensity checkup tares, (b) slipped soil block, (c) & (d) inclinometers showing deformation at the time of failure, (e) opened gap in slope crest due slipped soil (top view), (f) override of slipped soil on free drain sacks for FLM_07	215
Fig. A.23. Deposition, instrumentation and positioning for FLM_08	216
Fig. A.24. (a) to (f) sample preparation for FLM_08.....	217
Fig. A.25. (a) rainfall intensity checkup tares, (b) slipped soil block, (c) & (d) inclinometers showing deformation at the time of failure, (e) opened gap in slope crest due to slipped soil (top view), (f) override of slipped soil on free drain sacks in FLM_08.....	218
Fig. A.26. Deposition, instrumentation and positioning for FLM_09	219
Fig. A.27. (a) First layer placement, (b) placement of tensiometers and dry density checkup tares, (c) flume coverage at sample preparation stopages for more than 15 minutes, (d) fully placed sample for FLM_09.....	220

Fig. A.28. (a) high resolution filming from the opposite side, (b) wetting front at the opposite side (c) & (d) projectors and video camera, (e) wetting front after 130 minutes raining in FLM_09	221
Fig. A.29. Deposition, instrumentation and positioning for FLM_10	222
Fig. A.30. (a) First layer placement, (b) placement of tensiometers and dry density checkup tares, (c) flume coverage at sample preparation stoppage for more than 15 minutes, (d) fully placed sample, (e) trimmed and covered soil sample and (f) tilted flume, left for equalization for FLM_10	223
Fig. A.31. (a) high resolution filming from the opposite side, (b) wetting front and failure line at the opposite side (c) & (d) inclinometers showing deformation at the time of failure, (e) slipped soil (top view), (f) readings from inclinometer recordings in FLM_10	224
Fig. A.32. Deposition, instrumentation and positioning for FLM_11	225
Fig. A.33. (a) to (f) sample preparation for FLM_11	226
Fig. A.34. (a) high resolution filming from the opposite side, (b), (c) & (d) no failure in the slope subjected to 28 mm/hr rainfall intensity, (e) & (f) failure after 66 mm/hr rainfall application in FLM_11	227
Fig. A.35. Deposition, instrumentation and positioning for FLM_12	228
Fig. A.36. (a) to (f) sample preparation for FLM_12	229
Fig. A.37. (a) rainfall intensity checkup tares, (b) slipped slope, (c) & (d) inclinometers showing deformation at the time of failure, (e) slipped soil (top view) and (f) evidences of failure in rain infiltrated soils in FLM_12	230
Fig. A.38. Deposition, instrumentation and positioning for FLM_13	231
Fig. A.39. (a) to (f) sample preparation for FLM_13	232
Fig. A.40. (a) high resolution filming from the opposite side, (b) slipped slope surface (c) inclinometers showing deformation at the time of failure, (d) slipped soil (top view), (e) wetting front and failure line at FLM_13.....	233
Fig. A.41. Deposition, instrumentation and positioning for FLM_14	234
Fig. A.42. (a) to (f) sample preparation for FLM_14	235
Fig. A.43. (a) to (e) failure in FLM_14.....	236
Fig. A.44. Deposition, instrumentation and positioning for FLM_15	237

Fig. A.45. (a) to (f) sample preparation for FLM_15.....	238
Fig. A.46. (a) & (b) no failure in FLM_15.....	239
Fig. A.47. (a) to (f) sample placement in layers in laminar box for LAM_0.....	240
Fig. A.48. (a) & (b) soil sample placement in layers using clamping system for LAM_1, (c) & (d) laminar box positioned and (e) instrumented laminar box experiment.	241
Fig. A.49. (a) & (b) sample preparation and (c) & (d) slip after 105 minutes raining and then tilting to 42° in LAM_2	242
Fig. B.1. (a) Changes in pore pressure (suction) values throughout the test and (b) wetting front progress at different time steps and slip (failure) surface at the time of failure for FLM_01	244
Fig. B.2. wetting front progress at different time steps for FLM_02	245
Fig. B.3. (a) Changes in pore pressure (suction) values throughout the test and (b) wetting front progress at different time steps and slip (failure) surface at the time of failure for FLM_03	246
Fig. B.4. (a) Changes in pore pressure (suction) values throughout the test and (b) wetting front progress at different time steps and slip (failure) surface at the time of failure for FLM_04	247
Fig. B.5. (a) Changes in pore pressure (suction) values throughout the test and (b) wetting front progress at different time steps and slip (failure) surface at the time of failure for FLM_05	248
Fig. B.6. (a) Changes in pore pressure (suction) values throughout the test and (b) wetting front progress at different time steps for FLM_06	249
Fig. B.7. (a) Changes in pore pressure (suction) values throughout the test and (b) wetting front progress at different time steps and slip (failure) surface at the time of failure for FLM_08	250
Fig. B.8. (a) Changes in pore pressure (suction) values throughout the test and (b) wetting front progress at different time steps for FLM_09	251
Fig. B.9. (a) Changes in pore pressure (suction) values throughout the test and (b) wetting front progress at different time steps and slip (failure) surface at the time of failure for FLM_10	252

Fig. B.10. (a) Changes in pore pressure (suction) values throughout the test and (b) wetting front progress at different time steps for FLM_11	253
Fig. B.11. (a) Changes in pore pressure (suction) values throughout the test and (b) wetting front progress at different time steps and slip (failure) surface at the time of failure for FLM_12	254
Fig. B.12. (a) Changes in pore pressure (suction) values throughout the test and (b) wetting front progress at different time steps and slip (failure) surface at the time of failure for FLM_13	255
Fig. B.13. (a) Changes in pore pressure (suction) values throughout the test and (b) wetting front progress at different time steps and slip (failure) surface at the time of failure for FLM_14	256
Fig. B.14. Changes in pore pressure (suction) values throughout the FLM_15; no wetting front recording has taken place in this test.....	257
Fig. B.15. Changes in pore pressure (suction) values throughout the LAM_1.	257
Fig. C.1. (a) Distribution of simulated pore water pressures (suction) within the slope at the time of failure (b) simulated slip surface and (c) simulated pore water pressure changes in the location of tensiometers	260
Fig. C.2. (a) Distribution of simulated pore water pressures (suction) within the slope at the time of failure (b) simulated slip surface, (c) simulated pore water pressure changes in the location of tensiometers and (d) FS versus time for FLM_04	261
Fig. C.3. (a) Distribution of simulated pore water pressures (suction) within the slope at the time of failure (b) simulated slip surface, (c) simulated pore water pressure changes in the location of tensiometers and (d) FS versus time for FLM_05	262
Fig. C.4. (a) Distribution of simulated pore water pressures (suction) within the slope at the end of test FLM_08 (end of raining), (b) simulated potential slip surface, (c) simulated pore water pressure changes at the location of tensiometers and (d) FS versus time	263
Fig. C.5. (a) Distribution of simulated pore water pressures (suction) within the slope at the end of FLM_10 (end of raining), (b) simulated potential slip surface	

and (c) simulated pore water pressure changes at the location of tensiometers and (d) FS versus time	264
Fig. C.6. (a) Distribution of simulated pore water pressures (suction) within the slope at the end of test (end of raining), (b) simulated potential slip surface, (c) simulated pore water pressure changes in the location of tensiometers and (d) FS versus time for FLM_12	265
Fig. C.7. (a) Distribution of simulated pore water pressures (suction) within the slope at the end of test (end of raining), (b) simulated slip surface, (c) simulated pore water pressure changes in the location of tensiometers and (d) FS versus time for FLM_13	266
Fig. C.8. (a) Distribution of simulated pore water pressures (suction) within the slope at the time of failure (b) simulated slip surface, (c) simulated pore water pressure changes in the location of tensiometers and (d) FS versus time for FLM_14.....	267
Fig. D.1. (a) Measured and simulated pore water pressure changes in the location of instrumentations for FLM_03, (b) observed and (c) simulated failure surfaces.	270
Fig. D.2. (a) Measured and simulated pore water pressure changes in the location of instrumentations for FLM_04, (b) observed and (c) simulated failure surfaces.	271
Fig. D.3. (a) Measured and simulated pore water pressure changes in the location of instrumentations for FLM_05, (b) observed and (c) simulated failure surfaces.	272
Fig. D.4. (a) Measured and simulated pore water pressure changes in the location of instrumentations for FLM_08, (b) observed and (c) simulated failure surfaces.	273
Fig. D.5. (a) Measured and simulated pore water pressure changes in the location of instrumentations for FLM_10, (b) observed and (c) simulated failure surfaces.	274

Fig. D.6. (a) Measured and simulated pore water pressure changes in the location of instrumentations for FLM_12, (b) observed and (c) simulated failure surfaces.	275
Fig. D.7. (a) Measured and simulated pore water pressure changes in the location of instrumentations for FLM_13, (b) observed and (c) simulated failure surfaces.	276
Fig. D.8. (a) Measured and simulated pore water pressure changes in the location of instrumentations for FLM_14, (b) observed and (c) simulated failure surfaces.	277
Fig. F.1. Shear stress and vertical settlement in water content controlled direct shear tests in samples with $\gamma_d=1.2 \text{ gr/cm}^3$ and (a) 1%, (b) 5%, (c) 10% and (d) 15% water content subjected to different normal stresses.....	296
Fig. F.2. Shear stress and vertical settlement in water content controlled direct shear tests in samples with $\gamma_d=1.27 \text{ gr/cm}^3$ and (a) 1%, (b) 5%, (c) 10% and (d) 15% water content subjected to different normal stresses.....	297
Fig. F.3. Shear stress and vertical settlement in water content controlled direct shear tests in samples with $\gamma_d=1.35 \text{ gr/cm}^3$ and (a) 1%, (b) 5%, (c) 10% and (d) saturated water content.....	298

LIST OF ABBREVIATIONS

AEV	Air Entry Value
ANN	Artificial Neural Network
DSR	De-Saturation Ratio
DST	Direct Shear Test
EWS	Early Warning Systems
FLM	Label for flume tests
FE(M)	Finite Element (Method)
GIS	Geographic Information System
HCF	Hydraulic Conductivity Function
I-D	Intensity-Duration threshold
LAM	Label for laminar box test
LEM	Limit Equilibrium Method
PDE	Particle Differential Equation
PDCR	A probe to measure pore water pressure in soil (by PROCON)
PSD	Particle Size Distribution
PTF	Pedo-Transfer Function
QS	Quartz Sand soil
RTL	Rainfall-Triggered Landslide
SWCC	Soil Water Characteristic Curve
TDR	Time-Domain Reflectometry
TNS	Tensiometer

CHAPTER 1

INTRODUCTION

Chapter one, as an introduction to current research, presents research motivation, goals of the research, summary of methodology and outline of the dissertation.

1.1. Research Motivation

1.1.1. Precipitation-triggered landslides

“Landslides are one of the most widespread and effective agents in sculpting the earth’s surface” (Eckel, 1958). They occur in mountainous and hilly environments in many regions of the world and are an important agent in moving geo-material from upland to downhill (Lu and Godt, 2013). According to a recent survey, about half of the 40 most destructive landslide phenomena worldwide in the past century resulted from prolonged or intense rainfall (Sidle and Ochiai, 2006). Despite small volume ($<1000 \text{ m}^3$) of these landslides they are still destructive due to flow like debris and extensive affected area (Iverson et al., 1997).

Landslides in Turkey, similar to many regions in the world, have caused significant damages and loss of life especially in recent years. For instance, in Feke (Adana, southern Turkey), two rainfall triggered landslides occurred on March 2009 and December 2010. Some buildings collapsed and a highway was blocked due to these landslides (Fig. 1.1 (a) & (b)). Another rainfall triggered flow slide occurred in Gündoğdu (Rize, north eastern Turkey) in August 2010, in which 14 people died, 7 were

injured, some buildings collapsed, many buildings and roads were damaged and many vehicles were buried by landslide mud (Fig. 1.1 (c) & (d)).

A recent study by Can et al. (2013) has revealed inventory map of landslides in Turkey, which shows presence of 45475 active landslides throughout Turkey, 7.5% of which may react flow like. Fig. 1.2 shows older versions of this map published by Turkish General Directorate of Disaster Affairs (2008). Clearly Black Sea region, in northern Turkey, is remarked as the most susceptible region for the rainfall triggered landslides in Turkey (Fig. 1.3).



Fig. 1.1. (a) & (b) Damage due to landslides in Feke-Adana, in December 2010 (left) and March 2009 (right), (c) & (d) Landslide after heavy rainfall in Gündoğdu district in Rize, August 2010

Detailed studies (Huvaj et al., 2013) over these landslides summarized their general characteristics as;

- They are generally observed within the 3-5 m depths from the ground surface,

- Many of them are triggered after an intense rainfall in a short time or after a couple of days of lower intensity rainfall
- They are in fine grained soils and in disintegrated/weathered rocks (Fig. 1.4),
- The failure mode is translational and/or rotational flow slide,
- Groundwater level is typically at significant depths

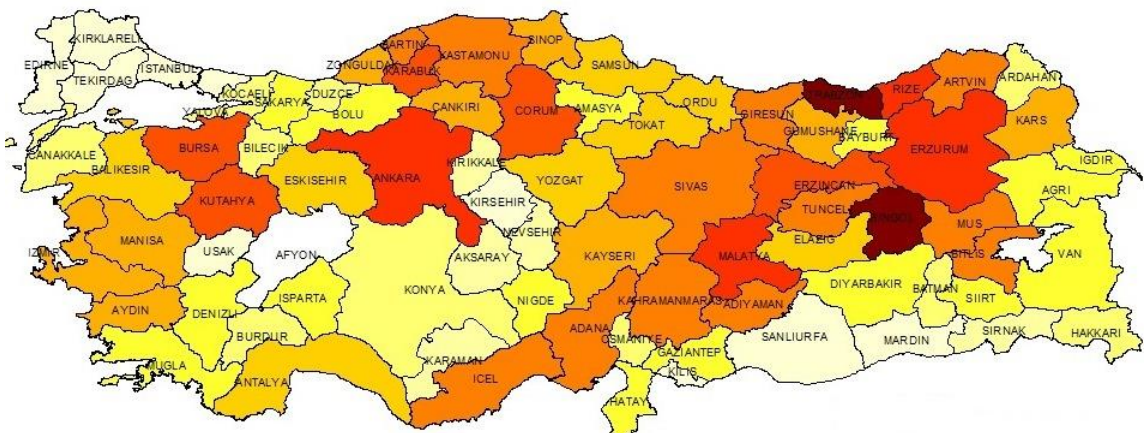
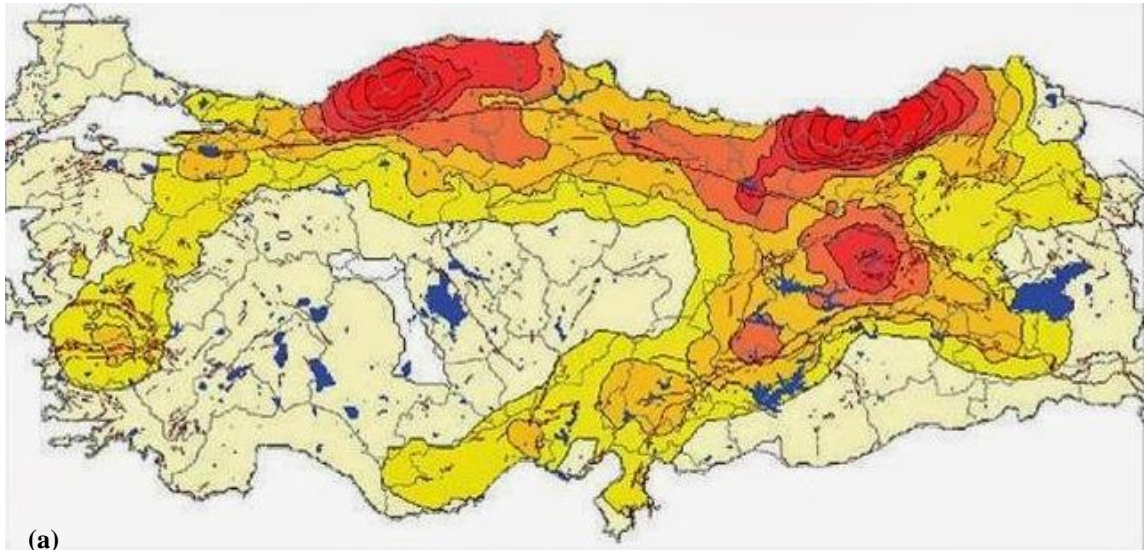


Fig. 1.2. Map of landslide occurrence distribution in Turkey considering (a) occurrence frequency and (b) volume of moved mass based on recorded landslide data in 1950-2008, (General Directorate of Disaster Affairs, 2008). Legend at the right belongs to (b) in m³

Dark Red	3,000 to 3,950	(2)
Red	2,000 to 3,000	(4)
Dark Orange	1,500 to 2,000	(5)
Orange	1,000 to 1,500	(12)
Light Orange	750 to 1,000	(9)
Yellow-Orange	500 to 750	(8)
Yellow	250 to 500	(15)
Light Yellow	100 to 250	(11)
Very Light Yellow	50 to 100	(5)
White	1 to 50	(9)

On the other hand, as the triggering factor, due to changes in the global climate system, the intensity and frequency of rainfall events, therefore the number and frequency of rainfall triggered landslide events are expected to increase in the coming decades. For example, in western Black Sea Region, in 1965-2005 mean annual rainfall increased from 600 mm to 1000 mm (Can et al., 2005). Also due to increased population, and limited available land, more and more buildings are being constructed on sloping ground, which may also increase the damages due to landslides in the near future.



Fig. 1.3. (a) Shallow landslides occur after an intense rainfall in a part of Black Sea Region, (b) threatening and destroying buildings

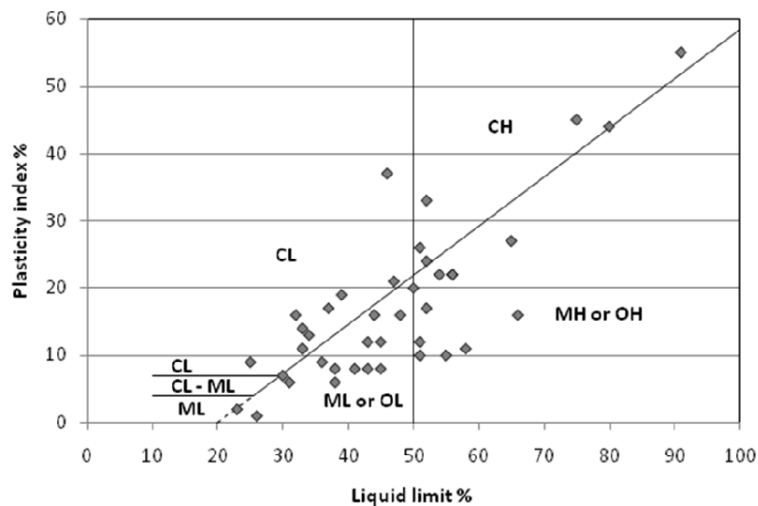


Fig. 1.4. Plasticity index of soils in recent rainfall triggered landslides in the Black Sea Region, Turkey (Huvaj et al. 2013)

1.1.2. Impacts on society and economy

Generally, landslides cause a significant impact on the society and its economy. They are considered major natural hazards that can result in high number of fatality and tremendous economic losses, directly and indirectly (Lu and Godt, 2013). According to a report by U.S. Geological Survey at 2001, United States has experienced economic loss (direct and indirect) of about US\$2 billion and fatalities of about 25-50 per year. Based on this report, in South American countries, despite smaller economic losses, numbers of casualties in major individual landslide events are huge. As extremes, 20,000 were killed in the 1970 Huascarán debris avalanche in Peru, approximately 25,000 died in the 1985 Nevado del Ruiz debris-flow disaster in Colombia, and as many as 30,000 were killed or are missing as a result of the 1999 landslides and floods in northern Venezuela (Schuster and Highland, 2001). Petley (2012) has reported 2620 fatal landslides with 32322 fatalities for the study period of 2004 to 2010. He has concluded that the spatial distribution of landslide occurrence is being strongly concentrated in Asia, particularly along the Himalayan Arc and in China, the Philippines and Indonesia, which drives the temporal occurrence through the annual cycle.

In Turkey, referring to a contribution by Ildir (1995), landslides in a period of 35 years between 1959 and 1994 damaged 76995 buildings throughout Turkey. This constitutes 27% of the entire loss from all natural hazards and is second after earthquakes. There is no other available data on either direct or indirect losses due to landslides on a national scale (Duman et al., 2005).

1.1.3. The mechanism of rainfall-triggered landslides and early warning

Landslide risk reduction is a pressing societal need in mountainous countries as well as along many coasts, lakes and rivers. Engineering measures to stabilize dangerous slopes can be costly or impractical in many cases (Sassa et al., 2007). Early warning systems have been applied to reduce the risk from natural hazards and are defined as “monitoring devices designed to avoid, or at least to minimize, the impact imposed by a threat on humans, damage to property, the environment, or/and to more basic elements like

livelihoods” (Medina-Cetina and Nadim, 2008). They can reduce risk by alerting people exposed to the landslide hazard so that they can take action to avoid or reduce their risk and prepare for effective response.

Today a significant effort is being spent in some countries of the world to develop reliable methods for landslide prediction to be used in early warning systems. Approach to these methods requires a deep knowledge of soil behavior and great experience (Picarelli, 2009). In fact, only a clear understanding of the physical and mechanical processes which lead to slope failure, and of the processes which govern resulting movement of soil or rock masses, can help in the setting up of effective actions for risk mitigation.

Slope instability (landslide) is defined as downward and outward movement of a slope forming material under the influence of gravitational and other forces as a result of shear failure at the boundaries of the moving mass. Rainfall is the most frequent triggering factor for landslides in many regions of the world and researchers have long attempted to determine the amount of precipitation needed to trigger slope failures. However, it is not simply the rainfall that causes a slope to fail; rather it is a change in pore water pressure in the soil resulting from rainfall infiltration.

Different mechanisms are stated as the reason for these failures. Some recent studies refer to the context of classical soil mechanics and declare that failure surfaces are saturated. This approach implies slides are because of excess pore water pressure regardless of rainfall infiltration (Reid et al., 1997) or ground water exfiltration due to rainfall (Montgomery et al., 1997). On the other hand, several studies (Morgenstern and de Matos, 1975; Lu and Likos, 2004; Rahardjo et al., 2007 and Godt et al., 2009) show failures as a result of suction changes due to infiltration/exfiltration rather than saturation pressure. Ng and Shi (1998) and Rahardjo et al. (2007) proved this numerically.

Due to this approach, in many slopes, particularly in the more dry/unsaturated regions of the world, pore water pressures exist at negative values relative to atmospheric pressure (i.e. suction). The suction (or negative pore water pressures) contribute to increasing the

shear strength of the soil and keep the slope stable. When rainfall infiltrates, the suction reduces, leading to a strength reduction that can initiate a failure (Toll et al., 2011). The factor of safety of the slope (F.S.) decreases as suction in the soil (and therefore the shear strength) decreases. In Fig. 1.5 schematic illustration of this process, for a soil initially existing in dry unsaturated state, in a slope where the groundwater level is at significant depth, is presented.

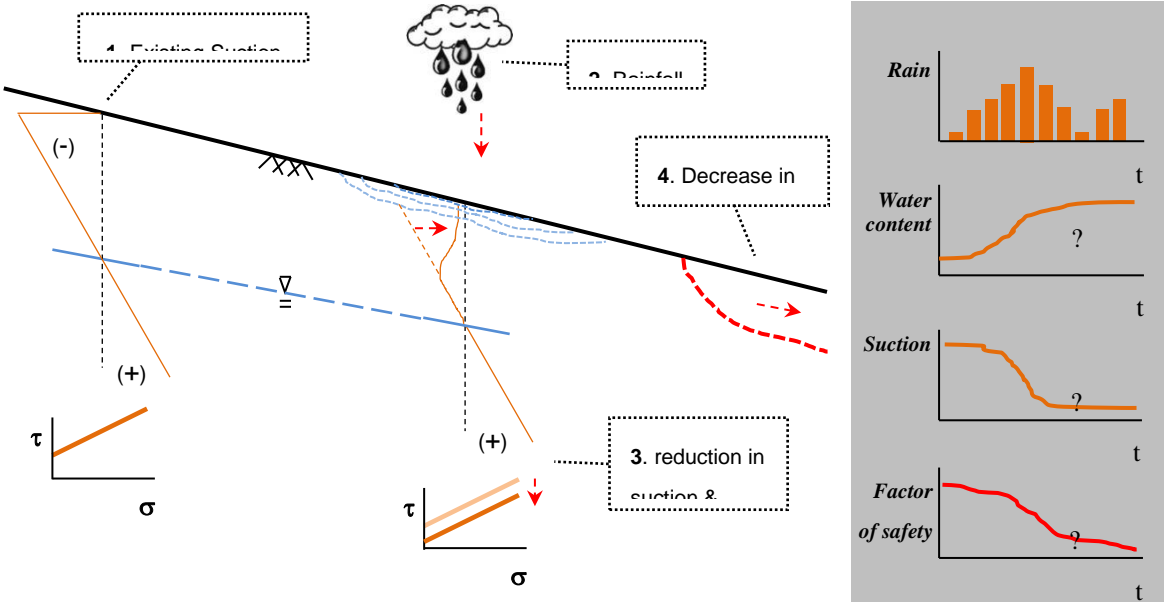


Fig. 1.5. Schematic illustration of the processes leading to failure in rainfall-triggered landslides in unsaturated soils

Nadim et al. (2009) revealed another point of view about mechanical mechanisms of flow like slides; shear failure due to build-up of pore water pressure and erosion by surface water runoff when flow velocity exceeds a critical value. Because of this argument, slip surface of a landslide often occurs along the top of a relatively impermeable layer located at some depth within the soil profile. Then shear strength along this surface and hence the stability of the slope is governed by the pore water pressure, which is under control of water seepage through the slope, either from infiltrated rain, or from exfiltration of groundwater. When the infiltration rate of the underlying layer is too low for further downward penetration of water or when a wetting

front forms, pore water pressure builds up, reducing the soil shear strength. Nadim et al. (2009) also reports field studies, which have proven that during high intensity rainfall, surface water runoff will exert shear stresses on the bed material which may cause erosion depending on the grain size distribution and specific gravity of the material when the flow velocity exceeds a critical value. As erosion progresses and sediment concentration increases, the flow regime may become unstable with heavy erosion at high flow velocity locations triggering a debris flow.

Studies on large-scale landslide experiments have proven the absence of widespread positive pore water pressures at failure (Abramento and Carvalho, 1989; Wolle and Hachich, 1989; Iverson et al., 1997; Reid et al., 1997 and Torres and Alexander, 2002). This finding has highlighted the context of mechanics of variably saturated soils, to study the mechanism of failure in precipitation-triggered landslides.

Protocols used in early warning systems for precipitation-triggered landslides have introduced three approaches.

First - Generally, prediction of rainfall-triggered landslides is performed using empirical correlations between landslide occurrence and amount of precipitation. Triggering thresholds are predominantly expressed as rainfall intensity and duration, or cumulative and antecedent rainfall, and can be defined as the line fitting the minimum intensity of rainfall associated with the occurrence of landslide (Caine 1980; Hong et al., 2006). Landslide triggering thresholds differ from one region to another based on hydro-climatological and geomechanical properties, as well as temporally e.g. seasonal changes. Guzzetti et al. (2007) distinguish between rainfall thresholds on three spatial scales; global, regional and local.

Second - Although rain is regarded as the prime triggering factor of landslides, infiltration and the development of positive pore water pressures at potential shear surfaces initiate landslide processes (Reichenbach et al. 1998; Leroueil 2004). There is, however, no established standard procedure for calculation of pore pressure in relation to rainfall events. A common procedure is to calculate pore pressure conditions required for slope instability which are then compared to observed pore pressures and checked

for reasonability. Based on multiple regression analysis of piezometric measurements Matsushi and Matsukura (2007) established rainfall intensity-duration thresholds. Godt et al. (2006) applied a similar approach and derived rainfall thresholds by comparing rainfall data with measurements of volumetric water content. Terranova et al. (2007) also derived critical rainfall situation for landslide triggering based on modelled infiltration and comparison with piezometer data.

Third - Coupled hydrology and stability models have been widely applied to predict the effects of rain storms, and to define critical situations. Examples for local scale (Berardi et al. 2005; Pagano et al. 2008), and regional scale (Dhakal et al. 2002; Crosta and Frattini 2003) approaches can be found in the respective literature.

1.2. Objectives of the current study

Empirical studies define the rainfall intensity and duration threshold that are likely to trigger landslides when reached or exceeded. Rainfall thresholds are defined through a statistical analysis of past rainfall events that have resulted in slope failures, and can be global, national or regional thresholds (Guzzetti et al., 2007). Empirical thresholds are limited by the availability, completeness, precision and bias of the archived records of rainfall and slope instability. In some countries such data may not be available, or can be very limited to carry out a statistical evaluation. As for the bias, the databases may include mostly the rainfalls that triggered landslides and not sufficient data about rainfalls that did not trigger landslides. Registered records may include more data about the events in populated urban areas, which obviously attracts more attention, especially the events with major damages and consequences and not much data in uninhabited areas (which may be in different geological formations and slope angles). In addition, while each type of landslide has a different mechanism, these studies do not identify different landslide types such as rockfall, debris flow, deep landslides in clayey soils, and shallow landslides in unsaturated soils etc.). For example, shallow landslides in unsaturated soils are typically triggered by reduction in suction in the ground due to rainfall infiltration into the soil, reducing the shear strength of the soil and causing

failure. On the other hand, for example, rockfalls may be triggered by increasing water pressures in the joints due to rainfall.

In order to develop a useful early warning system for landslides, the physical mechanism of landslides should be taken into consideration. In addition, it may be more feasible to aim for an early warning system and triggering rainfall thresholds, that are developed for smaller regions where the material types and landslide mechanisms can be similar, and not generalized for a country. Therefore defining a numerical model for typical slopes in the region, applying typical unsaturated soil properties (considering their range and variability) and obtaining rainfall intensity-duration thresholds could be more meaningful. Then, by studying sensitivity of the numerical model to changes in material properties and boundary conditions it may be possible to assess reliability of the obtained I-D thresholds.

Goals of this research, in brief, are

- to contribute to early warning systems by understanding the mechanism of rainfall infiltration and consequent shear strength changes in unsaturated soils
- establishing a sound methodology for realistic numerical simulation of rainfall induced landslides
- developing correlations between affecting parameters to predict landslide triggering time from rainfall forecasts
- develop rainfall Intensity-Duration thresholds using numerical simulations and laboratory flume experiments

1.3. Research scope

Referring to the goals of study, some sub-tasks were defined and performed. To digest correlations between different parts of mechanism of rainfall triggered slope instabilities, after detailed literature review, the author focused on numerical simulation of older experiments (field and laboratory) found in the literature. By this means, effect of changes in different parameters (model geometry, soil properties, boundary conditions, analyses method) were well investigated employing some commercial softwares (GeoStudio 2007/2012). The outcome from these studies resulted in the back

analysis of an instrumented field case and a parametric study over an instrumented laboratory flume model (scale model of a soil slope).

To study the effect of changes in soil properties over shallow landslides in greater detail, the author constructed various laboratory scale slope models. Laboratory study was preferred because of its

- reproduceability,
- ability to control (change) independently the variables such as slope angle, material type etc. in the lab,
- variability/heterogeneity of material properties in the field
- ease of taking measurements in the lab compared to field

Before performing laboratory model tests, unsaturated soil properties (soil-water retention capacity, soil-water transition capacity and shear strength changes due to changing suction) were determined using laboratory tests. To perform some of the tests, new setups were designed and manufactured at METU geotechnical laboratory. Using obtained data from these tests, soil water characteristic curve (SWCC) (representing soil-water retention capacity) in drying and wetting states, unsaturated hydraulic conductivity function (HCF) (representing soil-water transition capacity) and changes in shear strength of soil due changes in water content (which is controlling suction in soil) were assessed.

Laboratory model tests were performed in a flume setup designed and manufactured at METU geotechnical laboratory. Soil samples were in three different dry densities subjected to different rainfall intensities. The experiments were instrumented to monitor rainfall intensity, dry density, negative pore water pressure and deformation in soil body. Elapsed time to failure for each of the experiments plotted with the rainfall intensity composed rainfall intensity-duration threshold (I-D) for any specific dry density and slope geometry.

The soil parameters used in numerical models were validated through back-analysis of experiments in the laboratory. Results of the experiments were verified numerically and I-D plots from the numerical models were generated.

1.4. Thesis organization

Following this introduction, an overview of available literature focusing on summary of mechanics of variably saturated soils, characteristics of slope stability assessment and recent studies on rainfall-triggered landslides are presented in Chapter 2.

In chapter 3, the author has revealed results of numerical studies (back analyses and prediction) acquired in an international prediction competition in 2013. In addition, through a parametric study, the effects of different soil properties on behavior of unsaturated slopes subjected to rainfall are studied.

Chapter 4 is devoted to description of material property (element) tests, details of laboratory testing program, description of the equipment and testing procedures for flume and laminar box tests and detail of all applied instrumentation.

Chapter 5 is dedicated to the numerical studies. It is divided into subsections of finite and infinite slopes and reveals detail of numerical analyses of seepage and slope stability. In this chapter detail of excel spreadsheets and Matlab codes developed for infinite slopes are presented, as well as the procedure used for modeling with GeoStudio 2007/2012 software packages.

All of the obtained results from element tests, laboratory model experiments and numerical analyses are provided in chapter 6.

Chapter 7 includes detailed discussion of obtained results and comparison of experimental data and numerical simulations. In this chapter rainfall intensity-duration charts for the constructed slopes are presented.

Finally, a summary of the research, major conclusions, and recommendations for future area of study are presented in Chapter 8.

CHAPTER 2

LITERATURE REVIEW

2.1. Variably saturated soils

2.1.1. Basics

Explaining phenomena in unsaturated soil mechanics generally addresses back to the discovery of some mechanical features of water such as tension durability and interfacial properties. Scientifically, the true tensile strength of pure water is not easily observable because water fails in tension at its interfaces with other materials. Therefore, tensile strength of water is strictly limited to the tensile strength of water at surrounding material interfaces.

2.1.1.1. Soil suction

Soil suction plays a critical role in geotechnics since it controls three main concerns of a geotechnical engineer (e.g. strength, deformation and permeability). Rumpf (1961) believes suction as one of the five mechanisms that keep particle agglomerates together (others: solid bridges, bonding materials, molecular attraction and interlocking). Therefore, characteristics of this bonding mechanism (e.g. intensity, type ...) need to be determined before studying its impact on geotechnical properties.

Total Potential of Soil-Water – Amount of work per unit quantity of pure water that must be done by external forces to transfer reversibly and isothermally an infinitesimal amount of water from the standard state to the soil at the point under consideration (Aitchison, 1960). Its value can be obtained counting the work by the act of forces exerted to overcome to any of gravity, water and air pressures and solute concentration difference (osmotic). Toker (2002) has summarized these effects schematically in Fig. 2.1. Potentials due gravitational and air pressure are absent in soil medium and only

matric and osmotic ones are in effect. The term soil suction (i.e. total suction, moisture tension) is defined as summation of these two potential components.

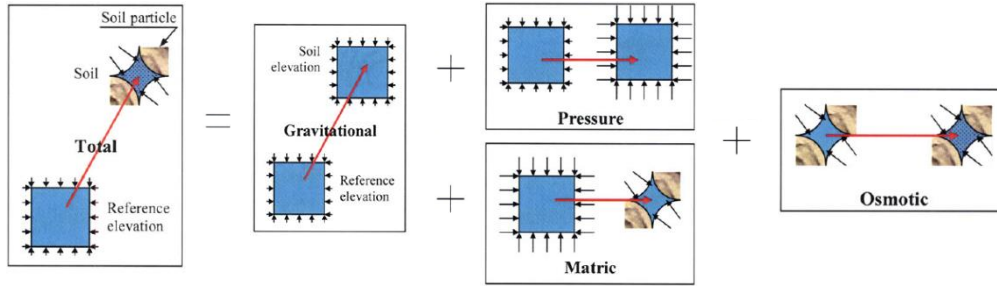


Fig. 2.1. Components of soil water potential (Toker, 2007)

Osmotic suction – Part of soil suction that may exist because of solute concentration differences. It is defined as the positive of the osmotic potential value. Osmotic suction (h_s) can be expressed as

$$h_s = n/V \cdot R \cdot T \quad (2.1)$$

where n/V is the total ion molar concentration, R is the universal gas constant and T is the absolute temperature in Kelvins (Petrucci, 1989). This suction type can be observed in soils with solute solids. In this research osmotic suction is ignored due nature of test materials (clean fine sands) and absence of solute solids.

Matric suction – Part of soil suction that can exist in response to physics of the water-air interfaces, and is equal to positive of the matric potential value. Soils with pores small enough, where the surface forces are large enough to prevent the body forces from draining the pores, will experience matric suction. Suction value relates to the energy that has to be applied to withdraw the water from the pores by overcoming the tensile forces created due to curved air-water interfaces. Matric suction is also called capillary potential or negative pore pressure.

Mathematically, it is the pressure differences across a curved surface, as illustrated in Fig. 2.2, and can be formulated as the following chain of force equilibrium equation (Young-Laplace):

$$(u_a - u_w) \cdot \rho \cdot d\eta \cdot r \cdot d\beta = 2 \cdot \sigma_{ST} \cdot \left(\rho \cdot d\eta \cdot \frac{d\beta}{2} - r \cdot d\beta \cdot \frac{d\eta}{2} \right) \rightarrow \quad (2.2)$$

$$(u_a - u_w) \cdot \rho \cdot r = \sigma_{ST} \cdot (\rho - r)$$

$$u_a - u_w = \left(\frac{1}{r} - \frac{1}{\rho} \right) \cdot \sigma_{ST} = 2\kappa \cdot \sigma_{ST} \quad (2.3)$$

where κ is the mean curvature, and σ_{ST} is the air-water interfacial tension (Laplace, 1806).

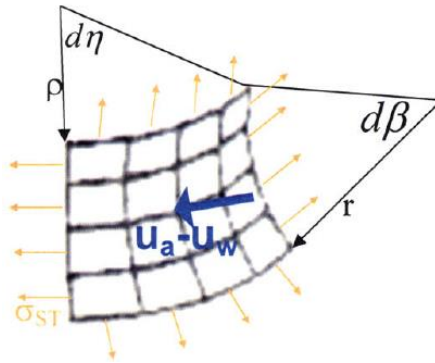


Fig. 2.2. An element of an air water interface (Toker, 2007)

Suction Units – Suction has the same units as pressure. In this research, pressure and suction terms are in kPa. Also note that throughout current thesis, pressure is denoted as P , while ψ and $u_a - u_w$ interchangeably are used to note suction.

2.1.1.2. Soil suction measurement

Intricacy of suction application and suction measurement techniques is much enough that they get studied/catalogued at once. There are long lists of soil suction application/measurement techniques that are catalogued in literature (Fredlund and Rahardjo, 1993 and Lu and Likos, 2004). These methods are categorized considering type of measured suction (total, matric or osmotic), range of applicability (varying between zero to 35 bar), field of application (laboratory and/or field) and if they measure suction directly or indirectly. Table 2.1 summarizes some of well-known techniques.

Table 2.1. Well-known techniques for applying/measuring soil suction (After Toker 2002)

	Technique (References and ASTM codes)	Type	Range (bar)	Usage field	Direct/Indirect (measured parameter)
Suction Application	Controlling Air pressure				
	Pressure membrane (D3152-72)	matric	1-15	Lab.	Indirect (controlled air)
	Pressure axis translation (Southworth, 1980)	matric	1-15	Lab.	Indirect (controlled air)
	Controlling RH				
	Humidity chamber	total	1-10000	Lab.	Indirect (relative humid.)
	Divided air flow	total	1-10000	Lab.	Indirect (relative humid.)
Suction Measurement	Centrifuge				
	Centrifuge (D422-88-R08)	matric	0-30	Lab.	Indirect (capillary)
	Measuring pore ion concentration				
	Squeezing	osmotic	0-350	Lab.	Indirect (ion content)
	Measure RH in pore air				
	Psychrometer	total	0.5-700	Lab.	Indirect (temperature at evap. or condensation)
	Filter paper (D5298-10)	total	4-1000	Lab.	Indirect (humidity in nearby filter paper)
	Chilled mirror hygrometer				
	Measure water content in a material of known retention curve				
	Filter paper (D5298-10)	total	0.3-1000	Lab.	Indirect (humidity in contact filter paper)
Heat dissipation sensor	matric	0-7	Lab.&field	Indirect (thermal conductivity of device)	
Gypsum porous block	matric	0.1-30	Lab.&field	Indirect (electrical conductivity of device)	
Measuring water content (conventional & TDR)	matric	0-5	Lab.&field	Indirect (dielectric constant of soil for TDR device)	
Direct measurement of water tension					
Osmotic tensiometer	matric				
Tensiometer	matric	0-0.98	Lab.&field	direct	
High capacity tensiometer	matric	0-15	Lab.	direct	

2.1.2. Soil Water Retention

Similar to grain size distribution of the soil which determines quantity of any specific sized particle in soil medium, there is another soil property which shows water retaining capacity of the soil against any applied suction; Soil Water Characteristic Curve (SWCC). In the other words, “the SWCC describes the corresponding constitutive relationship between soil suction and soil-water content” (Lu and Likos, 2004). It is considered as the most primitive characteristic of an unsaturated soil which can be referred in definition of many of physical/physicochemical mechanisms of unsaturated soils.

2.1.2.1. Characteristics of SWCC

Pore water retained in the soil skeleton is divided in three portions of “absorbed water”, “capillary water” and “bulk water” (Briggs, 1897). Under applied suction on a saturated soil sample there is a limit exceeding which bulk water starts to be drained from the soil sample. It is named as Air Entry Value (AEV or ψ_b). By termination of all bulk water drainage, again there is another limit from there on pendular water (Capillary water) will start to drain. Only after application of very high air pressures and temperatures tightly absorbed water will be wiped from surface of particles. Fig. 2.3 (a) shows aforementioned limits and main parts of an SWCC.

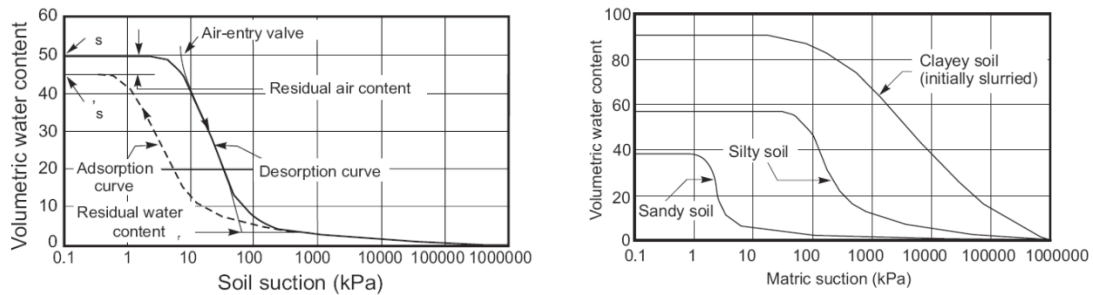


Fig. 2.3. (a) Main features of a typical SWCC and (b) Typical SWCCs for different types of soils (Fredlund and Xing, 1994)

Considering sequences of suction application (e.g. increasing or decreasing) two types of SWCC can be obtained. Desorption curve (drying SWCC) will be assessed by application of suction on a saturated soil sample and adsorption curve (wetting SWCC) will be obtained by decreasing suction from fully dry state of soil and letting it to adsorb water (Fig. 2.3 (a)).

The general shape of the SWCC can be influenced by many soil properties such as pore size distribution, grain size distribution, density, organic material content, clay content and mineralogy. For example soils with different grain size distributions (different soil types) result in different SWCCs (Fig. 2.3 (b)). Ahmadi-adli et al. (2014) also have summarized some of these effects in a more scientific way (Fig. 2.4).

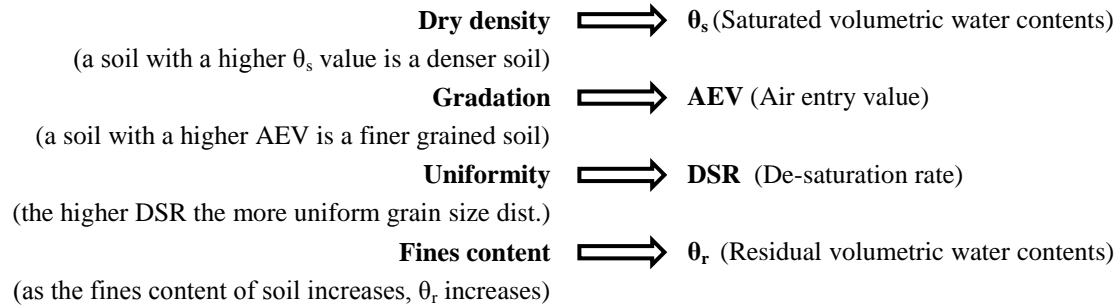


Fig. 2.4. Soil properties affecting characteristics of SWCC (Ahmadi-adli et al., 2014)

2.1.2.2. Experimental methods to assess SWCC

Four methods for determining the soil water characteristic curve were introduced in the literature and authorized by ASTM D 6836. According to ASTM D 6836 hanging column method is suitable for making determinations for suctions in the range of 0 to 80 kPa and is typically used for coarse soils with little fines, i.e. soils that drain readily. Pressure chamber methods with volumetric and gravimetric water content measurements are suitable for suctions in the range of 0 to 1500 kPa and are used for finer soils which retain water more tightly. Hygrometer method also is used when suctions near saturation are not required and commonly is employed to define the dry end of the soil water characteristic curve (that is, water contents corresponding to suctions > 1000 kPa). Centrifuge method also is typically used for coarser soils where an appreciable amount of water can be extracted with suctions up to 120 kPa. The above methods may be combined to provide a detailed description of the SWCC. Some innovative techniques which could resolve some shortcomings of above methods are also introduced in the literature. Znidarcic et al. (1991), Kong and Tan (2000) and Toker et al. (2004) proposed methods of faster methods and Lu et al. (2004) introduced a test method through which hydraulic conductivity also could be assessed.

2.1.2.3. SWCC models

As early as mid-19th century soil scientists have understood that a roughly similar trend can be seen in shape of SWCC for different soils. Therefore, time to time, researchers focusing on different sets of soils proposed different SWCC models. Leong and

Rahardjo (1997) proposed a generic equation (2.4) by which many of well-known models for SWCC could be generated using appropriate constants.

$$a_1\theta^{b_1} + a_2 \exp(a_3\theta^{b_1}) = a_4\psi^{b_2} + a_5 \exp(a_6\psi^{b_2}) + a_7 \quad (2.4)$$

where $a_1, a_2, a_3, a_4, a_5, a_6, a_7, b_1$ and b_2 are constants; ψ is suction pressure; θ is normalized volumetric water content and equal to $(\theta_w - \theta_r)/(\theta_s - \theta_r)$ where θ_w is the volumetric water content. If $a_2 = a_5 = a_7 = 0$ and $b_1 = 1$, then equation (2.4) can be simplified as

$$\theta = \frac{a_4}{a_1} \psi^{b_2} \quad (2.5)$$

by letting $b_2 = -\lambda$ and $a_4/a_1 = \psi_b^\lambda$ in equation (2.5), the Brooks and Corey (1964) equation for soil-water characteristic curve is obtained as

$$\theta = \left(\frac{\psi_b}{\psi}\right)^\lambda \quad (2.6)$$

If we let a_2, a_5 be 0 and $a_1 = a_7$ in equation (2.4), the following equation is obtained:

$$\theta = \left(\frac{a_4}{a_1} \psi^{b_2} + 1\right)^{-b_1} \quad (2.7)$$

now by letting $a_4/a_1 = \alpha^n$, $b_1 = m$ and $b_2 = n$ in equation (2.7), the van Genuchten (1980) equation is obtained as

$$\theta = \left[\frac{1}{1 + (\alpha\psi)^n}\right]^m \quad (2.8)$$

where a, m and n are constants. In equation (2.4) if a_1 and a_5 are set equal to zero and let a_3 is set to 1, the following equation is obtained

$$\theta^{b_1} = \ln\left(\frac{a_7}{a_2} + \frac{a_4}{a_2} \psi^{b_2}\right) \quad (2.9)$$

The following equation suggested by Fredlund and Xing (1994) can be obtained by substituting $a_7/a_1 = e$, $a_4/a_2 = (1/a)^{b_2}$, $b_1 = m$ and $b_2 = n$ in to equation (2.9).

$$\theta = \left\{ \frac{1}{\ln \left[e + \left(\frac{\psi}{a} \right)^n \right]} \right\}^m \quad (2.10)$$

where a , m and n are constants and e is the natural base of logarithms.

Most of the SWCC equations defined earlier were empirical in nature and the main difference between them was their shape. For an instance, the equation proposed by van Genuchten (1980) had a sigmoidal shape in contrast to Brooks and Corey (1964). Fredlund and Xing (1994) attempted to establish a theoretical basis for the SWCC by considering the pore-size distribution curve of the soil. The soil is considered to contain an interconnected set of pores that are randomly distributed and the distribution can be described by a function $f(r)$. The volumetric water content in the pores can be expressed as

$$\theta_w R = \int_{R_{min}}^R f(r) dr \quad (2.11)$$

where $\theta_w(R)$ is volumetric water content when all the pores with radius less than or equal to R are filled with water; and R_{min} is minimum pore radius in the soil. Fredlund and Xing (1994) showed that the BC equation (Brooks and Corey, 1964) is valid only when the pore size distribution is close to the distribution $f(R) = A/r^{m+1}$ where A and m are constant. It was also shown that pore-size distribution function suggested by Fredlund and Xing (1994) is a modification of the pore size distribution function by van Genuchten (1980). Fredlund and Xing (1994) introduce a correction factor $C(\psi)$ where by equation (2.10) becomes

$$\theta = C(\psi) \left\{ \frac{1}{\ln \left[e + \left(\frac{\psi}{a} \right)^n \right]} \right\}^m \quad (2.12)$$

where $C(\psi)$ is given by

$$C(\psi) = 1 - \frac{\ln\left(1 + \frac{\psi}{\psi_r}\right)}{\ln\left(1 + \frac{1000000}{\psi_r}\right)} \quad (2.13)$$

in which ψ is the suction value at residual volumetric water content, θ_r . The choice of suction value of 1000000 kPa in equation (2.13) is based on experimental evidence that the volumetric water content in soils approaches zero as the suction tends to 1000000 kPa. This suction value is also supported by thermodynamic considerations. At a temperature of 20°C a relative humidity of 0.01% gives $\psi=1026289$ kPa.

2.1.2.4. Methods for estimation of SWCC

The cost of performing a direct measurement of unsaturated soil property functions in the laboratory is excessive. The costs associated with measuring an entire unsaturated permeability or shear strength function, are in the order of 10 times as much as the cost of measuring the saturated soil properties. This has encouraged the pursuit of new means of implementing unsaturated soil mechanics into routine geotechnical engineering practice. The newly emerging procedures involve the use of the soil-water characteristic curve (SWCC) and saturated soil properties to estimate the unsaturated soil property functions (Fredlund et al., 1997). Costs can be further reduced if it is possible to estimate the SWCC from a grain-size distribution curve (Fredlund et al., 2002).

Estimation techniques are attractive, but the associated assumptions and limitations must be kept in mind. For example, in the methods to estimate SWCC from particle size distribution (PSD), the PSD is first assumed to estimate, and later “trained” to better estimate, an approximate desorption curve for a soil that is initially slurried near the liquid limit. The effects of stress history, fabric, confinement, and hysteresis are not addressed. Therefore, it must be kept in mind applying this technique.

SWCC mainly depends on the pore size distribution of the soil, which is primarily controlled by the particle size and secondarily the density. Therefore, the PSD and density of the soil may reasonably be correlated to SWCC. Here, different approaches of most well-known SWCC estimation methods have been summarized.

Point regression methods - In this approach, PSD parameters are correlated with water content at various suction levels of SWCC. Gupta and Larson (1979) method is an example work based on this approach.

Functional Parameter Regression Methods - This method assumes that functional parameters of the final equation can be correlated to basic properties of the soil. For instance, Rawls and Brakensiek (1985) presented some regression equations to estimate parameters of Brooks and Corey (1964) formula. Although the estimation of the air-entry value for most soils was quite reasonable, the de-saturation rate appears to be overestimated for most soils. This is likely due to the sharp initial slope inherent in the Brooks and Corey equation. In another study, Vereecken et al. (1989) used a dataset of forty soils to fit to van Genuchten (1980). Then using a sensitivity analysis and factorial analysis they concluded that by having PSD, dry density and organic carbon content, SWCC is predictable.

Physical Model Based Methods – These methods calculate water retaining capacity of the soils by referring physical properties of the soil (for instance, pore sizes), considering some simplifying assumptions. Arya and Paris (1981) pedo-transfer function (PTF) is one of the first methods proposed to estimate SWCC using physico-empirical approach. It estimates pore sizes from the PSD and converts pore radii to equivalent soil suction through capillary theory. Then the volumetric water content, θ_i , is obtained by summing the water-filled pore volumes. This method requires a reasonably well defined grain size distribution. The Fredlund and Wilson (1997) is another prominent PTF based on physico-empirical approach which assumes that a soil is composed of a series of uniform, homogeneous particles, each leading to a unique SWCC. The general shape of the SWCC for pure sand, pure silt, and pure clay is assumed to be known. Using a best-fit analysis for the Fredlund and Xing (1994) equation, three parameters were computed for each soil type. These parameters are assumed to be associated with a dominant particle size on the grain-size plot. It is hypothesized that as a soil tends towards being uniform in size, the values of the fitting parameters show a trend towards a particular value. The fitting parameters for particle sizes falling between pure clays, pure silts, and pure sands are approximated. The particle-size distribution curve can be divided into small divisions with uniform soil

particles. The analysis starts from the smallest particle sizes. A packing porosity is estimated for each soil division. The divisional SWCCs are then summed starting with the smallest particle size and continuing until the volume of the pore spaces are equal to that of the entire heterogeneous soil. The result is a theoretically estimated SWCC.

SoilVision 2007 software package has prepared a complete and user friendly interface to estimate SWCCs using most of the predefined methods. In a paper by Ahmadi-adli et al. (2012), applicability of each of these methods to different soils has been investigated briefly.

In a very recent study by Sattari (2014), a more reasonable approach both in terms of accuracy and cost presented in which the pore-scale drainage of soil medium simulated with application of computer modeling techniques (e.g. Matlab). In this study the amount of applied suction is gradually increased and resulting drainage scheme of bulk pores is visualized and finally the SWCC of the soil is determined using the residual water content of bulk pores and liquid bridges observed at the end of each suction increment. The research for development of this method is going on.

2.1.3. Soil Water Transition

Understanding flow rules through unsaturated soil medium has a critical importance since it defines the pattern under which the most important parameter in unsaturated soil mechanics (e.g. suction value) would change. Flow through an unsaturated soil medium will change water content and suction. Some major flow rules are discussed in the following sections.

2.1.3.1. Water flow through porous media

The mechanism that drives the movement of a liquid or vapor (or their mixture) in slopes is the gradient of total potential. For unsaturated slopes, the total potential (in terms of head) is expressed as the summation of the head due to gravity h_g , the head due to pore-water pressure h_m , the head due to osmosis h_o and the head due to kinetic energy h_v (generally is negligible due low velocity water movement).

For fluid flow in multi-dimensional porous media, the magnitude and direction of liquid water flow in saturated porous media under the different driving mechanisms of pressure and gravity can be unified by the total water potential concept and Darcy's law:

$$q = -K \nabla h_t = -K i \quad (2.14)$$

where q is the specific discharge vector (m/s), K is the hydraulic conductivity tensor, and i is the gradient of the total head. For unsaturated soil, both hydraulic conductivity, K , in the three global directions of x , y , and z and matric suction head are highly nonlinear functions of soil water content, i.e.,

$$q_x = -K_x(\theta) \frac{\partial h_m(\theta)}{\partial x} \quad (2.15)$$

$$q_y = -K_y(\theta) \frac{\partial h_m(\theta)}{\partial y} \quad (2.16)$$

$$q_z = -K_z(\theta) \frac{\partial h_m(\theta)}{\partial z} - K_z(\theta) \quad (2.17)$$

where θ is the volumetric water content defined as the relative volume of water to volume of soil. For isotropic materials, the three hydraulic conductivity functions (HCF) reduce to one, and hydraulic conductivity can be considered a scalar variable.

For transient flow through porous material, governing equations are (2.18) and (2.19) where ρ is the density of water (kg/m^3) and S_s is the specific storage of the soil.

$$-\rho \left(\frac{\partial q_x}{\partial x} + \frac{\partial q_y}{\partial y} + \frac{\partial q_z}{\partial z} \right) = \frac{\partial(\rho\theta)}{\partial t} \quad (2.18)$$

$$\frac{\partial}{\partial x} \left(K_x \frac{\partial h}{\partial x} \right) + \frac{\partial}{\partial y} \left(K_y \frac{\partial h}{\partial y} \right) + \frac{\partial}{\partial z} \left(K_z \frac{\partial h}{\partial z} \right) = S_s \frac{\partial h_m}{\partial t} \quad (2.19)$$

In unsaturated soil medium considering functionality of hydraulic conductivity to suction and/or water content, solution for equation (2.19) will need some specific boundary conditions and simplifying assumptions. For one dimensional case many solutions based on Richards (1931), Green and Ampt (1911) and Srivastava and Yeh

(1991) are available in the literature. Many recent analytical and numerical tools are based on the Richards (1931) solution (e.g. Jackson, 1992, 1993; Philip, 1993; Iverson and Baum, 2008; Lu et al., 2012).

2.1.3.2. Hydraulic conductivity function

Unsaturated hydraulic conductivity (HCF) is fundamental to hydrologic characterization of unsaturated soils and is required for most analyses of water movement in soils. For instance, HCF is a critical parameter to analyze the movement of water during infiltration or evaporation from soil specimens (Lagrega et al., 2001).

Hydraulic conductivity is a soil property that describes the ease with which the soil pores permit water movement. It depends on the variables describing the pores structure (e.g., void ratio and porosity), the pore fluid properties (e.g., density and viscosity), and the relative amount of pore fluid in the system (e.g., water content and degree of saturation). Therefore, flow through an unsaturated soil is more complicated than flow through continuously saturated pore spaces. Macropores are filled with air, leaving only finer pores to accommodate water movement. The movement of water in unsaturated soils is not dictated necessarily by gravity but with differences in matric potential which is the difference in the matric potential of moist soil and nearby drier areas (Brady and Weil, 1999). Thus, the unsaturated hydraulic conductivity function describes the dependence of hydraulic conductivity on the relative amount of pore fluid in the soil structure (Lu and Likos, 2004). As a common definition, HCF is defined as the relationship between hydraulic conductivity (k) and either matric suction (Ψ), volumetric water content (θ), gravimetric water content (w), or the degree of saturation (s). Similar to SWCC, when expressed as function of suction, there are different HCFs for drying and wetting state of water flow through soil but there is no such hysteresis in K - θ space resulting in a unique curve/function.

2.1.3.3. Experimental methods to assess HCF

In order to determine the hydraulic conductivity in unsaturated soils, more complex experimental methods are required than in saturated soils. There are three main methods to obtain unsaturated hydraulic conductivity (Muñoz et al. 2008);

- 1- Transitory method - Well known as Gardner's method that proposes to use Richards cell (Richards, 1931). It consists of measuring the time evolution of water volume that move out of the sample due to gas pressure increments.
- 2- Stationary method - A constant suction is applied to the sample by means of axis translation method. By applying constant gas and pore fluid pressure at the top and bottom of the sample, evolution of fluid volume due head difference between sample heads at given time increments are used to obtain HCF.
- 3- Instant Profile Method - In this method, the changes of the suction profile within a column of soil are measured as a function of time during the infiltration. The suction measurements can be performed by means of tensiometers or psychrometers, depending on the expected suction range. The water content profile can be measured directly using TDRs or determined using the Soil Water Characteristic Curve (SWCC) of the soil and the measured suction profiles. Direct measurement of water content is preferred since it can diminish the uncertainties of the SWCC such as the hysteresis and the scale effects (Daniel 1982 and Askarinejad et al 2012).

Methods for measurement of unsaturated hydraulic conductivity function have been issued by ASTM D 7664 (2010). In this standard three categories of methods such as Column tests, Axis translation tests and centrifuge permeameter tests has been proposed for direct measurement of HCF. In column test method HCF can be assessed using one-dimensional profiles of measured volumetric water content or suction along the height in a column of soil compacted into a rigid wall permeameter during imposed transient and steady-state water flow processes. In axis translation method the HCF can be obtained using outflow measurements from a soil specimen underlain by a saturated high-air entry porous disc in a permeameter during imposed transient water flow processes. There is also centrifuge parameter test method in which the HCF is determined using measured volumetric water content or suction profiles in a column of soil confined in a centrifuge permeameter during imposed steady state water flow processes. The methods in this standard can be used to measure hydraulic conductivity values ranging from the saturated hydraulic conductivity of the soil to approximately 10^{-11} m/s (ASTM D 7664).

2.1.3.4. HCF models

Similar to SWCC, there is a variety of mathematical models that are developed to model the unsaturated hydraulic conductivity function from limited experimental data sets or to predict the hydraulic conductivity function from more routinely obtained constitutive functions, e.g. SWCC (Lu et al., 2004). Regarding the functionality of any of these methods, they are classified as empirical, macroscopic, and statistical models (Mualem, 1978; Fredlund et al., 1994 and Leong and Rahardjo, 1997).

Empirical models are generally come from the need for systematic expression of directly measured unsaturated hydraulic conductivity values. They typically incorporate saturated hydraulic conductivity and one or more fitting parameters optimized to capture the general shape of a given set of data. Methods by Averjanov (1950), Campbel (1973) and Davidson et al. (1969) are of this type.

In macroscopic models, by assuming a laminar flow even in macroscopic scale (porous media), the flow is solved for a simple laminar system by interrelating hydraulic gradient, hydraulic radius and permeability. Obtained expressions are generally in the shape of equation (2.20) where S_e is the effective degree of saturation and δ is a fitting constant.

$$k = S_e^\delta \quad (2.20)$$

Different methods are available in the literature that their difference is in δ value such as Brooks and Corey (1964) and Leong and Rahardjo (1997).

The methods presented by Fredlund et al. (1994) and van Genuchten (1980), which are categorized as statistical methods, focus on estimation of HCF using the SWCC of the soil. These models are based on the presumption that the soil matrix can be represented as a network of interconnected capillary tubes of various sizes and that flow through the network occurs only through the liquid-filled tubes. Therefore, statistical distribution of tube sizes and their connectivity across a given plane in the soil can be the controlling parameters for the overall hydraulic conductivity. Because the distribution of fluid-filled pores is dependent on suction, and may be specifically quantified given the SWCC and

capillary theory, measurements or models for the characteristic curve become an indirect means to predict the hydraulic conductivity function.

2.1.4. Stress and Strengths in unsaturated soils

Throughout the literature the process of improvements in effective stress theory for soils from Terzaghi (1925 and 1943) to Lu et al. (2010) can be observed. Main theories/approaches are summarized in Table 2.2 with some related details.

2.1.4.1. The parameter χ

In general, majority of discussions and research are focused on determination of the parameters are available in any of approaches. Several studies have been conducted theoretically (e.g. Aitchison, 1960) and experimentally (e.g. Donald, 1960) in order to formulate χ . Some of these are summarized as;

- Aitchison (1960) derived the following equation, which was used by Donald (1960) in his results that are included in Fig. 2.5.

$$\chi = u_w \cdot S + \sum_0^u 0.3 \cdot u_w \cdot \Delta S \quad (2.21)$$

- Öberg and Sällfors (1995) used Fig. 2.5 to conclude that χ can be considered equal to S for engineering purposes.

- Karube et al. (1996) proposed a linear relationship (2.22) in which χ is zero at residual saturation (S_r) and 1 at full saturation:

$$\chi = \frac{S - S_r}{1 - S_r} \quad (2.22)$$

- Khalili and Khabbaz (1998) examined data from over a dozen different sources and over 200 soils. They proposed a general correlation that is not based on the degree of saturation, but on the air entry pressure (u_{AE}):

Table 2.2. Effective stress and shear strength theories for unsaturated soil mechanics

Approach/theory	Illustration	Effective stress definition	Shear strength definition	Parameters
Terzaghi's effective stress theory (1943)		$\sigma' = \sigma_n - u_w$	$\tau = c' + (\sigma_n - u_w) \tan \phi'$	-
Bishop's contribution (1959)		$\sigma' = (\sigma_n - u_a) + \chi \cdot (u_a - u_w)$	$\tau = c' + [(\sigma_n - u_a) + \chi(u_a - u_w)] \tan \phi'$	χ
Coleman's approach for effective stress (1962)		$\sigma' = (\sigma_n - u_a) + (u_a - u_w)$	$\tau = c' + (u_n - u_a) \tan \phi' + (u_a - u_w) \tan \phi_b$	ϕ_b
Lu et al.'s suction stress theory (2010)		$\sigma' = \sigma - u_a - \sigma^s$	$\tau = [\sigma - u_a - \sigma^s] \tan \phi'$	σ^s

$$\chi = \left(\frac{u_w}{u_{AE}} \right)^{-0.55} \quad (2.23)$$

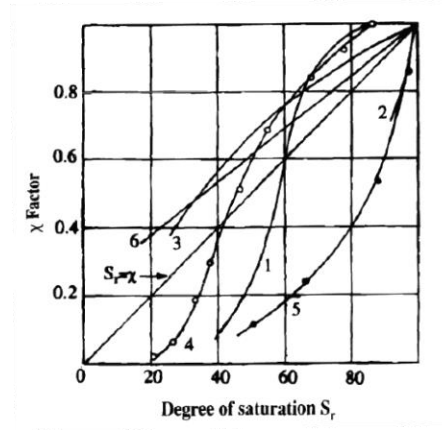


Fig. 2.5. Relation between χ and degree of saturation (from Öberg and Sällfors ,1995)

2.1.4.2. The parameter ϕ_b

ϕ_b is the shear strength contribution due to matric suction, and it changes nonlinearly with matric suction (Gan et al., 1988). Fig. 2.6 shows shear strength changes by suction for Madrid clayey sand by Escario and Juca (1989).

To obtain ϕ_b , Fredlund et al. (1995) proposed

$$\tan \phi_b = a_w \cdot \tan \phi' \quad (2.24)$$

For a_w also following definitions are presented by Fredlund et al. (1995) and Vanapalli et al. (1996) respectively,

$$a_w = \frac{S - S_r}{1 - S_r} = \frac{\theta - \theta_r}{\theta_s - \theta_r} \quad (2.25)$$

$$a_w = S^k \quad (2.26)$$

where k is fitting parameters that can be determined from strength testing with suction measurements.

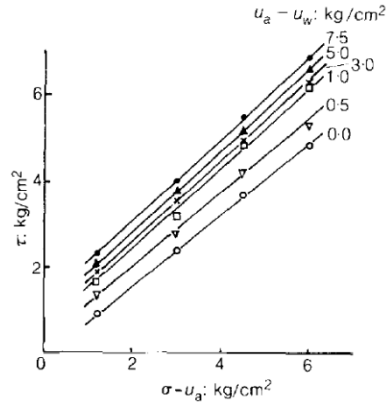


Fig. 2.6. Shear strength changes for Madrid clayey sand (Escario and Juca, 1989)

2.1.4.3. The parameter σ^S

Experimental validations have shown that suction stress (σ^S) can be obtained using direct shear test results. Therefore it can be calculated as,

$$\sigma^S = f(u_a - u_w) = -\frac{c}{\tan \phi'} \quad (2.27)$$

where c is the strength intercept for a given matric suction (apparent cohesion) and ϕ' is internal friction angle. To obtain its value using triaxial test results equation (2.28) has been proposed by Lu et al. (2010),

$$\sigma^S = -\frac{d + M(p - u_a)_f - q_f}{M} \quad (2.28)$$

where d is the intercept on the deviatoric stress q axis when p is zero, M is defined by the internal friction angle ϕ' . p and q are orthogonal stress components. Zehtab et al. (2012) has also tried to correlate σ^S with SWCC of the soils.

In one of recent studies Toker et al. (2014) has investigated unsaturated shear strength for moist spheres.

2.2. Stability of slopes

Landslides are mode of slope instability in which “propensity for a slope to undergo morphologically and structurally disruptive landslide processes” (Glade and Crozier 2005). Stable slope which is converted to a marginally stable state due to preparatory factors (e.g. weathering, deforestation, tectonic uplift or environmental change) will become actively unstable in response to dynamic triggering factors exceeding certain thresholds (e.g. intense rainstorms, seismic shaking or slope undercutting). In the meantime, sustaining factors control the behavior of the activated instability and therefore dictate the duration of movement, form and run out distance of slope failure (Thiebes, 2012).

Slope stability analyses, can quantify the above mechanism using variety of methods (e.g. limit equilibrium, finite element and probabilistic methods). Limit equilibrium method (LEM), which is the method used in current study, assumes factor of safety (FS) as a global parameter for the entire failure surface. In this method, FS can be determined with respect to force or moment equilibrium within the slope. LEM includes variety of methods that differ in calculation of resisting trusts, each of which are suitable for specific material or a geotechnical case. A summary of these methods are presented by Pockoski and Duncan (2000) in Table 2.3 which are commonly used in recent commercial softwares.

As the output of any of these methods, the stability of slope is generally assessed by calculating the Factor of Safety (FS), which is the ratio of driving and resisting forces/moments (Crozier 1989). In theory, a slope is stable as long as the FS is greater than unity and slope movement commences if the FS is 1.0 or smaller. However, many researchers (e.g. Petley et al., 2002; Glade and Crozier, 2005; Cheng and Lau, 2008 and Suryo, 2013) stress the point that the FS is only a relative measure of stability as it gives no information on the magnitude of destabilization that is needed until slope failure occurs.

Table 2.3. Well-known LEMs showing considered equilibrium types and assumptions (Pockoski and Duncan, 2000)

Method	Equilibrium				Assumptions	Comments
	Overall Moment	Individual Slice Moment	Horizontal Force	Vertical Force		
Swedish Circle	Yes	No	No	No	Circular Slip Surface	Only for $\phi=0$
Ordinary Method of Slices (Fellenius 1927)	Yes	No	No	No	Circular Slip Surface Side Forces Parallel to Base	Conservative Very inaccurate for high pore water pressures
Bishop's Modified Method (Bishop 1955)	Yes	No	No	Yes	Circular Slip Surfaces Side Forces Horizontal	Very inaccurate for high pore water pressures
Morgenstern and Price's Method (Morgenstern and Price 1965)	Yes	Yes	Yes	Yes	Slip surface of any shape Pattern of Side Force Orientations	Much engineering time required to vary side force assumptions.
Spencer's Method (Spencer 1967)	Yes	Yes	Yes	Yes	Slip surface of any shape Side Forces Parallel	Simplest Method
Corps of Engineers Modified Swedish (1970)	No	No	Yes	Yes	Slip surface of any shape Side Forces Parallel to Slope	High factor of safety
Lowe & Karafiath (1960)	No	No	Yes	Yes	Slip surface of any shape Side Force Orientations Average of Slope and Slip Surface	Best side force assumption
Janbu Simplified (Janbu 1954)	No	No	Yes	Yes	Slip surface of any shape Side Forces Horizontal	Low Factor of Safety
GLE - General Limit Equilibrium	Yes	Yes	Yes	Yes	Slip surface of any shape Pattern of Side Force Orientations	Much engineering time required to vary side force assumptions.
GoldNail Method* (Golder)	Yes	*	Yes	Yes	Slip surface of any shape Normal Stress Distribution	Toe circles only
SNAIL Method (CALTRANS)	No	No	Yes	Yes	Slip surface of any shape Two or three wedges, with side force angle = ϕ	Limited shapes of slip surfaces

2.3. Studies on Rainfall-Triggered Landslides

Studies on rainfall triggered landslides (RTL) are focused more or less on two aspects, prediction and mitigation. For accurate prediction of landslides, like any other phenomenon, the mechanism must be studied in detail, hypotheses must be generated, numerical tools developed and verified in different laboratory and field experiments. There could also be some prediction themes that could propose a method that relies on statistic of previous landside events and their triggering factors. In this part highlights from previous studies on prediction of landslides are reviewed.

2.3.1. Statistical studies

From the literature, it is understood that some approaches in predicting rainfall-induced slope failures use historical rainfall data to determine the rainfall threshold. The rainfall threshold is defined as the critical amount of rainfall, above which a landslide will be

triggered (Reichenbach et al., 1998). Prediction of these thresholds, which have an important role in EWS, is one of the key issues in landslide research (Berardi et al. 2005).

Among studies to establish triggering rainfall thresholds, a predominant work by Caine (1980) focused on rainfall intensity and durations which trigger landslides. Many researchers after Caine (1980) expressed rainfall intensity and duration for cumulative and antecedent rainfall and fitted a line to the minimum intensity of rainfall associated with the occurrence of landslide (Fig. 2.7). Following works (Terlien, 1998; Glade, 1998 and Crozier, 1999) added rainfall intensity and duration thresholds that did not cause landslides. Therefore, minimum and maximum thresholds should be acquired, where rainstorms below the minimum threshold never cause landslides (lower bound), and storms above maximum threshold always lead to landslides (upper bound). Between these thresholds landslides may occur under certain conditions.

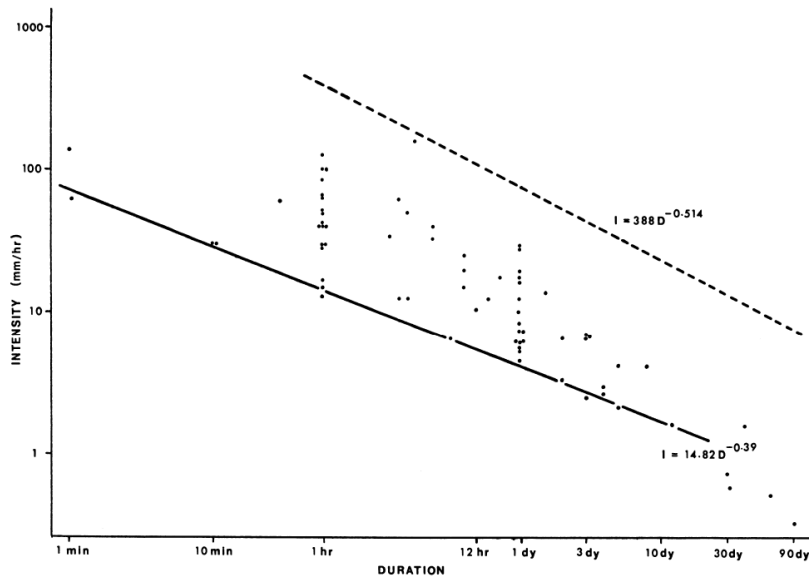


Fig. 2.7. Rainfall intensity and duration of shallow instabilities (Caine, 1980)

Crosta (1998) did a major categorization on rainfall intensity and duration thresholds by classification of employed landslides based on their location since geomechanical properties, hydro-climatical properties (Crozier, 1999) and vegetation type (Wieczorek and Glade 2005) are different from a region to region. Terlien (1998) revealed a set of

landslide triggering rainfall thresholds with distinction between statistical/empirical and deterministic thresholds. Deterministic thresholds were used when rainfall intensity and duration data are limited (Fig. 2.8 (a)). Guzzetti et al. (2007) also distinguished between rainfall thresholds on three spatial scales, for example, global, regional and local scale (Fig. 2.8 (b)).

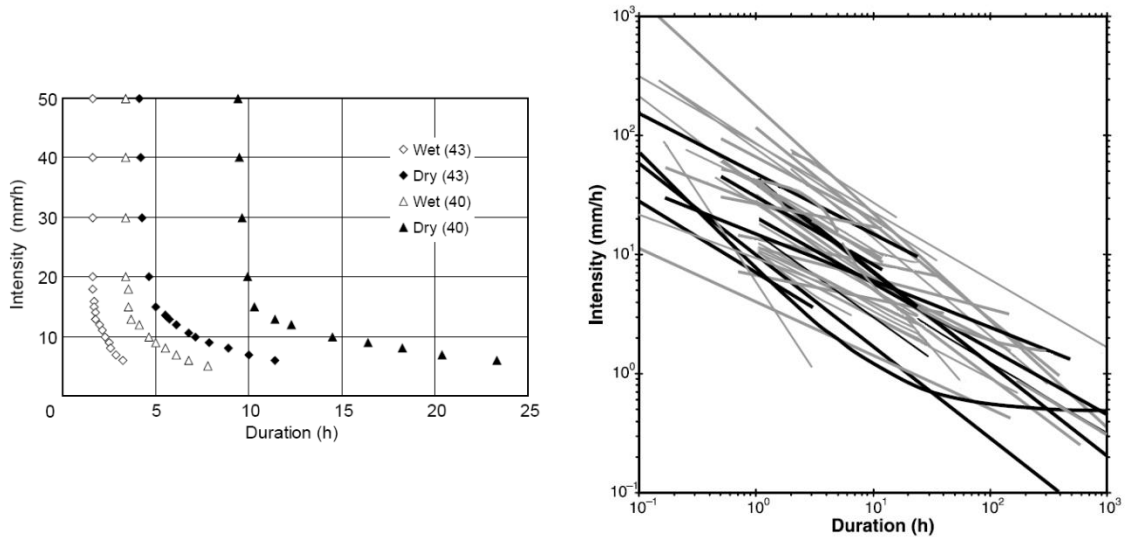


Fig. 2.8. (a) Critical combinations of rainfall intensity and duration needed for saturation of shallower 1.2m of slope as a function of slope and soil properties (e.g. slope angle (for 40° and 43°) and antecedent soil moisture (wet and dry)) by Terlien (1998) and (b) rainfall intensity - duration thresholds with distinction on scale by Guzzetti et al. (2007). (e.g. very thick line, global threshold; thick line, regional threshold; thin line, local threshold. Black lines show thresholds determined for regions or areas pertaining to the Central European Adriatic Danubian South-Eastern area)

As a revolution in classical landslide prediction studies (e.g. statistical methods), some of soil parameters such as soil pore water pressure and volumetric water content were substituted for rainfall intensity and duration thresholds. Negative pore water pressure monitored by many such as Matsushi and Matsukura (2007) and Godt et al. (2006) were used in more detailed and complicated statistical studies to obtain critical pore water pressures in a spatial pattern exceeding which failure will/would happen. Terranova et al. (2007) developed the same tactic using piezometer data.

2.3.2. Numerical studies

Majority of numerical studies on rainfall triggered landslides focus on two major topics; using numerical methods for susceptibility study of landslides triggered by rainfall (e.g. van Westen et al., 2007, Chen and Wang, 2007, Rossi et al., 2010, ...) and employing numerical methods in infiltration and stability studies of slopes (e.g. Rahimi et al., 2011, Lu et al., 2012, Eichenberger et al., 2013, ...).

In susceptibility studies, correlations between landslide inducing factors (geomorphological, hydraulic, hydrological, and anthropogenic factors) and the area where the landslides have been recorded can be evaluated all together with a multiple regression technique, such as weighted linear regression (Hong et al. 2007), logistic regression (Chen and Wang 2007; Dai and Lee 2002 and Guzzetti et al. 1999), or discriminant analysis (Santacana et al. 2003); or individually in a bivariate statistical method (Lee and Pradhan, 2006). More recent efforts have developed artificial neural network (ANN) approaches (Arora and Gupta 2004 and Lee et al. 2007).

Study of infiltration and slope stability of slopes using numerical methods can be classified in to two categories of (i) uncoupled unsaturated infiltration and slope stability studies and (ii) deformation coupled infiltration and slope stability studies.

(i) Some commercial finite element (FE) codes such as GeoStudio 2007 (GeoStudio International, 2007), FLEXPDE 6 (PDE solutions, 2014), etc. are capable to assess pore water pressure employing 1D/2D unsaturated seepage rules and use them in stability analysis of slopes subjected to fluid infiltrations/exfiltrations.

(ii) Some other codes also are developed to incorporate calculations, deformation and thermodynamics into hydraulic conductivity and shear strength such as Code Bright (implementing Basic Barcelona Model (Alonso et al., 1990) by Olivella et al., 1996), ACMEG-S & -2S (implementing nonlinear elasticity coupled with multi-dissipative plasticity by Nuth and Laloui, 2008), Z-soil (user defined hydro-mechanical coupled infiltration by Zace services Ltd.), etc.. Current state of the art is focused on improvement of numerical analysis methods and on implementation of different unsaturated soil plasticity rules in coupled analyses.

SEEP/W as a part of GeoStudio 2012 software package can make numerical simulation for constant and transient seepage through porous media. Because of using this software in different parts of current research, some features of this interface are summarized here.

- SEEP/W uses Darcy flow rules (see equation (2.14)).
- It uses Galerkin method of weighed residual for solving the governing differential flow equation (2.29),

$$\frac{\partial}{\partial x} \left(k_x \frac{\partial H}{\partial x} \right) + \frac{\partial}{\partial y} \left(k_y \frac{\partial H}{\partial y} \right) + Q = m_w \gamma_w \frac{\partial H}{\partial t} \quad (2.29)$$

in which, H is the total head, k_x & k_y are the hydraulic conductivity in the x and y directions, respectively, Q is the applied boundary flux, θ represents the volumetric water content, t shows time and m_w indicates the slope of the storage curve (SWCC).

- SEEP/W considers constant total stress, therefore volumetric water content changes are stress/deformation independent.

SLOPE/W also as another part of GeoStudio 2012 software package is used by many researchers to study stability of slopes subjected to infiltration/exfiltration. SLOPE/W can employ variety of methods for slope stability (e.g. Morgenstern-Price, Spencer, Corps of engineers, Lowe-Karafiath, Janbu Generalized, Sarma, Bishop, Janbu, Ordinary, etc.). SLOPE/W also used pore water pressure results of SEEP in a decoupled analysis.

- A numerical case by Rahimi et al. (2011)

As one of 2D infiltration coupled stability studies over slopes subjected to rainfall, a numerical study by Rahimi et al. (2011) focuses on antecedent rainfall over slopes. Fig. 2.9 shows the geometry of defined slope model in SEEP/W and SLOPE/W softwares and the boundary conditions. Two soils of high and low hydraulic conductivity (HC & LC, respectively) were assigned to the model and their SWCCs and HCFs are shown in Fig. 2.10.

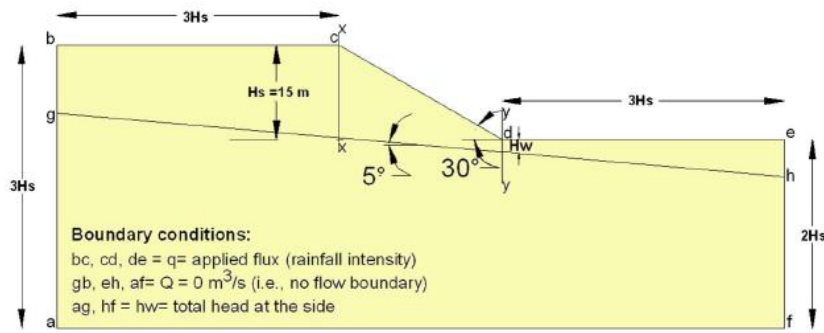


Fig. 2.9. Geometry of slope (Rahimi et al., 2011)

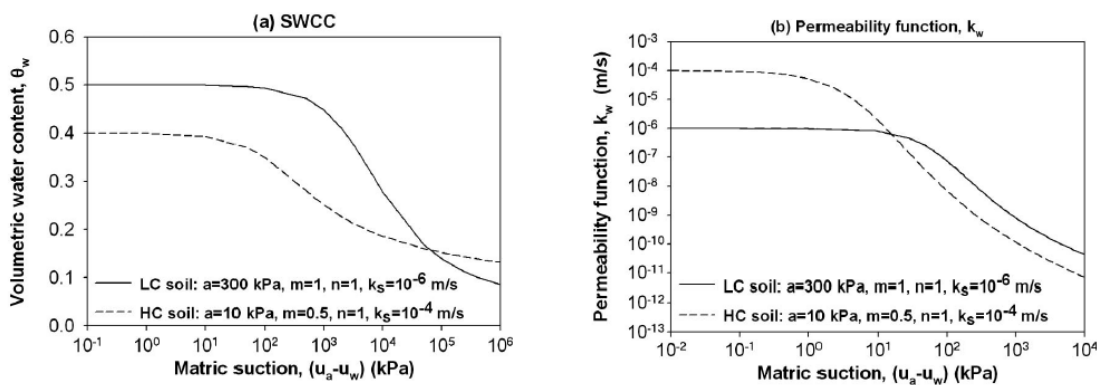


Fig. 2.10. (a) SWCC and (b) HCF of assigned soils to the model (Rahimi et al., 2011)

Shear strength properties for both of the soils were defined as $c' = 10 \text{ kPa}$, $\phi' = 26^\circ$ and $\phi_b = 26^\circ$ as typical soil properties of Singapore (Rahardjo et al. 2007). Unit weight also was set $\gamma = 20 \text{ kN/m}^3$.

For initial condition, as it is obvious in Fig. 2.9, a water table between nodes g & h was considered. Considering typical hazardous rainfall patterns of Singapore, three scenarios were analyzed: delayed rainfall pattern, normal rainfall pattern and advanced rainfall pattern. All the scenarios, as shown in Fig. 2.11, have the time discretized in intervals of 5 days (120hrs).

Stability of the slopes was investigated by examining factor of safety during rainfall over slopes (Fig. 2.12). Changes in pore water pressures also were presented in detail in illustrative sections of x-x and y-y at crest and toe of the slope (see Fig. 2.9) respectively in Fig. 2.13.

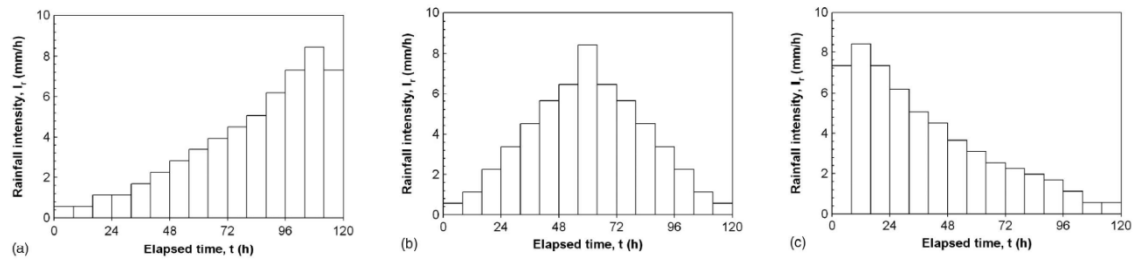


Fig. 2.11. Rainfall patterns, (a) delayed rainfall pattern, (b) normal rainfall pattern and (c) advanced rainfall pattern (Rahimi et al., 2011)

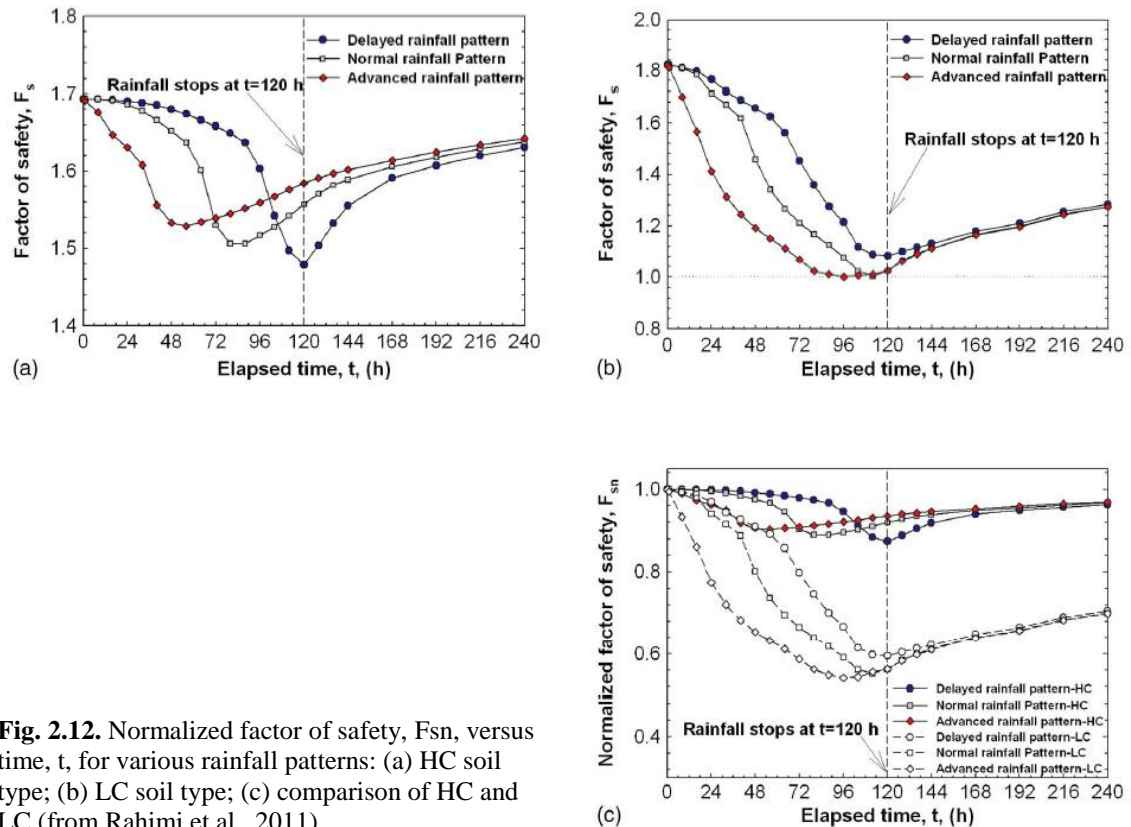


Fig. 2.12. Normalized factor of safety, F_{sn} , versus time, t , for various rainfall patterns: (a) HC soil type; (b) LC soil type; (c) comparison of HC and LC (from Rahimi et al., 2011)

Rahimi et al. (2011) concluded that antecedent rainfall affects the stability of LC soil slope more significantly than HC soil slope. Antecedent rainfalls could cause up to 45% reduction in the factor of safety of LC soil slope and up to 13% reduction in the factor of safety of HC soil slope before the occurrence of major rainfall.

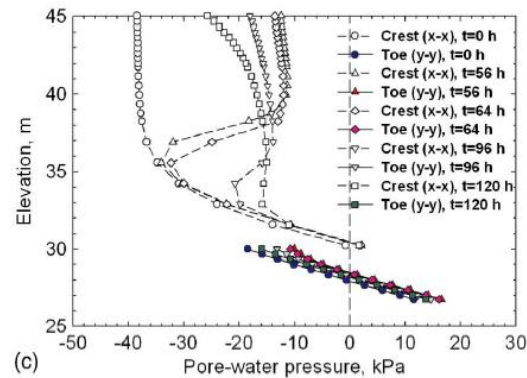
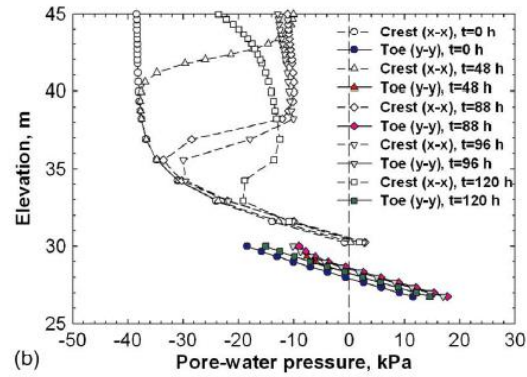
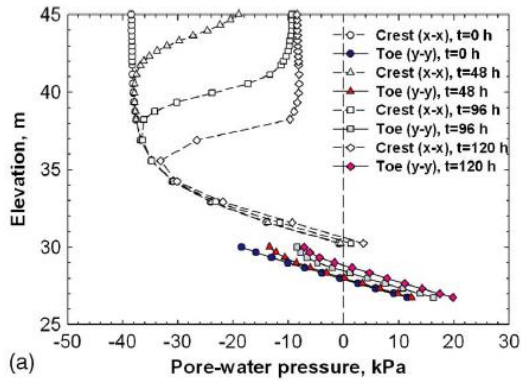


Fig. 2.13. Pore-water pressure distribution caused by antecedent rainfall at crest (x-x) and toe (y-y) cross section for HC soil type: (a) delayed rainfall pattern; (b) normal rainfall pattern; (c) advanced rainfall pattern (from Rahimi et al., 2011)

2.3.3. Field studies

Field studies over rainfall triggered landslides are generally focused over well instrumentation of a natural slope in the field, making record of different hydro-mechanical properties (e.g. deformation of soil body, pore water pressure, volumetric water content, etc.) and trying to simulate their response to different natural events (infiltration/exfiltration) numerically. However, it is very rare possibility that a real slope failure occurs during measurements; thus, artificial infiltration/exfiltrations are done to see slope response to extreme cases. The specifications of nine full scale landslide triggering experiments using artificial rainfall are summarized in Table 2.4.

In these cases generally focused to monitor pore pressures in potentially unstable zones as the main parameter supposed by changing which slope failures may occur. It was observed that various buildups of positive pore water pressure along a slope in response to vertical (up-to-down or down-to-up) infiltration and following shear strength reduction can generally can be considered as the most prominent triggering mechanism.

- Field study by Askarinejad (2013)

As one of major examples of field cases, Askarinejad (2013) has presented detail of field activities and results from Rudlingen case. In framework of TRAMM research project a steep slope of 38° (with maximum of 43° in the middle of the slope) at about the altitude 350 m above sea level, in a forested area near Ruedlingen village (northern Switzerland), was instrumented. The study area with 35m length and 7.5m width was located on the east facing bank along the river Rhine. The geology of the site was mainly consisted of Molasse which is the sediment deposited in the foreland basin of the Alps, containing alternate depositions in the Tethys Sea (Seawater Molasse) and on land (Freshwater Molasse). Soil layer above bedrock (ranging 0.75 to 4.5m) was investigated (Fig. 2.14) and using some test pits (TP), disturbed and undisturbed samples were obtained and geotechnical properties were assessed.

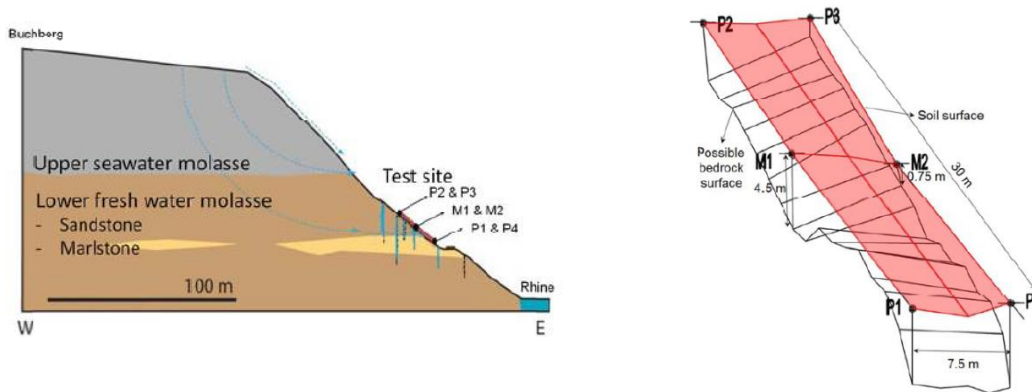


Fig. 2.14. (a) Geology of study site and (b) soil layer thickness above bedrock (Askarinejad et al., 2012)

The soil classified as medium to low plasticity sand (ML) according to USCS, in which fine fraction increases and activity decreases with depth increase. Using triaxial and direct shear tests, shear strength properties were also assessed. Fig. 2.15 shows plot of normal and shear stresses at failure obtained from direct shear tests.

Hydraulic properties of unsaturated soils were also determined through laboratory tests. Fig. 2.16 shows SWCC and HCF of the study soil.

One of the advantages of this study was employing detailed instrumentations. Askarinejad (2013) has plotted all instrumentation over the slope plan (Fig. 2.17).

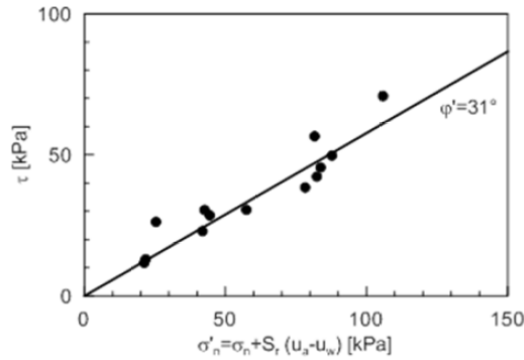


Fig. 2.15. Normal vs. shear stress at failure for Rudlingen soil case (Akarinejad et al., 2012)

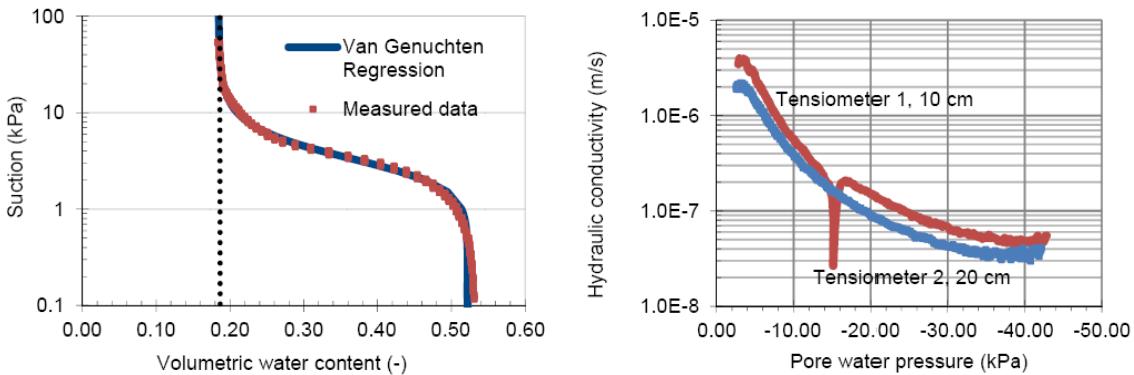


Fig. 2.16. (a) SWCC and (b) HCF of typical study soil obtained from laboratory test data, with van Genuchten curve fit (for SWCC) (Askarinejad et al., 2012)

In the study site two rainfalling scenarios were performed. First rainfall was in October 2008 and the second one was applied to the experiment on March 2009 (Fig. 2.18).

As the results from the tests, suction response of some of tensiometers placed in different depths within slope are demonstrated in Fig. 2.19 for second experiment. Detailed results for both of the experiments are revealed in Askarinejad (2013).

The first experiment despite subjecting to the rainfalls of higher intensity and longer duration in comparison to second experiment experienced no failure. It was concluded that in second experiment generated positive pore water pressures due exfiltration has reduced shear strength well enough to lead to failure.

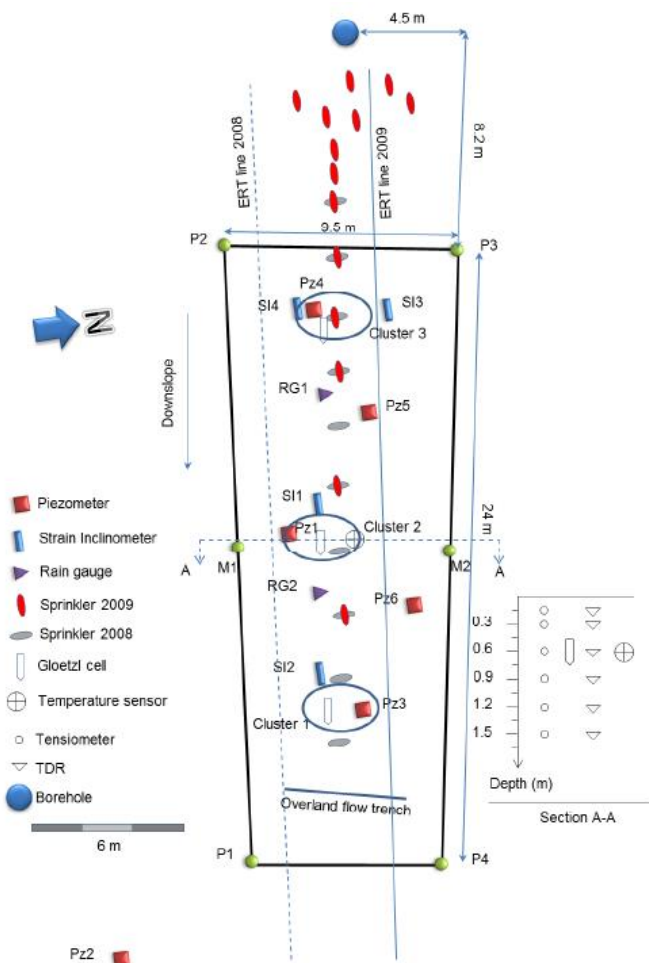


Fig. 2.17. Instrumentation plan of the Ruedlingen slope (Askarinejad et al., 2012).

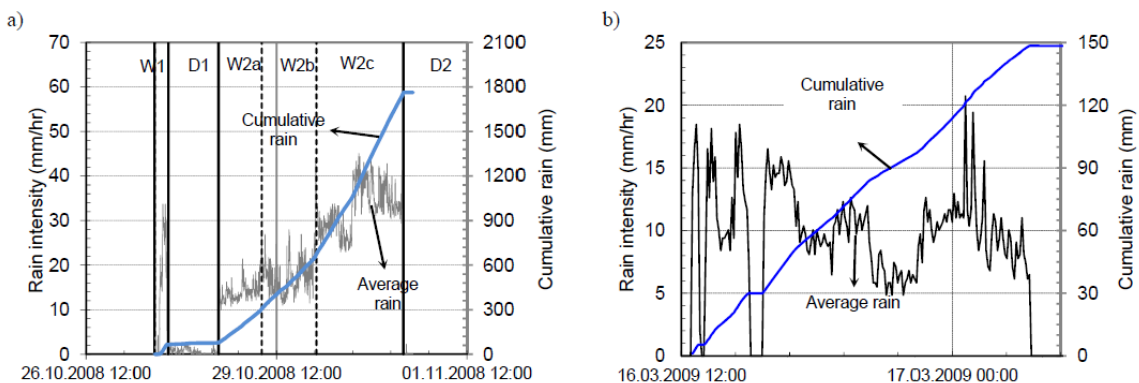


Fig. 2.18. Applied rainfall scenarios (a) First experiment and (b) second experiment (Askarinejad et al., 2012)

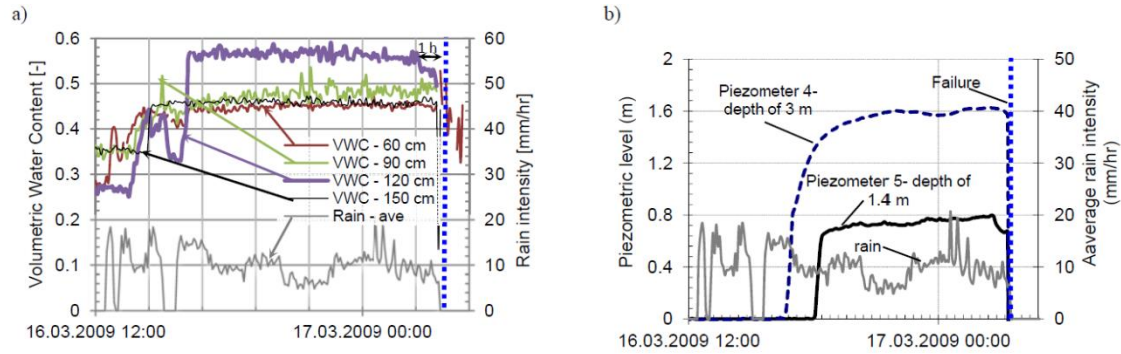


Fig. 2.19. (a) Changes in the volumetric water content profile in cluster 3, (b) changes in the piezometric level at two points on the upper part of the slope (Askarinejad et al., 2012)

- Field study by Godt et al. (2009)

As one of the older field case studies, Godt et al. (2009) showed that the partially saturated shallow landslide at a coastal bluff in the Seattle, WA, USA, was predictable using measured soil suction and water content and based on suction stress concept (which was novel at the time of research, 2009). In Fig. 2.20 cross section of the slope and the location of the instrumentations are shown.

In this study, instrumental observations from the site where a shallow instability occurred in the apparent absence of positive pore water pressures under partially saturated soil conditions was also reported (Fig. 2.21).

2.3.4. Laboratory Flume studies

To study effect of different parameters on behavior of the slopes subjected to rainfall, laboratory slope models are investigated by many researchers. In these studies, generally on a slope model in the laboratory (in different scales) artificial rainfalls are applied and changes in different soil parameters (pore water pressure, water content, deformation, etc.) are monitored. Centrifuge tests also are done to monitor more detailed behavior of the slopes subjected to rainfall. Table 2.5 is summarizes some of these studies.

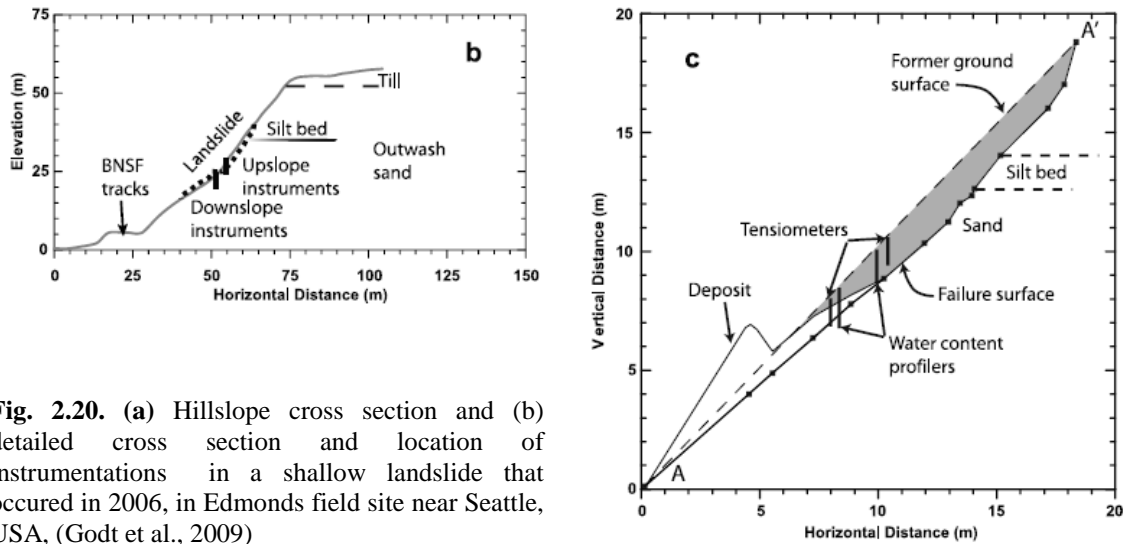


Fig. 2.20. (a) Hillslope cross section and (b) detailed cross section and location of instrumentations in a shallow landslide that occurred in 2006, in Edmonds field site near Seattle, USA, (Godt et al., 2009)

- Laboratory experiment by Daminao (2004)

In one of prominent studies by Daminao (2004), a set of laboratory flume experiments were carried out using a uniform mix of typical Cervinara soil (southern Italy) and subjected to artificial rainfalls of different intensities. Extensive instrumentation of the experiments made it possible to prepare a complete set of geotechnical data (e.g. pore water pressure using tensiometers and miniature pore water pressure transducers, volumetric water contents using Time Domain Reflectometers, deformation assisting Particle Image Velocimetry technique). More details about this study are presented in 3.1.

- Laboratory experiment by Schnellmann et al. (2010)

In another study by Schnellmann et al. (2010) a physical slope model was used to study the effect of rising groundwater table on pore-water pressures of an unsaturated soil slope. In addition, finite element analyses were carried out to simulate infiltration in slopes under steady state and transient conditions. To perform model tests, a laboratory setup was employed to apply rainfall in controlled intensities. It was possible to generate

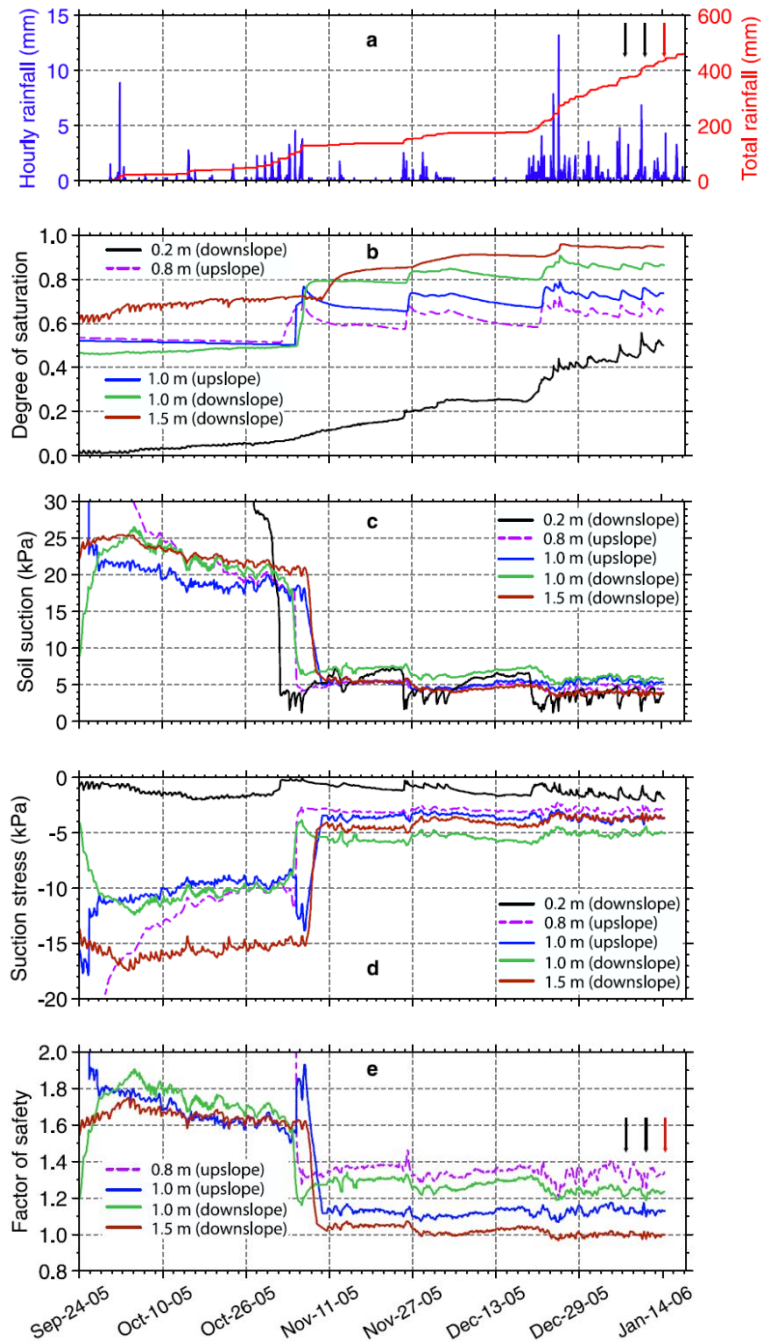


Fig. 2.21. (a) Hourly and cumulative rainfall, (b) soil saturation, (c) soil suction, (d) suction stress and (e) factor of safety for the period 24 September 2005 to 14 January 2006 at various depths from the upslope and downslope instrument arrays (Fig. 2.20). Black and red arrows indicate the times (6 and 10 January 2006 and 14 January 2006, respectively) of the occurrence of several landslides along the 15 km stretch of bluffs in the vicinity of the field site and the study site.

independently controllable ground water table inside the model at the side boundaries. The setup has capability to be instrumented to capture different geotechnical properties (Fig. 2.22).

For this study, drying and wetting SWCCs obtained from independent measurements in Tempe cell and capillary rise open tube tests. HCF also estimated using saturated permeability and SWCC data (Fig. 2.23). Volumetric water content and pore water pressures were measured in different points in the model using Time Domain Reflectometers and tensiometers.

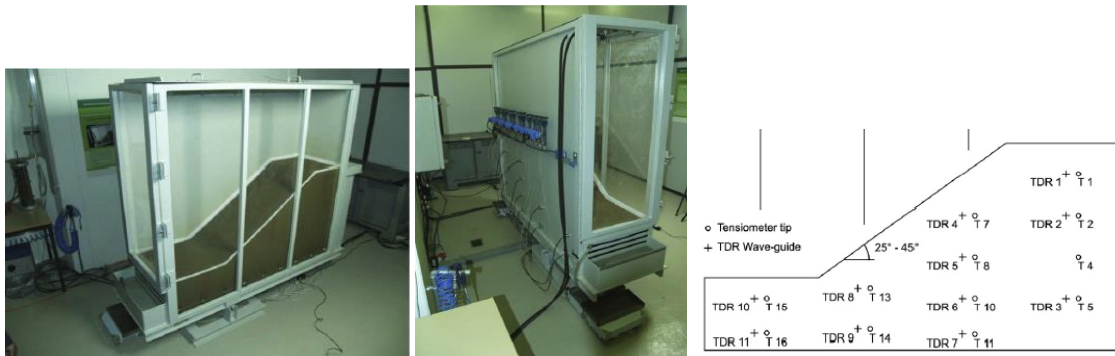
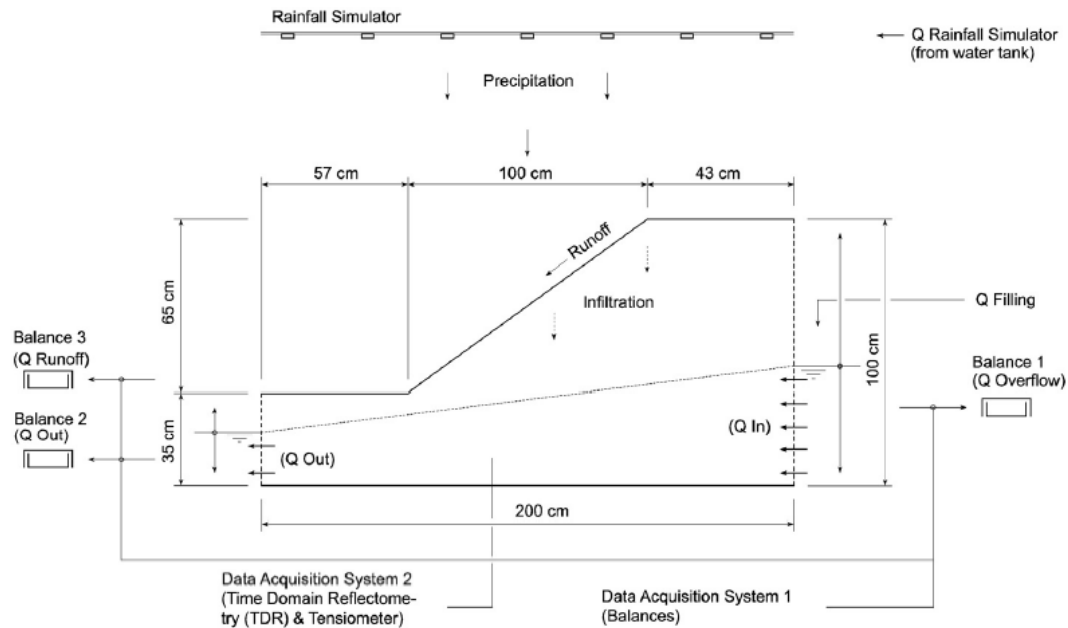


Fig. 2.22. Experimental model for suction change monitoring due rainfall in slopes (Schnellmann et al., 2010)

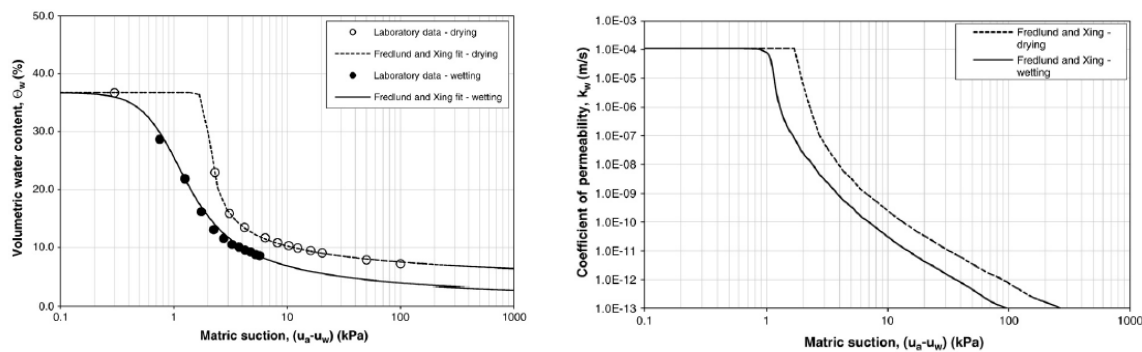


Fig. 2.23. (a) SWCC and (b) HCF of used soil

The pore water pressure measurements in this experiment were always found to be higher than -4 kPa. This effect was explained by the steep permeability function of this particular sand. It was interpreted that the permeability drops significantly when the pore water pressures are lower than -1 kPa. This causes a time dependent equalization process which prevents quick pore water and water content changes in the unsaturated zone (Fig. 2.24).

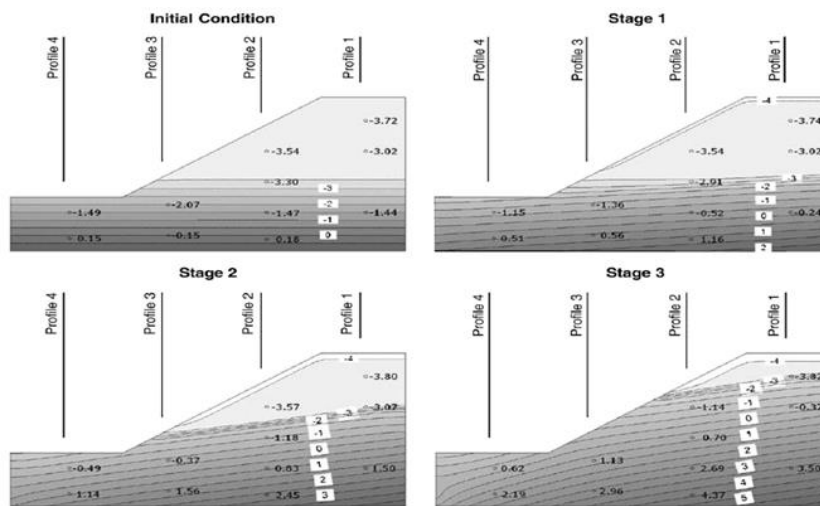


Fig. 2.24. Pore water pressure response, (Schnellmann et al., 2010)

Both, experimental data and numerical analyses demonstrate a delayed response in pore-water pressure in the unsaturated zone due to the rising of water table. A conceptual framework was also presented (confirmed with measurements and numerical results) to

describe the possible lower and upper limits of pore water pressures in a slope resulting from the rise in water table. This research demonstrated that a delay in pore-water pressures may cause a delayed failure. Specially for fine-grained soil slopes, failure may not occur at the end of rainfall, but may occur at some time after the end of rainfall. Hence, time to failure for an unsaturated slope should be analyzed incorporating unsaturated–saturated seepage analysis.

Table 2.4. Landslide triggering experiments on natural field slopes (modified after Askarinejad, 2013)

Reference	Location	Sprinkled area, Triggered vol./area (T)	Rainfalling method	Instrumentations	Slope angle	Soil type
Oka, 1972	Japan	500	Sprayed form	-	-	-
Yagi et al., 1985	Japan	10 × 25	Rainfall	Ext/P	-	-
Yamaguchi et al., 1989	Japan	10 × 25	Upper trench	Ext/P/Inclinometer	-	-
Harp et al., 1990	USA	1.6 × 1.3 30 × 5.0 3.2 × 4.0	Upper trench	Ext/P	30 43 70	Gravelly silty sand Weathered disintegrated Coarse to medium sand
Olivares and Picarelli, 2003	Italy	-	Natural rainfall	T/P/RG	38	Volcanic ashes and Pumice
Ochiai et al., 2004	Japan	30 × 5.0	Sprinklers	Ext/T/Strain probe	33	Weathered disintegrated granite sand
Teyssere, 2005	Switzerland	55	Sprinklers	Ext/TDR/T/Moisture	42	Moraine (gravelly silty sand)
Godt et al., 2009	USA	11 × 25 (T)	Natural	T/P	45	Loose sandy colluvium
Askarinejad, 2013	Switzerland	130	Sprinklers	TDR/T/P/Soil deformation probe/ERT/Soil pressure sensors/ Photogrammetry/RG/Meteorological station	38	Silty sand with clay

Ext: Extensimeter, P: Piezometer, PPT: Pore Pressure Transducer, RG: Rain Gauge and TDR: Time Domain Reflectometry

Table 2.5. Landslide triggering experiments in the laboratory (flume and centrifuge tests)

Reference	Location	Soil type	Rain intensity (mm/hr)	Instrumentation	Slope angle (°)	Failure mechanisms	Slope shape
Okura et al., 2002	Japan	Sand	100	PPT, RG	10 & 32	“Fluidization”	
Take et al., 2004 (Centrifuge)	UK	Fine & coarse granite sand	4.2 (250)	PPT, PIV	45	Static liquefaction	
Orense et al., 2004	Japan	Omigava sand	42-72	TDR	40	“Fluidization”	
Tohari et al., 2007	Indonesia	River sand & granite sand	0-100	PPT	32-45	Water table increase	
Montrasio and Valentino, 2007	Italy	Pyroclastic soils	84	TDR and PPT	38	Water table increase	
Huang et al., 2010	Hong Kong	Silty sand	47	T/RG/PPT/TDR	29 & 30	Water table increase	
Olivares et al., 2009	Italy	Pumice & Fly ash	18-105	T/PPT/RG	0-40	Static liquefaction	
Schallmann et al., 2010	Switzerland	Well graded sand with silt	40	TDR	33	-	
Askarnejad, 2013 (Centrifuge)	Switzerland	Silty fine sand	1.27-2.5 (10-45)	TDR/T/P/PIV	38	down to up effect	

P: Piezometer, PPT: Pore Pressure Transducer, RG: Rain Gauge and TDR: Time Domain Reflectometry, PIV: Particle Image Velocimetry

CHAPTER 3

INITIAL STUDIES – A LANDSLIDE PREDICTION ATTEMPT AND A PARAMETRIC STUDY OVER A FLUME CASE

To become more familiar with suction coupled slope stability analyses in unsaturated soil slopes using available commercial softwares, it was focused on back analysis of a field case study and back analysis and parametric study over a well-documented flume case. In addition, a study of effects of unsaturated hydraulic properties on the rainfall triggering mechanism was carried out in order to get a better sense of the process. In following sections each of these study packages are described in detail.

3.1. Back analyses and predictions for Cervinara field case and flume models

During the third Italian Workshop on Landslide (IWL2013) which took place on 23 and 24 October 2013 in Naples (Italy), a special session was dedicated to a landslide hydrological modeling competition entitled as Round Robin test. The test was designed to provide geological and geotechnical data of a monitored field slope and two flume model tests for calibration of the models and ask participants to do blind predictions over infiltration progression and time to failure in a flume model and the monitored field site. A research team from Middle East Technical University (METU) composed of two faculties (Dr. Nejan Huvaj and Dr. Kartal Toker) and the author participated in Round Robin test. The sequences followed for calibration of numerical models and predictions of pore water pressures and time to failure, prepared for Round Robin test, are presented in following sections. Contributions by Bogaard et al. (2014) and Ahmadi-adli et al. (2014) summarized the findings.

3.1.1. Summary of prepared data

Data provided for the participants consisted of physical characteristics of soils covering study site, data of controlled infiltration flume tests with deformation monitoring data and also field infiltration data. Summary of provided data follows.

3.1.1.1. Geological/geotechnical characterization of the study site

Slope of Cervinara (northeast slope of Mount Cornito of Cervinara, around 40 km north-east of Naples) is covered with granular volcanic pyroclastic soil which is notorious for the disruptive flow-like sudden shallow landslides. The soil cover consists of an alternation of loose volcanic ashes and pumices lying upon fractured limestone bedrock. To assess basic geotechnical characteristics of these soils, laboratory tests were performed on small undisturbed or reconstituted soil samples (with width ranging 70mm to 100mm and height of 20mm to 150mm). Table 3.1 gives the main physical properties of the ashes, which usually represent the thickest layer within the profile. These data obtained from suction-controlled triaxial strength and infiltration tests, details of which are available at Picarelli et al. (2006), Olivares & Damiano (2007), Olivares et al. (2009), Damiano & Olivares (2010) and Greco et al. (2010). Throughout Round Robin, for possibility of more complicated numerical analyses more detailed information from these tests was made available for the participants. These detailed data were such as the axial, radial and volumetric strains and water content changes observed before applying deviator load and measured step by step during applying deviator load.

Table 3.1. Main physical properties of the investigated volcanic ashes (Bogaard et al., 2014)

specific weight, γ_s (kN/m ³)	25-26
unit volume weight, γ (kN/m ³)	11-14
porosity, n	0.67-0.75
saturated hydraulic conductivity, k_{sat} (m/s)	1.5×10^{-7} - 5.7×10^{-6}
effective friction angle, ϕ' (°)	38
Cohesion, c' (kPa)	0

3.1.1.2. Data from infiltration flume experiments

The complete record of two infiltration experiments in a slope covered with a layer of the ashes of Cervinara were provided to the participating modeling teams. The experiments were done in the geotechnical laboratory of the Seconda Università di Napoli and well instrumented by minitensiometers; pressure transducers; TDR probes and laser sensors to capture complete response of the slope. The inclination of the slopes was 40° and the width of the experiment 50 cm. The bottom and walls of the flume were impervious (made of Plexiglas). The toe of the slope was made up of a supporting element, geotextile wrapped gravel. It was draining the layer only when the soil at the foot of the slope approached saturation. Table 3.2 summarizes the main characteristics of the two experiments. More detailed data about the flume and the installed devices can be found in Olivares et al. (2009).

Table 3.2. Main characteristics of the flume infiltration tests (Bogaard et al., 2014)

Test	Soil Thickness (cm)	Slope Length (cm)	Initial porosity, n_0	Rainfall intensity (mm/h)	Initial mean suction (kPa)	Duration of test (min)
D3	10	100	0.75	55	17.5	36
D4	10	120	0.76	56	41	30

3.1.1.3. Data from field monitoring

Close to the location of the catastrophic landslide which occurred in 1999, an automated monitoring station was launched later in August 2009 at the slope of Cervinara. In this station, measurements of volumetric water content and capillary tension (suction) were taken every two hours. In addition, a rain gauge for hourly automatic acquisition was installed to monitor rainfall intensities.

Participants in the Round Robin were provided with hourly rainfall and air temperature recordings, soil suction and soil volumetric water content measured between 01.01.2011 and 27.07.2011 (Damiano et al., 2012 and Greco et al., 2013).

3.1.1.4. Blind prediction

The participants in the Round Robin were asked to do two blind predictions;

- (a) Modeling of response of an infiltration experiment in a reconstituted slope in the same laboratory flume as in D3 and D4 experiments

Table 3.1 reveals general characteristics of the test, response of which was to be predicted. Soil suction at some locations, the settlements at some locations along the slope surface and the pore water pressure at various locations at the bottom of the soil cover were also given as initial conditions of the problem. For this part, the participants were asked to simulate time of slope failure and suction response in specific points inside soil model.

Table 3.3. Main characteristics of the flume infiltration test to be blindly predicted during the Round Robin contest (Bogaard et al., 2014)

Test	Soil Thickness (cm)	Slope Length (cm)	Initial porosity n_0	Rainfall intensity (mm/h)	Initial mean suction (kPa)
C4	10.0	100	0.65	60	52

- (b) Simulation of the hydrologic response of the slope of Cervinara to the experienced weather condition (rainfall and temperature) in a specific time period.

Participants were provided with soil suction and soil volumetric water content measured between 01.01.2011 and 27.07.2011 (Damiano et al., 2012 and Greco et al., 2013).

To perform the blind prediction of field conditions, the modelers were supplied with hourly rainfall and air temperature recordings between 1st September 2011 and 12th February 2012. As initial state for soil medium (to be considered in simulations), soil suction at four depths and volumetric water content at three depths (every 2 or 6 hours recordings) between 28.10.2011 and 29.10.2011 were used.

The participants were asked to simulate soil suction between 01.01.2012 and 12.02.2012 and soil volumetric water content between 07.01.2012 and 12.02.2012 at specific depths within monitoring station at the slope of Cervinara.

3.1.2. Contribution by METU team in Round Robin test (IWL2013)

As a participant to round robin test, Middle East Technical University (METU) team performed infiltration and slope stability analyses to simulate flume infiltration test and a field experiment and had an estimation of suction distribution and stability change in the slopes due to climatic changes (mainly rainfall and evaporation). Model definitions, calibrations to assess accurate soil properties and estimations for both flume and field case are explained in this section. Also results of estimations are presented in following parts.

3.1.2.1. Controlled infiltration flume experiments

The Round Robin test is basically an inter-laboratory comparison test performed independently. Recordings from two of D3 and D4 infiltration flume tests were to be used in calibration of soil properties. Then pore water pressure distribution and time to failure in a similar but independent flume test (C4) was to be estimated.

- Numerical simulation of flume models

The pore fluid flow due to rainfall in D3 and D4 flume models was simulated numerically in 2D using SEEP/W. The longitudinal cross sections of 10 cm thickness and 100 or 120 cm length were selected along planes where majority of instruments exist. The bottom and upper side (right) boundaries of the model were impervious, whereas lower side (left) boundary was simulated as free drain. Rainfall intensities of 55 and 56 mm/h, modified by the slope angle, have also been applied constantly from the upper boundary (Fig. 3.1).

Properties of assigned soil to the model such as grain size distribution, porosity, water retention and hydraulic conductivity data, as well as shear strength in saturated and unsaturated conditions were provided from laboratory experiments on small disturbed/undisturbed specimens. Some of these properties were calibrated using records from previous flume tests on the same material (e.g. D3 and D4).

Numerical seepage analysis was performed in two separate stages. In order to let suctions to be equalized throughout the soil (representing time between construction of

flume and rainfall initiation) an equalization stage was introduced in which drying soil hydraulic properties were used. For modelling rainfall infiltration a raining stage was also defined where wetting properties of the soil were assigned to the model.

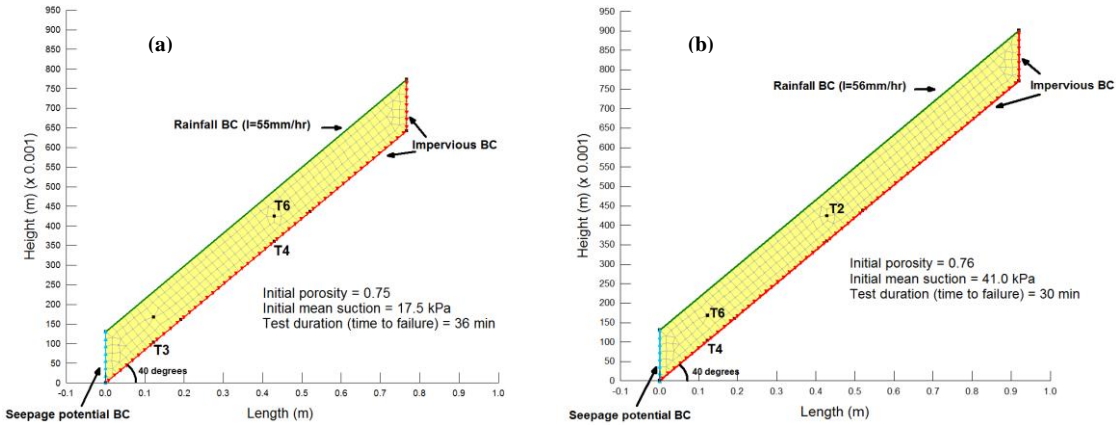


Fig. 3.1. Numerical models for simulation of D3 (a) and D4 (b) infiltration flume tests

- *Calibration of soil properties for the Flume case*

Available hydraulic properties soil water characteristic curve (SWCC) and hydraulic conductivity function (HCF) for Cervinara soil were used as initial guesses for accurate data. Prepared suction-volumetric water content value pairs at exfiltration and evaporation states through reconstituted soil samples and water extrusion trough pressure plate were employed directly as drying SWCC data. Wetting SWCC data points, on the other hand, were assessed indirectly using TDR records adjacent to T3 tensiometer data which are subjected to infiltration due to rainfall. Saturated volumetric water content was calculated using porosity of test specimens and estimated air entry value. Fredlund & Xing (1994) formula was fitted to the data points consequently (Fig. 3.2).

Hydraulic conductivity of Cervinara soil was assessed separately for drying and wetting states. As initial guess for drying HCF, the estimation method proposed by Fredlund et al. (1994) was used with reference to obtained drying SWCC. Required saturated hydraulic conductivity value was also available using constant head tests. For wetting hydraulic conductivity, initial guess was assessed using drying HCF data points. In this

approach, suction value of any data point on drying HCF was used to obtain corresponding suction of a point with same hydraulic conductivity on wetting HCF curve. This conversion assumes there is a unique hydraulic conductivity value for each water content and constant water content on drying and wetting SWCCs corresponds to two different suction values.

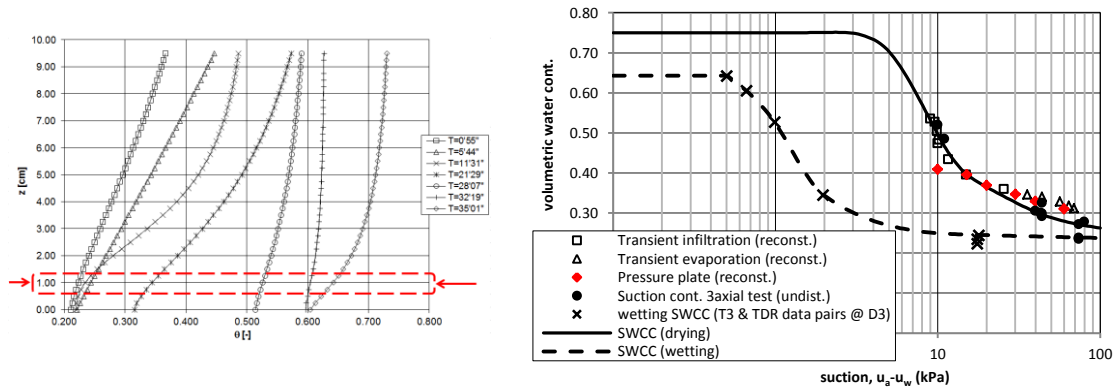


Fig. 3.2. (a) TDR records in time used to obtain wetting soil water characteristic curve (SWCC) and (b) SWCC at drying and wetting states

Estimated HCFs must be used carefully since generally they may contain significant error (Fredlund and Xing, 1994 and Leong and Rahardjo, 2007). Therefore obtained HCFs are only used as initial guesses and more accurate HCFs are obtained using a back analysis to capture suction values recorded by tensiometers. Fig. 3.3 has plotted calibrated drying and wetting HCFs for Cervinara soil.

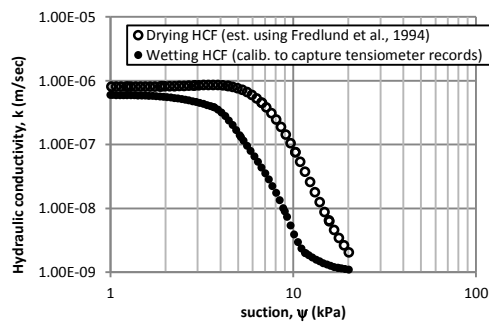


Fig. 3.3. Drying and wetting hydraulic conductivity function (HCF)

Fig. 3.4 shows modeled suction values using calibrated hydraulic properties of Cervinara soil in comparison with recorded suction values in tensiometers.

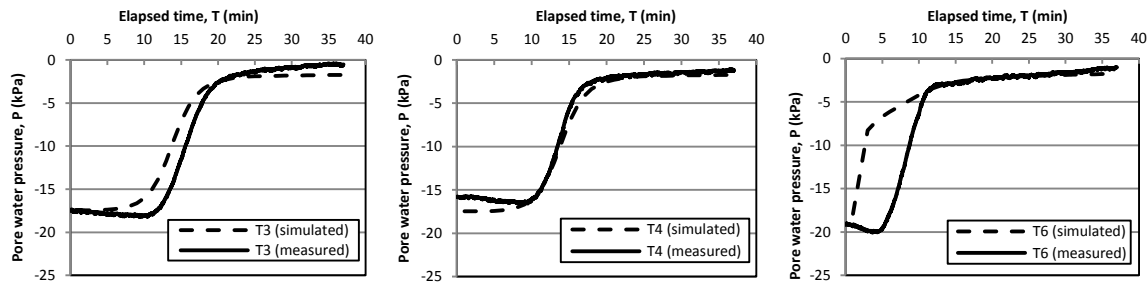


Fig. 3.4. Simulated versus measured pore water pressure at location of T3, T4 and T6 tensiometers for flume test D3

To do a slope stability analyses it's also required to obtain unsaturated shear strength of the test material. Provided data for this purpose included results of a set of unsaturated triaxial shear tests which demonstrated nonlinear shear strength change due suction changes. Considering inability of SLOPE/W software to define nonlinear shear strength, an innovative technique was applied. It must be noted that Slope/W can only use the method proposed by Vanapalli et al. (1996) which uses SWCC of the soil to assess unsaturated shear strength. Therefore, in this technique, unique hypothetical SWCCs were generated using relative volumetric water content, S_e and $\tan\phi_b/\tan\phi$ which were available from triaxial test results. This hypothetical SWCC were used only in calculation of shear strength as input for Vanapalli method, but not in infiltration simulation.

Performing coupled analysis using calibrated hydraulic soil properties in seepage simulation (SEEP/W) and hypothetical SWCCs in slope stability analysis (SLOPE/W) showed good agreement between assessed time to failure in numerical model (which considered time to F.S.=1.0) and the time lasted in flume tests D3 and D4 to observe failure (excessive deformations).

- *Round Robin Competition (Flume Test)*

In round robin test, the objective was estimation of pore pressure response and time to failure in an independent flume test, C4. This experiment consists of a slope with 10cm thickness and 110cm length which tilted 40 degrees. C4 constructed from Cervinara soil. Therefore, after definition of the model in SEEP/W and SLOPE/W, calibrated hydraulic

and strength properties of Cervinara soil were assigned. Defined model and obtained pore pressure responses are plotted in Fig. 3.5. Deeper tensiometers (T2, T4, T7, T8) have shown almost similar response and tensiometers in the middle (T3, T5, T6) responded similarly. As a criterion for failure, suction values at the time of failure in D3 and D4 were used. These suctions are the highest values, lower than which will indicate “failure” at each test. Considering 1 and 2 kPa as suctions at failure in D3 and D4, 220 and 90 minutes were obtained as failure time in C4 test. Therefore, it was proven that “time to failure” is very sensitive to the shear strength criterion.

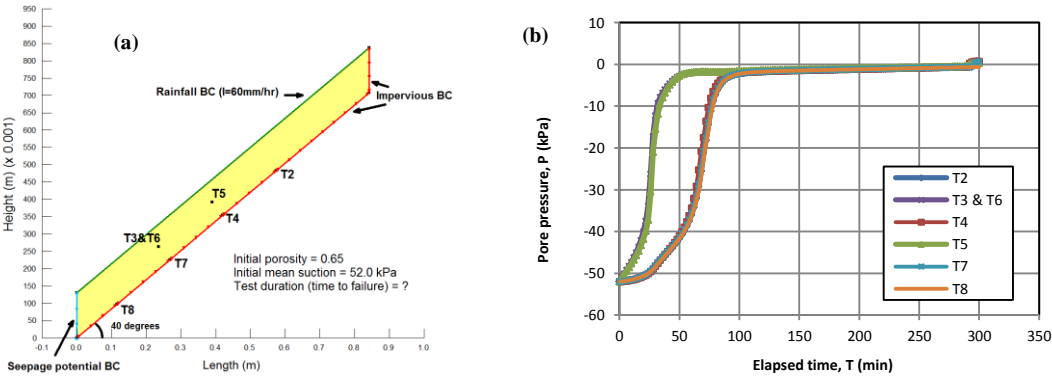


Fig. 3.5. (a) Defined numerical model for C4 and (b) calculated suction response at T2, T3, T4, T5 and T6 in test C4

3.1.2.2. Cervinara Field Experiment

Beside the flume infiltration case, second half of Round Robin test involved estimation of pore water pressure in a real scale slope which is subjected to incidental rainfalls. The case was located at Cervinara and an instrumentation station was constructed in the study region, recorded rainfall intensities and infiltration response of the ground since 2008.

- *Numerical modelling*

To assess geometry of the slope, topographic map of an almost 850 x 850m area which contains location of instrumentation station was provided based on GIS database. In order to prepare a 2D model representing real geometry of the slope, critical cross section (that includes steepest slope and passes through instrumentation station) was

selected. Fig. 3.6 shows a slope of 530m length and 270m height with various surface and bedrock steepness at different locations.

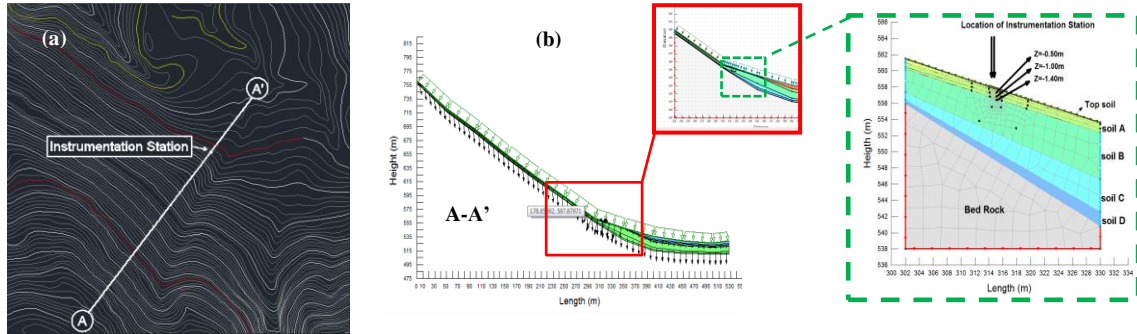


Fig. 3.6. (a) Topography of the study region and (b) selected slope cross section

Fig. 3.7 (a) indicates composition of soil layers at the location of instrumentation station. In contrast to the flume case, no laboratory data were provided for any of the typical soils in the slope. Therefore, assessment of their properties was only possible by using field data recorded from instrumentations. Tensiometer and TDR records could be used in back analyses to assess soil hydraulic properties. However, this option also was limited to two upper layers (Fig. 3.7(b)).

Therefore, as a solution, two coupled numerical models defined to study infiltration and slope stability for this slopes. For assessment of hydraulic soil properties using calibration a local cross section at the location of instrumentation station (Fig. 3.6, the most right) was studied, whereas for slope stability the global cross section was used (Fig. 3.6, A-A').

Rainfall records which were provided for the time period of almost 10 months (28/10/2010 – 16/07/2011) were applied to the upper boundary condition in numerical model. The lower boundary was restrained by impervious bed rock which had variable different depth.

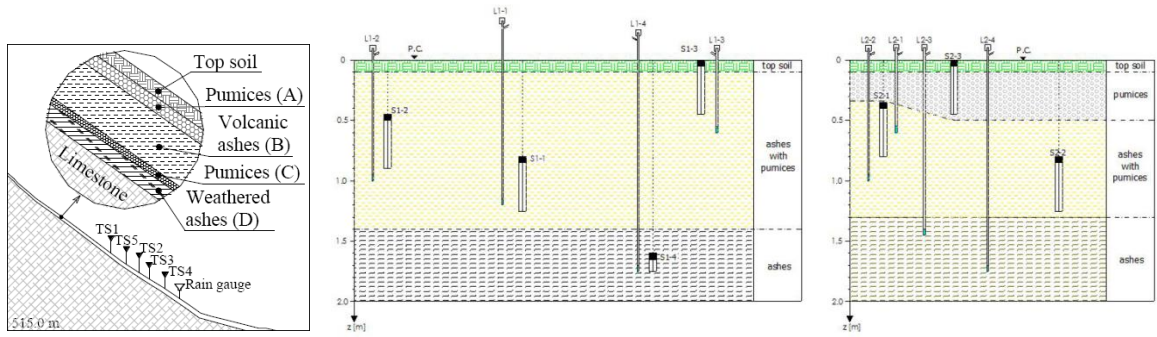


Fig. 3.7. (a) Soil composition in location of instrumentation station and (b) buried measurement devices at the instrumentation station

In order to accurately simulate suction response to the rainfall which is very sensitive to hydraulic properties of the soils, three time periods including major rainfall events were selected for numerical study (Fig. 3.8).

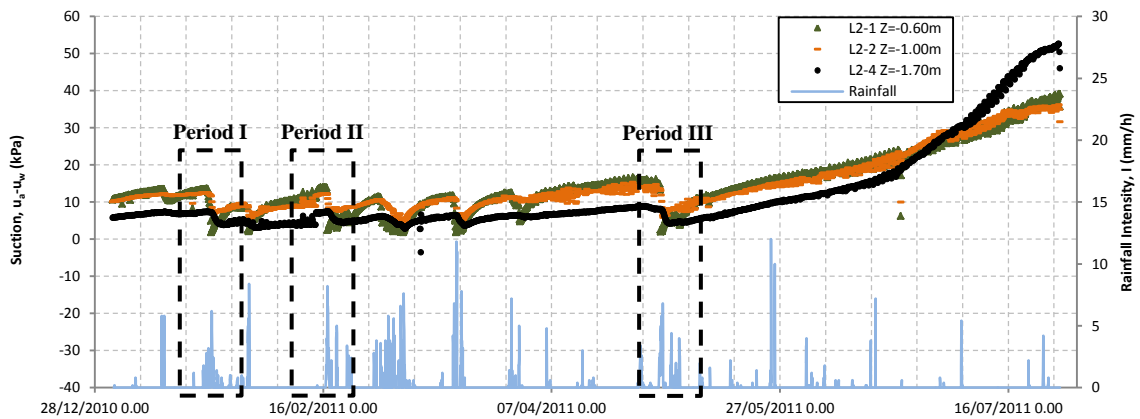


Fig. 3.8. Suction response in different depths at instrumentation station, rainfall records and calibration periods

- *Calibration of soil properties*

Initial guess of soil hydraulic properties were done using two methods. Pairs of Tensiometer and TDR data were available for only soil A. Therefore, for soil A, SWCC was obtained directly by plotting suction and volumetric water content. Using grain size distribution, initial guess for SWCC and HCF were made for soils B, C and D referring database of PLAXFLOW software. Then, using back analyses, accurate soil properties were assessed by capturing suction records at specific locations during the three periods of rainfall events. Fig. 3.9 shows calibrated hydraulic soil properties.

Fig. 3.10 also shows the suction records versus calculated suction values obtained from numerical analysis using calibrated soil properties.

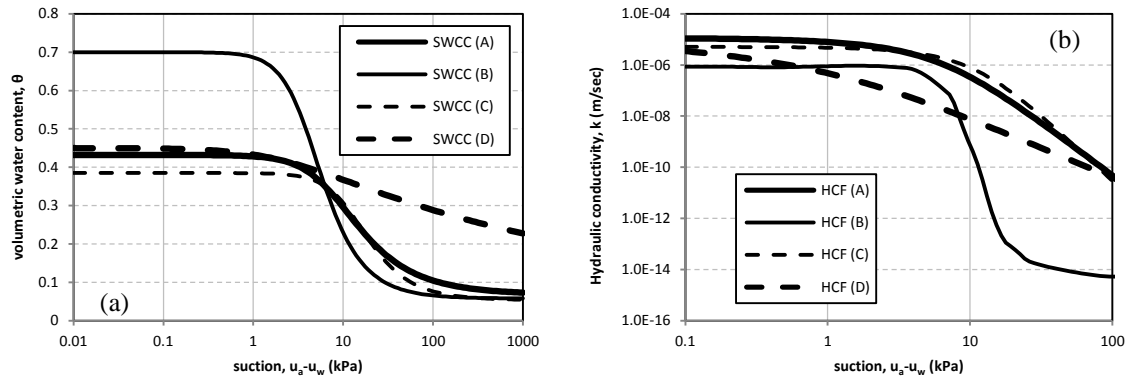


Fig. 3.9. (a) SWCC & (B) HCF of soils A, B, C and D

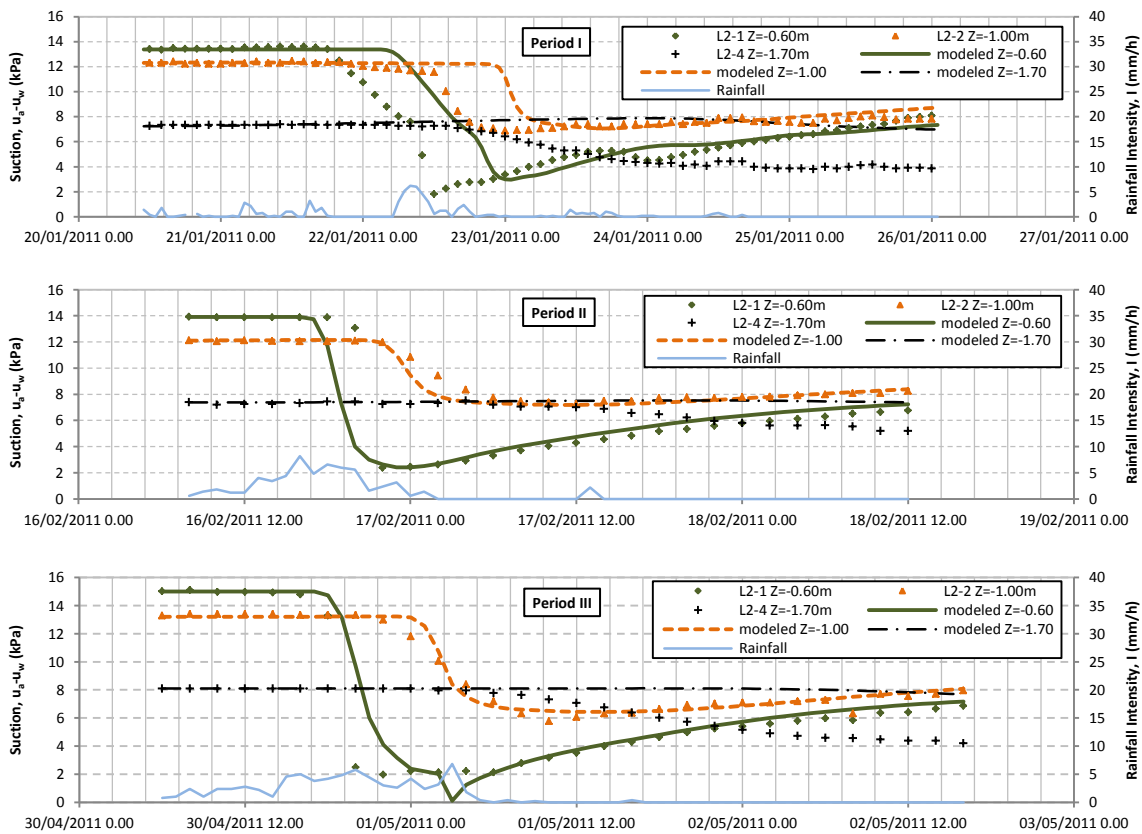


Fig. 3.10. Measured suctions in various depths at instrumentation station versus calculated suctions using calibrated soil materials at three calibration time periods

- *Round robin competition (Field Experiment)*

Part of the round robin test was estimation of tensiometer and TDR responses due climatic changes at specific depths in the time period of 01/01/2012 and 12/02/2012. Precipitation and weather temperature recordings in the mentioned time period were provided. The modelers had to be able to predict suction and volumetric water content using the models which were calibrated to the soils of study region.

Fig. 3.11 shows results of the study by METU team. In modelling climatic changes for the periods of no rainfall, a constant evaporation rate of 2 mm/h were assumed and applied. This assumption was very rough since there are many evaporation models which are coupled to temperature records. This part of study also assumed that vegetation has no effect on infiltration and evaporation. Constant initial suctions were assigned to all parts of each soil layer.

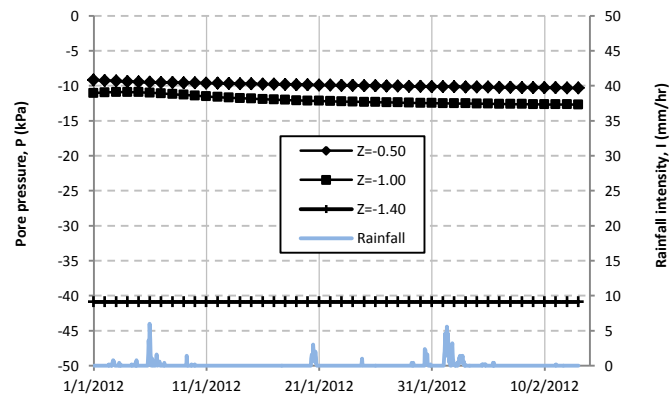


Fig. 3.11. Calculated suctions at required depths due climatic changes between 01/01/2012 and 12/02/2012

3.1.2.3. Conclusions and remarks

The lessons learnt from this activity are valuable and they can be summarized as follows;

- 1- Hydraulic properties of Cervinara soil was assessed accurately using provided laboratory test data and calibration due to suction response to be used numerical simulations. High sensitivity of the calculated suctions to the small changes in SWCC & HCF curves was also observed.
- 2- It was observed that numerical simulation of a real scale steep slope in the field challenged with a number of difficulties such as the uncertainties in the boundary conditions, non-uniformity in soil properties, groundwater table and evaporation. Among these factors, evaporation was observed to be the dominant factor.
- 3- Review of other solutions for this exercise clearly show that complex physically-based models allow a better description and deeper interpretation of the processes actually leading to the triggering of a landslide. However, this comes at the price.
- 4- Use of separate wetting and drying soil hydraulic properties are found to be necessary for accurate infiltration simulations.
- 5- For rainfall triggered landslides, to determine correctly the “time to failure” of a slope, the definition of the “time of failure” becomes critical and influential. $FS=1.00$, specific threshold deformation/strain value, development of a failure plane inside the soil or dramatic drop in the factor of safety are the common criterias.

3.2. Effects of SWCC on unsaturated slope stability (A parametric study)

Part of current research it was focused on the effects of changes in main unsaturated soil properties on the stability of slopes. To do so, the effect of unsaturated soil properties (such as properties of soil water characteristic curve, SWCC) on the distribution of suction in the slope, the shape of the failure surface, failure time, and rainfall intensity-duration threshold were investigated. As the properties of SWCC, author considered SWCC of Edosaki sand from Gallage and Uchimira (2010) and generated SWCCs with

different air entry values (AEV – suction corresponding to the border of saturated and unsaturated states of the soil), saturated volumetric water contents (θ_s), de-saturation rates (DSR – defined as the rate of change of volumetric water content, θ , with matric suction, ψ , i.e. $-d\theta/d\log\psi$ and residual volumetric water contents (θ_r) (Fig. 3.12). These soils, then, were used in a 2D numerical model that was defined in GeoStudio 2007 software package (SEEP/W and SLOPE/W). The numerical model is first validated by predicting the triggering rainfall-intensity duration for a well-instrumented laboratory slope model test on Edosaki sand by Gallage and Uchimura, 2010 (Ahmadi-adli et al., 2012). Suction distribution in the slope, the shape of the slip surface, time to failure and slope instability triggering rainfall intensity-duration threshold were investigated by performing staged seepage (equalization and raining) analysis followed by limit equilibrium slope stability calculations.

Although this general topic had been studied in the literature, the novelties in this study was (i) modeling seepage and slope stability numerically without the assumption of infinite slope, considering the equalization and rainfall stages using the drying and wetting unsaturated properties of the soils separately; (ii) characterizing SWCC through independent physical soil properties, rather than curve fitting parameters.

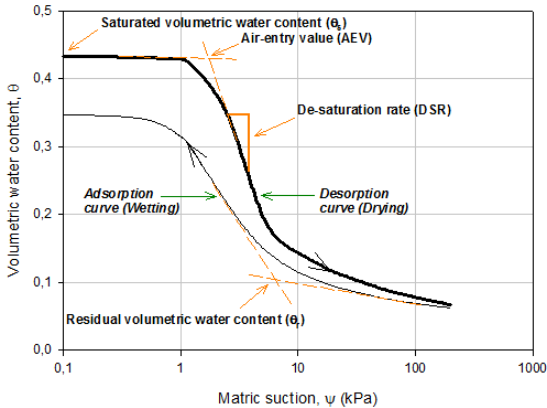


Fig. 3.12. Drying and wetting soil-water characteristic curve and its characteristic parameters

3.2.1. Numerical model

A numerical model is defined and calibrated with the well-instrumented experimental study documented by Gallage and Uchimura (2010).

3.2.1.1. Geometry and material properties

The laboratory flume model of Gallage and Uchimura (2010) consisted of a 0.7-m-high, 0.80-m-wide, 45-degree slope constructed in a 2-m-long flume box (Fig. 3.13). Reviewing literature showed that typical laboratory flume setups for studying slope stability are in the ranges of 0.5 to 1.0 m width and 2 to 3 m length. Therefore, dimensions of numerical model in this study are selected such that it would be possible to verify the results by laboratory scale model tests.

Edosaki sand (from a natural slope in Ibaraki prefecture in Japan) had been used by Gallage and Uchimura (2010) as testing material in the laboratory flume model. It is classified as silty sand (SM) according to Unified Soil Classification System. The specific gravity of solids and maximum and minimum void ratios of the soil were reported as 2.75, 1.59, and 1.01, respectively, by Gallage and Uchimura (2010).

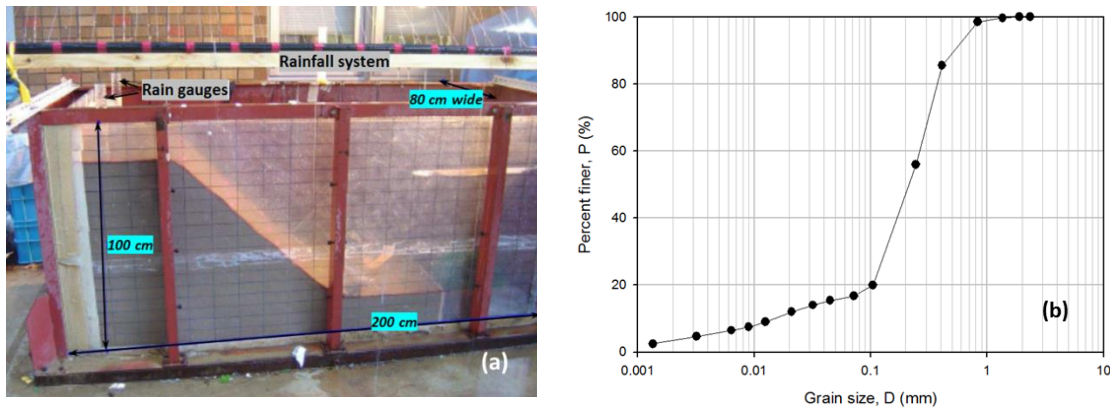


Fig. 3.13. (a) Laboratory flume setup used by Gallage & Uchimura (2010) and (b) grain size distribution of Edosaki sand (data from Gallage & Uchimura, 2010)

Fig. 3.14(a) includes drying and wetting soil water characteristic data for Edosaki sand which had been obtained using Tempe Pressure Cell method for a sample of the same dry density as that in the flume, 1.22 g/cm^3 (Gallage and Uchimura, 2010). Appropriate curves had been fitted to these data using the equation proposed by Fredlund and Xing (1994). In addition, drying hydraulic conductivity of this soil had been measured as a function of suction by using a Permeameter by Gallage and Uchimura (2010) and Gallage et al. (2013). Wetting hydraulic conductivity for Edosaki sand had not been measured. Therefore, we deduced it from measured drying hydraulic conductivity data

points through drying and wetting SWCCs, assuming there is a negligible hysteresis in HCF when plotted against volumetric water content (Fredlund and Rahardjo, 1993; Lu and Likos, 2004). In Fig. 3.14(b) HCF data for Edosaki sand are plotted with respect to

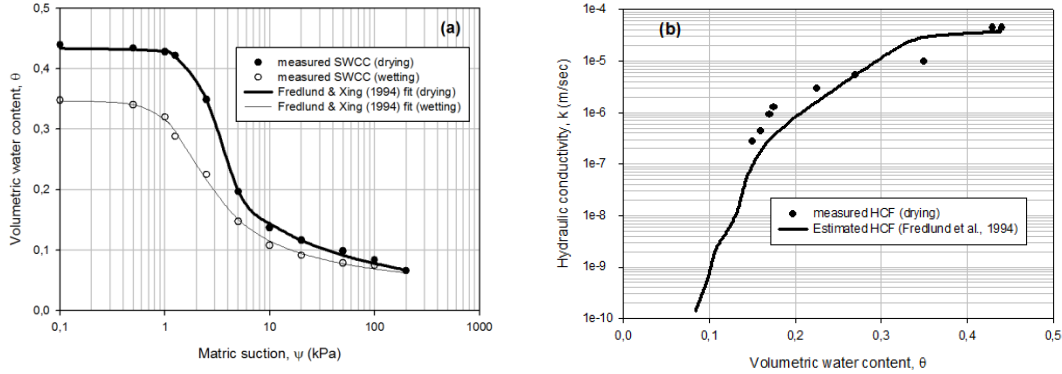


Fig. 3.14. (a) Soil-water characteristic curves and (b) hydraulic conductivity function (data from Gallage and Uchimura (2010) and Gallage et al. (2013)) (FX: Fredlund and Xing, 1994)

volumetric water content. These data are compared to some HCF predictions such as Fredlund et al. (1994). The method proposed by Fredlund et al. (1994) was found to predict hydraulic conductivity function for this material successfully.

In order to interpret shear strength of Edosaki sand in unsaturated state, independent stress state variable method proposed by Fredlund and Morgenstern (1977) is used. Based on this method, shear strength in unsaturated soils can be defined as,

$$\tau = c' + (\sigma_n - u_a) \tan \phi' + (u_a - u_w) \tan \phi^b \quad (3.1)$$

where τ denotes shear strength of unsaturated soil; c' is effective cohesion of saturated soil; ϕ' is internal friction angle; ϕ^b is angle of shearing resistance with respect to suction; σ_n is total normal stress on the plane of failure; u_a and u_w are pore air and water pressures, respectively, and $u_a - u_w$ is the matric suction of the soil in the failure plane. In this estimation, the relationship between τ and $u_a - u_w$ is assumed to be linear. Such a simplified strength model is deemed sufficient since the aim of current study was the investigation of changes specifically in SWCC on slope stability. Friction angle and shearing resistance angle with respect to suction are deduced by back analysis, matching

time of failure observed in the flume test under the assumption of $\phi^b = 0.5\phi'$ (proposed by SLOPE/W). Resulting values are $\phi' = 30.3^\circ$ and $\phi^b = 15.15^\circ$ (Ahmadi-adli et al., 2012).

3.2.1.2. Numerical Analyses

The numerical model is defined in GeoStudio 2007 software (SEEP/W and SLOPE/W) (Fig. 3.15(a)). SEEP/W can model both saturated and unsaturated flows and SLOPE/W can model stability of slopes considering variable pore-water pressure conditions using limit equilibrium method.

A seepage analysis is carried out in two time-dependent (transient) stages at SEEP/W. These stages were;

- **Equalization stage** which is a 30-day period of waiting, during which suction equilibration took place. Time period for this stage is selected so long to eliminate the effect of different drying hydraulic conductivities on equalization of suctions.
- **Rainfalling stage** during which rainfall is applied and slope stability analyses are carried out.

The pore water pressure distributions obtained for each time increment of seepage analysis are used in stability analyses to determine the factor of safety of the slope using SLOPE/W.

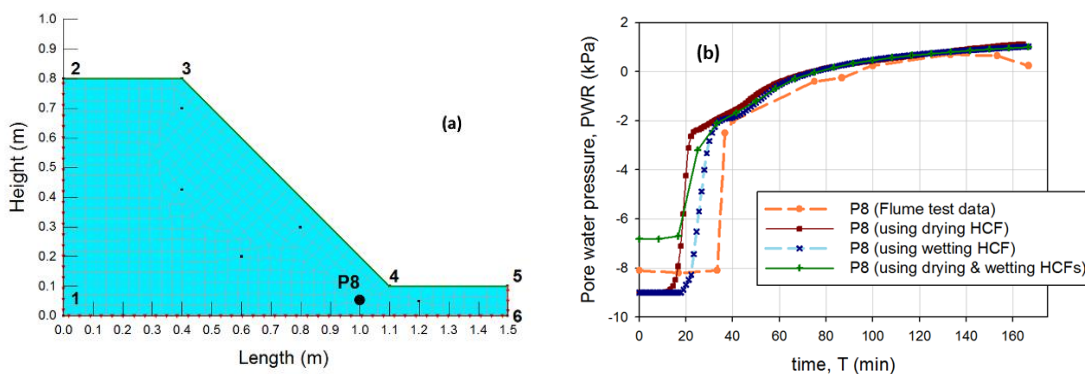


Fig. 3.15. (a) Numerical slope model defined in SEEP/W and SLOPE/W and (b) comparison of suction versus time after start of rainfall, for one of the selected points, P8, in the slope (Ahmadi-adli et al. 2012)

Finite element (FE) mesh shown in Fig. 3.15(a) is used in the numerical seepage analyses of the model. In this model, boundaries 1-2, 1-6 and 5-6 are considered as “no-

flow” boundaries as no water flow was allowed through these boundaries during laboratory flume test. During equalization stage no flow boundary is assigned to the 2-3, 3-4 and 4-5 sides, prohibiting evaporation and let the suction be balanced due to gravity alone. Then rainfall R_1 ($R_1 = 40$ mm/hr) is applied on boundaries 2-3 and 4-5, and rainfall R_2 ($R_2 = R_1 \times \cos 45^\circ$) is applied on boundary 3-4. The initial pore water pressure (before equalization stage) is assigned as 4.8 kPa suction which corresponds to volumetric water content of 0.2 as in the original test. After equalization stage, the values of suction are taken as the initial suction values for rainfall stage (see 3.2.2.2). For stability analyses, the pore water pressure obtained from numerical seepage analyses are used to determine the factor of safety of the slope. Bishop’s limit equilibrium method is applied.

In Fig. 3.15(b) calculated suction versus time values at an example point in the slope are shown together with the measured values in the flume experiment (Ahmadi-adli et al., 2012). Assessment of suction-time response of other points in the slope and landslide triggering rainfall intensity-duration (40 mm/hr) were successful. The results obtained from numerical model agree with the results obtained from experimental flume model. Therefore, the numerical model using SEEP/W and SLOPE/W can successfully model rainfall infiltration and consequent landslide occurrence in an unsaturated slope.

3.2.2. Parametric study

In this part of the study, SWCC is defined with four parameters: AEV (air entry value), θ_s (saturated volumetric water content), DSR (de-saturation rate) and θ_r (residual volumetric water content). Definitions of these parameters have been depicted schematically in Fig. 3.12. The parameters are used for qualitative definition and are different from the curve fitting parameters of the equations that describe SWCC in the literature. In the following sections the effect of changes in any of these parameters on suction distribution, failure surface, time to failure and I-D plots are explained.

3.2.2.1. Hypothetical soils

In order to study effect of changes in characteristics of SWCC, realistic hypothetical soils are assumed. SWCC of these soils are generated by changing one of the characteristic parameters (AEV, θ_s , DSR, θ_r) keeping others constant. These parameters relate to physical soil parameters e.g. grain size distribution, dry density, soil uniformity and fines content (Fig. 3.16). Using a built-in application in SEEP/W, corresponding HCFs for these soils (Fig. 3.17) are estimated based on method proposed by Fredlund et al. (1994) which requires the saturated hydraulic conductivity (K_s) as an additional input parameter.

AEV – The first set of soils focus on the effect of changes in air entry value of the soil which is a measure of its grain size. Four hypothetical SWCCs are generated from SWCC of Edosaki sand by multiplying all suction values of Edosaki sand (on the entire curve) with 0.5, 2.0, 4.0 and 6.0 (Fig. 3.16(a)). Air entry values for these soils are then their respective multiples of the AEV of Edosaki sand (1.75 kPa) resulting in AEV values ranging from 0.88 to 10.5 kPa. Saturated hydraulic conductivity is assumed to be proportional to the square of particle or pore size, based on pipe flow equations and correlation by Hazen (1930). Particle or pore sizes are assumed to be inversely proportional to AEV, based on capillary tube analogy as well as correlations by Sjoblom (2000) and Toker (2002). Hence the original K_s value is multiplied by 4, 1/4, 1/16 and 1/36 for respective AEV values.

θ_s – Fig. 3.16(b) shows some SWCCs with different saturated volumetric water contents. To obtain these SWCCs, saturated volumetric water content of soils is varied by increments/decrements of 0.04, and θ_s values in the range of 0.36 to 0.52 are obtained. Physical interpretation of this action is increasing and decreasing dry density of hypothetical soil. For example, soil with a higher θ_s value is a looser soil. Saturated hydraulic conductivity of these newly generated soils, to be used as an input in HCF estimation at SEEP/W, are deduced from permeability of Edosaki sand considering density of each hypothetical soil. Flow equation and volume mass relations are used to derive a relation between K_s and volumetric water content (Fig. 3.17(b)).

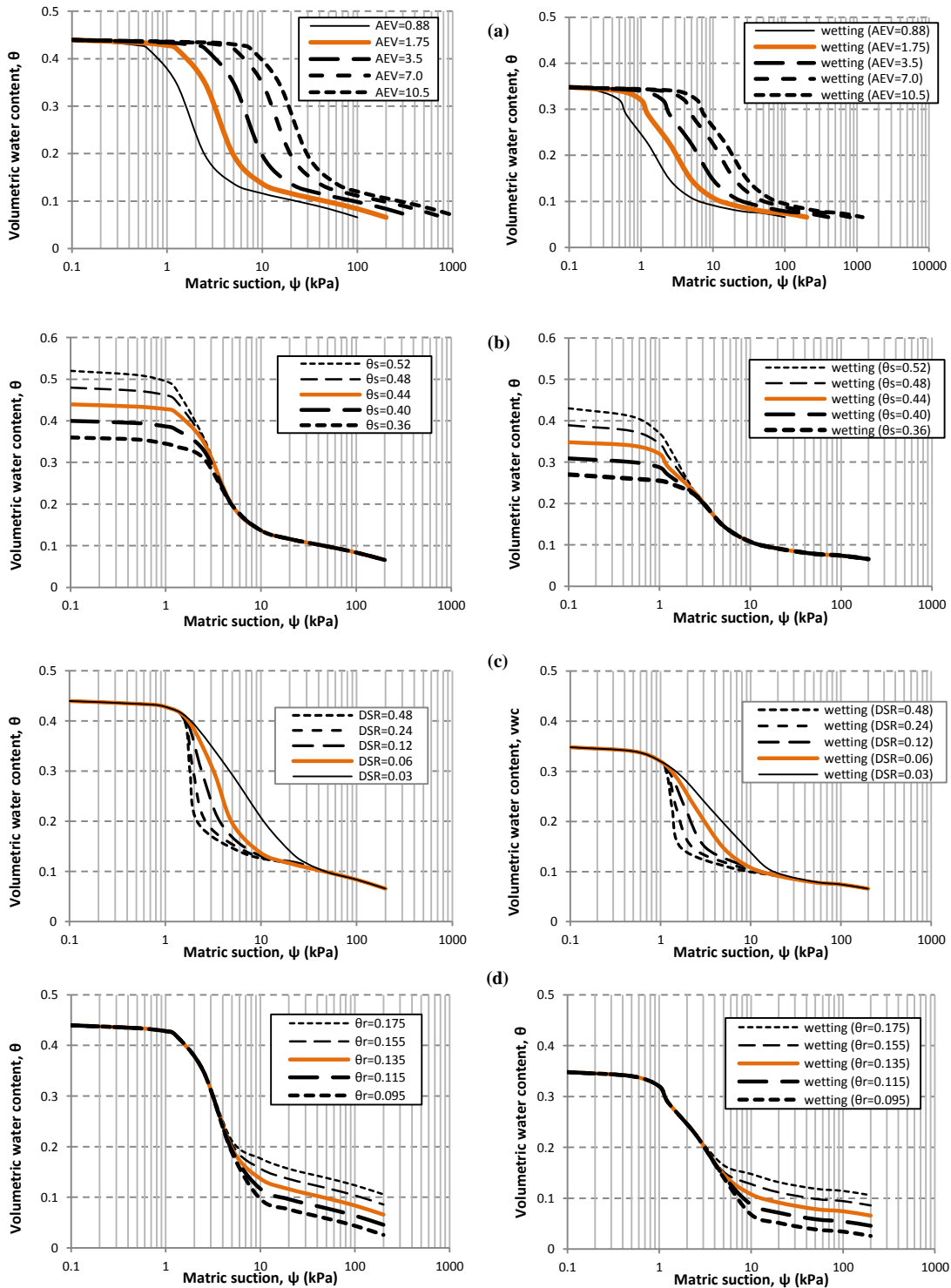


Fig. 3.16. Drying (left) / wetting (right) SWCCs for hypothetical soils with different (a) AEV, (b) θ_s , (c) DSR and (d) θ_r values. SWCC of Edosaki sand is shown by the solid bold line

DSR – To obtain soils with different rates of desaturation, DSR of Edosaki sand (0.06) is multiplied by 0.5, 2.0, 4.0 and 8.0. Higher DSRs represent soils with more uniform grain size distribution curves (Fig. 3.16(c)). HCF of these soils can be seen in Fig. 3.17(c). It was assumed that changes in DSR of a soil have no significant effect on its K_s .

θ_r – As finer portion of a soil increases, amount of remaining volumetric water content at high suctions (residual) increases. Soils with increased and decreased residual water content are generated from original SWCC data set of Edosaki sand. To do so volumetric water contents of data set at residual tail (part of SWCC with suction higher than 10 kPa) are increased and decreased by 0.02 (Fig. 3.16(d)). Fig. 3.17(d) shows corresponding HCF of these soils.

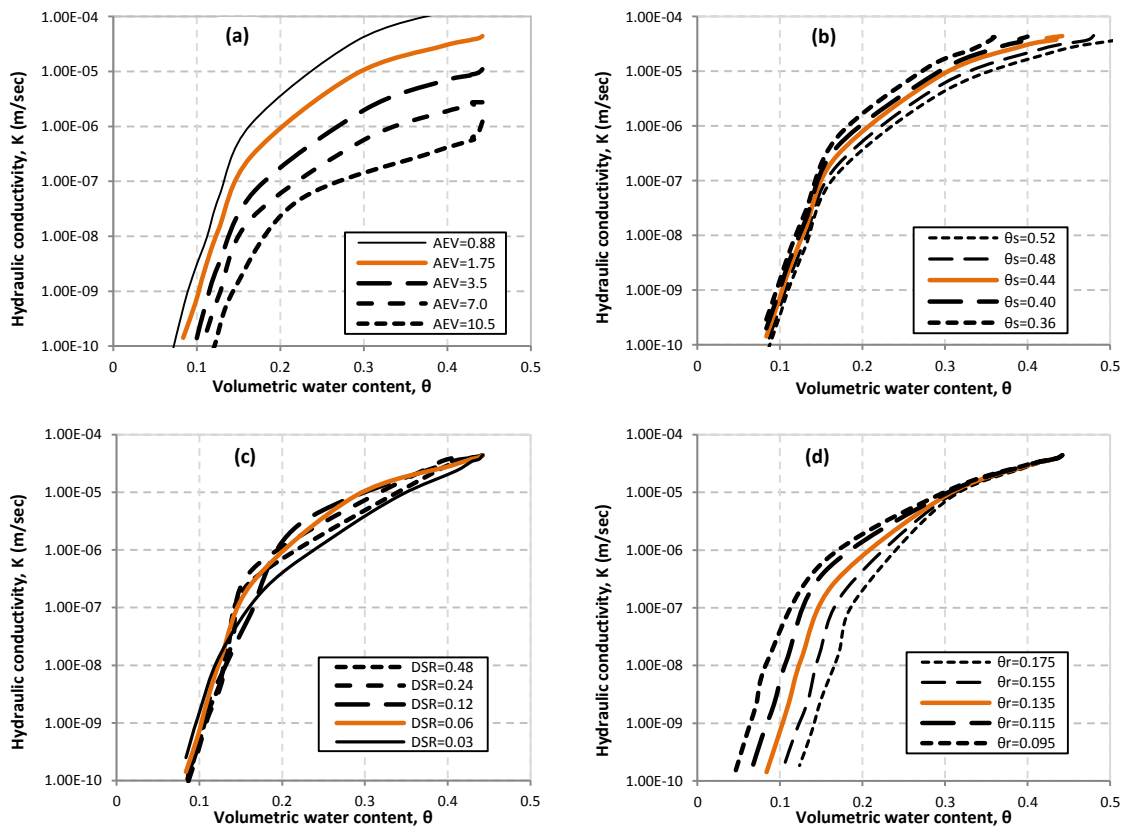


Fig. 3.17. Estimated HCFs corresponding to SWCC of hypothetical soils with different (a) AEV, (b) θ_s , (c) DSR and (d) θ_r values. HCF of Edosaki sand is shown by the solid line

3.2.2.2. Seepage and stability analyses

By using unsaturated properties (SWCC & HCF) of hypothetical soils seepage and stability analyses of the model are performed under the intensity of 40 mm/hr rainfall. Pore water pressures and slip surfaces calculated at the time of failure (FS=1.0) are demonstrated in Fig. 3.18.

Before starting to study the effects of changes in SWCC of the soils, in order to decide on initial pore water pressure in any of the numerical models, preliminary analyses were carried out on a single model with different initial water contents. The results showed that initial suction in the soil body can significantly affect behavior of slope. In all of the cases with different initial suctions, failure modes are observed to be very similar (at the time of failure). Higher initial suctions postpone failure and lower initial suctions make slopes eligible to fail sooner. On the other hand, assuming constant initial suctions for all models (models with different SWCCs) causes different initial water contents. Therefore, in different models, we decided to assume constant water content instead of constant suctions at the initial state. Consequently, in all analyses initial suction is set to correspond to 0.20 volumetric water content except the analyses set for θ_r for which θ_0 was 0.13. In this way, in the models with finer soil type (e.g. higher AEVs), initial suctions (onset of analyses) are set to higher values.

AEV – After analysis of the set of models with different AEVs, we observed that pore water pressure values within the soil vary from -26 to +2 kPa for different soil types. Suctions remains high in the depths of slopes with finer soil types while it is reduced only at the surface, even after a period of rainfall long enough to reach failure. This is because lower hydraulic conductivity at high suctions prevents infiltration more than a few centimeters beyond the surface. Therefore, only shallow failures occur in slopes composed of finer material.

θ_s – Soils with higher θ_s values represent looser soils. However, this does not significantly change suction distribution and failure surface at the time of failure for the slopes composed of these soils. Numerical analyses show that for denser soils (lower θ_s) water table at the time of failure is deeper (Fig. 3.19) and slip surface is slightly shallower. However, this analysis does not consider increase in ϕ due to greater density.

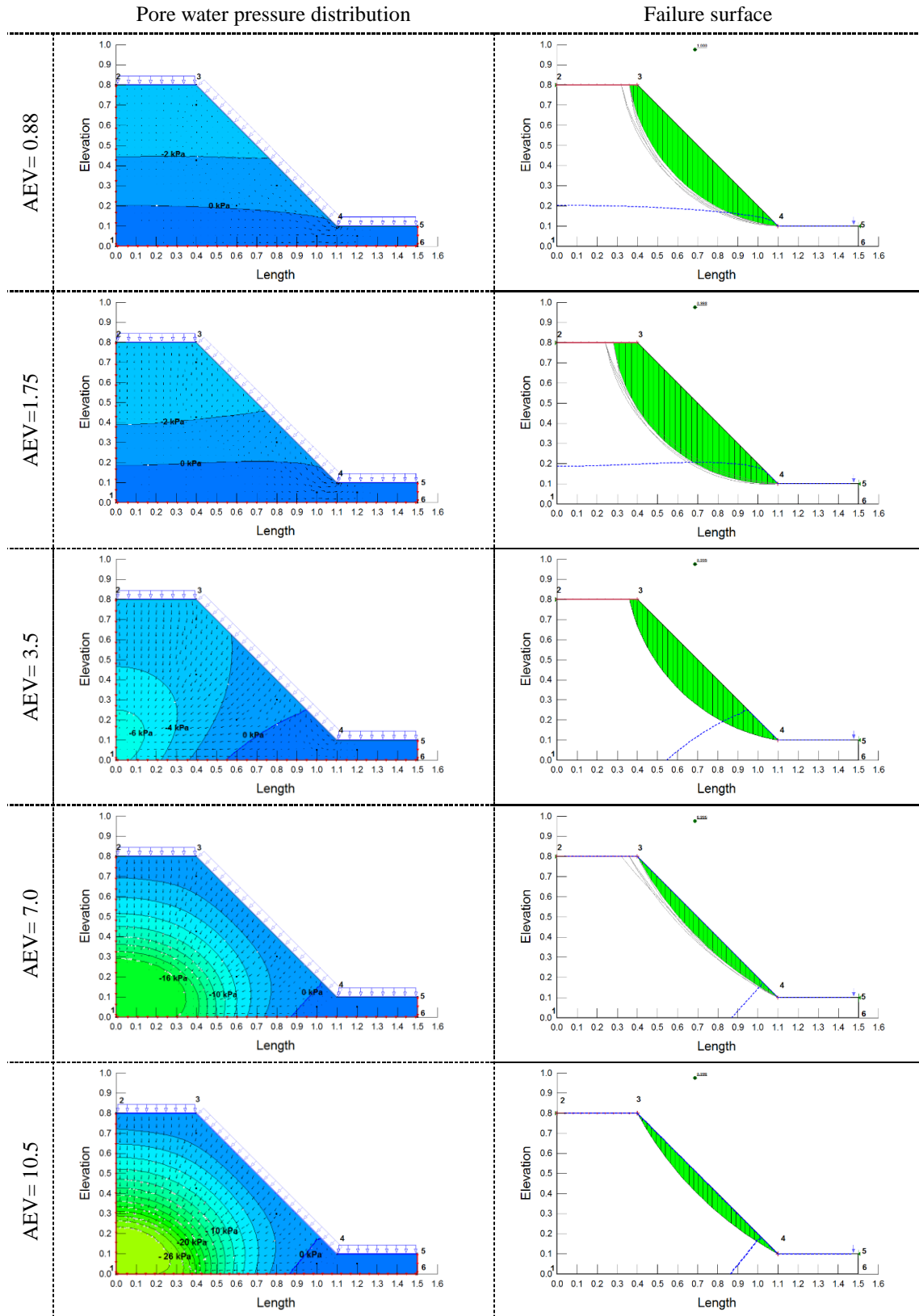


Fig. 3.18. Pore water pressure distribution and failure mode of slopes composed of hypothetical soils with different AEVs

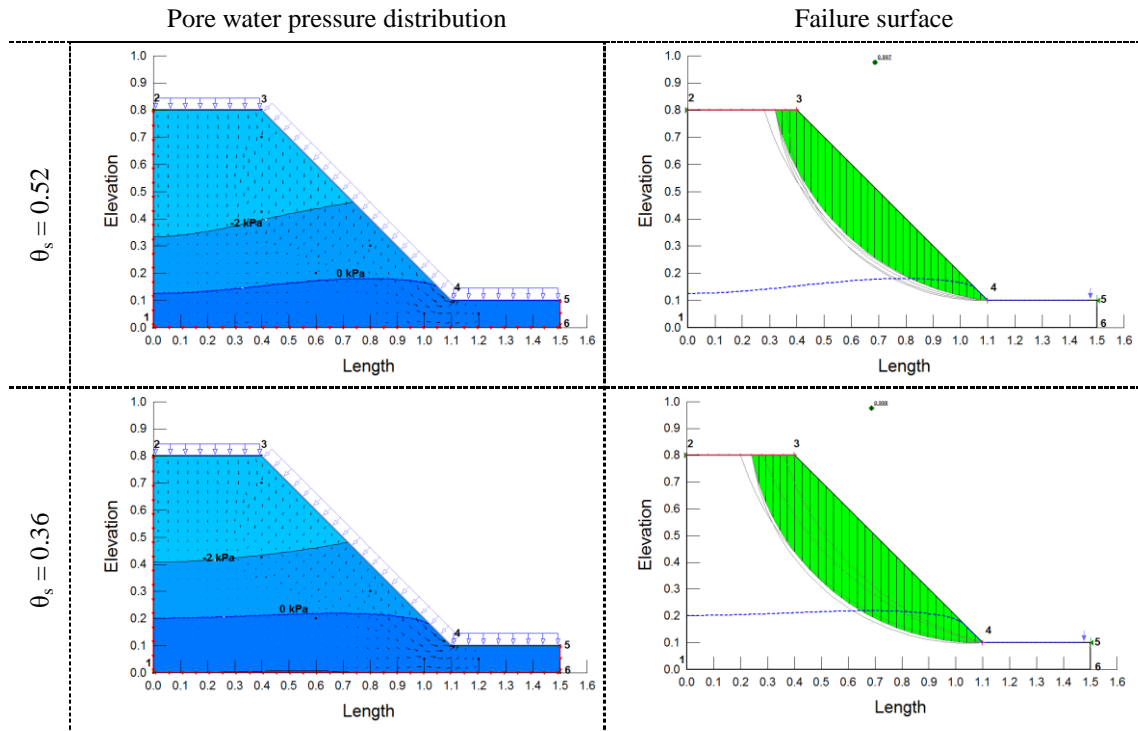


Fig. 3.19. Pore water pressure and failure mode of slopes composed of hypothetical soils with highest and lowest θ_s values

DSR – Desaturation rate is mostly controlled by uniformity of the soil. Pore water pressure distribution for highest and lowest DSR values, 0.48 and 0.03, respectively, are demonstrated in Fig. 3.20. In non-uniform soils (lower DSR) due to higher initial suction values and consequently lower hydraulic conductivities, less infiltration occurs. Because of this a lower level of water table at the time of failure is observed. It also causes later failures.

θ_r – Changes in fine content causes significant changes in the shape of SWCC but this does not affect suction distribution in the slope of this soil. Suction distribution and the shape of slip surface in slopes with soils of different θ_r values are very similar to that of Edosaki sand (Fig. 3.21). Water tables at the time of failure in these analyses are very similar despite the differences in θ_r . However differences would arise if the initial water contents were smaller.

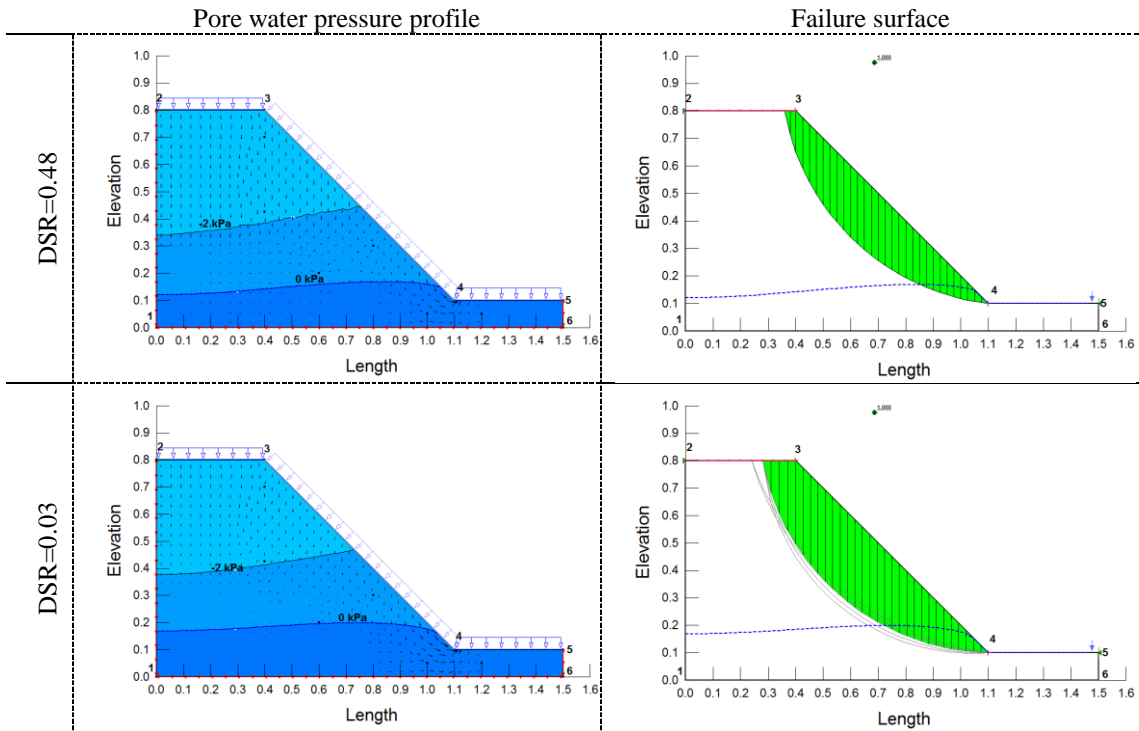


Fig. 3.20. Pore water pressure and failure mode of slopes composed of hypothetical soils with highest and lowest DSR values

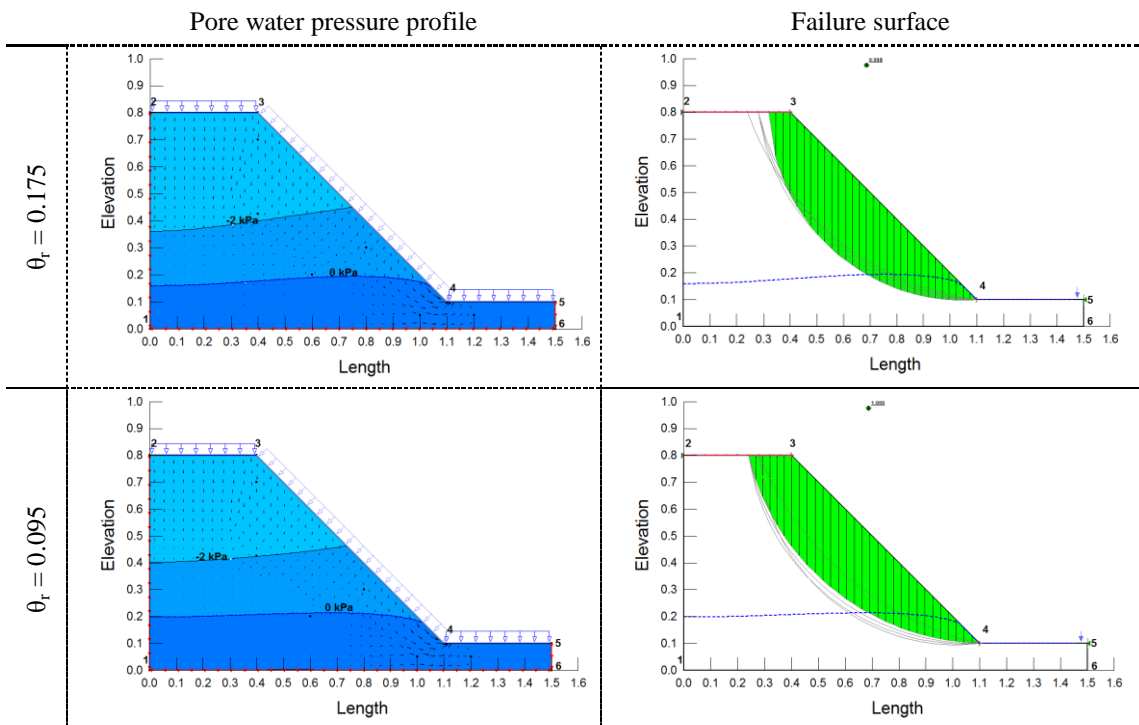


Fig. 3.21. Pore water pressure and failure mode of slopes composed of hypothetical soils with highest and smallest θ_r values

Required time after rainfall initiation till failure is also a critical parameter in the core of early warning systems. In this study the effect of changes in SWCC on “time to failure” is investigated for the hypothetical soils (Fig. 3.22). Summary of results are;

- Slopes consisting of finer soils fail later due to lower hydraulic conductivity. Difference in the time to failure for AEV between 0.88 to 7.0 kPa soils is very small.
- The time required to failure in slopes with denser soil is shorter because there are less voids to saturate.
- Uniform soils fail earlier due to greater infiltration and faster rise of water table.
- Slopes of soils with different fine content need a similar rainfall duration to reach failure as long as the initial θ is constant.

3.2.2.3. Rainfall intensity-duration (I-D) thresholds

Intensity and duration are primary rainfall properties controlling the infiltration into a slope and instability. Rainfall intensity-duration threshold that triggers a landslide is a unique relationship for a slope. In Fig. 3.23 the effect of different rainfall intensities on factor of safety of a slope is demonstrated. Higher rainfall intensities cause a sharp drop in F.S. and a short duration of this rainfall is sufficient to cause failure. However, a rainfall with very small intensity might not cause failure even if it rains for a prolonged duration. Performing a number of numerical analyses with different rainfall intensity-duration combinations makes it possible to obtain a rainfall threshold that triggers a landslide on a particular slope. Fig. 3.24 shows rainfall I-D thresholds for different FS values for the generic slope model of Edosaki sand, with safe and unsafe zones labeled as such. We can also see I-D lines for different factors of safety.

I-D thresholds for different hypothetical soils and the effect of SWCC characteristics are shown in Fig. 3.25. Changes in AEV (i.e. grain size) of a soil appear to have a significant effect on I-D threshold that triggers a landslide. For a given rainfall intensity, longer duration is required to fail a slope composed of finer soil in comparison to a slope composed of coarser soil. As the soil gets finer, the difference between the durations required to trigger a landslide for high-intensity and low-intensity rainfalls decreases (i.e. the slope of the I-D threshold line on log-log plot increases). In other words, a high-

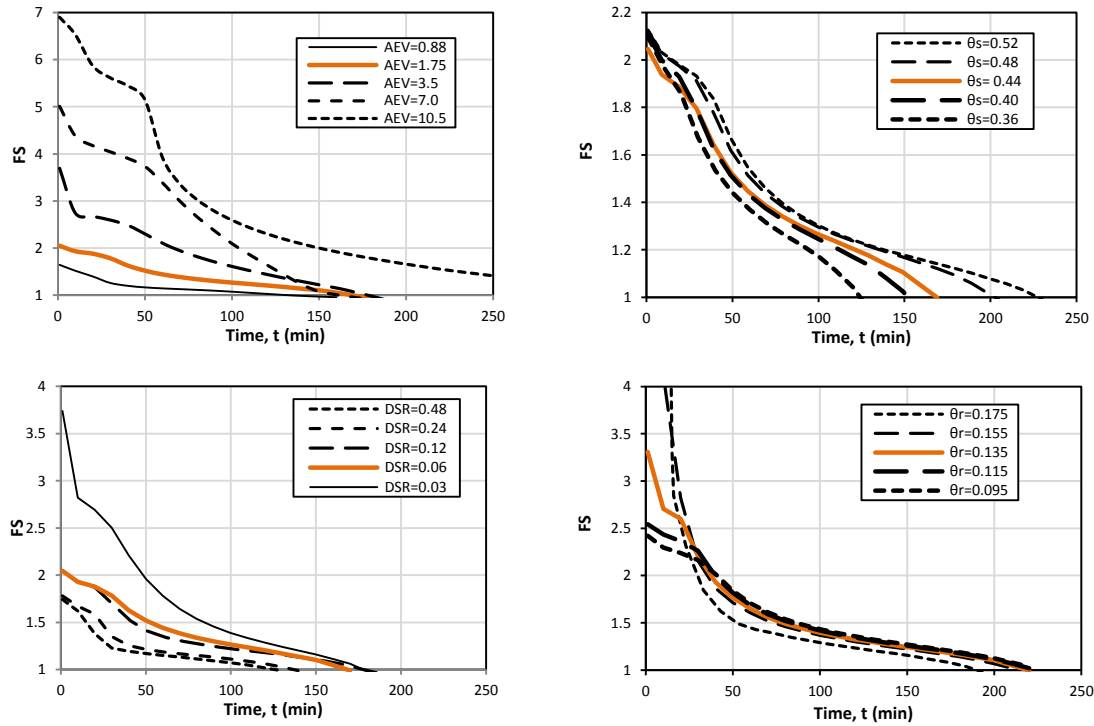


Fig. 3.22. Decrease of factor of safety in the slopes with soils of different AEV, θ_s , DSR and θ_r values. Time zero is the time rainfall starts, and rainfall is applied till failure

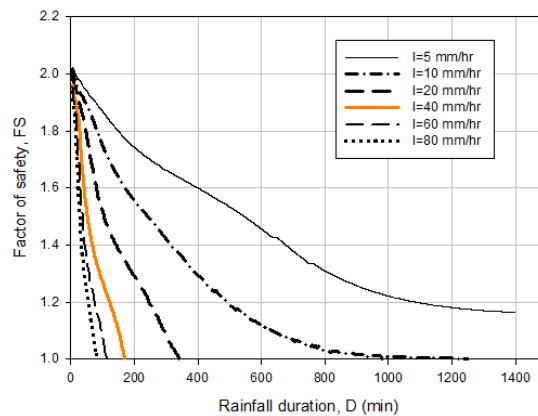


Fig. 3.23. Changes in factor of safety of slope made up of Edosaki sand under different rainfall intensities

intensity rainfall may trigger a landslide in a coarser soil in shorter duration in comparison to a finer soil. On the other hand, a low-intensity rainfall triggers landslides in both coarser and finer soils in similar durations. The exception to this is if the soil is very coarse, then failure is unreachable with a rainfall that has a low intensity since the

water can freely be drained through the soil by gravity, never increasing the degree of saturation.

As the saturated volumetric water content, θ_s , of the soil changes (i.e. dry density), the durations on the I-D threshold change but its inclination remains constant. For a given rainfall duration, for greater θ_s (looser soil) higher intensity rainfalls are needed to make the slope fail. In other words, for a given rainfall intensity, longer duration rainfall is needed to cause failure as the soil gets denser. It must be noted that at lower intensities no significant difference is observed for different values of θ_s .

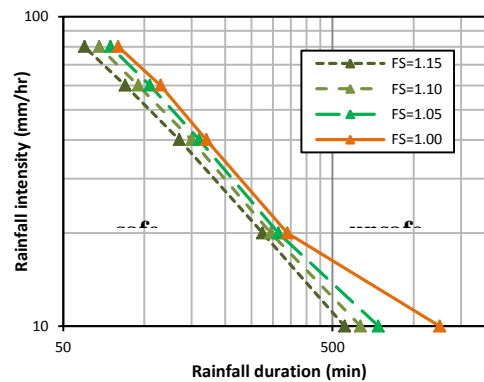


Fig. 3.24. Rainfall intensity-duration plot for slope composed of Edosaki sand with different factor of safety values

Increasing of desaturation rate, DSR, (i.e. uniformity) can also affect I-D plot. Slopes of soils with more uniform particle size distribution (higher DSR) tend to fail in shorter time for a given rainfall intensity. This is probably because a greater amount of water infiltrates the uniform soils faster and consequently suction is reduced sooner, reducing shear strength. In soils with non-uniform particle size distribution (low DSR) there seems to be no significant changes in stability due to DSR changes.

Value of θ_r (i.e. fine content) also affect I-D threshold offset slightly. Soils composed of higher percent of fine particles may fail in shorter time while soils of less fine content do not tend to fail at low rainfall intensities. Fig. 3.25(d) shows that at low rainfall intensities (less than 20 mm/hr) no failure (data point) has been observed in slopes of soils with less fine content (low θ_r value).

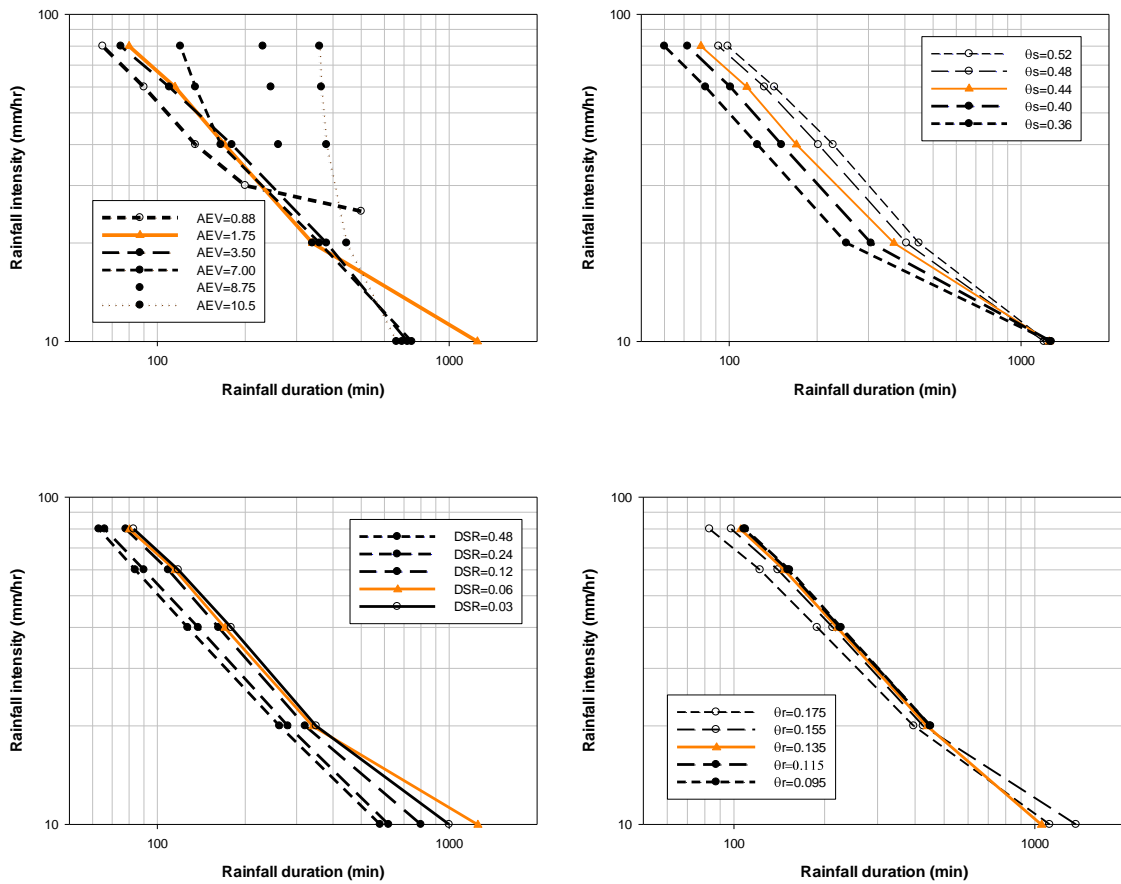


Fig. 3.25. I-D thresholds for soils of different AEV, θ_s , DSR and θ_r values

3.2.2.4. Conclusions and remarks

Understanding the effects of wetting/drying SWCC and HCF on I-D thresholds is a necessary first-step towards an integrated early warning system for rainfall triggered landslides that considers the physical mechanism of the problem and natural variability of soils. To the author's knowledge, the conclusions below have not been explicitly discussed in the literature.

1. The intensity-duration threshold that triggers a landslide can be computed successfully given that the unsaturated hydraulic and shear strength properties of the soil are known. It is discovered that for such an accurate prediction, it is necessary to perform separate analyses for different stages (evaporation/equalization and rainfall)

using their corresponding unsaturated soil properties (drying and wetting respectively).

2. This study shows that unsaturated soil properties such as SWCC and HCF play a critical role in the behavior of unsaturated slopes. Current study has focused on the effects of changes in controlling parameters of SWCC, namely the air entry value (AEV), saturated water content (θ_s), de-saturation rate (DSR) and residual water content (θ_r).
 - a) In coarse-grained soils, for a given rainfall intensity, as the particle size gets smaller (i.e. AEV gets larger) time to failure becomes longer due to the existence of higher suctions and slower infiltration. In other words longer duration of rainfall is needed to cause failure, and shallower slip surfaces are expected.
 - b) It is observed that θ_s (the density of the soil) does not significantly change the failure surface and suction distribution at the time of failure. For a given rainfall intensity, a looser soil (with larger θ_s) requires slightly longer duration rainfalls to cause the slope to fail. However, this effect will probably be countered by increased friction angle in denser soils.
 - c) In soils with uniform particle size distribution (i.e. greater DSR) infiltration occurs more quickly and failure occurs in shorter time as compared to a soil with lower DSR.
 - d) Changes in θ_r (i.e. fines content) cause significant changes in the shape of SWCC but this does not affect suction distribution at the time of failure, unless the slope is initially very dry. θ_r also offsets the I-D threshold slightly without changing its inclination.
3. The change of FS with time due to rainfall in unsaturated slopes can be computed successfully by numerical methods with physical basis. The rate of decrease of FS with time is different for different soils and this rate changes with time for a given soil.
4. Both “high intensity short duration” rainfalls and “low intensity long duration” rainfalls can cause landslides in unsaturated soils, as characterised by I-D thresholds.

- a) Based on the analyses carried out in this study for rainfall intensities between 10-100 mm/hr it is observed that I-D threshold that triggers a landslide is nonlinear in log-log plot.
- b) For very low intensity rainfalls (less than 20 mm/hr) no matter how long rainfall occurs it does not cause a landslide. This is because the soil is able to exfiltrate all the rainfall that infiltrates.
- c) As the soil gets finer, the difference between the durations required to trigger a landslide for high-intensity and low-intensity rainfalls decreases (i.e. the slope of the I-D threshold line on a log-log plot increases). In other words, a high-intensity rainfall may trigger a landslide in a coarser soil in shorter duration in comparison to a finer soil.
- d) For finer grained soils, time to failure is independent of rainfall intensity above a certain level. This is because above that certain intensity, only surface runoff increases and infiltration into the soil does not change.

CHAPTER 4

MATERIAL, EQUIPMENT AND PROCEDURES

This chapter explains detail of all experimental activities in the thesis. It reveals detail of the procedures for deterministic tests of the material used throughout current thesis, explanation of the employed apparatuses and detail of calibration (if any) and narration of the procedures for index tests, flume tests and laminar box tests.

4.1. Material properties and index tests

Different soils were checked in current research to select the right material. Soil material to be used in this thesis is selected as uniformly graded fine sand that is factory-made crushed quartz (Fig. 4.1). This material was purchased specially for current research from POMZAEXPORT Mine Industries & Trade Company. The material is named as “Quartz Sand” and will be called as QS throughout this dissertation.

Some index tests were performed on this soil to determine basic geotechnical properties such as Grain size distribution (ASTM D422), Specific gravity of soils (ASTM D854), Minimum/maximum void ratio of soils in dry state (ASTM D4253) and permeability (ASTM D2434). Results of these tests are summarized in table 6.1.

Obtaining the minimum dry density of the material in wet state was necessary for the flume tests considering soil material are placed in the flume/laminar box with slight moisture. The reasons were first, ability to control dry density of the soil in sample preparation, and second, applying soil suction of almost 15-20 kPa as initial suction into the prepared sample (which corresponds to 1.5% water content in SWCC, see section 6.1.1). Therefore, as an unconventional procedure, it was assessed by trial and error by pouring soil with 1.5% humidity in cubes of 20×20×20cm and checking dry density.

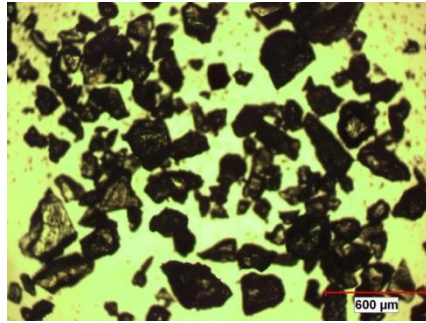


Fig. 4.1. Microscopic view of the grains in QS soil

As a restrictive limit for the lowest dry density of the wet soils which would be placed in the flume, potential for volume change of the prepared soil samples due to wetting (hydro compression) in lowest dry densities were considered. To do so, four samples of moist soil (1.5% moisture content) were compacted in 20×20×20cm cubes of Plexiglas (Fig. 4.2) with different dry densities. The samples were subjected to the rainfall



Fig. 4.2. Cubic samples subjected to rainfall to obtain minimum dry density with no volume change under rainfall, (a) & (b) before and (c) & (d) after applying rainfall

intensity of 55 mm/hr for 10 minutes and then volume changes (settlement at the sample surface) were measured in them. Obtained results are presented in section 6.1.

4.1.1. Assessment of Soil Water Characteristic Curve (SWCC)

Drying SWCC of the QS soil was assessed using proposed methods by ASTM D6836 (hanging column and pressure methods) and for wetting SWCCs (at different dry densities) capillary tube method were used. These test setups were designed by the author and constructed by FORE Testing Equipment Industries in METU geotechnical laboratory.

4.1.1.1. Hanging Column

Hanging column setup at METU geotechnical laboratory was able to obtain suction-gravimetric water content relation in the range of 0-60 kPa. The schematic and photos from the manufactured setup are shown in Fig. 4.3. The mechanism of the setup is applying (increasing) suction ($u_a - u_w$) to the soil specimens by decreasing pore water pressure (u_w) and obtaining water content corresponding to the applied suction.

Specimens are prepared in required density from moist soil compressed in sampling ring made of stainless steel with 1.0cm height and 4.0cm inner diameter. Specimens are then placed on the pressure plate and rotated quarter of a turn and pushed on the plate. After placement, saturation of the specimens is performed by leaving them submerged for at least 24hrs (Fig. 4.4).

Before starting suction application, water for saturation of samples is drained manually. Then, by applying initial suction step, remaining water on the disc (at the edge of the sampling ring and in the corners of the plate) drains. Stabilization of water drainage discharge may take more than one day at the initial suction step. After stabilization, one (or two) specimens are removed to obtain their water content and suction is increased to the next level. This cycle is repeated till highest planned suction value. Applied suction values and the final water content of each specimen (i.e. at each suction level) results in a point on the SWCC of the soil.

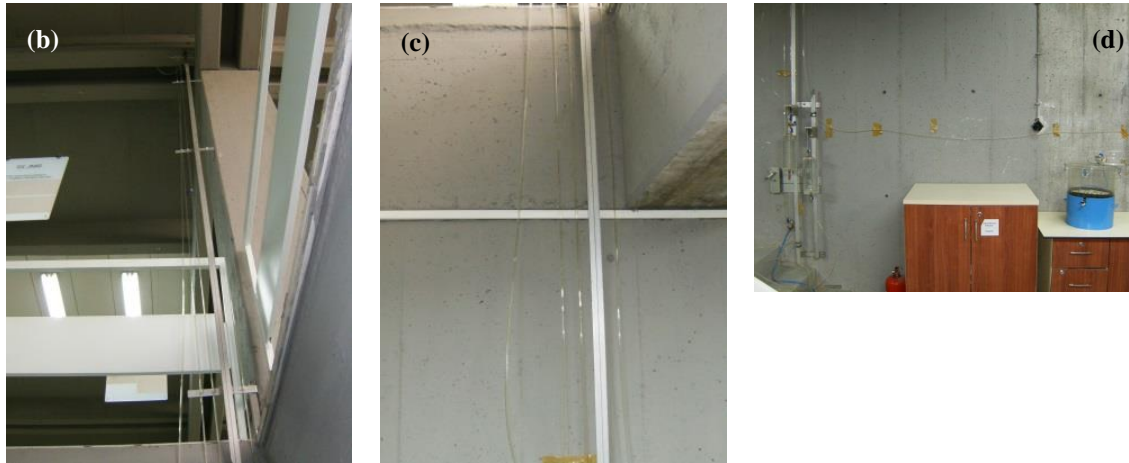
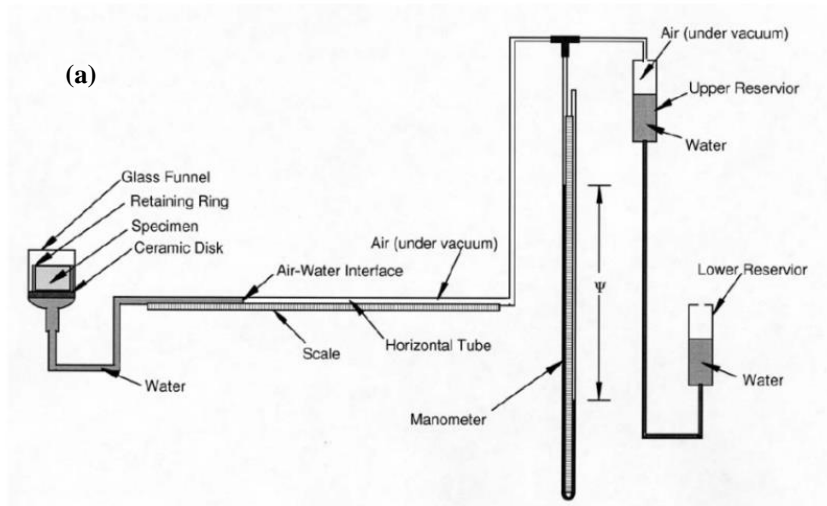


Fig. 4.3. (a), (b), (c) and (d) Hanging column setup designed, manufactured and mounted in METU geotechnical laboratory

4.1.1.2. Pressure plate extractor

To obtain water retention of QS soil at higher suctions in the range of 50-1000 kPa, pressure plate setup was used. Sketch and more detailed view of constructed setup are shown in Fig. 4.5. The only difference between hanging column and pressure chamber setups is in the method for application of suction. In pressure chamber setup suction ($u_a - u_w$) is applied (increased) by increasing pore air pressure (u_a).

Preparation and saturation of the specimens to be tested in pressure chamber and hanging column is the same. Suction must be applied in steps and a specimen must be retrieved for water content measurement the end of each step. A small difference in testing procedure is; in hanging column setup, there is no need for suction removal at the

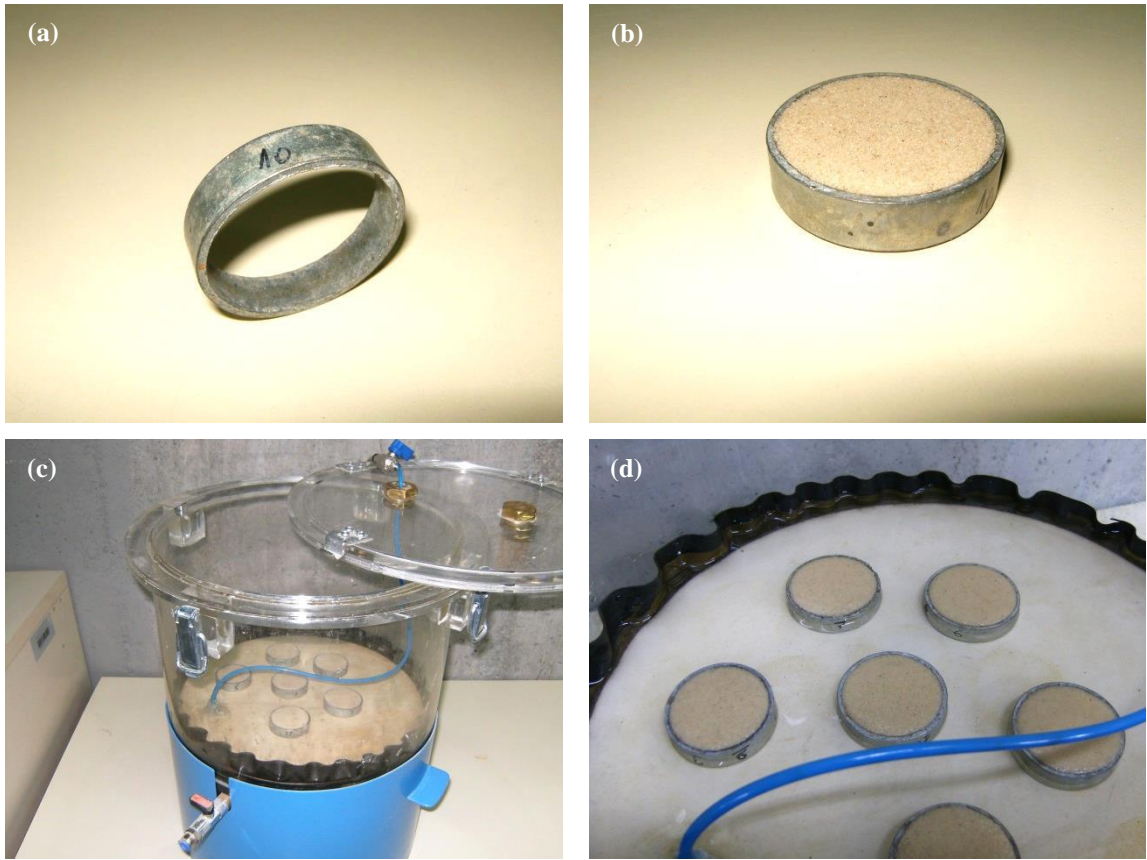


Fig. 4.4. Specimen preparation for hanging column setup (a) Sampling ring, (b) prepared sample in the ring, (c) placed samples on the pressure plate and (d) submerged samples left for saturation.

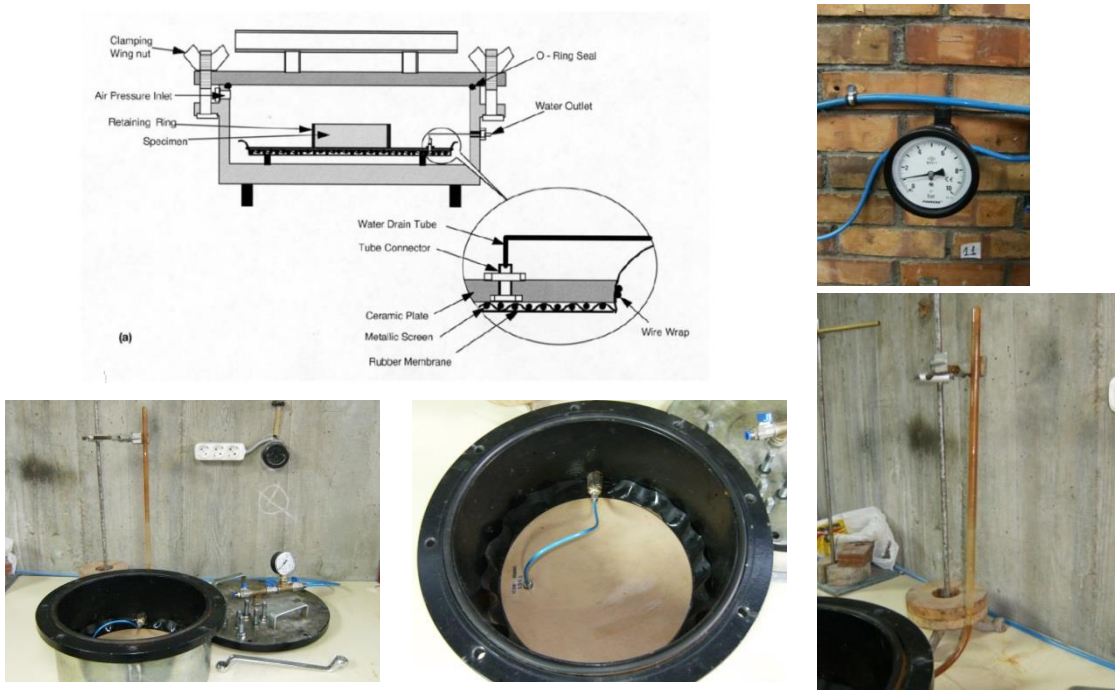


Fig. 4.5. Pressure plate setup at METU geotechnical laboratory

end of each stage for taking water content sample, whereas in pressure chamber method pore air pressure (and consequently suction) must be removed before opening the chamber. Fig. 4.6 shows soil specimens in pressure chamber setup.

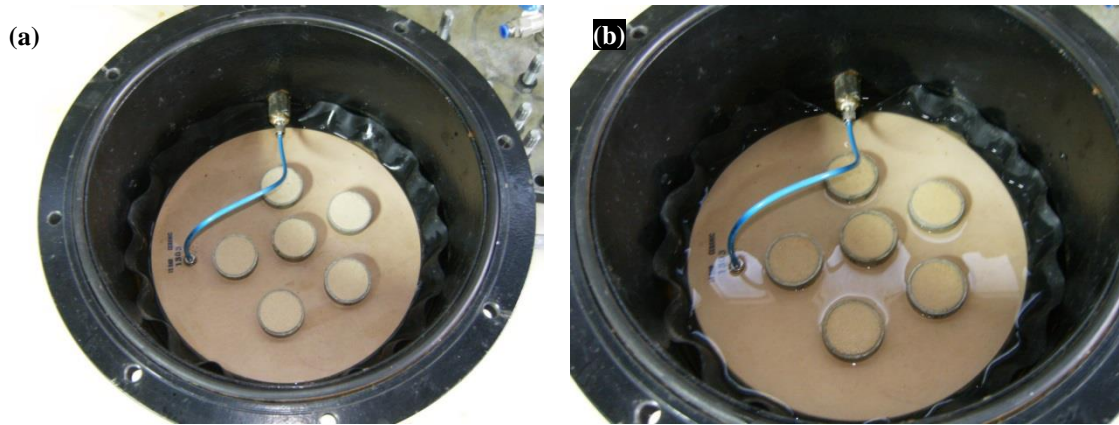


Fig. 4.6. Samples in pressure chamber setup, (a) placed and (b) submerged

4.1.1.3. Capillary Column

To obtain wetting SWCC of the QS soil, a column of soil was used to simulate capillary rise phenomenon, which is a wetting process. Fig. 4.7 includes detailed sketch and some figures from the manufactured setup for this purpose.

To prepare sample for this test, capillary column segments is filled with QS soil in desired dry density and then mounted to form vertical capillary tube (Fig. 4.8). Then the lower opening of the composed tube is left in the water (inside container). Because of generated suction due to capillarity, water moves upward. Because of difference in hydraulic head (and matric suction) water in different segments is different when equilibrium is established. After equalization of the system (water movement) the tube was dismantled and the water content at each of the segments was determined.

Obtained results for SWCC of QS soil at different dry densities are presented in 6.1.1.

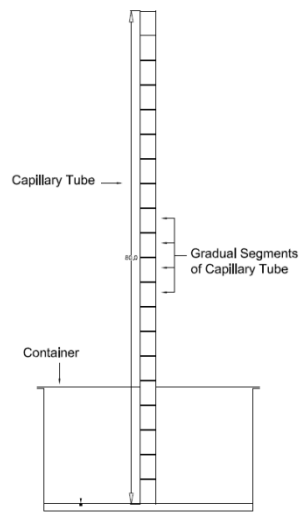


Fig. 4.7. Capillary tube setup

4.1.2. Hydraulic Conductivity Function Assessment

Properties of water transition throughout the QS soil samples were assessed using infiltration column method (ASTM D7664). To have an apparatus with capability to do infiltration tests in granular soils (methods A & B in ASTM D7664) an infiltration

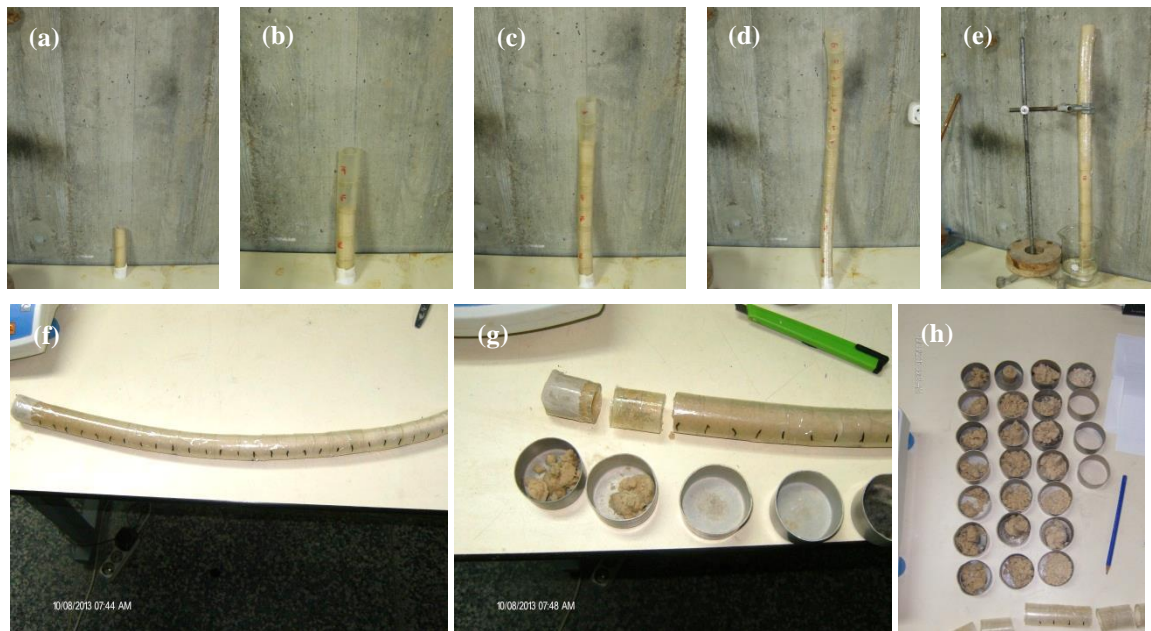


Fig. 4.8. Test in Capillary tube (a, b, c & d) specimen placement in the tube segments, (e) mounted tube, (f) moved water in the column due capillarity and (g & h) water content specimens.

column setup was designed by the author and manufactured by FORE Testing Equipment Industries.

Infiltration column setup at METU geotechnical laboratory was able to handle changes in suction values due to water transition through sample. The schematic diagram and detailed photos of the manufactured setup are shown in Fig. 4.9. It consists of a transparent Plexiglas cylindrical container, the holding board and five miniature tensiometers.

- The container has inner diameter, $D_i = 20\text{cm}$; height $H = 120\text{cm}$; thickness, $t = 0.6\text{cm}$ and number of holes for insertion of tensiometers, $n = 5$. The soil sample and ponding setup (to apply water) on top of the sample. For ponding a combination of water cup and cotton wicks were used in current research.



Fig. 4.9. Infiltration column setup designed, manufactured for METU geotechnical laboratory (a) sketch proposed by ASTM D7664, (b) dispatched parts and (c) montaged infiltration column setup, (d) water drain on pedestal and filter close up and (e) tools for ponding into the sample (water cup + cotton wicks).

- The holding board was designed to carry the container, keep it vertical and place tensiometers. Where the container is located on the board, a perforated mesh is set to drain water down from the sample. Water drained from the sample can be collected in a beaker that is placed under the setup using a collector funnel.
- F2100 miniature tensiometers by Soilmoisture Equipment corp. are used for monitoring suction values at different heights.

In this study tests could be initiated from either states of fully saturated or fully dry samples according to the standard, however, author performed an initially dry test and an unconventional test in which soil sample was unsaturated at the beginning.

To perform test, samples were prepared by pouring QS soil (and compacting to the required density) inside the infiltration column, and left for 24 hours to let suctions to be equalized. During sample placement, by reaching sample surface to the levels of tensiometer insertions, miniature tensiometers were mounted (Fig. 4.10). After equalization time, ponding was allowed (started) and suction values were recorded. Throughout the tests ponding rate was kept (approximately) constant on the surface of the samples (50ml/day) and suction value recording carried on till test termination at a rate of 1 measurement/day. Test is considered terminated when the wetting front reaches to the bottom of the column.

The infiltration column setup was designed to take suction recordings at five stations (elevations). This is the minimum number of suction recordings due to ASTM D 7664, but for faster infiltration tests, experiments done with limited number of tensimeters over QS soil. Furthermore, regarding lower hydraulic conductivity of dry soils, test lasted for weeks which caused drying in tensiometers and zero recordings. In those cases tensiometers were refilled regarding instructions by the manufacturer. In the course of this research, infiltration column tests are done over samples of 1.2 and 1.35 g/cm³ dry densities. Suction vs. time data are used in governing flow equations and hydraulic conductivity of the soil sample is assessed from there. Detailed calculations are presented in 6.1.2.

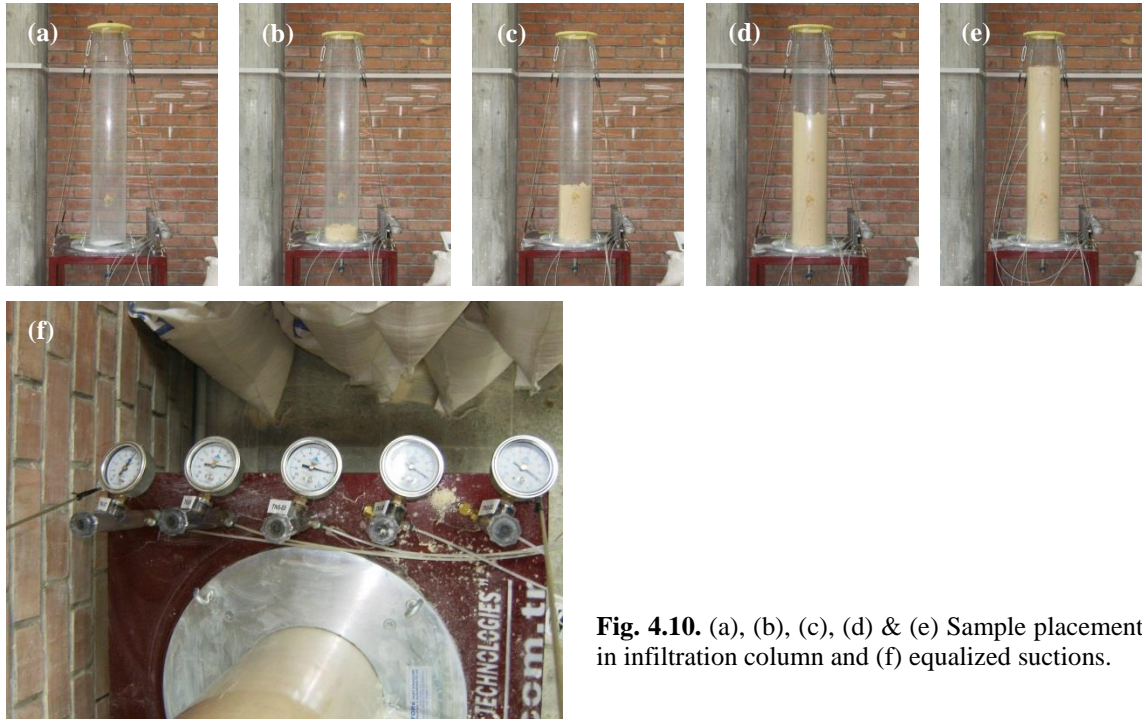


Fig. 4.10. (a), (b), (c), (d) & (e) Sample placement in infiltration column and (f) equalized suctions.

4.1.3. Unsaturated shear strength tests

Considering variably saturated condition of the soils in rainfall triggered landslide phenomena, shear strength of these soils also must be assessed in unsaturated state. Therefore this research also focused on measurement of unsaturated shear strength of QS soil.

Proper unsaturated strength tests would require complicated apparatuses to perform suction controlled shear tests (e.g. direct shear test or 3axial test apparatuses) or shear apparatuses with suction measurement capability. But because such apparatuses were not available in geotechnical laboratory at METU, water content controlled tests were done instead of suction controlled tests. After some trial tests in direct shear test setup and after partial verification of the results (outcomes published in a contribution by Ahmadi-Naghadeh et al., 2013) this method deemed suitable for unsaturated shear strength assessment.

To perform tests, a procedure similar to conventional direct shear tests was followed. The only difference was sealing top and bottom of the specimen while testing (shearing)

using plastic Nylon pieces placed between grooved plate and porous plates. Fig. 4.11 shows procedure in more detail.

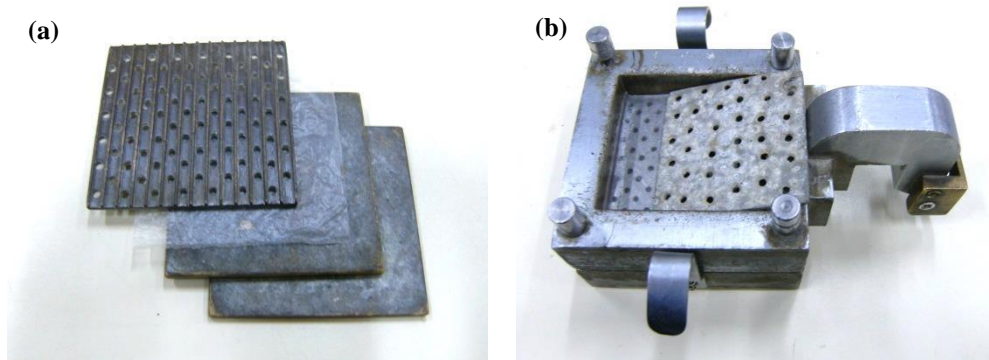


Fig. 4.11. Water content controlled direct shear test procedure, Nylon sealant placement in (a) top and (b) down of the sample.

Water content controlled direct shear tests were performed on samples with three dry densities of 1.20, 1.27 and 1.37 gr/cm^3 and four water contents of 1, 5, 10 and 15% as well as tests on dry soil specimens at each density. To have capability to obtain cohesion and internal friction angle for each dry density and water content, tests were repeated at different normal stresses (5.1, 12.0, 24.5 and 37.1 kPa). In selection of normal stresses, range of generated stresses in flume and laminar box tests were considered. Test results are presented in more detail in 6.1.3.

4.2. Flume tests

In order to verify findings from numerical analyses (see chapters 5 & 6) which support main argument of current thesis, experimental model tests were planned. Indeed these tests replicate rainfall triggered slope instability.

In the scale model tests, soil slope experiments constructed in the flume setup were subjected to the artificial rainfall with known intensity and their behavior (e.g. infiltration and failure) was studied. These tests are labeled as “flume test” throughout current thesis.

In following sections, the constructed flume setup is described and then the schedule of the flume tests is explained. Also a detailed explanation of sample preparation and testing procedure for all experiments are presented.

4.2.1. Flume Setup

To perform flume tests, an original exclusive flume setup was designed by the author and manufactured by Akdoğan Reklam Industries. Fig. 4.12 shows schematic of the flume setup. The flume setup consists of a flume box, raising system and adjustable rainfalling system.

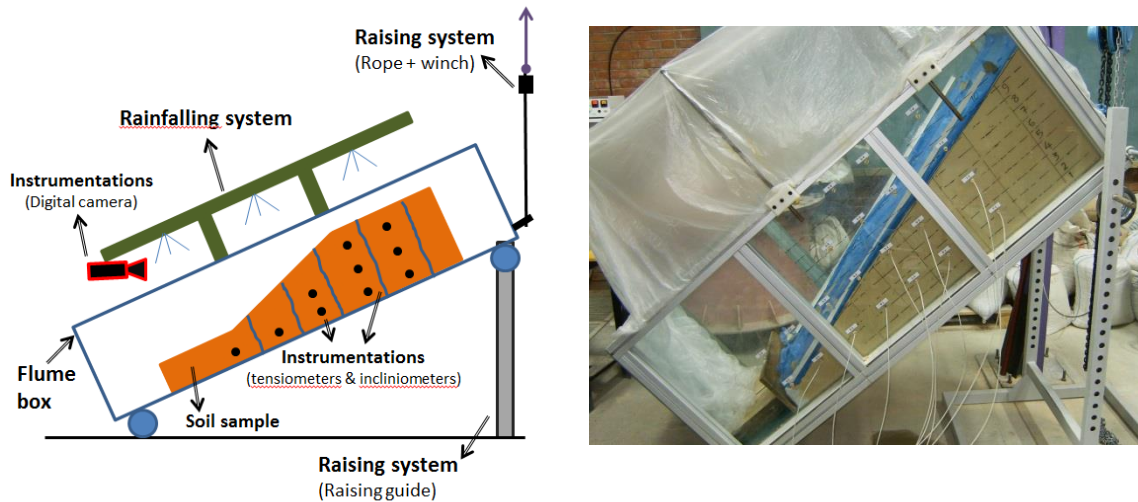


Fig. 4.12. Schematic view of the flume setup designed and manufactured for METU geotechnical laboratory

As shown in Fig. 4.13 the flume box is a modular container which could carry up to 1.5 tons of material and be tilted in desired (planned) inclination (55 degrees at most). The internal dimensions of the box are 187 (length) \times 48 (width) \times 70cm (height). It is suitable to be instrumented with different devices (miniature tensiometers, PDCRs, TDRs, inclinometers, digital camera).

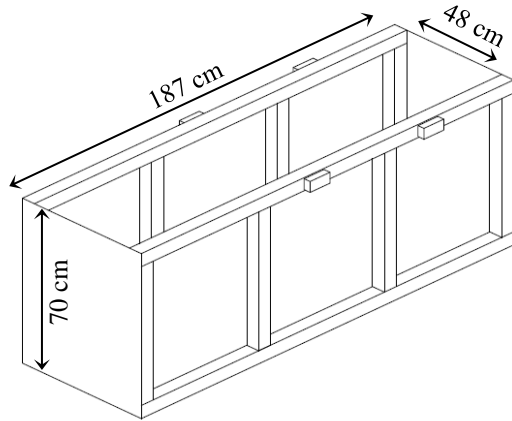


Fig. 4.13. Dimensions of the flume box

The box consists of a frame and side and bottom coverings. The frame was made up of jointed carbonized aluminum profiles. The long sides of box are made of, the short side walls are of galvanized steel sheets and bottom is compressed hard plastic sheets. Employed tempered glass sheets (prepared by Merkezcam Glass & Frame Industries) can withstand soil pressure and shocks from dynamic compaction of soil specimen. They also have a set of holes with 12mm diameter to insert any of tensiometers and PDCRs or to pass cables of TDRs (if any). Side glass walls are also shown in more detail in Fig. 4.14. Handmade rubber plugins (made of eraser rubber) are used to seal

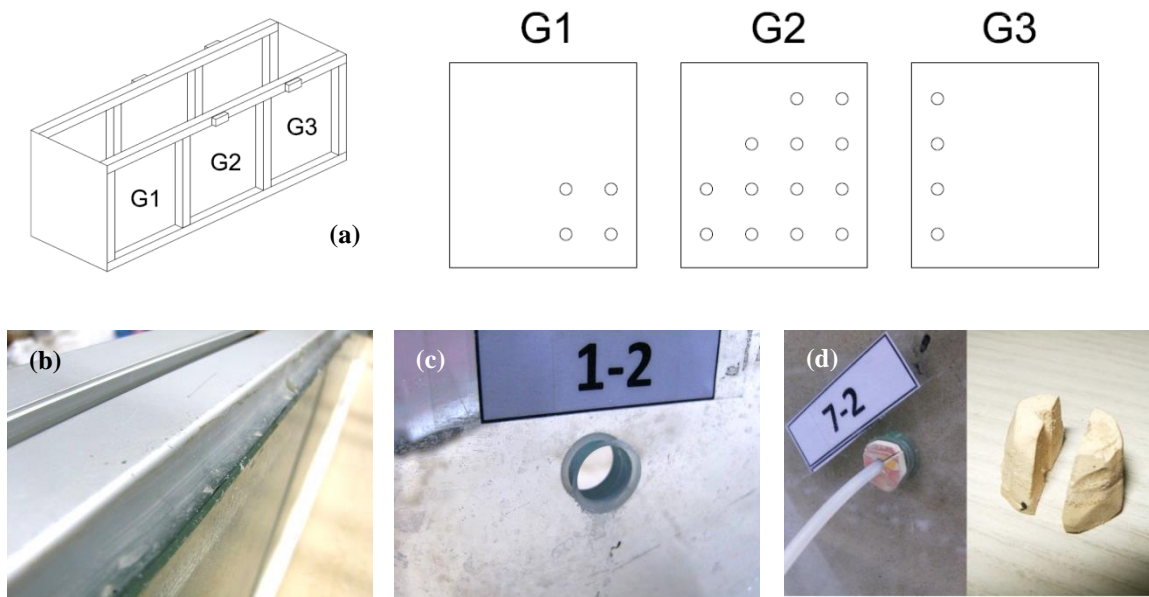


Fig. 4.14. (a) Distribution of openings, (b) sealant of glass walls, (c) an openings and (d) rubber sealants

instrumentation holes on glass sheets. This figure also shows views of galvanized steel sheets and compressed hard plastic sheets. Fig. 4.15 presents some close up views from different parts and details of the flume box.

A raising mechanism is used to tilt the flume box. It consists of a portal frame made up of IPE 240 steel sections, 1 ton differential hoist and a holding (leaning) pedestal. Fig. 4.16 shows these parts in detail. The system was able to tilt the flume box (raise a side) smoothly, without initial/terminal shocks and keep it at a determined angle safely.

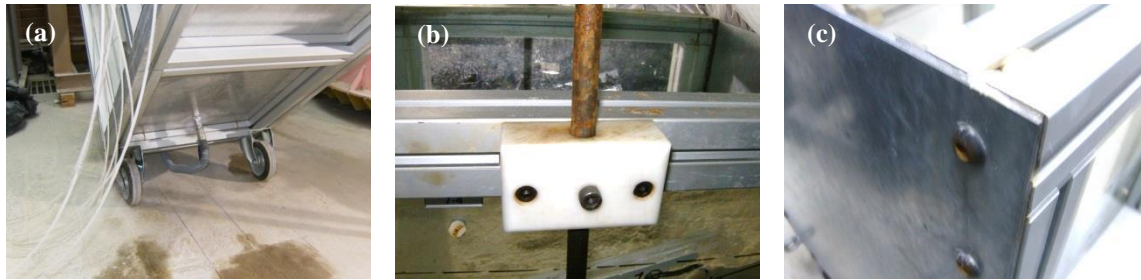


Fig. 4.15. Close up of some details in flume box, (a) drainage from the flume, (b) up/down and right/left moveable rainfalling system montage and (c) removable upstream and downstream walls

A rainfall system was designed and manufactured (by Süsoy Ltd.) to apply artificial rainfall on soil sample in the flume and laminar box experiments. Fig. 4.17 shows the system which consists of a digital control panel (composed of spraying-resting control circuits, temporary water reservoir and actuators) and sprinklers array.

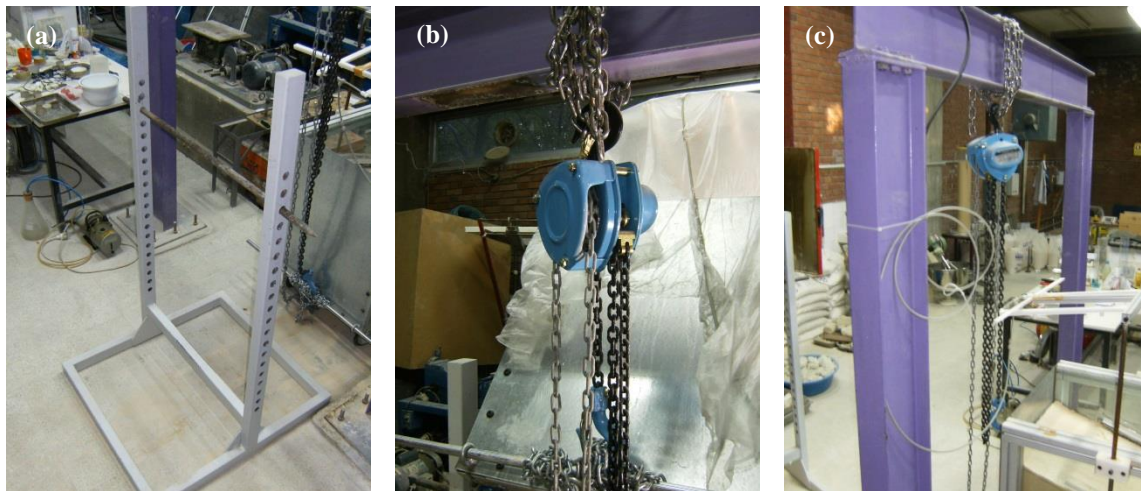


Fig. 4.16. Lifting system (a) holding pedestal, (b) winch and (c) Steel frame

was mounted on an adjustable (elevation and inclination) aluminum frame which could support pressurized water hoses and nozzles.

The system is capable of applying different rainfalls by adjusting spraying (rainfall) and resting (no rainfall) time pairs within a minute. Applying uniform rainfall with lower intensities was quite difficult since slower rates caused water droplet formation (rather than spray) in nozzles. Therefore, to obtain a specific rainfall intensity it was decided to adjust spraying/resting time pairs.

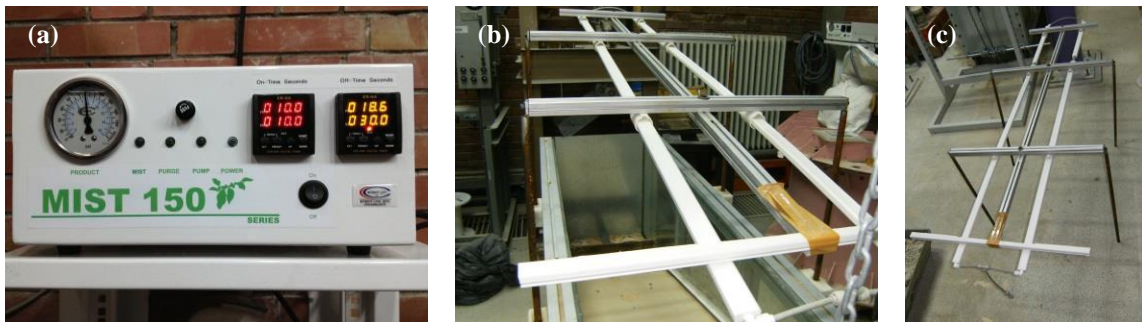


Fig. 4.17. Rainfalling system in detail (a) control panel, (b) & (c) rainfalling pan

The system was able to apply spraying for 0-120 seconds and resting for 1-120. The flow from each nozzle was varied in 0.06-3.87 lt/hr range if the sprinkler array stays horizontal. These values might change considerably by tilting the array or changing its elevation (due to water head differences). Fig. 4.18 shows the experiment for measuring from any nozzle.

This made it necessary to measure rainfall intensity on each soil surface considering its elevation, inclination and also status of the sprinkler array. Therefore, rainfall intensity was measured multiple times throughout the thesis for different spraying/resting pairs and different soil model surfaces.

Fig. 4.19 shows an experiment measuring rainfall intensity on an inclined surface which is similar to the surface of one of the flume experiments (FLM_06). It's obvious that in the upper region of the experiment rainfall intensity is significantly lower than the middle and lower parts. This was considered in numerical simulation of the flume experiments.

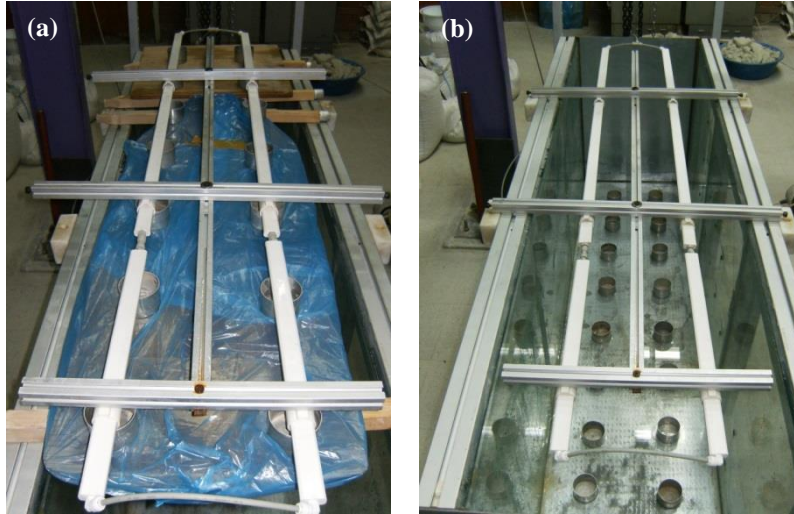


Fig. 4.18. (a) Measuring water discharge from each of nozzles and (b) Rainfall intensity measurement over flume bottom



Fig. 4.19. Rainfall intensity checkup over inclined surface

4.2.2. Measurement devices

To assess changes in pore water pressure throughout the tests, soil samples are equipped with tensiometers and PDCR devices. To capture deformations, a combination of side and wall inclinometers and a digital camera for image processing are used. In following sections, devices and their application are described in more detail.

4.2.2.1. Tensiometers

2100F Soilmoisture Probes are field and laboratory tensiometers that work in the range of 0-90 kpa. In current research nine 2100F miniature tensiometers were used to

measure soil suction in different experiments (e.g. infiltration column, flume tests and laminar box tests).

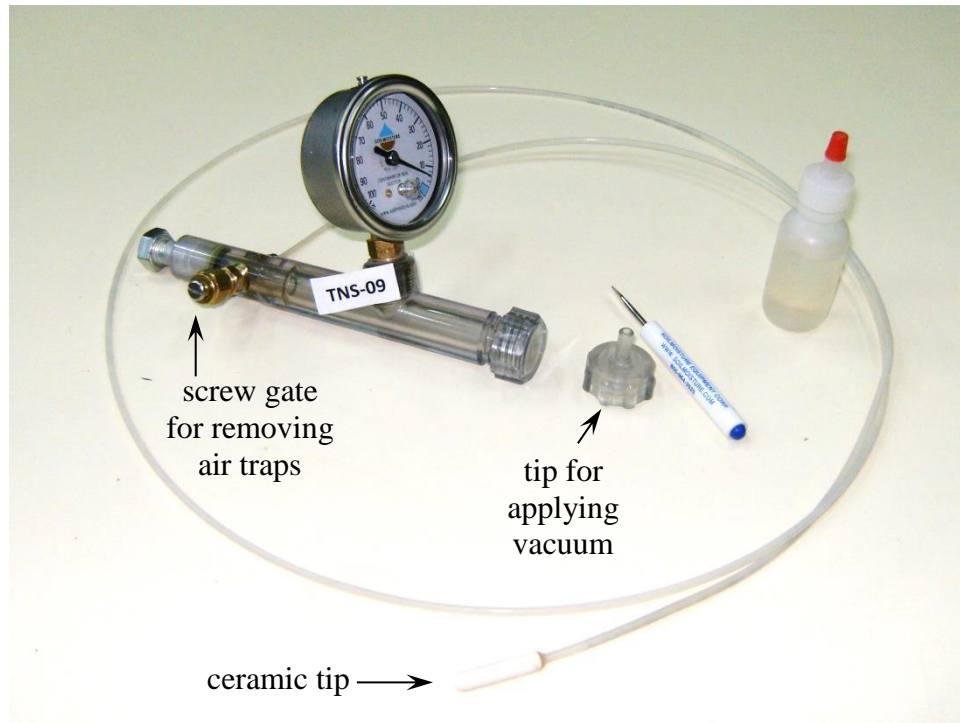


Fig. 4.20. 2100F Soilmoisture Probes

4.2.2.2. PDCRs

Miniature tensiometers are the devices that can measure positive and negative pore water pressures within soil medium. Druck PDCR-81 is a miniature pore pressure transducer produced by PROCON Systems Inc. and well-known for its accuracy and precision. The PDCR were used in METU geotechnical laboratory is equipped with a 3 bars ceramic disc and a 10 bars pressure transducer. Detail of this apparatus is presented in Fig. 4.21.

- Saturation of PDCRs

Generally, the most challenging part of using miniature tensiometers is their saturation. Saturation is necessary for suction (negative pore water pressures) measurements since the pressure transducer will work only if the water reservoir between ceramic disk and transducer diaphragm would be filled with water. Saturation also is not a simple process

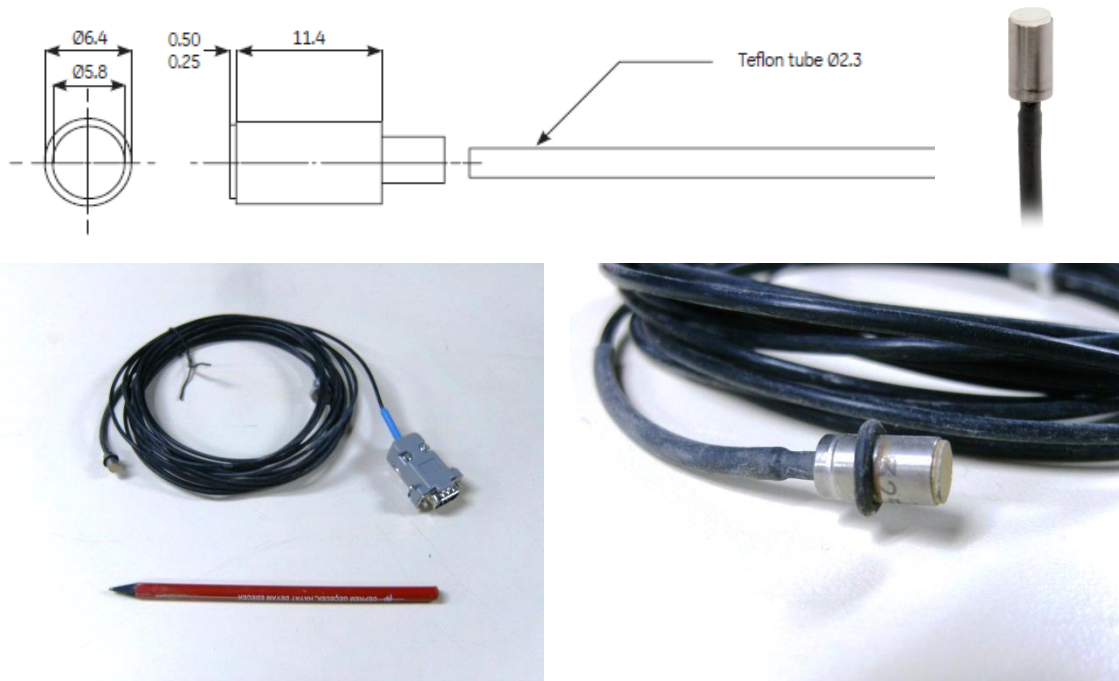


Fig. 4.21. Druck PDCR-81 probe

since this gap (water trap) is very small and generally it's very difficult to force water through ceramic disc to the otherwise sealed gap to fill it completely. Therefore a special procedure was developed for saturation of PDCRs.

To develop a saturation process some comments by Take and Bolton (2003) were considered. A new setup for this purpose were designed by the author and manufactured by ALFA Laboratories Company. The setup is shown in Fig. 4.22 in more detail.

For saturation, briefly, PDCRs are inserted into a chamber and subjected to initial direct vacuum (approximate gage pressure of -100 kPa) for 60 minutes. At the end of 60 minutes while vacuum is still applied, the chamber rotated upside down. Then, vacuum is removed by opening to the atmosphere. Former studies and also author's trials revealed that at the end of this stage PDCR can read suction up to -60 kPa. Thus, further steps were followed to make PDCR capable to measure higher suction. These steps were pre-pressurization cycles in which cycles of pressurizing (up to 3 bars) and following vacuum could increase suction to the ranges even higher than the reported air

entry value of porous disc. In current research 3 cycles of pressurization were done and suction measurement capability in PDCRs increased to -155 kPa.

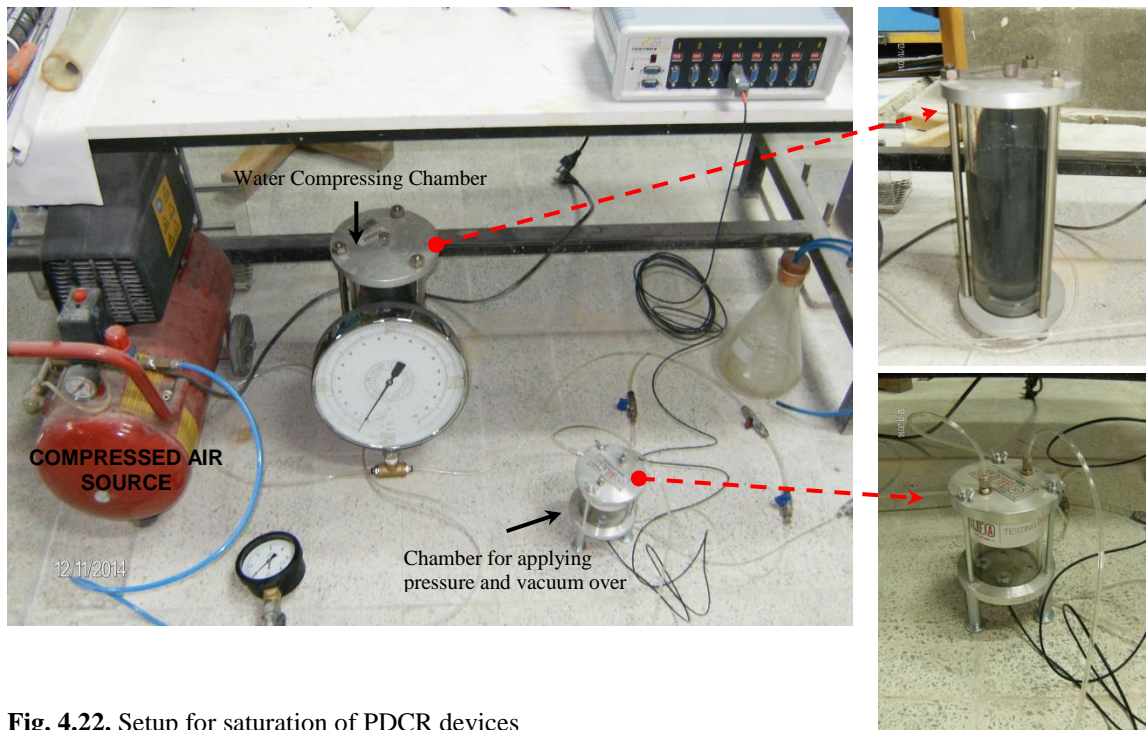
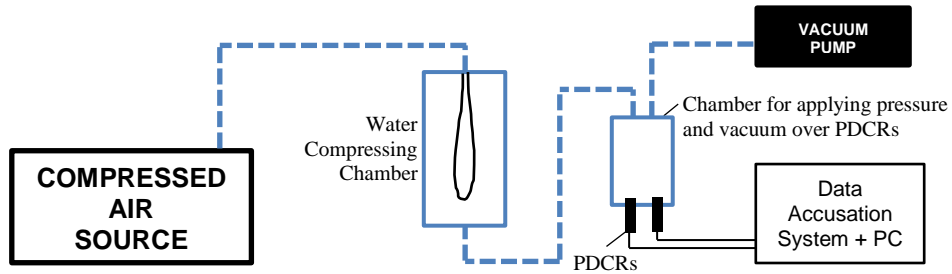


Fig. 4.22. Setup for saturation of PDCR devices

- **Calibration of PDCRs**

Saturated PDCRs before usage needed to be calibrated. To do so, available setup in METU geotechnical laboratories for hanging column tests were used (Fig. 4.23). For doing calibration positive and negative water pressures were applied in the range of ± 50 kPa. Applied water pressures and measured voltage values are plotted against each other and shown in Fig. 4.24 with the resulting calibration equations.

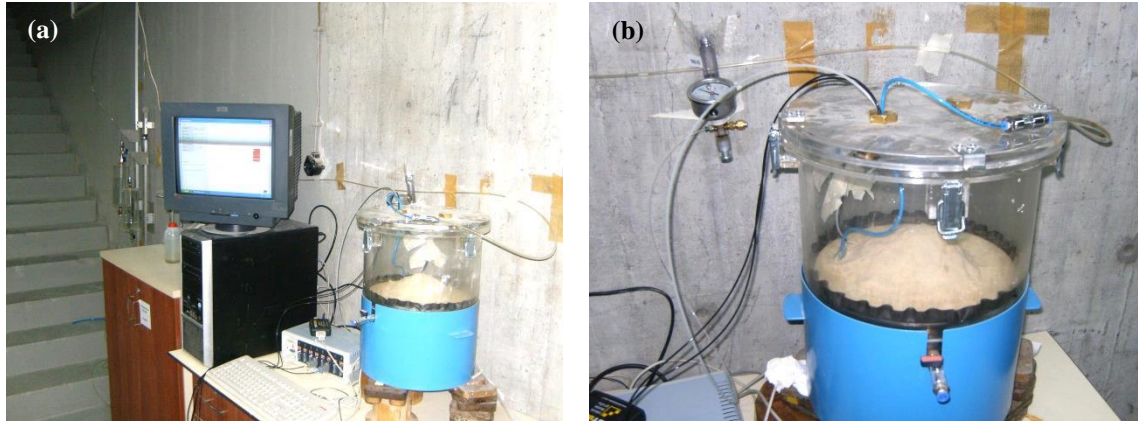


Fig. 4.23. (a) Setup for calibration of PDCRs, (b) detail of connections

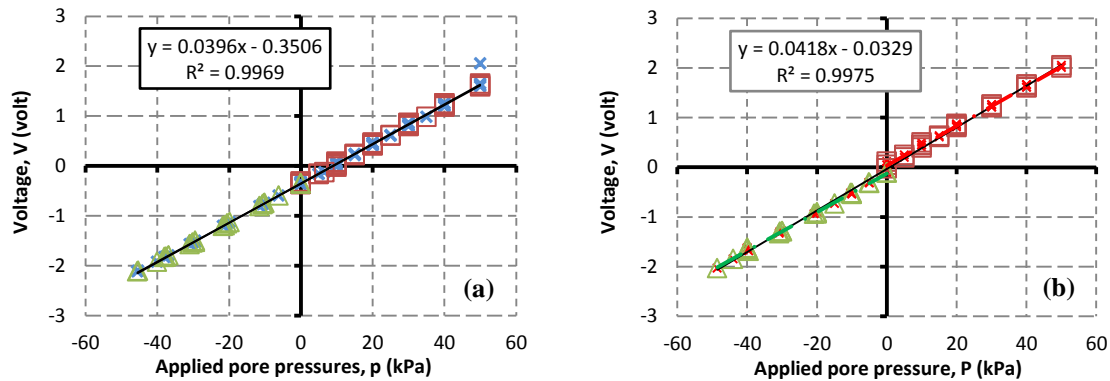


Fig. 4.24. Calibration charts for (a) PDCR-1 (yellow) and (b) PDCR-2 (blue)

4.2.3. Inclinerometers

Inclinometers are the tools that can be used to show lateral movement/deflection in a mass of a soil. Real sized inclinometers in the field are generally composed of a propylene flexible tube that is placed into a borehole and also a recording probe that can be slipped into the grooves inside tube. Usage of these inclinometers is limited to the field jobs due their size.

In current research need for inclinometers in laboratory scale were obvious. Therefore various methods were considered for this purpose such as miniature inclinometers that are equipped with MEMS (Micro-Electro-Mechanical Systems) chips, miniature inclinometers that use radio frequencies to locate stations, some passive tools like spaghetti rods. Finally we settled on the innovative idea of non-electronic elastic

inclinometers, considering the time and financial resources available. Fig. 4.25 shows detail of the central and side inclinometers.

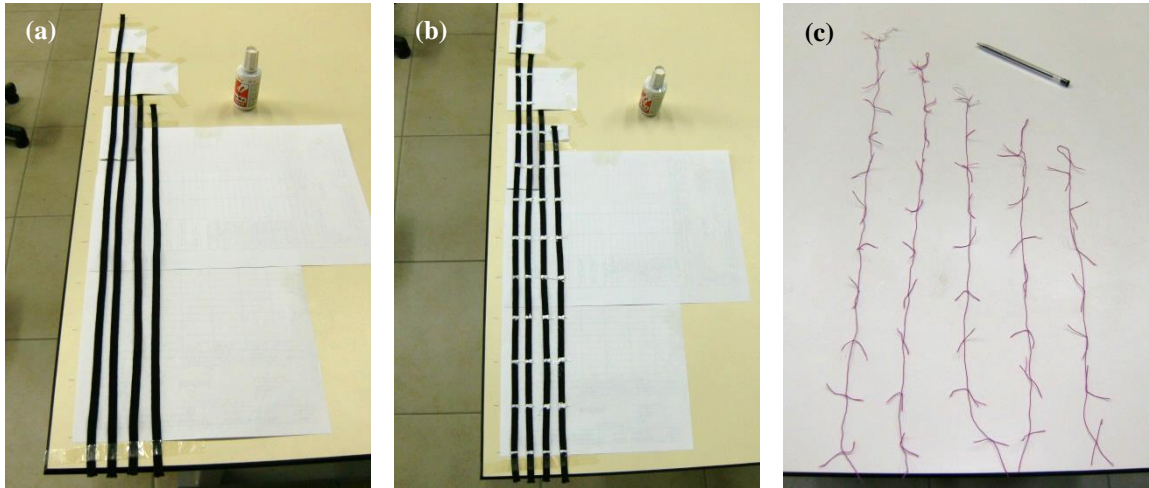


Fig. 4.25. (a) & (b) Preparation of side and (c) central inclinometers

Inclinometers used here are made up of elastic woven strip that could be prepared easily from hosiery. As shown in Fig. 4.25, side inclinometers are made up of black and 5mm wide elastic bands and central inclinometers are from very thin elastic ropes. In order to leave some reading stations on the inclinometers, for side inclinometers white ink were used but for thin central inclinometers one tiny knot were left. Spacing between these reading stations in both tools are 5.0cm.

4.2.4. Testing program

In total 16 flume tests have performed. These tests were named as FLM_00 to FLM_15 in which FLM was the abbreviation of flume and following double numbers were denoting number of the tests.

Tests FLM_00 to FLM_02 were trial flume tests to study sample preparation processes, checking up montaged parts and instrumentations. In tests FLM_03 to FLM_15 rainfall intensity changed and failure time recorded to compose intensity-duration (I-D) plot. Three relative densities of 34, 48 and 61% corresponding to 1.20, 1.27 and 1.35g/cm³ dry densities were checked and two I-D plots assessed. Table 4.1 is summarizes test

program (average values for relative density, rainfall intensity and other testing parameters).

Table 4.1. Flume tests program

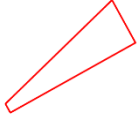
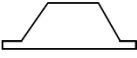
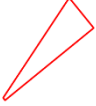
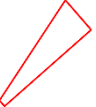
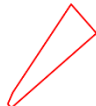
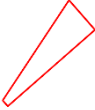
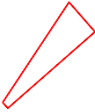
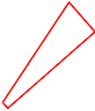
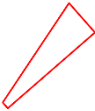
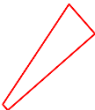
Test lable	Test date	Slope shape	Slope angles (°)	Relative density (%) *	Rain intensity (mm/hr) **	Employed instrumentations ***
FLM_00	27 Aug. 2013		44	61	15/60 (10.6)	T, P, D, V
FLM_01	10 Dec. 2013		45 & 50	61	5/60 (4.1) 30/60 (24.8)	T, P, D, V
FLM_02	01 Jan. 2014		55 & 60	61	15/60 (10.6)	T, P, D, V
FLM_03	12 Apr. 2014		56.5	34	55/60 (54.4)	T, P, D, V
FLM_04	04 May 2014		56.5	34	43/60 (46.3)	T, P, D, V
FLM_05	12 May 2014		56.5	34	25/60 (28.3)	T, P, D, I, V
FLM_06	25 May 2014		56.5	34	15/60 (15.6)	T, D, I, I _w , V
FLM_07	30 May 2014		56.5	34	0/60	T, D, I, I _w , V
FLM_08	18 June 2014		56.5	34	20/60 (21.6)	T, D, I, I _w , V
FLM_09	13 July 2014		58	61	55/60 (59.6)	T, D, I, I _w , V

Table 4.1 (continued). Flume tests program

Test lable	Test date	Slope shape	Slope angles (°)	Relative density (%) *	Rain intensity (mm/hr) **	Employed instrumentations ***
FLM_10	28 July 2014		56.5	48	55/60 (63.0)	T, D, I, I _w , V
FLM_11	13 Aug. 2014		56.5	48	25/60 (28.9) 55/60(66.7)	T, D, I, I _w , V
FLM_12	22 Aug. 2014		56.5	48	40/60 (48.8)	T, D, I, I _w , V
FLM_13	28 Aug. 2014		56.5	34	22/60 (25.5)	T, D, I, I _w , V
FLM_14	02 Sep. 2014		56.5	48	22/60 (26.0) 40/60 (48.3) 55/60 (62.8)	T, D, I, I _w , V
FLM_15	06 Oct. 2014		56.5	48	18/42 (20.2)	T, D, I, I _w , V

* Relative densities 34, 48 and 61 % correspond to 1.2, 1.27 and 1.35 gr/cm³ dry densities. For more detain in asseemnet and calculations see 4.1 and 6.1.

** Rainfall intensities are stated as spraying time per cycle length, in seconds. In the parenthesis also average rainfall intensities are presented in mm/hr.

*** T: Tensiometers, P:PDCRs, D:Density checkup tares, I: Inclinometers, I_w: Wall inclinometers, V: Video cameras

4.2.5. Sample preparation

Procedure for preparation of sample for a test in the flume box is explained in detail in current section. Following the procedure, which generally took more than 5 hours, had been repeated at every FLM test.

4.2.5.1. Plotting geometry of the experiment on the glass walls

This was the very first stage of the sample preparation for the flume. In general after different trial numerical analyses, geometry was determined for the flume test.

In order to create a sample with an accurate geometry, it was useful to plot the side sections of the sample on the glass walls. This was done by board marker pen (easily erasable) from the outside of the flume. In this drawing, soil sample boundary, location of filter boundaries, sample placement layers and location of side inclinometers were included. Fig. 4.26 has shown geometry drawings for the test FLM_06 on the monitoring and closed side walls.



Fig. 4.26. Drawing of layers of sample placement and geometry of specimen

4.2.5.2. Providing and placement of supports and filter barriers

Many flume tests were planned to have free drainage in the lower boundary of the soil sample, therefore granular material with high permeability was used for this purpose.

These material before usage were packed in bags of appropriate dimensions (e.g. $5 \times 10 \times (24+24)$ cm) made of filter paper, and then placed in their location. This tactic was used due to two main reasons, (i) difficulty in reuse of blended filter material and soil sample after test termination and (ii) difficulty in shaping filter material and creation of distinct smooth boundary between filter and soil sample considering their loose nature at the time of placement.

After test termination, these filter boxes were removed and left drying in the oven. They could be used several times till the shape of the boxes was unacceptably deformed. Fig. 4.27 has shown detail of the preparation; usage and desiccation of filter boundaries (filter boxes).

4.2.5.3. Placement of inclinometers

Innovative elastic inclinometers (explained in detail in section 5.2.3.3) have been used in many of the flume tests. In order to place inclinometers in the soil sample, instead of

inserting them after sample deposition, they are placed in the correct (planned) location inside the box and then place the soil sample.

To place the inclinometers in the correct location and in correct shape, they are hung from a wooden supporting bar which is located on top of the flume box. By this means, by adjusting elevation of the inclinometer, reading stations could be set in the middle of each deposition layer. Fig. 4.28 has highlighted detail of the inclinometer placement in flume test FLM_06.



Fig. 4.27. Filter material preparation, placement and removing after test.

4.2.5.4. Sample placement and compaction

Sample placement is both the most important and the most sensitive stage. The criterion was uniform placement of soil material in the flume box with a predefined dry density. Therefore, the procedure was configured to deposit soil material in layers of more than 5cm and compact to the known density using tamping on a steel plate. It was also understood that for shaping and compacting sandy material to a specific dry density its necessary to make them wet before deposition and compaction. Humidity of 1.5% was found to be appropriate using trial and error. A bakery blender with capacity of 50kg was used for mixing soil and water and making it uniform paste (Fig. 4.29).

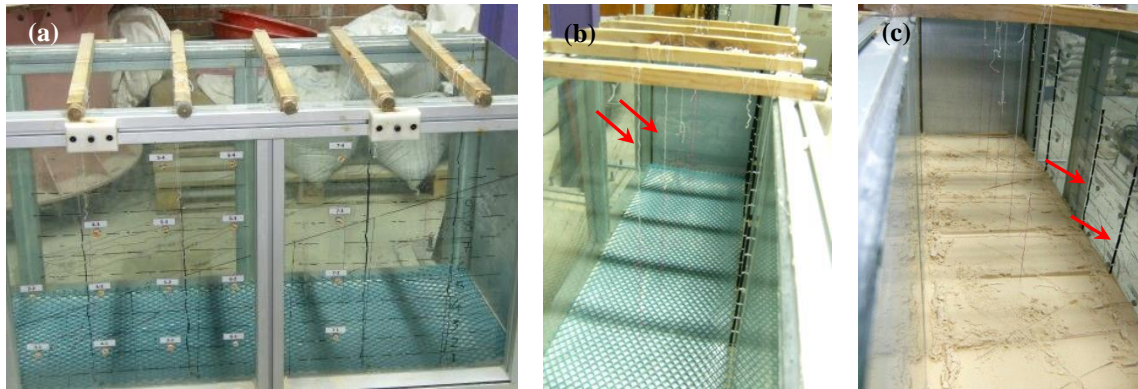


Fig. 4.28. (a) Inclinometer placement (hanging from wooden bars), (b) middle inclinometers and (c) wall inclinometer



Fig. 4.29. Bakery blender used to mix misted soil

Thickness of the deposition layers and number of tamping and its intensity (steel bar drops and their height) for a specific dry density were assessed using trial and error before tests. Fig. 4.30 has shown the tools used in sample preparation for FLM_06 and FLM_14.

In this stage, the most difficult and time consuming part was pouring/depositing soil material in the vicinity of some instrumentations such as inclinometers. Generally the author was doing that manually.

Similar to the other layered but uniform soil sample reconstitution procedures, before placement of new layer, lower soil layer is surface was scarified to establish acceptable interlocking of layers, protect any possible slip from layers boundaries.

4.2.5.5. Tensiometers and PDCRs placement

As introduced in 4.2.2.1 and 4.2.2.2, tensiometers and pore pressure transducers as the means of instrumentations that can measure positive and negative pore water pressure should be saturated before placement in soil sample. Also due to geometry of the flume samples it was necessary to place them into the soils sample at the time of sample creations rather than inserting them. Therefore, it was planned to place these instrumentations in their correct position after deposition of underneath soil layer.



Fig. 4.30. Plate and weights used to compact soils sample

In order to place mentioned instrumentations in soil sample, prepared holes on glass walls were used. In some of the flume tests, tips of the inserted tensiometers and PDCRs were extended to the centerline of the sample. In other tests this was modified to 10 cm insertion into the soil to reduce slight resistance (e.g. reinforcing effect of tensiometer hoses or PDCR cables). Fig. 4.31 shows both types of placements and locations of tensiometer bodies.

4.2.5.6. Trimming sample edges

After deposition of soil sample completely and placing instrumentations in flume model, by trimming sample surface and removing the extra material final shape of the experiment emerges. For trimming, lateral geometry drawings were directive. In the

cases of experiments with inclinometers, trimming also was very time consuming. Fig. 4.32 shows soil sample in experiment FLM_04 before and after trimming.

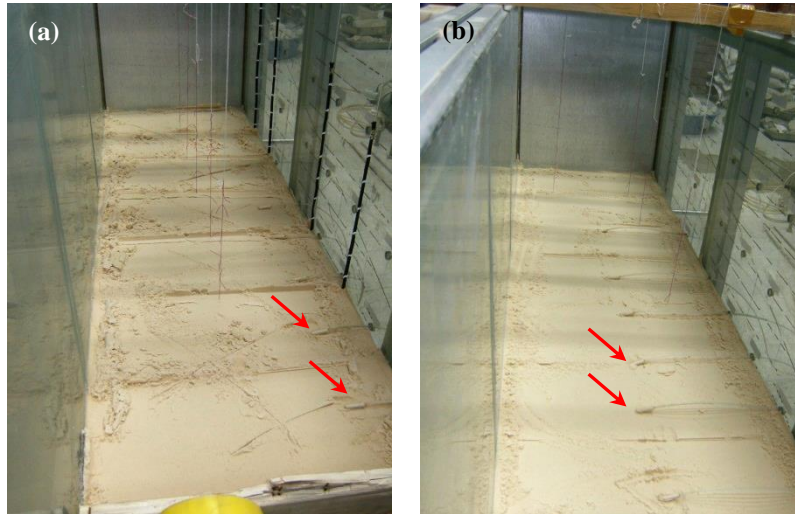


Fig. 4.31. Tensiometer placement with two distances from the flume wall, (a) FLM_03 and (b) FLM_06

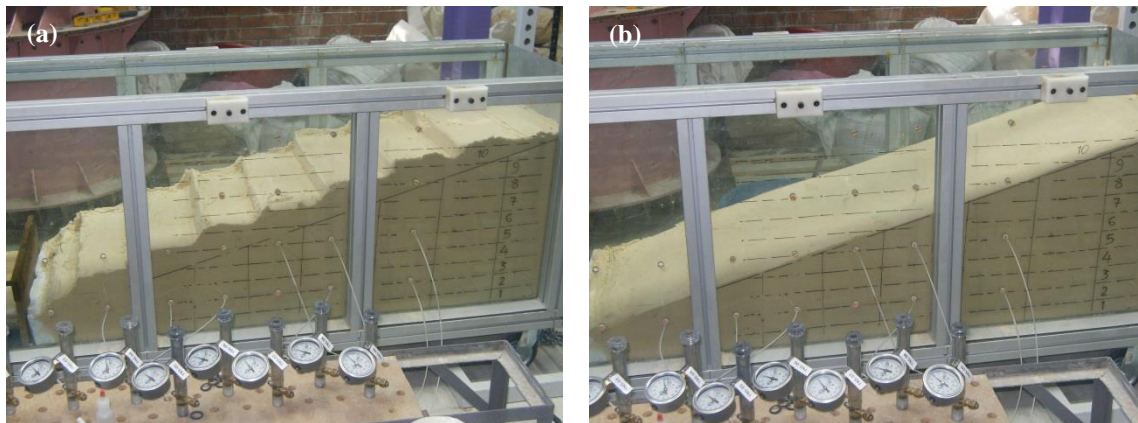


Fig. 4.32. Sample (a) after deposition (b) after trimming (FLM_04)

4.2.5.7. Droplet drain montage and covering flume box

Remember rainfalling system was applying precipitation using misting. When mist cores in contact to side wall glasses it turn in to water droplets that flow downward. This was considered as potential for increased infiltration along the side glasses. As a solution, plastic drop drains were prepared and attached on side glass walls, a couple of centimeters above the soil surface, to drain water drops to the filter material to drain freely. The cross section and view of the installed drain are shown in Fig. 4.33.

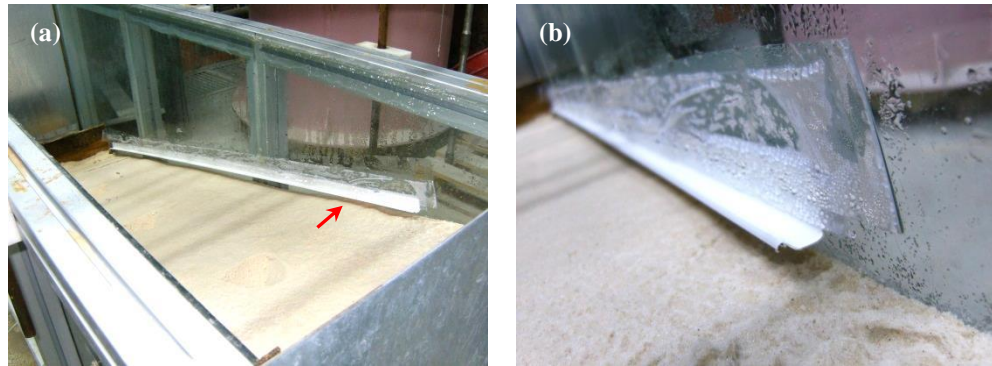


Fig. 4.33. Drop drain (a) mounted over the box wall and (b) close up

In order to avoid sample surface desiccation at the time between sample preparation and testing Nylon covers was placed on the surface. Sample surface desiccation in some of the tests caused changes in shape of the slope model which was due high inclinations in surface. By desiccation, suction disappeared so the soil material slipped down. This phenomenon is shown in Fig. 4.34 which was from test FLM_03. As extra protection, an additional covers was placed over the sprinkler array to minimize desiccation. Fig. 4.34 shows both of these means for FLM_04.

4.2.5.8. Positioning (tilting) flume box

Immediately after sample preparation completion and covering, the flume experiment is brought to the position and inclination of testing. This was done with the assistance of the lifting system and supporting frames.

This stage is also very sensitive in which no extra disturbance must be generated as it could cause failure prior to the test. Therefore it was done with considerable care. Experiment FLM_06, after positioning, is shown in Fig. 4.35.

4.2.5.9. Equalization stage

The flume tests are left for a period of time between the sample preparation and the test. This time period, which is at least 24 hours, is for equalization in suction values inside of the soil sample. This was deemed necessary based on the findings of chapter 3. This stage is needed in order to get rid of any local water accumulation as any possible defect of current soil blending method. Furthermore, initial water content must have been

balanced due to elevation head which has changed after positioning. During equalization stage sample surface is left covered and undisturbed.

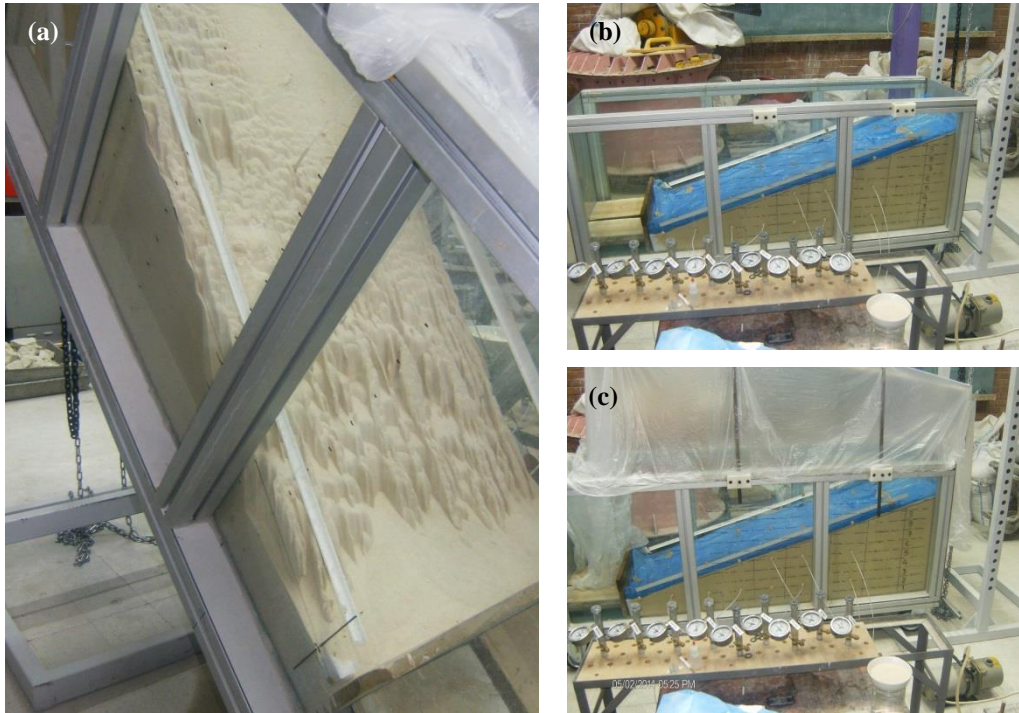


Fig. 4.34. (a) Desiccation over sample while equalization, (b) sample cover and (c) box (extra) cover



Fig. 4.35. Sample positioning, left for suction equalization

4.2.6. Testing

Testing stage started by uncovering the soil sample inside flume. Also in order to find a place for leaving rainfall intensity checkup tares some half cup like holes were carved

on the inclined surface of the model. Fig. 4.36 shows surface of the soil sample with these cups in experiment FLM_06 at testing stage before rainfall application.

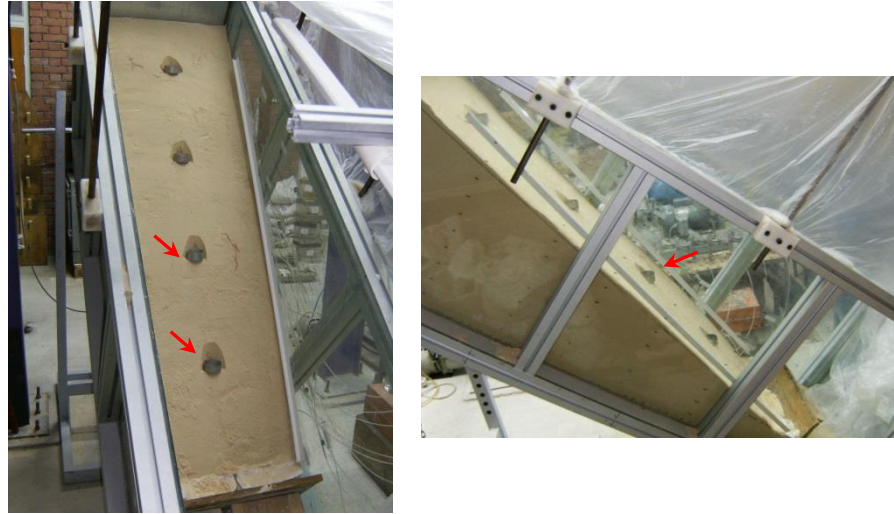


Fig. 4.36. Rainfall intensity checkup tares placed over sample surface

After placement of tares on soil sample, rainfall started and simultaneously recordings are also initiated. In the flume tests generally suction values, wetting fronts and inclinations were recorded. For each of flume tests recorded data are presented in Appendices A and B.

Considering granular nature of soil used in this study, it was used several times for different tests. After usage the material is dried in a low temperature oven and then stored till the next usage.

4.3. Laminar box tests

To verify numerical/analytical modeling of shear behavior in an infinite slope model laminar box setup was designed and constructed for this research for the first time. In the following sections detail of the setup, summary of test specifications, sample preparation and testing methods are explained.

4.3.1. Laminar Box Setup

The setup consists of 50 laminates located on each other without lateral guides all set on a tilting pan. After placement of soil in the setup, it could be tilted to the chosen degree and subjected to rainfall. The setup could be instrumented by the tensiometers and PDCRs at 5 possible elevations. Fig. 4.37 shows overview of the laminar box setup designed and constructed for this research.

The laminar box tests were performed within the flume box setup. Ability to apply rainfall and using adjustable positioning system were the reasons to prepare samples and perform triggering tests in laminar box setup inside flume box.

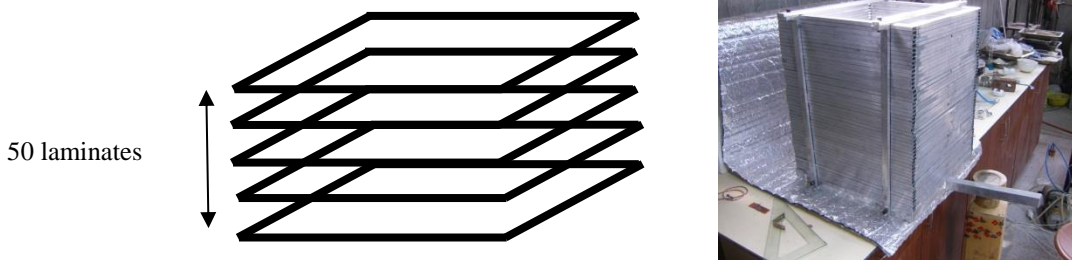


Fig. 4.37. Overview of designed and constructed laminar box setup

Inner dimensions of laminates are $40 \times 40 \times 2$ cm. Laminates were manufactured from 2×1 cm aluminum box profiles for minimum weight and maximum stiffness. Detail of a laminate and connections are shown in Fig. 4.38.

Due very light weight of the laminates in comparison to the weight of the soil placed in the laminar box and also smoothness of laminates, negligible friction was expected between laminates. This was the reason for eliminating laminate guides which are common in conventional seismic laminar boxes, thus, the laminates left resting on each other. To remove surface scratches due machinery works over laminates, a smoothening procedure including rubbing surfaces with a coarse textile coated with wax were applied. Fig. 4.39 shows laminate surface before and after smoothening.

Despite smoothening, a small resistance against sliding due friction remained between laminates. Therefore, to take into account the friction between laminates in calculation of factor of safeties, a simple system of pulley; rope and a sand bottle were used.

Fig. 4.40 shows detail of this system. Fig. 4.41 also shows result of the calculated friction angle between laminates.

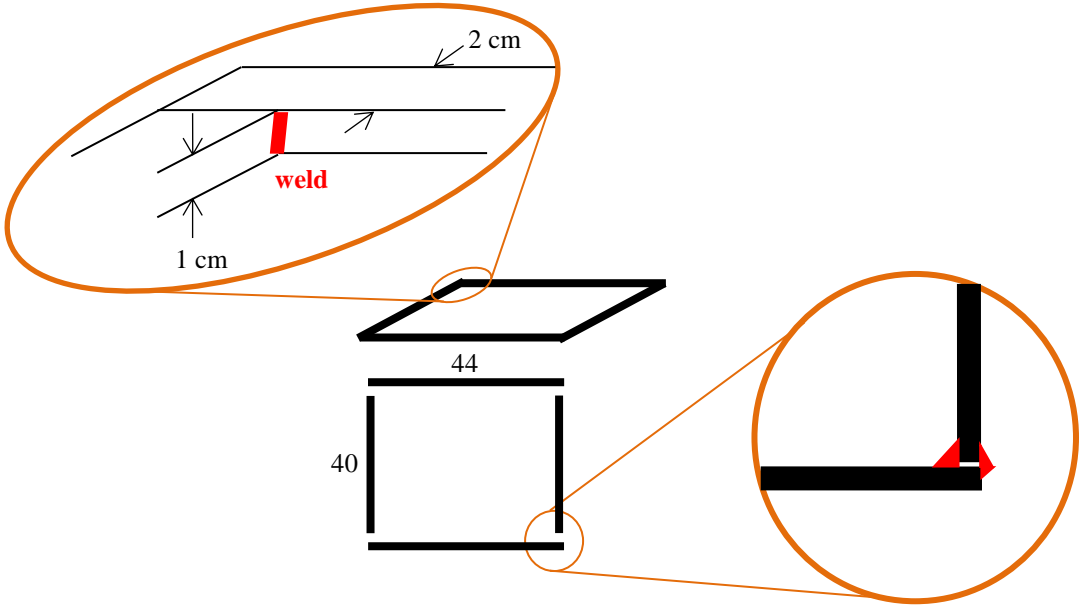


Fig. 4.38. Detail of laminate dimensions and connections

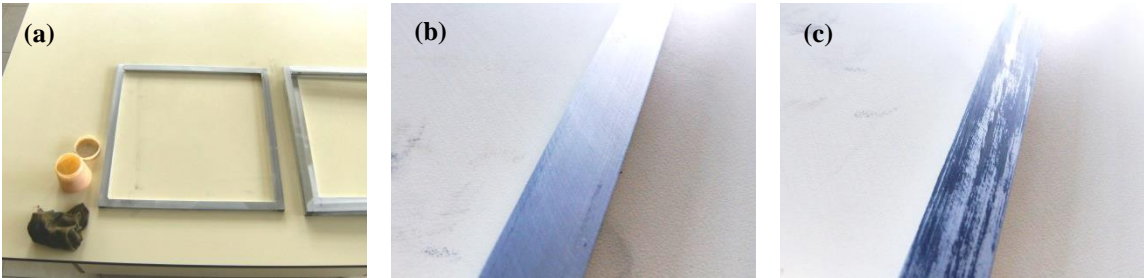


Fig. 4.39. (a) Laminate surface smoothing, (b) surface before and (c) after smoothing



Fig. 4.40. Setup for assessing friction between laminates

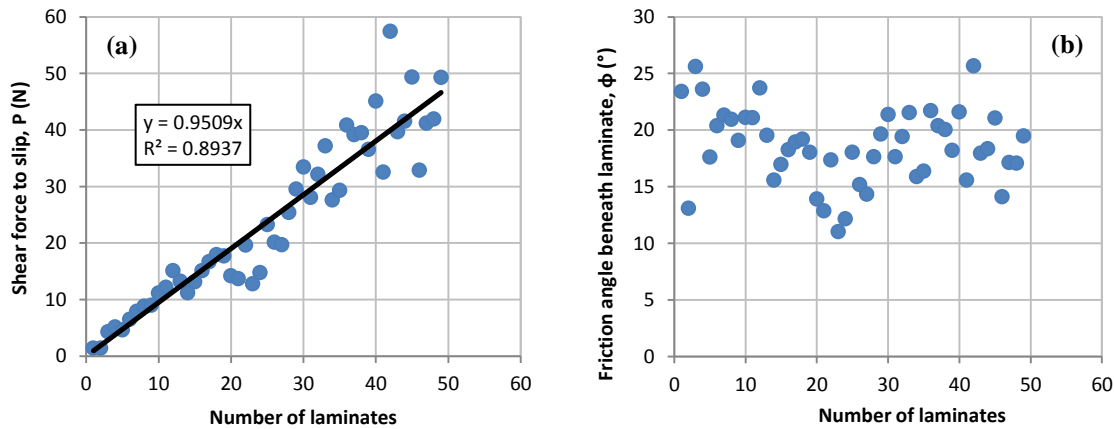


Fig. 4.41. (a) Needed shear force to slip laminates and (b) friction angle between laminates

4.3.2. Test program

In current research three laminar box tests were performed in total. These tests were named as LAM_0 to LAM_2 in which LAM is the abbreviation of laminar box and following numbers denote number of the tests.

The tests LAM_0 to LAM_2 were performed as trial laminar box tests to study sample preparation processes, checking up installed parts and instrumentations. The relative densities of 34 and 61% corresponding to 1.20 and 1.35g/cm^3 dry densities were checked. Table 4.2 is summarized tests program (average values for relative density, rainfall intensity and other soil properties).

Table 4.2. Laminar box tests program

Test lable	Test date	Slope angles (°)	Relative density (%) *	Rain intensity (mm/hr) **	Employed instrumentations ***
LAM_0	16 Aug. 2013	30	61	-	-
LAM_1	10 Sep. 2013	30	61	15/60 (10.6)	T, D, V
LAM_2	17 Oct. 2013	42	34	25/60 (28.3)	T, D, V

* Relative densities 34 and 61 % are correspondent to 1.2 and 1.35 gr/cm³ dry densities. For more detail in assessment and calculations see 4.1 and 6.1.

** Rainfall intensities are stated as spraying time per minute. In the parenthesis also average rainfall intensities are presented in mm/hr.

*** T: Tensiometers, D: Density checkup tares, V: Video cameras

4.3.3. Sample preparation

Sample preparation was the most challenging issue for the tests in the laminar box apparatus. In this section more detail about the procedure for sample preparation in laminar box tests, which generally took about 2 hours are presented.

4.3.3.1. Batching of the laminates

In the proposed method for sample preparation to the laminates were filled with the soil and soil was compacted in the layers of 5cm. Therefore, at each layer of sample preparation, 5 laminates (i.e. height of the laminates is 1cm) were placed and the soil samples poured and compacted inside laminates.

In order to mimic a vertical slice of an infinite slope, sample is placed inside inclined laminates and then the box is tilted to the slope angle. Therefore, at each layer of sample preparation, the laminates were placed in inclined form by sliding over each other. Some guides also are used for this purpose. Fig. 4.42 shows the view of laminates in sample preparation.

4.3.3.2. Fixing laminates using clamping system

Since the laminates were left resting each other at a high angle, the overall weight and vertical forces associated with the compaction procedure were enough to topple the stack. In order configure soil specimen it was necessary to keep laminates fixed in the preferred position throughout soil placement and compaction. This was achieved using a

clamping setup which was designed by the author and manufactured by the Oz-san industries. Fig. 4.43 shows the schematic view of the setup.



Fig. 4.42. Inclined placement of laminates in sample preparation

4.3.3.3. Sample placement and compaction

Similar to the procedure explained in 4.2.3.4, the soil specimen was configured by deposition of soil material, with 1.5% moisture content, in layers of 5cm and compacted to the target density using tamping on a steel plate.

4.3.3.4. Tensiometers and PDCRs placement

5 of the laminates have a hole on the back side to insert measurement devices through. Instrumentation is placed parallel to the sliding alignment to generate minimum friction against shearing.

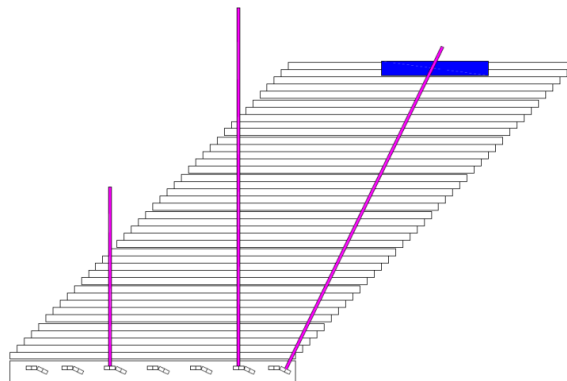


Fig. 4.43. Clamping system to fix laminates beside each other in sample preparation

4.3.3.5. Positioning laminar box

Similar to the procedure described in section 4.2.3.8, by completion of sample preparation, the flume box in which the laminar box is placed, is positioned (tilted) to the slope angle that the laminar box setup models. Experiment LAM_1 after positioning has been shown in Fig. 4.44.



Fig. 4.44. Positioning laminar box setup within flume box

4.3.3.6. Equalization stage

To let the suction values to be equalized in soil sample, similar to flume tests, it was considered to leave a period of time (at least 24 hrs) between the sample preparation and the test. During equalization stage, sample surface is left covered and undisturbed.

4.3.4. Testing

After uncovering the laminar box setup rainfall were applied. In laminar box tests only suction values are recorded continuously throughout the test.

CHAPTER 5

NUMERICAL SIMULATIONS

5.1. Seepage and stability analyses in infinite slopes

As part of current research, in order to better understand the physical processes to assess pore water pressure changes due to water infiltration into unsaturated soils and slope stability in infinite slopes, a simple code is developed to perform seepage and slope stability analyses in a representative infinite slope element. Another goal of this task was supplying a tool for numerically simulating 1D seepage in infiltration column tests (to verify laboratory data to assess HCF) and seepage and slope stability in laminar box tests (Fig. 5.1).

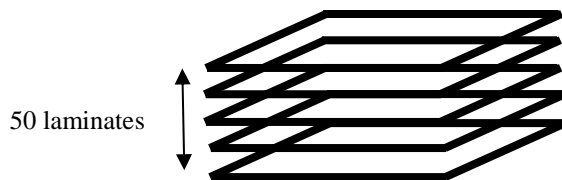


Fig. 5.1. Laminar box test setup representing a vertical slice in an infinite slope

5.1.1. Developed spreadsheets and Matlab codes

Microsoft Excel spreadsheets and then Matlab codes were developed to model seepage and slope stability for a representative element of infinite slope in unsaturated soils. The code has flexibility such that different hydraulic soil property models (e.g. different SWCC and HCF models), different element sizes, different time increments and

different boundary conditions (e.g. infiltration and exfiltration) can be modeled by the user. The code contains a 1D seepage and an infinite slope stability calculation parts. In the 1D seepage calculation part of the code, upward/downward seepage due to head difference is calculated using Darcy (1930) flow rule. Slope stability is calculated using force equilibrium in soil elements and factor of safety against sliding is calculated on the planes between soil elements.

5.1.1.1. 1D seepage analysis

In the 1D seepage analyses part of the code, the main goal is to find the time-dependent pore water pressure changes in the ground during and after rainfall infiltration. For this, changing pore water pressures (and volumetric water contents) in soil elements are calculated using the initial unsaturated pore water conditions in the ground, and the relations between the suction and water content (SWCC), and hydraulic conductivity (HCF) and also the suction and. The main scheme of the code for seepage calculation process is shown in Fig. 5.2. The code starts with the input data on pore water pressure values or volumetric/gravimetric water content values in the soil. In the case of absence of appropriate input data, any of pore water pressure and volumetric water content

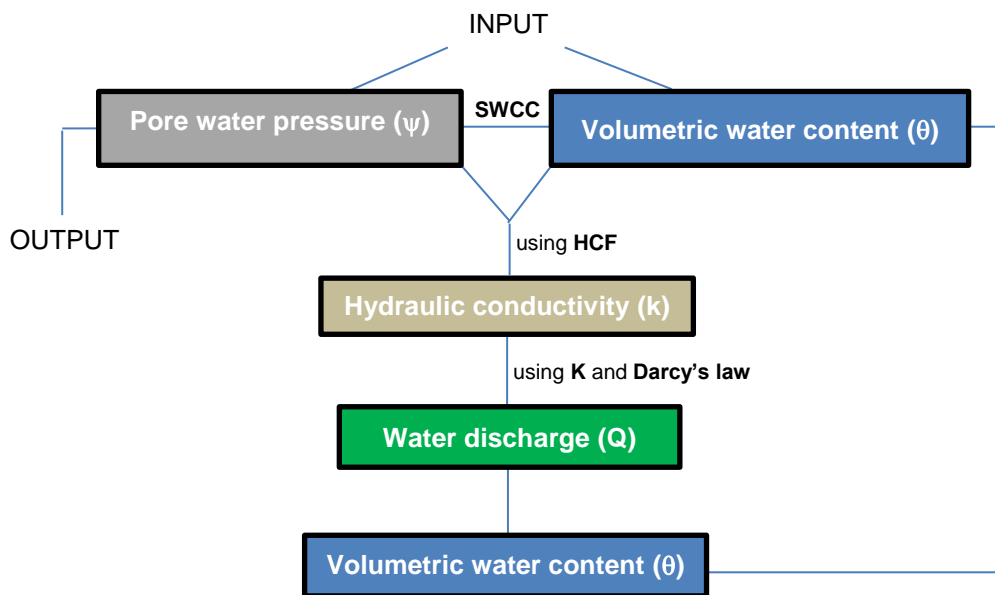


Fig. 5.2. The main scheme of the code for 1D seepage calculation process

values can be obtained by using preferred SWCC model. The input pore water pressure or water content values are used to calculate the hydraulic conductivity value by using the HCF function preferred by the user. Having hydraulic conductivity value and using Darcy flow law (1930) the water discharge from an element of soil to another element of soil can be assessed. This discharge would change the water content of elements which will result in changes in pore water pressure of elements. Changing pore water pressures also will change the head difference between the elements and the seepage will carry on. The output from this 1D seepage analyses is the pore water pressure in specific element(s) during and after rainfall infiltration. More detailed flowchart of calculations is also presented in Fig. 5.3.

5.1.1.2. Slope stability analysis

For stability investigation of a soil element in infinite slopes subjected to rainfall infiltration, limit equilibrium of forces on the plane between soil elements (laminates) were established incorporating Coleman's (1962) effective stress approach in unsaturated soils (see 2.1.4).

Fig. 5.4 shows an element of soil in an infinite slope subjected to rainfall and forces acting in this element. In this figure, γ_i is the unit weight and W_{soil} is the weight of the soil mass above the plane considered; $W_{\text{laminates}}$ is the cumulative weight of laminates; D is the driving force; S is the resisting force; α is the slope angle and ϕ_{laminate} is the friction angle between laminates.

Having volumetric water content value it is possible to calculate the changing unit weight of rainfall water infiltrated soil and then weight of soil mass divided by the sliding plane area can be used in calculating the driving force. Pore water pressure values are used in calculation of resisting forces (e.g. resisting forces due to suction). In laminar box tests, in the plane of sliding, friction between two laminates is also generating a resistance against sliding in addition to the soil resistance. Therefore, two resisting forces were considered in calculation of factor of safety and friction angle between each of the laminates are measured in the laboratory (explained in Chapter 4).

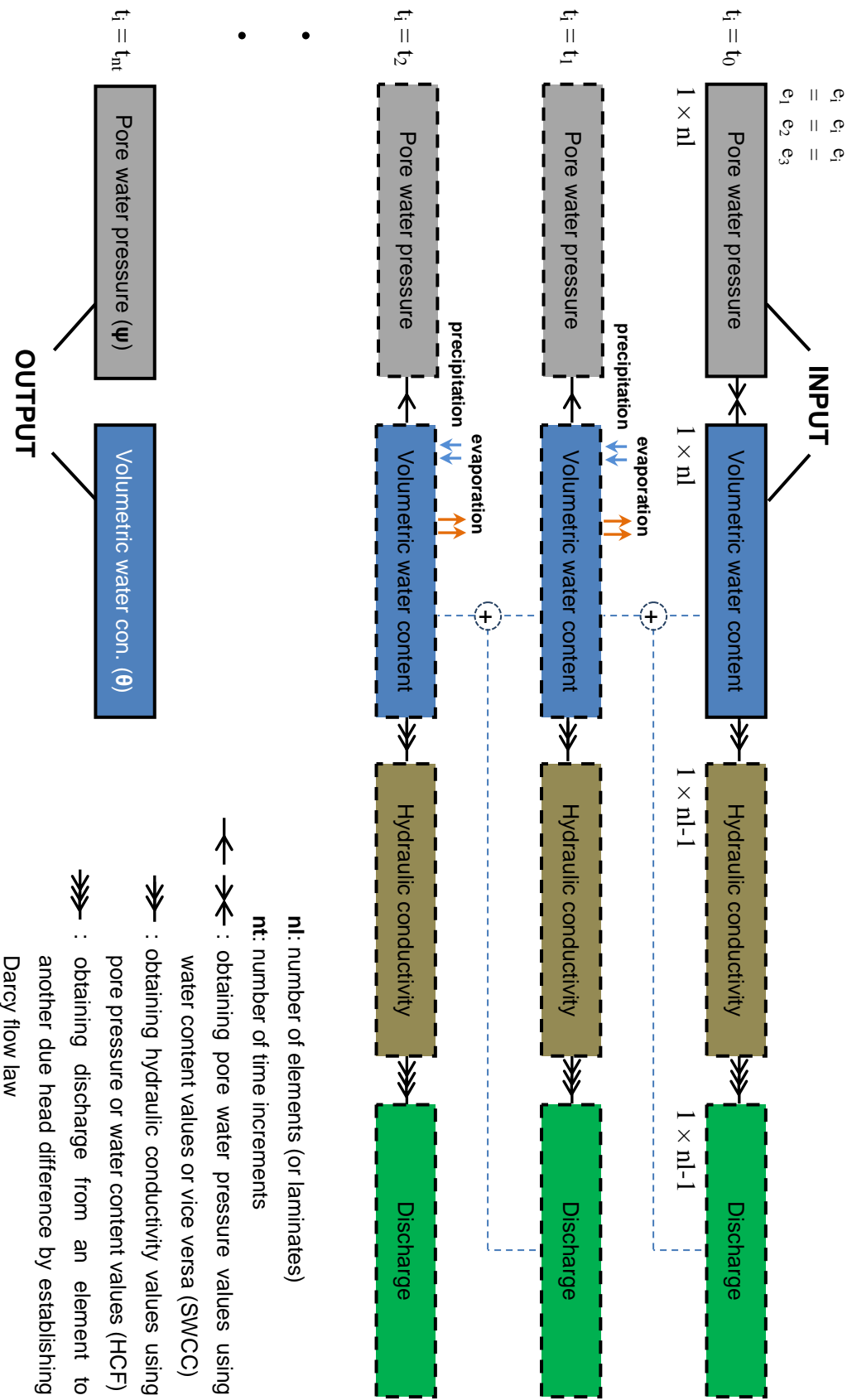


Fig. 5.3. Detail of calculations in 1D seepage analysis

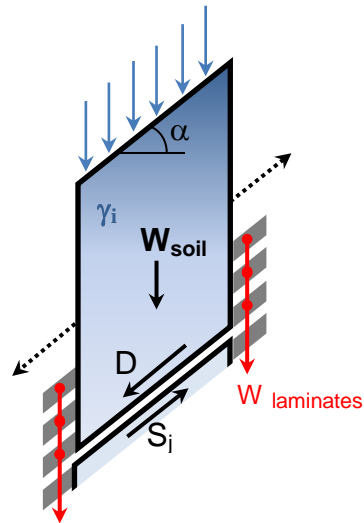


Fig. 5.4. A vertical slice of infinite slope subjected to rainfall infiltration

Fig. 5.5 shows the detail of calculations for slope stability analysis in an element of infinite slope. Developed Matlab code for seepage and slope stability analyses are presented in Appendix E.

5.1.2. Numerical simulation of laminar box tests

Using the spreadsheets and Matlab code, numerical simulation of seepage and stability for an infinite slope element can be carried out for the laminar box simulation.

The physical model is composed of a 40×40×40 cm cube of QS soil compacted in 34 % relative density and subjected to rainfall. Numerically simulated suction values at 4 locations within the soil element are compared with the measured suction values obtained from the laminar box test.

The major inputs for the current numerical simulation are summarized in Table 5.1 and Table 5.2. Obtained results are presented in detail in chapter 6.

Table 5.1. Inputs for numerical simulation of 1D seepage and stability in a laminar box test

Model Specifications	Nl:	40	Number of laminates
	Ll:	0.01	length (height) of laminates (m)
	tse:	5	duration of time steps at evaporation (sec)
	tsr:	2	duration of time steps at rainfall (sec)
	ne:	180	requested analysis time in evaporation (min)
	nr:	150	requested analysis time in rainfall (min)
	Si:	30	constant initial suction (kPa)
	alfa:	40	initial inclination of setup (°)
	Side:	0.4	internal sides of laminates (m)
	Sidew:	0.02	width of sides of laminates (m)
	Ir:	1.111e-5	Rainfall intensity (m/sec)
	Ie:	0.2e-9	Evaporation intensity (m/sec)

Table 5.2. Inputs for material properties

Material Properties	Gd:	13.75	Dry unit weight of soil (kN/m ³)
	Gw:	9.807	Unit weight of water (kN/m ³)
	phi:	30.3	Internal friction angle (°)
	c:	0	Apparent cohesion (kPa)
	phl:	18.5	Friction angle between laminates (°)
	phb:	phl/2	Internal friction angle (°)
	Ts:	0.484	Saturated volumetric water content
	Tr:	0.05	Residual volumetric water content
	a:	7.5	SWCC - Fitting parameters for Fredlund & Xing (1994)
	n:	3.6	
	m:	2.0	
	Sair:	150	
	Ks:	2.5e-7	HCF - Leong & Rahardjo (1997)
P:	4		

5.2. 2D seepage and stability analyses in finite slopes

SEEP/W and SLOPE/W applications from Geo-studio 2007/2012 software package are used to simulate seepage and slope stability numerically in finite slope experiments (i.e. flume tests). In the following sections more details about the numerical model definition

and analyses are presented. The outputs from simulations are suction distribution in the soil body at different depths and locations and at different times after the start of rainfall, the factor of safety versus time and the failure surface (if any).

5.2.1. Model definition

- Analyses type

Several different analyses types are predefined in SEEP/W and SLOPE/W such as steady state, transient and coupled seepage and stability analyses can be conducted.

In the current study due to mechanism of time-dependent seepage in rainfall triggered slope instabilities, a transient analysis is selected. Because of the immediate relation between the slope stability and unsaturated shear strength to rainfall infiltration and related pore pressure changes in the ground, the seepage analysis by SEEP/W is the main (parent) analysis for the stability analysis by SLOPE/W.

In the laboratory physical models, as part of the sample preparation procedure, the soil samples (after they are placed into the flume or laminar box setups) are covered and left for at least 24 hrs for equilibration of suctions in the samples. After this equilibration/equalization time, raining is started. Therefore, to represent this equalization (waiting) time period, another seepage stage is added in the numerical analyses to the beginning of the analyses. This initial analysis is named as “equalization stage” and the equalized suction values (e.g. the outcome of equalization stage) were considered as the initial suction values in the soil model at the beginning of raining.

Time intervals are selected and set at the beginning of the numerical analyses. For equalization stage due to small rate of changes in water flow and closed boundaries, the time increments of 60 minutes were considered. But for the main seepage analyses time increments were different considering applied rainfall intensity.

To perform slope stability analyses in finite slopes throughout the thesis, Morgenstern-Price methods of slices is used as the slope stability analysis method in SLOPE/W.

- Geometry

The final geometry of the soil specimen is drawn in AutoCAD and then it is imported to SEEP/W 2012 software which was available in METU geotechnical division to perform seepage analyses. Fig. 5.6 shows the geometry and boundary conditions defined in SEEP/W 2012 for FLM_04 flume test, as an example.

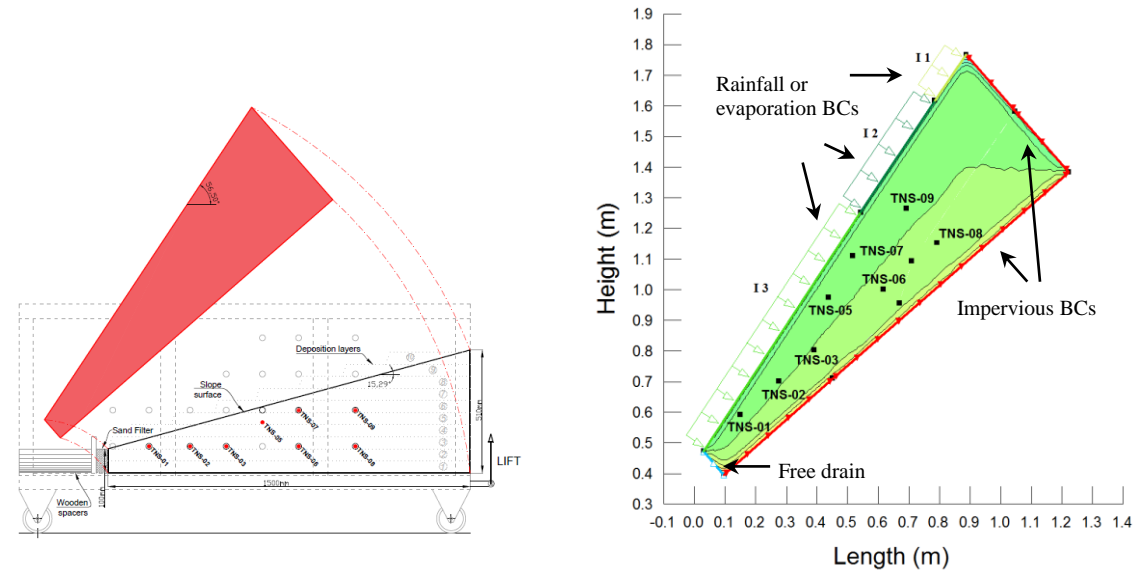


Fig. 5.6. Geometry and boundary conditions for FLM_04 flume test

5.2.1.1. Boundary conditions

- Rainfall BCs

Applied rainfall over flume experiments in the laboratory is simulated as a boundary condition in the numerical models. The boundary conditions (BCs) in SEEP/W 2012 could be defined as a constant or time dependent function, while in the current research a rainfall boundary which was constant with time is used.

The applied rainfall in the flume test setup is measured to have a non-uniformly distributed intensity over the length of the slope (Fig. 5.6). In the numerical analyses, one option was to consider an average rainfall intensity to be applied to the whole slope, and the second option was to use different rainfall intensity values on the slope to more realistically represent the different intensities in the slope length in the flume tests. The

second option is preferred in this study, i.e. the rainfall BCs with different intensity values are used along the slope length. The method for assessment of rainfall intensity distribution over the slope length of different slope angles is described in section 4.2.1. Fig. 5.7(a) shows a sample rainfall intensity diagram along the length of the slope. For simplicity three rainfall intensity values are used to numerically model this rainfall as shown in Fig. 5.7(b).

Each slope angle had a specific rainfall intensity distribution, for example the rainfall intensity distribution shown in Fig. 5.7 is used in all the slopes with 56.1 degree inclinations. For modeling different rainfall intensities (different spraying times), before each test, the rainfall intensity measurements is done by placing some tares over slope

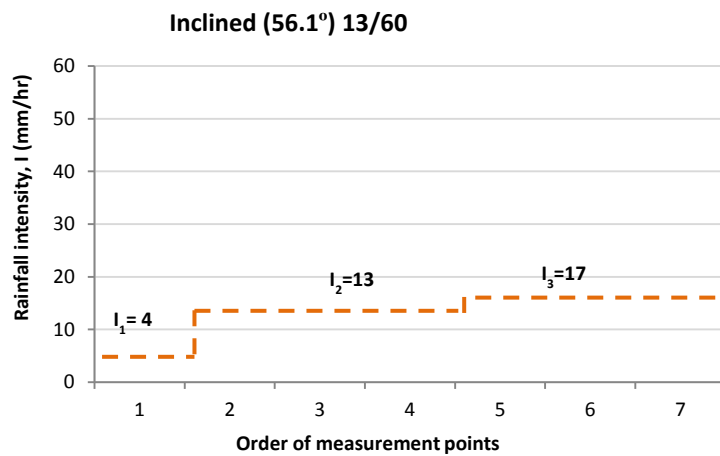
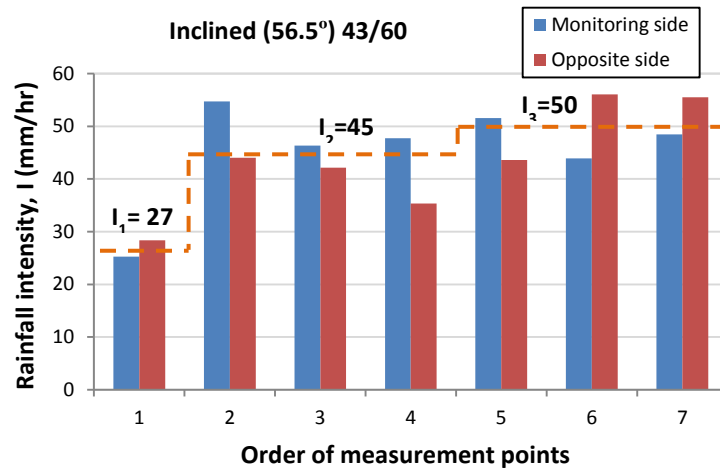
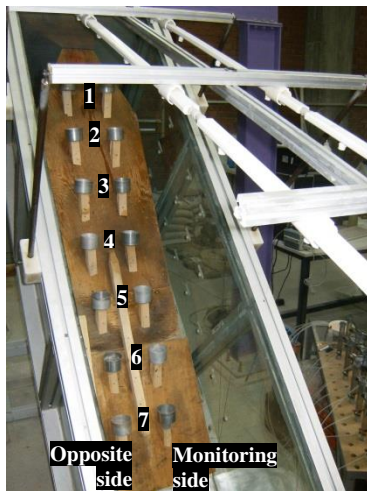


Fig. 5.7. (a) Assessment of rainfall intensity distribution over an inclined slope, (b) normalized rainfaling pattern on the FLM_03 test

(Section 4.2.4). Average of measured intensities (by tares) is used then to normalize rainfall pattern of the specific slope angle. Fig. 5.7(b) shows the normalized rainfall pattern for test FLM_03. Rainfall intensity patterns for all the flume tests are shown in Table 5.3.

- Impervious BCs

Side and bottom boundaries are assigned as impervious by setting constant hydraulic discharge as zero.

- Free drain BCs

SEEP/W 2012 has boundary type that can model free drain effect in seepage analyses. For simulation of the flume experiments with filter material in the downstream boundary, free drain BCs with the (Total flux, $Q=0$ and constant head, $H=0$) are used in current research.

5.2.1.2. Material properties

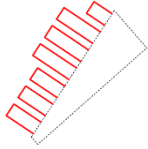
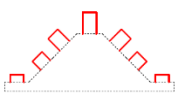
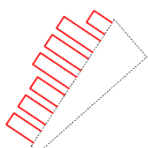
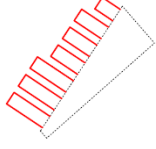
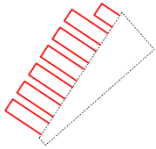
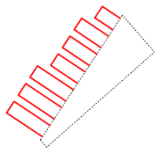
To perform seepage and slope stability analyses numerically, considering the state of rainfall triggered landslides in which slopes are variably saturated, unsaturated soil properties obtained from the laboratory tests has to be assigned to the material properties in the numerical models. To perform seepage analyses SWCC and HCF of the unsaturated soil are needed and for slope stability analyses, unsaturated shear strength properties are essential. In current research, considering the relative density of soil sample, preferred hydraulic (SWCCs and HCFs) and shear strength properties are assigned to the models (see chapter 6).

5.2.2. Analyses

Numerical simulation of flume model tests includes three numerical analyses (e.g. Equalization, Seepage and slope stability).

At equalization stage, initial suction is the average of suction values recorded via tensiometers immediately before raining starts. The outcome from this analyses (e.g. the suction distribution in the soil model after at least 24 hr being left in test position /

Table 5.3. Applied rainfall intensity for any of flume tests

Flume tests	Average rainfall (mm/hr)	Local rainfall intensity (mm/hr)				Shape
		I ₁	I ₂	I ₃	I ₄	
FLM_00	10.6	6	14	10	-	
FLM_01	4.1 24.8	9	10	12	14	
FLM_02	10.6	3 18	3.5 21	4.5 27	5 29	
FLM_03	54.4	30	66	47	-	
FLM_04	46.3	29	49	54	-	
FLM_05	28.3	17	31	-	-	
FLM_06	15.6	9	17	-	-	
FLM_08	21.6	12	23	-	-	
FLM_09	59.6	29	59	78	-	
FLM_10	63.0	31	62	83	-	
FLM_11	28.9 66.7	14 33	28 66	38 87	-	
FLM_12	48.8	33	66	87	-	
FLM_13	25.5	21	26	34	-	
FLM_14	26.0	21	26	34	-	
FLM_15	20.2	16	21	23	-	

inclination) was used as the initial condition (initial suction values) in seepage analyses.

Using seepage analyses changes in suction during raining is modeled. Therefore, more than the suction distribution during raining, suction changes at specific points

within the slope (e.g. location of tensiometers and pore water pressure transducers) can also be assessed.

Calculated (simulated) suction values for any soil element is later used in assessment of unsaturated shear strength which is a function of suction value (or volumetric water content). Slope stability analysis is then performed having unsaturated shear strength parameters and updated unsaturated soil density. Using slope stability analyses, the time to failure and failure slip surface is assessed for each finite slope analyses. Details of results from slope stability analyses are presented in section 6.3.

5.2.3. Calibration of Hydraulic properties

Considering possible heterogeneity in sample preparation in laboratory tests for assessing HCF and comparison of obtained results from numerical simulation of seepage in slope models with recorded suction values in flume experiments, a need for calibration of unsaturated soil properties understood.

Laboratory measured SWCC of QS soil at different dry densities did not have to be calibrated, while HCF data needed calibration since the observed differences in suction values recorded by tensiometers and pore water pressure transducers and simulated suctions using numerical model. The other reason for need for calibration was unavailability of HCF for sample with 48% relative density (required duration of a typical HCF test is 2-2.5 months). Therefore HCF for samples of relative density of 48% obtained using back analysis of a flume test.

Fig. 5.8 shows obtained HCF from laboratory test data and calibrated HCF using FLM_06 test data. Fig. 5.9 shows the simulated pore water pressures using calibrated HCF versus measured suction values in tensiometers in the flume test. HCFs of samples with 34% and 48% relative density are presented in chapter 6.

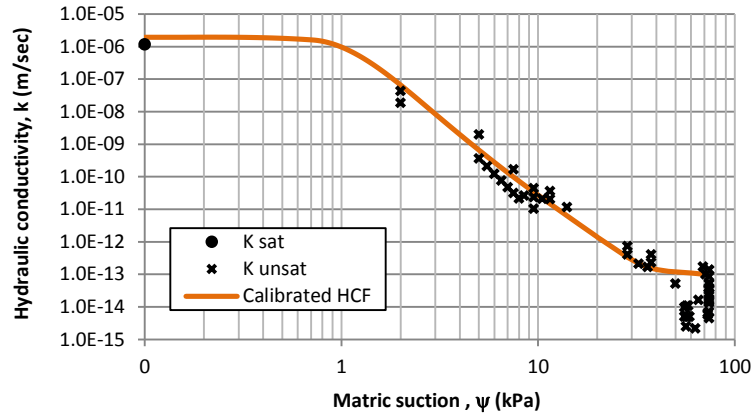


Fig. 5.8. Calibrated HCF of QS soil ($R_d:34\%$)

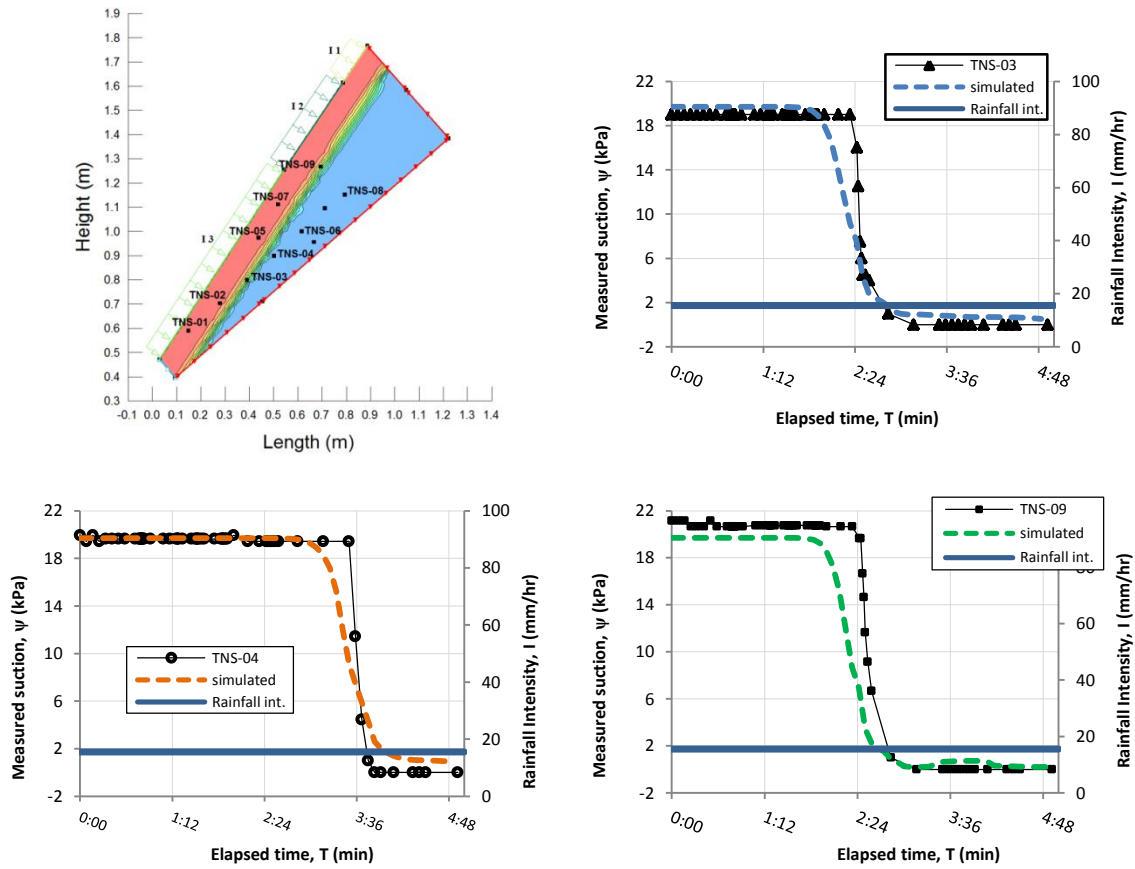


Fig. 5.9. Simulated pore water pressures using calibrated HCF and measured suction for TNS-06

CHAPTER 6

RESULTS OF TESTS AND NUMERICAL SIMULATIONS

This chapter presents results from all experimental activities and numerical simulations in the thesis. It contains details of the results from index tests for the materials used throughout the research, calibration details of the apparatuses, details of the flume tests and laminar box tests's results.

6.1. Material index test results

Detailed material properties of employed QS soil (quartz sand) are obtained using different routine geotechnical and an unconventional test and their results are presented in this part. Fig. 6.1 shows the particle size distribution of the QS and more detailed results are presented in Table 6.1.

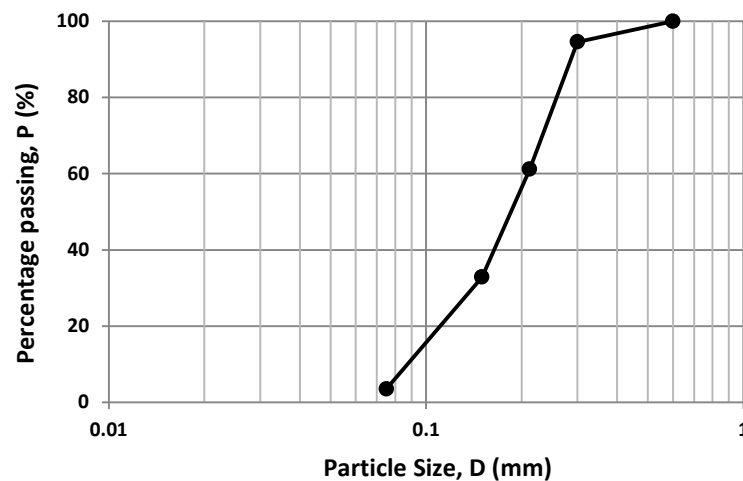


Fig. 6.1. Particle size distribution of QS

Minimum dry density of the sand in the moist state needs to be determined because the samples are prepared in laboratory tests at a moisture content of 1.5%. As described in

section 4.1, four cubes of Plexiglas filled with different soils of different dry density are subjected to rainfall to assess minimum dry density with negligible volume change under rainfall. Table 6.2 presents the obtained results.

Table 6.1. Some geotechnical properties of QS

D ₁₀ (mm) :	0.09	C _c :	1.08	G _s :	2.663
D ₃₀ (mm) :	0.14	C _u :	2.24	Y _{d max} :	1.648 g/cm ³
D ₅₀ (mm) :	0.18	PI (%) :	N.P.	Y _{d min} * :	1.332 g/cm ³
D ₆₀ (mm) :	0.202	USCS Soil Classification:	SP	K _{sat} :	1.145e-6 m/sec

* Y_{d min} here is obtained from ASTM D4253.

Table 6.2. Settlement after rainfall, in minimum dry density checkup cubes

Box NO	Dimensions (mm)	Dry density (g/cm ³)	Settlement after rainfall (mm)	Relative volume change (mm/mm)
#	L × W × D	Y _d	s	s/D
1	203×204×216	1.05	34	0.157
2	204×202×215	1.15	3	0.014
3	199×200×199	1.25	0.6	0.003
4	198×199×199	1.35	0.2	0.001

Reviewing obtained results it is understood that minimum dry density of QS in wet state is around 1.05 g/cm³ but the dry density which no significant volume changes due to rainfall will be around 1.20 g/cm³.

As other parameters that would be used in calculation of relative density of the samples, minimum and maximum void ratio of QS are also calculated (e_{min}=0.616 and e_{max}=1.536) using volume-mass relations.

6.1.1. SWCCs of QS soil

Three wetting SWCCs (in different dry densities of 1.20, 1.27 and 1.37 g/cm³) and a drying SWCC of QS soil are presented in this section. To do so, obtained suction-gravimetric water content pairs from SWCC assessment methods employed in current research (see section 4.1.1) are plotted. Using volume-mass relations suction-volumetric water content forms of SWCCs are also extracted (Fig. 6.2)

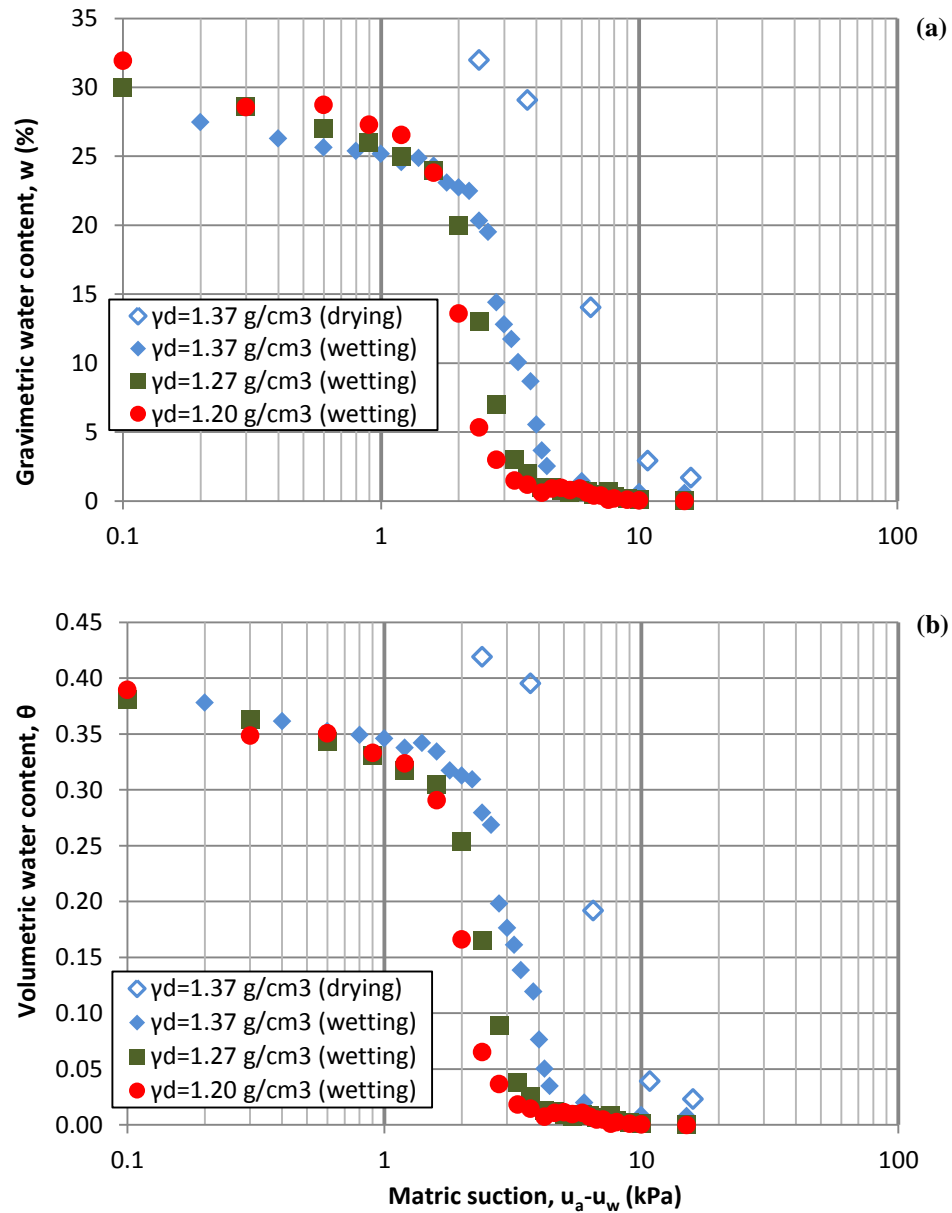


Fig. 6.2. Drying and wetting SWCCs of QS soil in (a) suction-gravimetric water content and (b) suction-volumetric water content space

To be used in numerical simulations, it was required to have experimental data in the form of one of the well-known SWCC models. Therefore, Fredlund & Xing (1994) model is fitted to any of the obtained data and the results are presented in Fig. 6.3. Assessed curve fitting parameters for each of SWCCs are also summarized in Table 6.3.

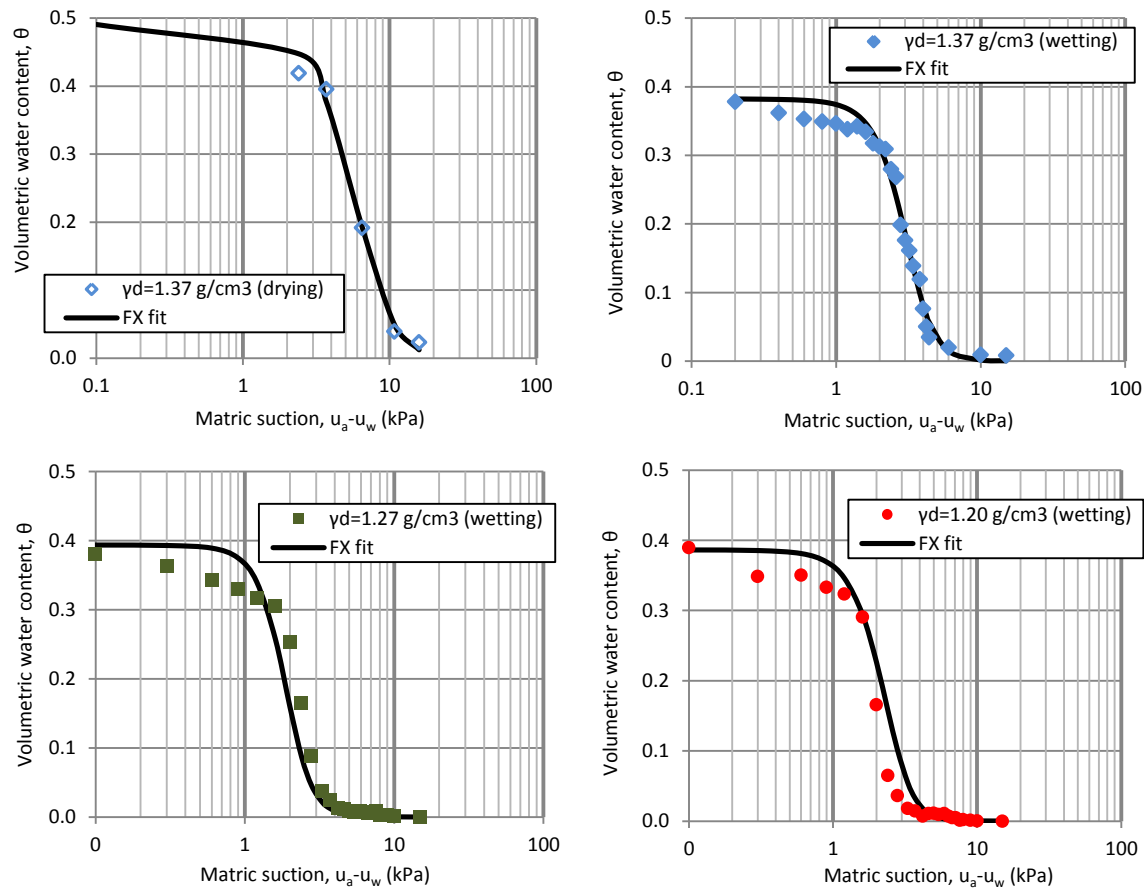


Fig. 6.3. Fx (Fredlund and Xing, 1994) fit to experimental data of SWCC

Table 6.3. Summary of fitting parameters for Fredlund and Xing (1994) SWCC model

	type	γ_d (g/cm ³)	SWCC fitting parameter			
			θ_s	a	m	n
QS soil SWCCs	Drying	1.37	0.484	7.50	4.50	2.55
	Wetting	1.37	0.378	3.51	4.00	3.60
		1.27	0.381	2.78	4.72	3.34
		1.2	0.39	2.05	3.50	4.10

6.1.2. Assessment of HCF for QS soil

More calculations are needed to assess the velocity of water transition through an unsaturated soil sample in different suctions (HCF) rather than assessing SWCC. Indeed, obtained raw data from infiltration column tests (suction values recorded in time

intervals as the water seeps into the unsaturated soil) needs to be first used to obtain corresponding water contents from SWCC and then, inserted in the governing flow equations to assess hydraulic conductivity. Fig. 6.4 shows measured suctions with time at different depths in the soil as measured by tensiometers TNS-01 to 05, in one of the infiltration column tests and correspondent volumetric water content changes plot (obtained from its SWCC). Plot of hydraulic conductivity values versus suction at each interval will give the HCF of the unsaturated soil sample.

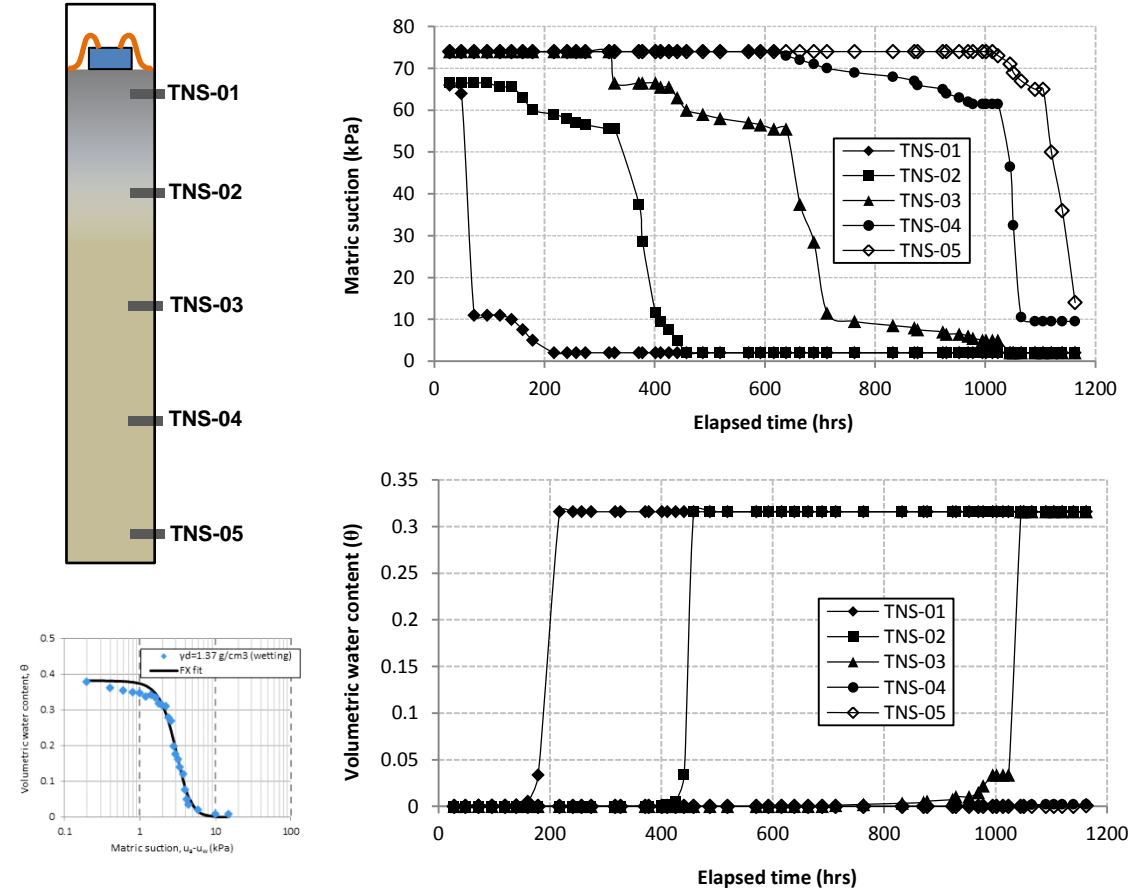


Fig. 6.4. (a) Sketch of infiltration column test (setup explained in more detail in Chapter 4), (b) used SWCC for assessing volumetric water content using suction values, (c) Matric suction and (d) volumetric water content changes with time

Establishing Darcy flow equations between any two tensiometer stations in the infiltration column setup can be used to obtain pairs of suction (ψ) and hydraulic conductivity (k) at any time increment. Calculation steps presented in Table 6.4 are

followed in the current research to obtain hydraulic conductivity (k) at any station in infiltration column subjected to water infiltration and obtained data are plotted in Fig. 6.5. Calibrations for these data were also assessed using suction responses in FLM_06, FLM_09 and FLM_10 laboratory flume tests.

Table 6.4. Unsaturated hydraulic conductivity calculation procedure

Matric Suction	ψ	kPa	ψ_s	recorded by tensiometers
Volumetric Water Content	θ	-	θ_s	assessed from suction values using corresponding SWCC
Hydraulic gradient	$\Delta h/\Delta z$	m/m	$\left(\frac{\Delta h}{\Delta z}\right)_{s,s+1} = 1 + \frac{1}{\gamma_w} \left(\frac{\psi_{s+1} - \psi_s}{z_s - z_{s+1}}\right)$	head difference between stations
Volume of water downstream	ΔV	m^3	$\Delta V_{s,s+1}^t = A \sum_{s=1}^n (\theta_s^{t+1} - \theta_s^t)(z_{s+1} - z_s)$	volume of the water that flowed downward from a station summing volumetric water change at any of stations in downstream*
Instantaneous hydraulic conductivity	k	m/s	$k_t = \frac{\Delta V_{s,s+1}^t}{A \Delta t \left(\frac{\Delta h}{\Delta z}\right)_{s,s+1}}$	hydraulic conductivity can be assessed between any stations

* A: infiltration column area

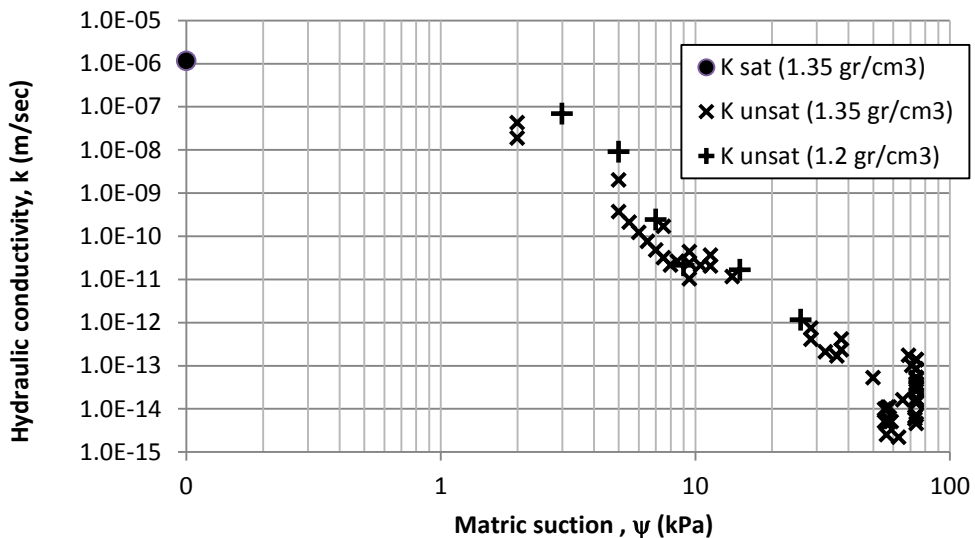


Fig. 6.5. Hydraulic conductivity of QS soil obtained from infiltration column test for relative densities of 34% and 61%.

6.1.3. Results of shear strength tests on QS soils

As described in section 4.1.3, a number of water content controlled direct shear tests are performed to assess the shear strength of QS soil in variably saturated conditions. Obtained data from the tests and processing of data are described in the present chapter.

Similar to conventional direct shear tests, generated shear force and settlement/swelling of top cap are plotted versus horizontal shearing displacement for each test (Fig. 6.6). In addition, water content values are also recorded before and after test at different parts of the sample to monitor water content changes (if any) during the test.

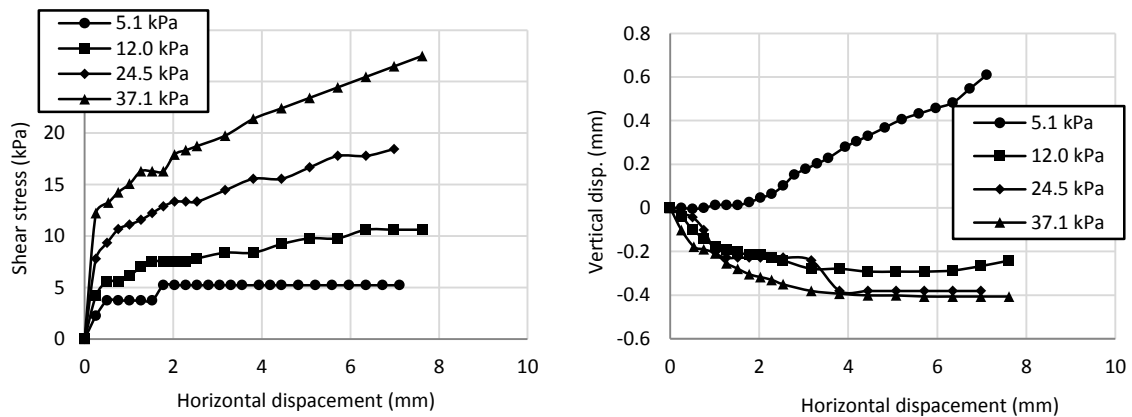


Fig. 6.6. Generated shear force and settlement/swelling in water content controlled direct shear tests (numbers in the legend are normal stresses)

As the failure criteria, similar to conventional direct shear tests, maximum developed shear stress is considered as “failure”. This is also proved by the volume change behavior of the tests in critical state. Shear force and settlement/swelling behavior for all of direct shear tests are available in Appendix F.

Repeating tests in different normal stresses, cohesion (c) and internal friction angle of samples (ϕ) are assessed plotting test results in normal/shear stress plain. Fig. 6.7 shows shear strength properties of QS sand at different dry densities and at different water contents.

Water content values recorded at the beginning and at the end of each of direct shear tests are also reported in Appendix F. As an example, in test DST-P-1%-1.2-37 (1%: initial water content, 1.2: dry density (g/cm^3) and 37: normal stress (kPa)) water content

shows less than 1% difference between the beginning and end of the test. Therefore the direct shear tests can be considered to be conducted at practically constant water content.

Although there are some discrepancies (especially at low normal stresses such as 5 kPa) it can be observed from the trendlines in Fig. 6.7 that, increasing suction (reducing water content) in the current sandy material, in general, causes slight increase in shear strength.

6.2. Flume Test Results

As part of current research, the results obtained from numerical seepage and stability simulations are tried to be verified experimentally in laboratory model tests. Another goal of the current study is to experimentally obtain the rainfall intensity-duration threshold for triggering landslides in unsaturated soils and to observe the relation between its intensity and duration. Values to be verified are: as the rainfall infiltrates into the soil, i.e. as the pore water pressure in the ground changes, the progression of the wetting front with time, development of the failure surface and the time to failure. In the following sections details of recordings of these values in laboratory flume tests are described.

6.2.1. Pore water pressure response

During the flume tests, pore water pressures within the soil samples are measured using an array of pore pressure transducers and tensiometers. Recorded pore water pressures, in the soil at different locations, are plotted with time after the start of raining. Fig. 6.8 shows the pore water pressure response in any of the measurement points for FLM_04 flume test. Time needed for the water to infiltrate and to reach to tensiometers and duration for the suctions to reduce to zero can be assessed referring to pore water pressure response charts prepared for each flume test. Graphs for all the tests are presented in Appendix B.

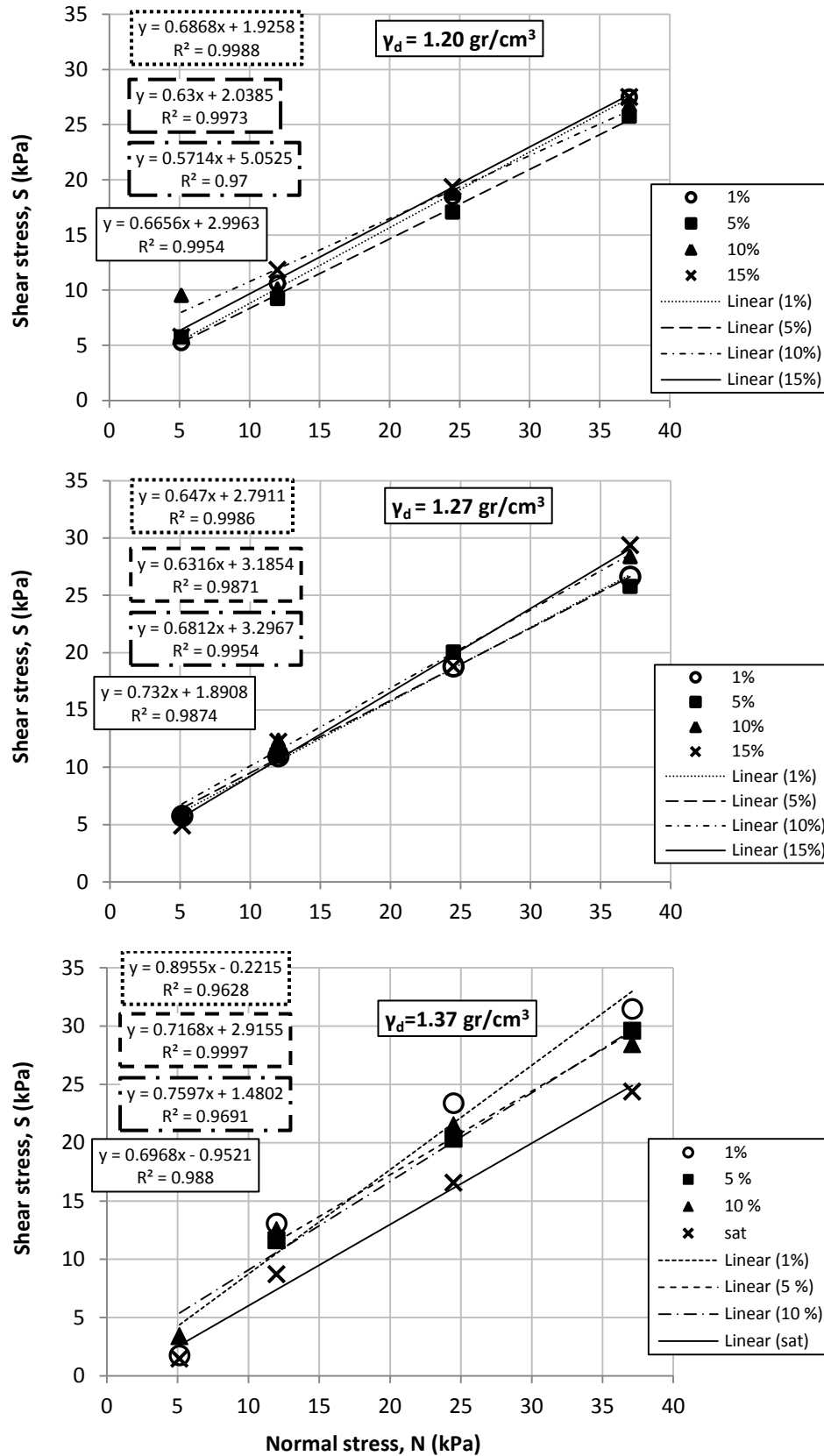


Fig. 6.7. Water content controlled direct shear test results on QS

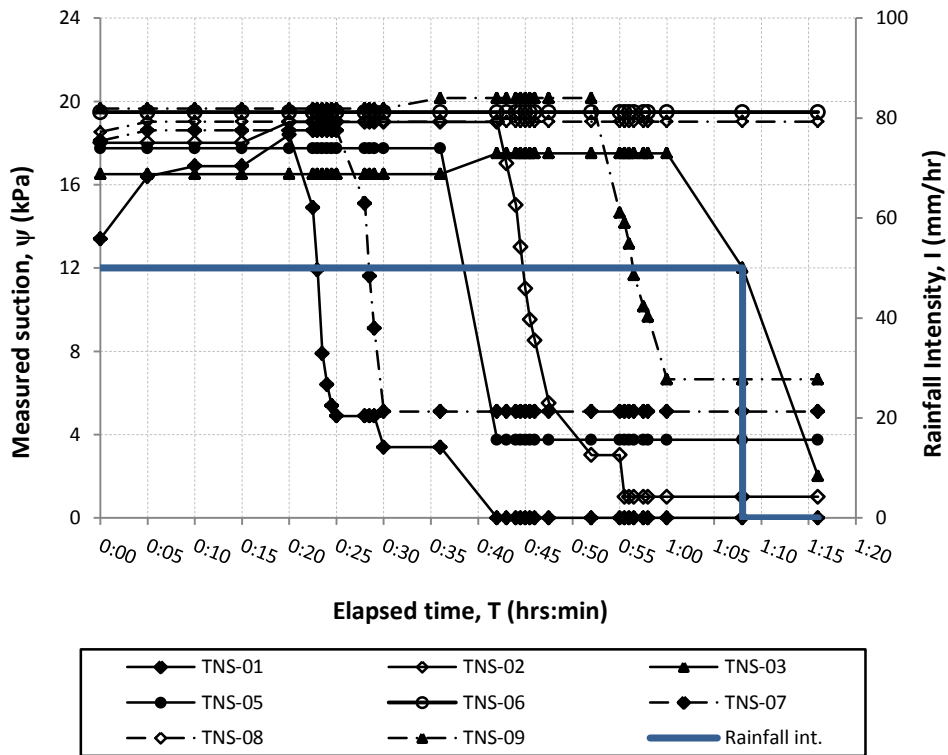
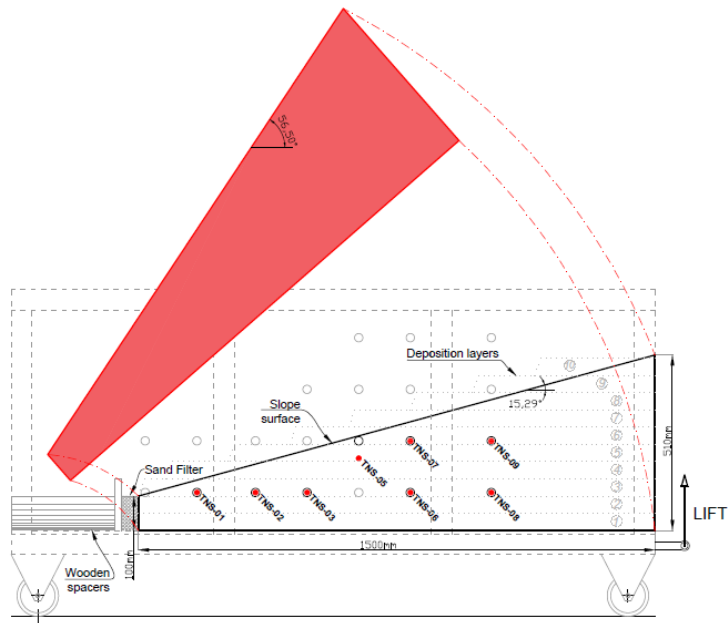


Fig. 6.8. (a) Location of instrumentation and (a) pore water pressure response to raining for FLM_04.

6.2.2. Wetting front

Wetting front progress as the rainfall infiltrates in slopes is another parameter that is recorded in laboratory flume tests. Wetting front recordings more than being used in study (verification) of numerical simulations, was also useful in assessment of difference in wetting front progress in the middle and in the sides of the flume experiments.

In order to assess the progression of wetting front with time for the flume tests, the vertical distance between the wetting front (i.e. the depth where the suction drops to zero) and the base of the flume setup were recorded from time to time (generally once every 20 minutes and faster recordings in tests with higher rainfall intensities) at 11 vertical sections in the flume box. Fig. 6.9 shows the progress of wetting front with time for FLM_06 flume experiment. Appendix B summarizes the wetting front charts for all the flume tests.

6.2.3. Failure surface

Specifications of failure surfaces (e.g. shape, depth and configuration of moved mass) are of significant importance in slope instability studies and generally can reflect triggering mechanisms.

In the current research, projection of failure surface on monitoring side of the flume box is recorded as the depth of sliding and the shape of the failure surface in flume experiments. In addition to these measurements, photos taken from the failed slopes, from the side view and top view are also used to assess the configuration of failure surface.

A set of miniature, in-house-developed primitive inclinometers (elastic ropes) also are used in flume experiments in the current study to detect the depth of sliding and the amount of movement. An array of inclinometers in the slopes were set in a way that recordings from different longitudinal and cross sections would be taken. Fig. 6.10 shows inclinometer recordings for the failure surface in FLM_08 flume test. Some side view and top views from the failed slope are also presented in Fig. 6.10. Detailed failure

surface loci on monitoring side of the flume box are presented in Appendix B for all the flume tests.

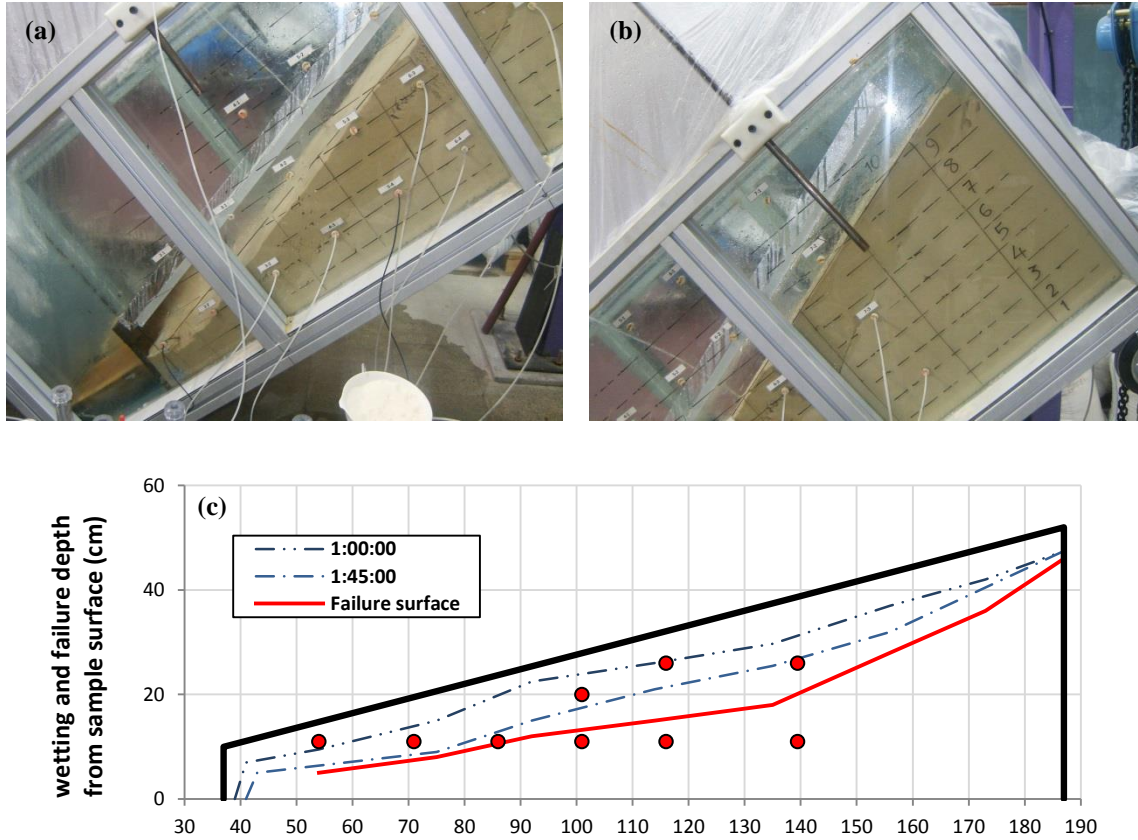


Fig. 6.9. (a & b) Location of vertical sections for measuring the depth of the wetting front and (c) the location of the wetting front at 1 hour and 1 hour+45 minutes after the start of rainfall in FLM_06 in response to rainfall infiltration (circle symbols show the location of tensiometers and pore pressure transducers)

6.2.4. Time to failure

Understanding the time that is left until failure after initiation of a rainfall over a slope plays a critical role in application of early warning systems. In the current research, the “time to failure” is considered as the “time to occurrence of major deformations in the soil” after the start of rainfall in the flume tests. Values of time to failure for flume tests are summarized in Table 6.5.



Fig. 6.10. (a) Failure surface projection on monitoring side wall of the flume box, (b, c & d) side and top views of the failed mass (M: middle inclinometers, W: wall inclinometers) for FLM_08 flume test and (e) plot of inclinometers and emerging failure surface

6.3. Numerical simulations for flume tests

Response of slopes with known material properties and constant geometry subjected to different rainfall intensities is simulated numerically in the current study and obtained

results are tried to be verified experimentally in the laboratory by flume experiments. Results from numerical simulation of seepage and slope stability are presented in more details in the following sections.

Table 6.5. Time to failure in flume experiments

Test #	Average rainfall intensity <i>I</i> mm/hr	Time to failure <i>t</i> min	Test #	Average rainfall intensity <i>I</i> mm/hr	Time to failure <i>t</i> min	Test #	Average rainfall intensity <i>I</i> mm/hr	Time to failure <i>t</i> min
Relative density, $R_d = 34\%$			$R_d = 48\%$			$R_d = 61\%$		
FLM_03	54.4	48	FLM_10	63.5	103	FLM_00	10.6	-
FLM_04	46.3	60	FLM_11	28.9 & 66.7	- & 93	FLM_01	4.1 & 24.8	-
FLM_05	28.3	69	FLM_12	48.7	134	FLM_02	10.6	-
FLM_06	15.6	-	FLM_14	22	205	FLM_09	59.6	-
FLM_07	-	-	FLM_15	20	-			
FLM_08	21.6	74						
FLM_13	18	105						

6.3.1. Suction response

Changes in the pore water pressure in slopes is one of the key parameters that can affect the stability, especially for the triggering of landslides in unsaturated soils. Numerical simulation of seepage in unsaturated slopes makes it possible to study the pore water pressure changes in response to rainfall infiltration.

Figure 6.11(a) shows the suction distribution in the slope at FLM_04 flume test at the onset of failure as an example. For FLM_04 test, the soil relative density is 34%, the slope angle is 56.5 degrees and the applied average rainfall intensity is 46.3 mm/hr. By defining extra nodes on the numerical model, pore water pressure changes were also assessed in the location of the instrumentation (e.g. pore pressure transducers, PDCRs and tensiometers, TNSs). Figure 6.11(b) presents the numerically obtained suction values at different locations in the soil, with time after start of rainfall, for the flume experiment FLM_04.

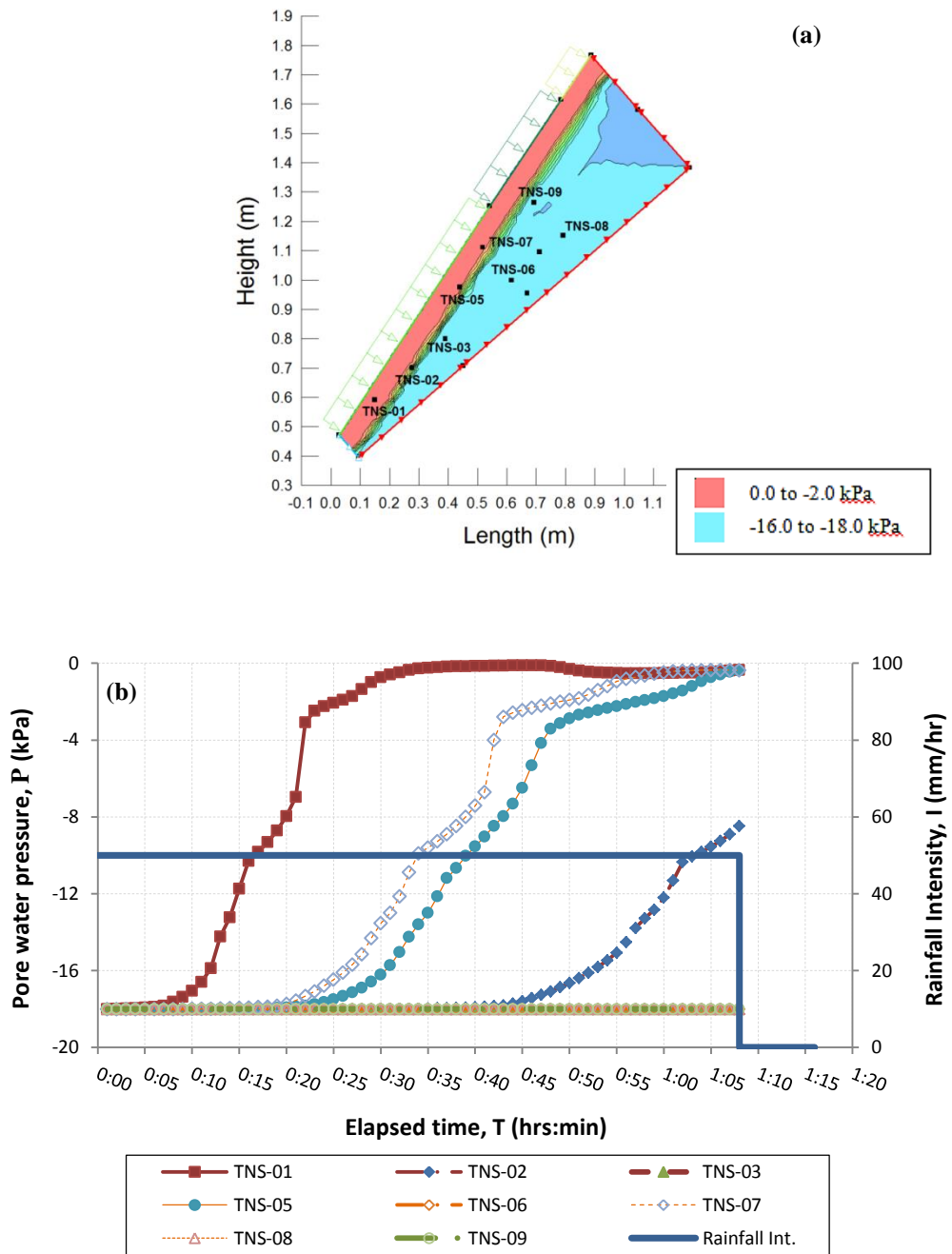


Fig. 6.11. (a) Pore pressure distribution in the slope at the time of failure for FLM_04 and (b) pore water pressure response to rainfall infiltration, at different locations in the soil with time

Appendix C includes numerically simulated behavior of slopes subjected to rainfall for all of the flume experiments.

6.3.2. Failure surface

Numerical assessment of the failure surface locus in 2D models was of high importance and a difficulty at the same time, in the current research. Simulation of the properties of the failure surface (e.g. the shape and the depth of failure surface) is performed incorporating the unsaturated shear strength of QS soil in slope stability analyses by SLOPE/W 2012.

Fig. 6.12 shows the slip surface at the time of failure for FLM_04 flume test, and the factor of safety value at the time of failure. Detailed failure surface loci in 2D slope stability modeling are presented in Appendix C for all the flume test simulations.

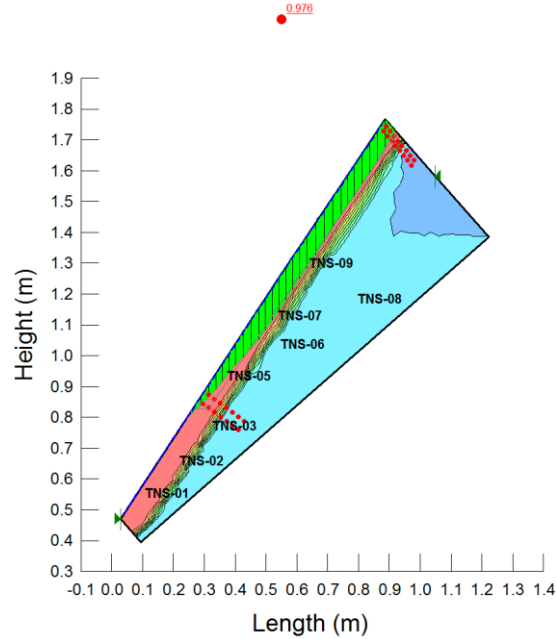


Fig. 6.12. Failure surface in 2D slope stability analysis for FLM_04

6.3.3. Time to failure

As it is a critical factor in simulation of behavior of rainfall triggered landslides, time to failure is investigated in numerical slope stability analyses in the current study. In current research, the time to failure is considered as time to reach the factor of safety equal to 1.0 in slope stability analyses. Fig. 6.13 shows changes in factor of safety with

time in flume slope for FLM_04 flume test. Also simulated time to failure values are summarized in Table 6.6.

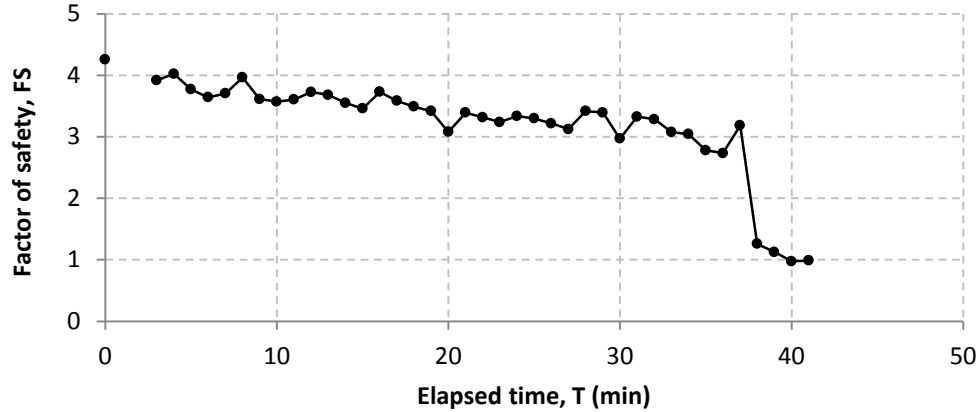


Fig. 6.13. Factor of safety versus time for FLM_04 flume test

Table 6.6. Time to failure (F.S. = 1.0) obtained from numerical simulations.

Test #	Average rainfall intensity <i>I</i> mm/hr	Simul. time to failure <i>t</i> min	Test #	Average rainfall intensity <i>I</i> mm/hr	Simul. time to failure <i>t</i> min	Test #	Average rainfall intensity <i>I</i> mm/hr	Simul. time to failure <i>t</i> min
Relative density, $R_d = 34\%$			$R_d = 48\%$			$R_d = 61\%$		
FLM_03	54.4	-	FLM_10	63.5	175	FLM_00	10.6	-
FLM_04	46.3	40	FLM_11	28.9 & 66.7	- & 93	FLM_01	4.1 & 24.8	-
FLM_05	28.3	48	FLM_12	48.7	295	FLM_02	10.6	-
FLM_06	15.6	-	FLM_14	22	186	FLM_09	59.6	-
FLM_07	-	-	FLM_15	20	-			
FLM_08	21.6	68						
FLM_13	18	46						

6.4. Laminar box tests

Obtained results from laminar box tests are limited to suction response to rainfaling and time to failure. Suction values are also simulated numerically while infiltration seepage is modelled using the developed Matlab code (see 5.1.1) and time to failure is assessed using slope stability analyses with SLOPE/W (see 5.1.2). In Fig. 6.14, as an example, measured and simulated suction values from LAM_1 are presented in detail. In LAM_1

test, the relative density of the soil is 61%, the slope angle is 30 degrees, and the rainfall intensity is 10.6 mm/hr. Simulation of changes in stability also shows that failure does not take place since the factor of safety has not fallen below 1.0. This was verified in laminar box test and no failure was observed.

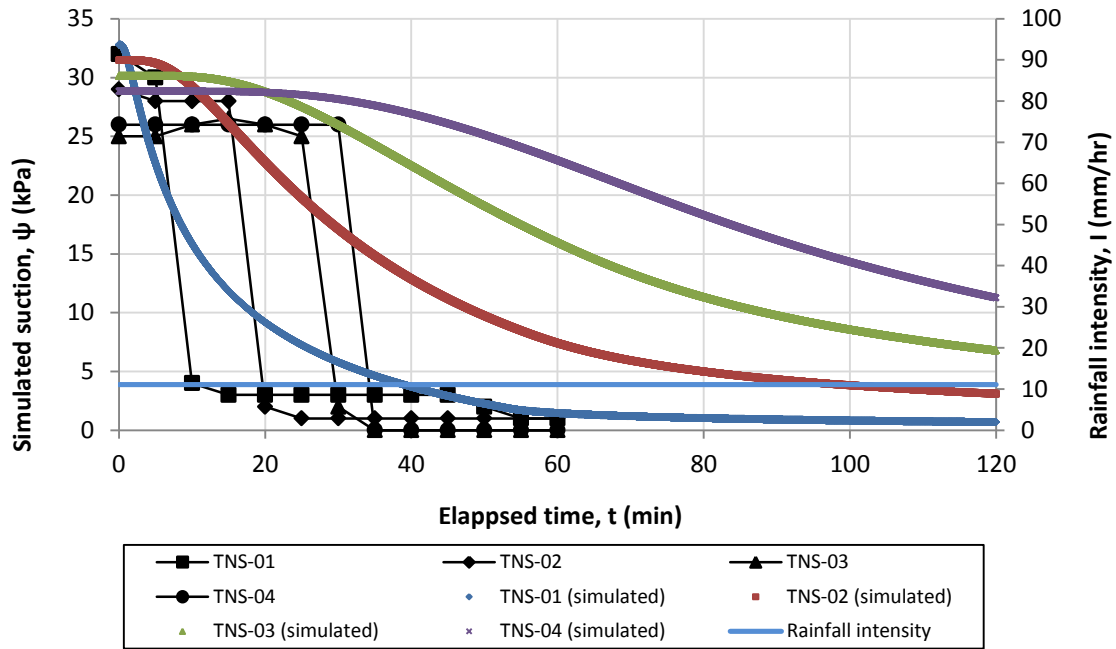


Fig. 6.14. Suction response in laminar box test and simulations (LAM_1 test)

CHAPTER 7

DISCUSSION OF RESULTS FROM EXPERIMENTS AND SIMULATIONS

Interpretation of findings from each of laboratory experiments is summarized in current chapter. Also the results from the numerical simulations are discussed here and compared with the results of the experiments. Discussions and comparisons are organized in seepage and slope stability subsections. At the end, plots of numerically and experimentally assessed rainfall intensity duration thresholds (I-D) are presented for two specific flume cases.

7.1. Seepage due to rainfall infiltration

7.1.1. Flume Experiments

Seepage in finite slopes due to rainfall which is simulated numerically by SEEP/W 2012 and verified with flume experiments are investigated considering pore water pressures and wetting front progress. In this section, comparison of measured and simulated pore water pressures are presented only for slopes with failure at the end of the test.

7.1.1.1. Pore water pressures

Simulated pore water pressures within infinite slopes are compared with measured pore water pressures (e.g. using tensiometers and PDCRs) in flume experiments. Appendix D summarizes detailed results from simulations and experiments (e.g. from Appendices C and B, respectively) and shows simulated and measured suctions at each measurement point in the flume.

For FLM_03 in which average rainfall intensity of 54 mm/hr was applied over a 56.5° degree slope with sample of 34% relative density, there exists a good agreement

between measured and simulated suction changes in the location of TNS-02 and TNS-04. Referring to Fig. 7.1, at the locations of TNS-05 and TNS-08, for a long period of time during the test no changes in suction values was observed and simulated and measured suctions remained the same.

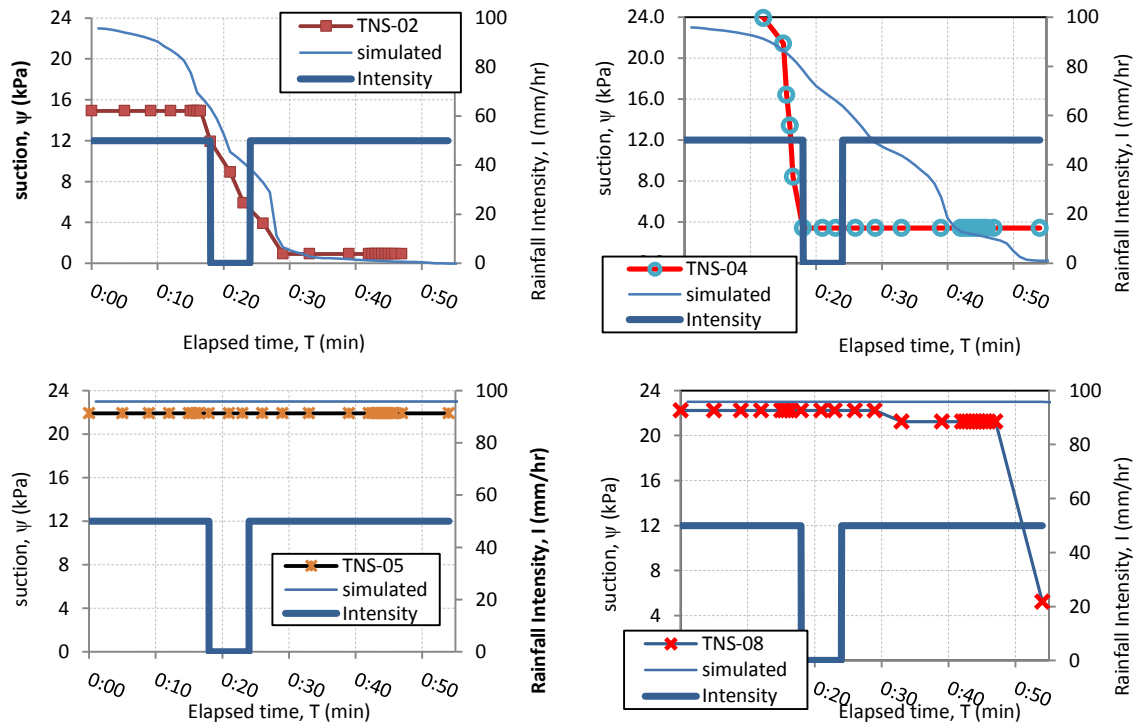


Fig. 7.1. (a) Measured and simulated pore water pressure changes in the location of instrumentations for FLM_03

At FLM_04, a soil sample with 34% relative density was subjected to 46 mm/hr rainfall intensity. Simulated suction values at the location of TNS-01, TNS-05 and TNS-07 shows a quite good match with recorded suctions. At TNS-08 and TNS-06 despite the agreement between the measured and simulated suctions, no suction loss was observed, meaning that the rainfall did not infiltrate enough to reach them (Fig. 7.2).

In another flume experiment with 56.5° degree slope, FLM_05, a lower intensity rainfall (28 mm/hr) was applied and continued till failure. TNS-02 and TNS-05 showed a suction response matching the simulated suctions, while in TNS-01 and TNS-07 there is a time lag between the measured and simulated suction values. This could happen

because of slight changes in relative density of soil samples in the vicinity of tensiometers or in the infiltration route.

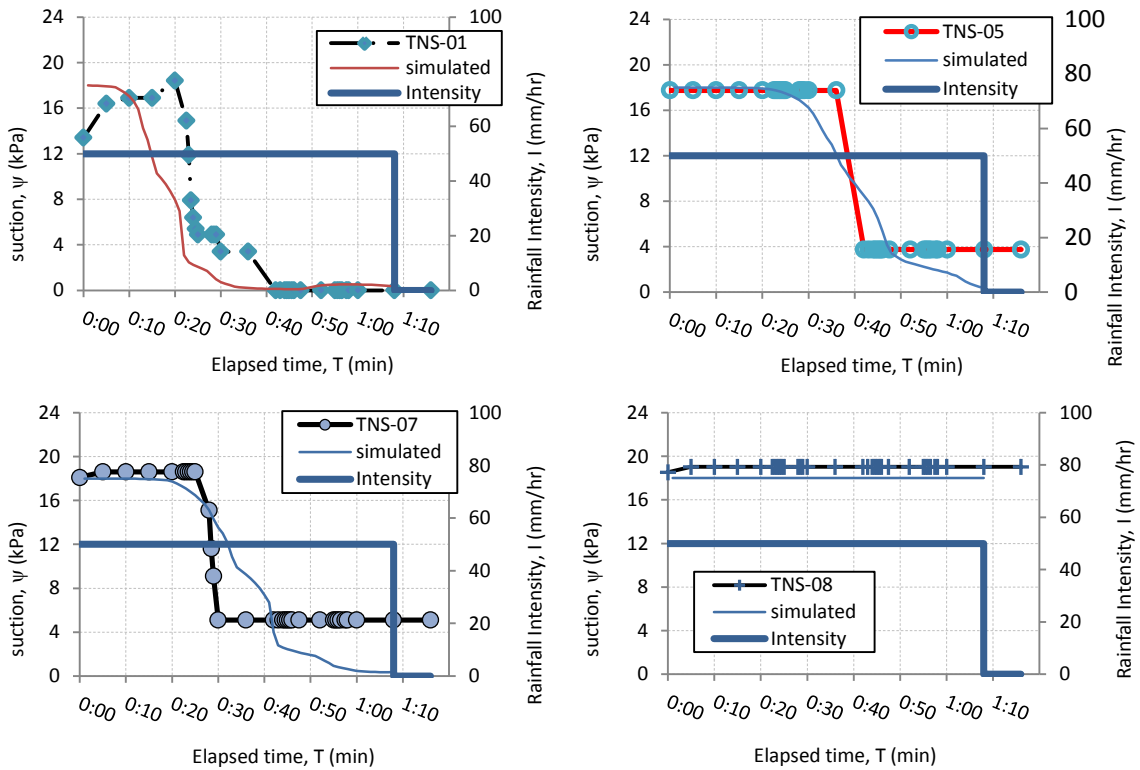


Fig. 7.2. Measured and simulated pore water pressure changes in the location of instrumentations for FLM_04

Soil experiment for FLM_08 experienced 22 mm/hr rainfall. In this test, tensiometers TNS-03, TNS-04, TNS-06 and TNS-08 have recorded no changes in suction while raining. There is a good agreement in location of these tensiometers between measured and simulated suction values. But in TNS-01 and TNS-07 measured suction values start to change almost 10-15 minutes later than simulated suctions.

In a flume experiment with 48% relative density, average rainfall intensity of 63 mm/hr was applied. In FLM_10, tensiometers TNS-05 and TNS-07 experience a very similar suction changes to simulations and TNS-03 and TNS-09 start to response to suction changes 4-6 minutes earlier in comparison to simulations.

As it is summarized in Appendix D, in FLM_12 that rainfall with intensity of 48 mm/hr is applied over a finite slope with soil sample of 34% relative density, TNS-03, TNS-04

and TNS-09 showed a very good agreement with simulated suction responses. In simulated suction response, suction at location of TNS-01 starts to change immediately after rainfall initiation but tensiometer TNS-01 starts to respond with almost 10 minutes lag. This is most probably because of any slight differences between the planned and really placed location of tensiometers in the soil sample. In other words, if a tensiometer was located slightly deeper, time period that was needed for its response would be longer.

For FLM_13, a rainfall with intensity of 18 mm/hr was applied over soil sample of 34% relative density. TNS-02 and TNS-03 showed a good match between the measured and simulated soil suctions. Similar to FLM_08, tensiometers detect water infiltration 5-10 minutes later than simulations which probably comes from slight density differences within the soil sample.

In FLM-14 that rainfall intensity of 22 mm/hr was applied over a soil of 34% relative density, recorded suction response at TNS-04, TNS-07 and TNS-09 are plotted against numerical simulations. Despite very similar trend in suction losses, a time lag of almost 5-15 minutes exist between measured and simulated suction responses. In TNS-06 simulation matches to experimental data but non of them is subjected to infiltration.

7.1.1.2. Wetting front

Study of detected wetting front progress in flume experiments subjected to rainfall and their comparison with numerically simulated wetting fronts was another way to evaluate the success in simulation of seepage of rainfall water into a partially saturated soil.

Fig. 7.3 shows observed (detected) wetting front and simulated one for FLM_03 flume test. It is clear that the wetting front at both 38 and 49th minutes after the test starts, progressed more than the numerically simulated wetting fronts. Despite observing the same trend in FLM_04 for which the wetting front is plotted in Fig. 7.4 numerical simulation is more successful in this test as both simulated and detected wetting fronts are very close to each other. Study of the results for the rest of the flume tests shows that some common findings from wetting front investigation in flume experiments and their numerical simulations are;

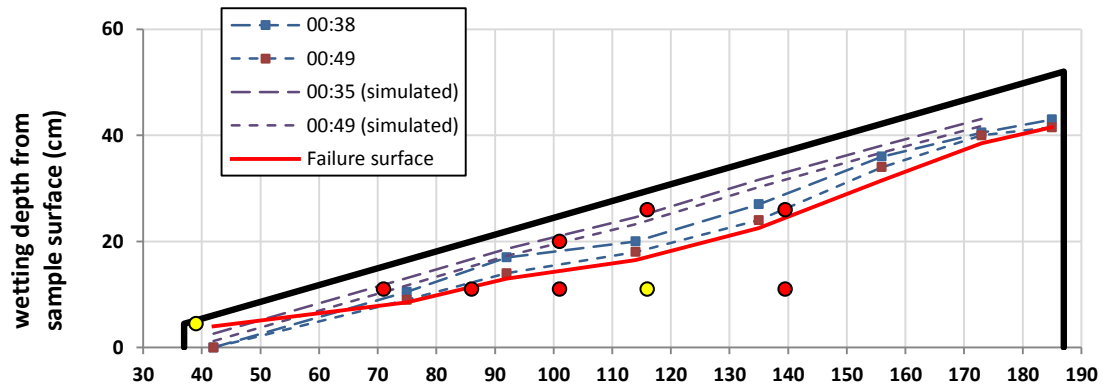


Fig. 7.3. Detected (measured) and simulated wetting front for FLM_03

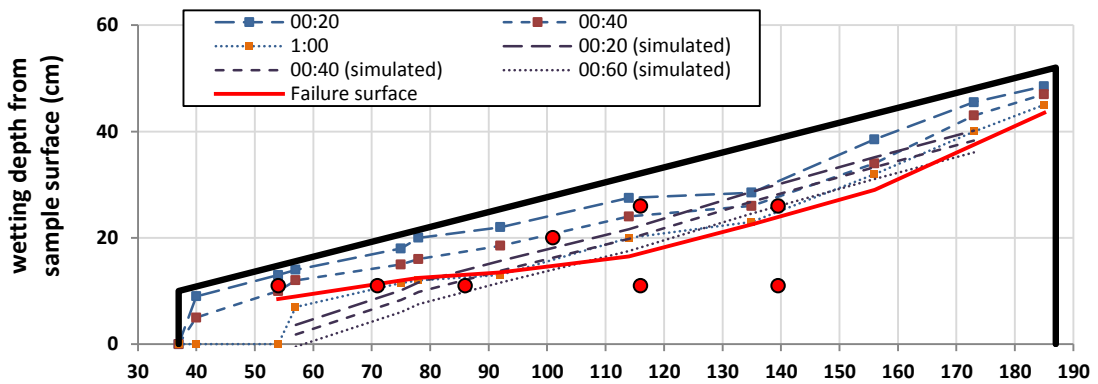


Fig. 7.4. Detected (measured) and simulated wetting front for FLM_04

- Wetting front in flume experiments generally were not straight/similar to straight line because of nonuniformity in soil sample. This was opposite to simulated wetting fronts. For instance in experiments FLM_05, FLM_08 and FLM_12 non-uniform infiltrations (i.e. different vertical distances to the wetting front) were observed along the slope length.
- Wetting front recordings were not necessarily matching with the suction changes recorded by tensiometers in flume experiments. Thus, it was deduced that wetting front progress in vicinity of side walls were different from the wetting

front in the middle of slope. For an example, in FLM_10, tensiometer TNS-09 despite monitoring suction loss 37 minutes after rainfall initiation, detected wetting front reaches tensiometer at $t = 45\text{min}$. This can be interpreted as slower infiltration in the vicinity of side walls of the flume, which was not possible to be considered in the numerical simulation due to the 2D nature of the numerical analyses.

Movement of the wetting front in an unsaturated soil, is observed in flume tests clearly by visually, which can be confirmed with the zero suction measurements in tensiometers (meaning that the wetting front reached at the depth).

7.1.2. Laminar box tests

Only results from laminar box test LAM-1 are simulated numerically and presented in this research. Fig. 6.14 shows the plot of measured and simulated suction changes in LAM-1. Despite correct trend of changes in suction values with depth in the soil sample due to raining, recorded and simulated values of suction do not match at all. Probably this is because of the non-precise hydraulic properties used in 1D seepage calculations.

7.2. Slope stability

7.2.1. Flume experiments

Stability of a slope in a laboratory flume experiment can be expressed by observing the deformations in the soil in different parts of slope, manually (observing deformations/movements/cracks by eye) or mechanically (detecting deformation by different mechanical means such as PIV methods, inclinometer readings etc). Considering the nature of rainfall triggered landslides, in the current research, large deformations/sliding of the mass are considered as the definition of "failure" at the flume experiments. For flume tests time to failure recorded as one of test results. But in numerical simulation of slope stability in flume experiments, the results presented as factor of safety versus time and time to failure.

7.2.1.1. Factor of safety versus time (FS vs. t)

In early warning systems for rainfall triggered slope instabilities, plot of factor of safety versus time plays a critical role. In the current research, slope stability analyses and assessment of changes in factor of safety during raining over laboratory flume models was of significant importance. Plot of factor of safety versus time for flume experiments are presented in detail in Appendix C.

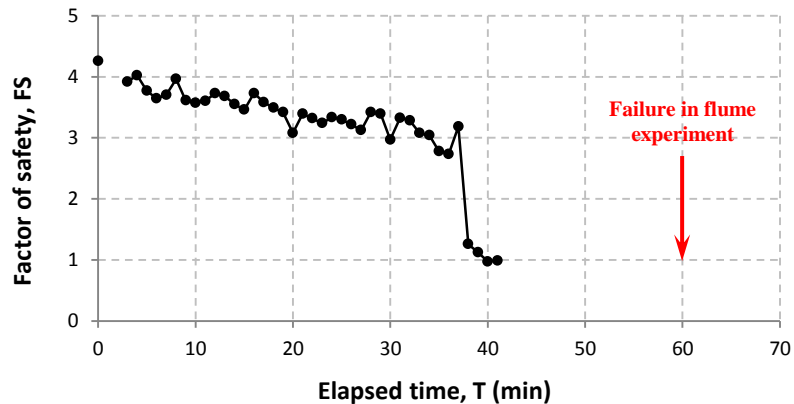


Fig. 7.5. Simulated time to failure in flume model FLM_04

As an instance, in flume test FLM_04, the slope failed at 60 minutes after rainfall initiation. Fig. 7.5 shows the results of numerical simulation of slope stability for FLM_04 and failure incident in flume experiment. There is an obvious difference between failure time in the laboratory experiment and simulation. Different reasons may cause such differences, for example possible lower estimation of unsaturated shear strength parameters.

Factor of safety versus time for other flume tests are also summarized in Fig. 7.6. Study of FS vs. time plots shows some similarities between the results of simulation of experiments with same relative density. In the group of the experiments with 34% relative density, after a steep fall in critical factor of safety (generally falling below 1.0) some abrupt increase in FS was observed which faded very fast. On the other hand, in the experiments with relative density of 48% after a severe decrease in FS during raining, it has been carried on decreasing till failure, moderately. In these simulations no increase in FS was detected.

7.2.1.2. Time to failure (t to failure)

As another parameter that can be considered/used in early warning systems, time to failure was considered in the current study, numerically and experimentally. Furthermore, in the current study, time to failure was probably the only parameter that could mention (or early warn) failure/instability in flume experiments.

Table 7.1 is summarised the time to failure in flume experiments and the time to failure obtained from slope stability analyses.

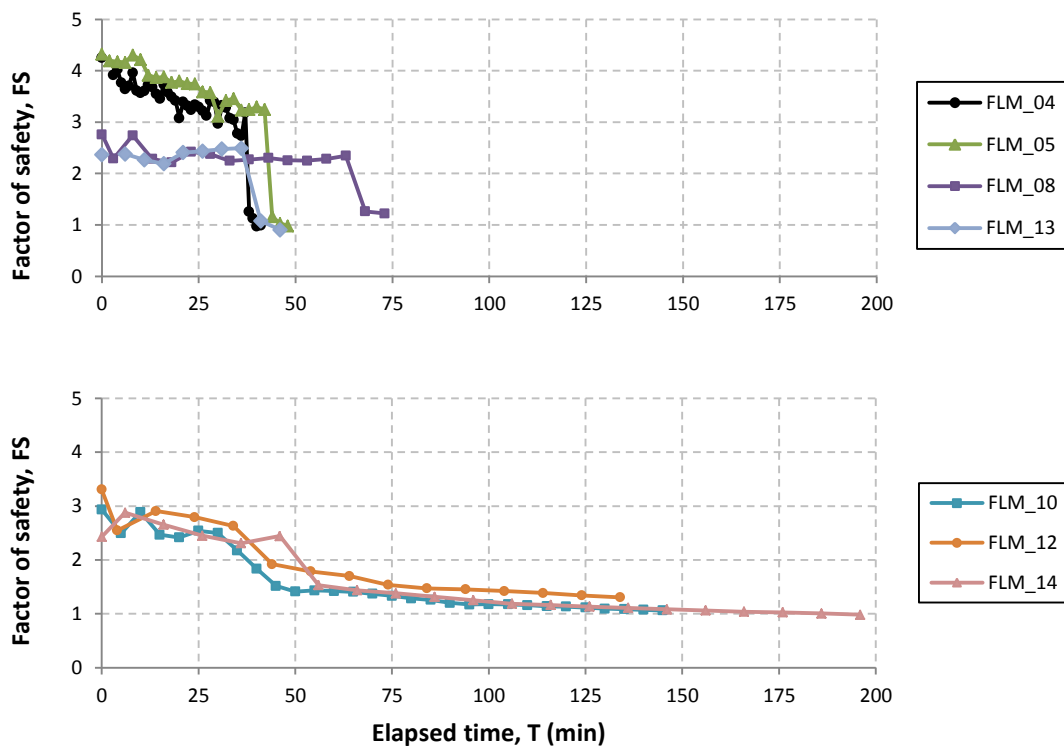


Fig. 7.6. Simulated time to failure for flume tests with (a) 34% and (b) 48% relative density

As a general observation, simulated time to failure in experiments with lower relative density (e.g. $R_d=34\%$) is smaller than the measured failure times in flume experiments. On the other hand, in experiments with higher relative density (e.g. $R_d=48\%$) simulated time to $FS=1.0$ is far longer than the observed failures in flume experiments. The rate of decrease in the factor of safety with time, is high for the tests at low relative density.

This is in contrast to a very smooth (i.e. a small rate of decrease in factor of safety) in denser soils.

Table 7.1. Recorded time to failure in flume experiments and their numerical simulation

Test #	Average rainfall intensity <i>I</i> mm/hr	Time to failure <i>t</i> min	Simulated time to failure <i>t_s</i> min	Test #	Average rainfall intensity <i>I</i> mm/hr	Time to failure <i>t</i> min	Simulated time to failure <i>t_s</i> min
Relative density, $R_d = 34\%$				Relative density, $R_d = 48\%$			
FLM_03	54.4	48	-	FLM_10	63.5	103	175
FLM_04	46.3	60	40	FLM_12	48.7	134	295
FLM_05	28.3	69	48	FLM_14	22	205	186
FLM_08	21.6	74	68				
FLM_13	18	105	46				

7.2.1.3. Slip surface

Projection of failure surface to the side glass walls (monitoring side of the flume box) and recordings of placed inclinometers clearly indicated the failure surface in flume experiments. Failure surface is also assessed from slope stability analysis using SLOPE/W 2012.

Numerically simulated and experimentally detected failure surfaces are presented in Appendices C and B, respectively, and in Appendix D comparison of these data (e.g. simulated and detected failure surfaces) are presented.

Study of these data show a weak agreement between simulated and detected failure surfaces. Some considerations in this regard are as the following;

- In simulations, generally in many of the flume tests, simulated failure surface is shallower than the reality.
- Simulated failure surface generally is located in water infiltrated zone almost for all of the tests. This is not the case for all of the detected failure surfaces in flume experiments. For instance, except FLM_05, FLM_10 and FLM_14 tests,

generally in many of flume experiments wetting front is coincident with the wetting front or is in its vicinity. Although the uniformity of soil placement is controlled by the tares placed inside the soils while it is being prepared, still, the observed differences may arise from the slight nonuniformity in sample density which affects its infiltration and shear strength characteristics.

As a side note, it is observed that the in-house-developed miniature inclinometers were able to detect the depth of the landslides reasonably accurately.

7.2.2. Laminar box

In both laboratory flume tests and in numerical simulations, for the limited number of laminar box tests, a failure is not observed (for the range of rainfall intensities and durations applied). Slope stability analysis shows factor of safety values higher than one and this is proved laminar box tests in which no failure was observed. For the soil samples prepared at large relative densities, causing a failure was not easy/or not possible for the ranges of rainfall intensity and durations employed in this study.

7.3. I-D thresholds

Plotting time to failure versus average rainfall intensity in flume experiments gives the rainfall intensity-duration thresholds (I-D plots) that triggers a landslide. Fig. 7.7 shows the obtained I-D threshold for the two sets of tests with 34 and 48% relative density. Then, numerical simulation of these tests are obtained and plotted by performing seepage and slope stability analysis of flume tests using SEEP/W and SLOPE/W 2012 softwares which have been explained in detail in section 5.2.

Solid filled symbols in Fig 7.7 are representing the experiments which have experienced failure, while the experiments in which no failure is observed till the end of raining are shown with points with no filling. In FLM_11 after applying rainfall with intensity of 28 mm/hr for 135 minutes and having no failure, the rainfall intensity is increased to

67 mm/hr and the time that is needed for failure after intensity increasing is recorded. This incident (FLM_11*) is shown with red colored point on I-D plot.

For each of the two category of flume tests with $R_d = 34\%$ (FLM_03, 04, 05, 08 and 13) and $R_d = 48\%$ (FLM_10, 12 and 14) a best function is fitted to the data on the I-D plot. This function can be used as the boundary between “safe” and “unsafe” rainfalls over 56.5° slope on QS soil. R-square value for regression also is higher in tests with higher relative density ($R_d = 48\%$) indicating a better fit.

To show the results from numerical simulation of intensity durations, the gray colored symbols are used. These points have the same rainfall intensity as their representing laboratory flume experiment, while the “simulated” time to failure is generally different from that of the experiment.

No specific trend line is fitted to the “simulated” intensity duration pairs because of their higher scatter. One of the reasons for this scatter seems to be the high sensitivity of the slope stability to any slight changes in the shear strength parameters of the unsaturated soils, or another could be using an average rainfall intensity in the vertical axis (although the applied rainfall had some non-uniformity over the slope length, which is taken into account in the numerical analyses), or the difficulty in precisely defining the “failure time” in both numerical study and in the flume. Although we tried to minimize the effect, it is noted in the laboratory tests that the density of the samples change after placement and during and at the end of raining, this could change the SWCC and the HCF of the soil slightly which could influence the results.

It should be noted that in almost all flume experiments, the deformations leading to failure occurred almost instantaneously, i.e. they are not like slowly developing movements visible in the soil, but rather they occur rather abruptly.

Although there are some discrepancies between the depth of the slip surfaces in the flume experiments and in the numerical simulations, we observed a general trend of a translational, infinite slope type movement mechanism, which is typical for rainfall triggered landslides in unsaturated soils in nature.

Overall, it is observed that the general shape of the I-D plot in log-log scale is linear. For very low intensity rainfalls, either the rainfall has to continue a very long time to cause failure, or it is impossible to cause failure in these very small values of rainfall intensity. It's because of that the infiltration is at such a slow rate that the water can be drained out of the soil before it causes any slope instability. It is also demonstrated physically and simulated numerically that, small intensity-long duration rainfalls, and large intensity-short duration rainfalls can both trigger landslides (except the very small rainfall intensities, in the range of less than 15 mm/hr).

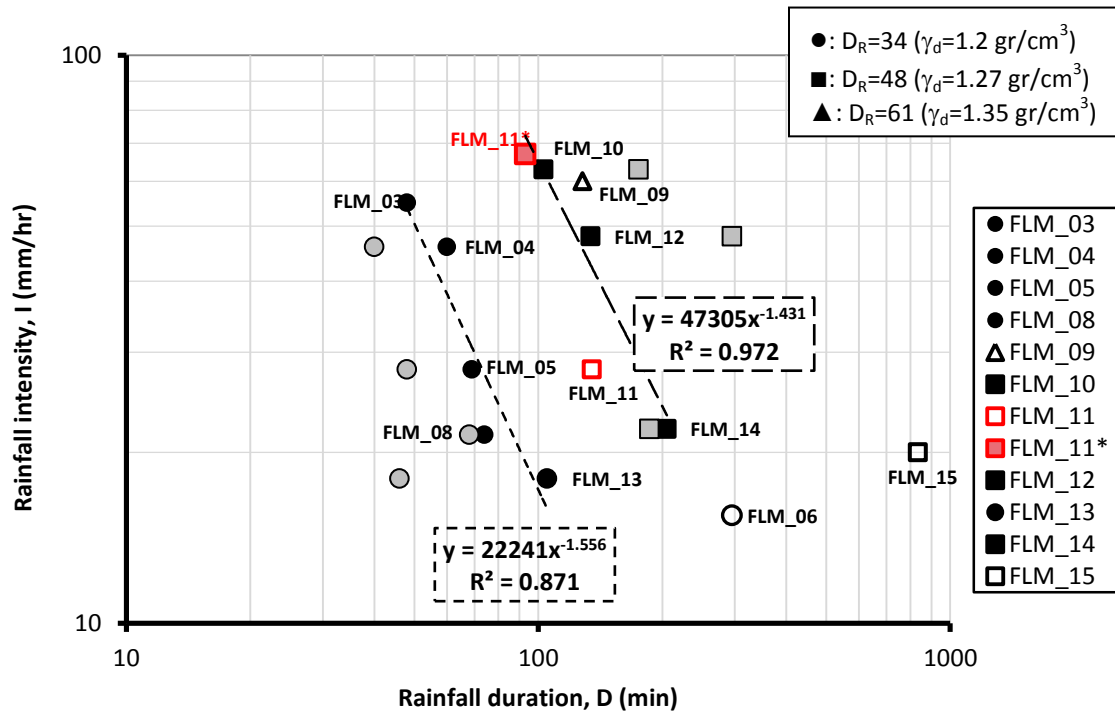


Fig. 7.7. Rainfall intensity duration pairs assessed experimentally and numerically

CHAPTER 8

CONCLUSIONS AND RECOMMENDATIONS FOR FUTURE STUDIES

This chapter highlights the achieved objectives of the research presented in section 1.3. Major findings are discussed in this chapter. Also, some of major concluded remarks from parametric studies, numerical simulations and laboratory experiments are summarized in following sections.

8.1. Achievements

Although all of the conclusions are valid for one type of soil (clean fine sand) used in this study; and that any further studies would definitely strengthen the conclusions by adding supporting evidences; the major achievements from the current research can be summarized as follows;

- 1- Available methods for predicting rainfall-induced landslides are based on the statistical study of records of past slope failures and actual rainfall data. However, such studies are limited by the availability, completeness, precision and bias of these records. Therefore, in order to develop a useful early warning system, the physical mechanism of landslides should be taken into consideration. In the current research, to the author's knowledge for the first time in the literature, rainfall intensity duration thresholds that would trigger a landslide (I-D plots) are obtained physically in the laboratory flume tests and by numerical simulations.
- 2- The shape of the I-D threshold curve (that triggers a landslide) is demonstrated to be a linear relation in log-log plot of rainfall intensity versus duration, for the soil used in this study. To the author's knowledge, this is the first study in the

literature that showed/proved the shape of the I-D plot, by physical experiments and by numerical simulations. The results of this study confirms that, both high intensity-short duration rainfalls, and low intensity-long duration rainfalls can trigger landslides. However, below a certain low rainfall intensity (in this study 15 mm/hr) landslides are not triggered for the material used in this study. This leads to a conclusion that the I-D relation could be asymptotic to the duration axis.

- 3- For the first time in the literature, the effect of density of the soil on the I-D threshold is demonstrated by physical laboratory tests (and supported by numerical simulations). As the relative density of the material increases, the triggering rainfall intensity-duration threshold line moves to the right (in the log-log plot of intensity versus the duration). For the soil used in this study, in flume tests with dense soil (at 61% relative density), failure is not observed for the rainfalls in the range of 4 to 67 mm/hr.
- 4- A sensitivity analyses is carried out in this study focusing on the effects of soil type and its properties on SWCC, and therefore on the I-D thresholds. It was concluded that an I-D plot is affected mostly by the grain size of the soil (rather than dry density, uniformity and fines content).
- 5- It is observed that the unsaturated shear strength parameters of soils can be obtained with reasonable accuracy (for practical geotechnical purposes), using a water-content-controlled direct shear tests instead of suction controlled sophisticated tests. Obtained data from those direct shear tests, despite the scatter, show an almost linear behavior such that as expected as the suction increases, the shear strength envelope moves up (i.e. an apparent cohesion due to suction develops).
- 6- In the current study, for the first time in the literature, the wetting and drying SWCCs and HCFs (i.e. the hysteresis effect) were used in numerical simulations of unsaturated slopes subjected to rainfall. Investigation of the simulations and test results showed the success of this approach and the importance of including the hysteresis in these soil characteristics. Therefore, this study proposes a

methodology for the numerical analyses of rainfall triggered landslides considering the unsaturated material properties with hysteresis in wetting/drying.

- 7- Laminar box setup, which is a widely used setup in earthquake studies, has not been used before in landslide studies. Laminar box setup for studying infiltration and slope instability in an element of infinite slope were designed and manufactured in the current research. To the author's knowledge, this is the first time that laminar box setup is used for landslide studies. The setup is calibrated and its employment is assessed using some trial tests. Although limited number of tests were conducted in soils at high relative densities (hence no failure was observed), the laminar box setup seems to be a promising tool for landslide triggering studies.
- 8- In-house-developed, simple inclinometers using elastic strips for detecting lateral deformations in the laboratory flume experiments were prepared and used successfully in the current study.

8.2. Conclusions

8.2.1. A Landslide prediction competition

As part of the PhD study, the author participated in an international landslide prediction competition organized during the Third Italian Workshop on Landslides in Naples, Italy in 2013 (Bogaard et al., 2014 and Ahmadi-adli et al., 2014). The lessons learnt from this activity are valuable conclusions and they can be summarized as follows;

- 6- Numerical simulation of a real scale steep slope in the field challenged with a number of difficulties such as the uncertainties in the boundary conditions, non-uniformity in soil properties, groundwater table and evaporation. Among these factors, evaporation was observed to be an important factor.
- 7- Review of other solutions for this exercise clearly shows that complex physically-based models allow a better description and deeper interpretation of

the processes actually leading to the triggering of a landslide. However, this comes at a price.

8.2.2. Parametric study

Understanding the effects of wetting/drying SWCC and HCF on I-D thresholds is a necessary first-step towards an integrated early warning system for rainfall triggered landslides that considers the physical mechanism of the problem. To the author's knowledge, the conclusions below have not been explicitly discussed in the existing literature previously.

- 1- The intensity-duration threshold that triggers a landslide can be computed successfully given that the unsaturated hydraulic and shear strength properties of the soil are known (or can be estimated).
- 2- Both “high intensity short duration” rainfalls and “low intensity long duration” rainfalls can cause landslides in unsaturated soils, as characterised by I-D thresholds.
 - e) Based on the sensitivity analyses carried out in this study for rainfall intensities between 10-100 mm/hr it is observed that I-D threshold that triggers a landslide, in general, is mostly linear in log-log plot, considering a range of different soil types. Observed slight non-linearity in I-D plot in sensitivity analysis is mainly due to the difference in boundary conditions in the numerical model with the real infinite slope type translational landslides, which causes positive pore pressure to be built up in the geometry of the sensitivity analyses.
 - f) For very low intensity rainfalls (less than 15 mm/hr) no matter how long rainfall occurs it does not trigger a landslide, for the clean fine sand material used in this study. This is because the soil is able to exfiltrate all the rainfall that infiltrates.
- 3- It was concluded that an I-D plot is mostly influenced by the grain size of the soil (rather than dry density, uniformity and fines content).

- 4- This study shows that unsaturated soil properties such a SWCC and HCF play a critical role in the behavior of unsaturated slopes.

8.2.3. Numerical simulations and laboratory experiments

All the observations and findings in this subsection are limited to a clean fine sand soil with specific grain size distribution.

- 1- Soil properties needed for numerically simulating unsaturated slopes subjected to rainfall, including hydraulic (SWCC and HCF) and shear strength parameters can be obtained in the laboratory accurately. The hysteresis in SWCC should be considered for drying and wetting. For correct shear strength parameters to be used in slope stability analysis of unsaturated slopes, the relevant range of normal stressess must be kept in mind.
- 2- Infiltration of rainfall into an unsaturated soil can be simulated accurately, numerically by SEEP/W 2012 and can be verifed with flume experiments. The results can be investigated considering pore water pressures and wetting front progress.
 - a) As the rainfall infiltrates into the soil, wetting front can be observed to move down into the soil (this can be checked with tensiometer measurements showing zero suction values as the wetting front reaches to their locations). Wetting front in flume experiments generally were not in the shape of a straight line along the slope length. This was opposite to the numerically simulated wetting fronts. The difference in the shape of the wetting front could be possible nonuniformities in soil sample during preparation especially near the boundaries of the flume box, or due to direct/fast infiltration of water at the front side of the flume box, where the wetting front depth is measured.
 - b) Wetting front recordings were not necessarily matching with the suction changes recorded by tensiometers in flume experiments. Thus, it was deduced that wetting front progress in the vicinity of side walls of the flume setup were different from the wetting front in the middle of slope. This can

be interpreted as slower infiltration in the vicinity of side walls of the flume, which was not possible to be considered in the numerical simulation due to the 2D nature of the numerical analyses.

- 3- In early warning systems for rainfall triggered slope instabilities, plot of factor of safety versus time could play a critical role. In the current research, slope stability analyses and assessment of changes in factor of safety (FS) during raining over laboratory flume models was of significant importance. Study of obtained FS versus time plots shows that, loose samples (prepared at relative density of 34%) showed a steep decrease in FS with time as the rainfall infiltrates and suctions in the soil decrease towards zero. In the experiments with relative density of 48%, a very gradual (less steep) decrease in FS is observed with time. At larger relative density value (61%) failure is not observed; i.e. probably failure never occurs, or in other words FS versus time plot becomes asymptotical to the time axis.
- 4- Projection of failure surface onto side glass walls (monitoring side wall of the flume box) and recordings of placed inclinometers clearly indicated the failure surface in flume experiments. Failure surface is also assessed from limit equilibrium slope stability analysis using SLOPE/W 2012. In both flume experiments and in numerical simulations the failure surfaces are mostly translational, and failure mechanism is infinite slope type landslide.
- 5- There is a weak agreement between simulated and detected depth of failure surfaces. Some considerations in this regard are as the following;
 - In simulations, generally in many of the flume tests, simulated failure surface is more shallower than the reality in the flume. Although the uniformity of soil placement is controlled by the tares placed inside the soil while it is being prepared, still, the observed differences may arise from the slight nonuniformity in sample density which affects its infiltration and shear strength characteristics.
 - Simulated failure surface generally is located in water infiltrated zone almost for all of the tests. Except a few tests, generally in many of flume

experiments the failure surface is coincident with the wetting front or is in its vicinity.

8.2.4. I-D thresholds

Plotting time to failure versus average rainfall intensity in flume experiments gives the rainfall intensity-duration thresholds (I-D plots) that trigger a landslide. Major conclusions obtained in this study can be summarized as;

- 1- Higher scatter in I-D plot is observed in numerically “simulated” intensity duration pairs. One of the reasons for this scatter seems to be the high sensitivity of the slope stability to any slight changes in the shear strength parameters of the unsaturated soils, or another could be plotting the average rainfall intensity in the vertical axis (although the applied rainfall had some non-uniformity over the slope length, which is taken into account in the numerical analyses), or the difficulty in precisely defining the “failure time” in both numerical study and in the flume. Although we tried to minimize the effect, it is noted in the laboratory tests that the density of the samples change after placement and during and at the end of raining, this could change the SWCC and the HCF of the soil slightly which could influence the results.
- 2- It should be noted that in almost all flume experiments, the deformations leading to failure occurred almost instantaneously/abruptly.
- 3- General trend of a translational, infinite slope type movement mechanism, which is typical for rainfall triggered landslides in unsaturated soils, was observed despite some discrepancies between the depth of the slip surfaces in the flume experiments and in the numerical simulations.
- 4- Overall, it is observed that the general shape of the I-D plot in log-log scale is linear. For very low intensity rainfalls (less than 15 mm/hr), either the rainfall has to continue for a very long time to cause failure, or it is impossible to cause failure in these very small values of rainfall intensity, which would be because of the entering water is entering at such a slow rate that it can be drained out of the

soil before it causes any slope instability. It is also demonstrated physically and simulated numerically that, low intensity-long duration rainfalls, and high intensity-short duration rainfalls can both trigger landslides (except the very small rainfall intensities less than 15 mm/hr in this study).

- 5- For the first time in the literature, dependency of I-D plot to relative density of soils is investigated numerically and verified experimentally by the laboratory flume tests. It was observed that as the relative density increases, the I-D plot moves to the right, meaning having safer slopes for a specific rainfall in denser soil.

8.3. Recommendations for future works

Moving forward in different steps of current research highlighted the need for vast and detailed researches in the future.

- Current research focused on one material type and all the observations and findings are limited to a clean fine sand soil with specific grain size distribution. More material types can be tested to prove obtained major findings.
- Conduct numerical simulations in real scale slopes subjected to climatic changes and verify the results using well instrumented field tests.
- Employing I-D plots generated considering physical mechanism in early warning systems and evaluation of the outcome.
- SWCC, HCF, and shear strength properties of unsaturated soils can be evaluated in terms of a probabilistic approach. The possible range of values for these soil properties can be developed. This would generate I-D thresholds considering uncertainty and variability in material properties. I-D values then would be based on probability of failure, rather than FS.
- Black Sea Region has a fertile ground and agricultural managing organizations are active in the region. Some of unsaturated soil parameters (e.g. SWCC and HCF) of typical soils of the region can be obtained from them and be used in numerical simulations to obtain I-D plots.

- Performed numerical simulation of unsaturated seepage and slope stability in current study which was verified with flume experiments can be improved by different means such as;
 - o using more precise material properties – This can be done by using more sophisticated tools in the laboratory to obtain precise hydraulic properties (SWCC and specifically HCF) and performing suction measured/controlled tests to measure sophisticated shear strength parameters.
 - o using more sophisticated coupled finite element analysis methods to take into account different aspects such as constitutive modeling of unsaturated soils, thermodynamic properties and boundary conditions such as temperature and evaporations. Many recent studies are focused to prepare numerical tools to implement hyper plasticity and thermodynamic analyses for simulation of behavior in unsaturated slopes and they can be used to repeat simulation of flume experiments in new studies.
- In the current study, soil samples prepared for laboratory flume and laminar box experiments had 1.5% initial gravimetric water content. In real case, in unsaturated natural slopes, preceding rainfall and evaporation change the water storage of the soils. Therefore, more detailed study is needed to incorporate initial suction effect and also repeat tests with preceding rainfall.
- Some limited measurement devices were employed in this study. Particle image velocimetry (PIV) method as one of better and more improved tools to assess precise deformation during rainfall was used by the author to detect deformations in a number of tests. In this method using different frames of a video taken from soil specimen during rainfall deformations and displacements could be measured. For a future work, available videos from all of flume tests can be processed to determine deformations throughout the tests.
- Laminar box setup despite being designed and manufactured for the first time, calibration and prove of application, were not used comprehensively in the current research. Only a limited number of tests were carried out, at high relative

density (61%) where slope failure is not observed under rainfall. It's highly recommended to do tests using this setup and obtain experimental I-D thresholds.

- Prepared Matlab code can be used in numerical assessment of I-D thresholds in infinite slopes. It's recommended to do numerical simulations using this tool and verify the results using slope stability tests in laminar box setup.
- Matlab code can be implemented in interfaces to use geographic information systems (GIS) and hydrologic data of any region to assess rainfall triggered landslide hazard maps.

REFERENCES

- Abramento, M., & Carvalho, C. (1989). Geotechnical parameters for the study of natural slope instabilization at Serra do Mar, Brazil. *Proceedings of the 12th International Conference on Soil Mechanics and Foundation Engineering*. Rio de Janeiro.
- Ahmadi-adli, M., Huvaj, N., & Toker, N. K. (2010, April 22-27). Rainfall triggered landslides in unsaturated soils: a numerical sensitivity analysis for rainfall threshold. Vienna, Austria: European Geosciences Union general assembly.
- Ahmadi-adli, M., Huvaj, N., & Toker, N. K. (2014). Effects of air entry value on rainfall induced slope instability. *Geo-Congress 2014*. Atlanta: American Society of Civil Engineering.
- Ahmadi-adli, M., Huvaj, N., Toker, N. K., & Korkucu, M. G. (2012). Comparative study of Soil Water Characteristic Curve prediction methods. *Proc. of 3rd International Conference on New Developments in Soil Mechanics and Geotechnical Engineering*. Nicosia: Near East University.
- Ahmadi-adli, M., Toker, N. K., & Huvaj, N. (2014). Prediction of seepage and slope stability in a flume test and an experimental field case. *Procedia Earth and Planetary Science*, 9, 189-194. doi:10.1016/j.proeps.2014.06.022
- Ahmadi-Naghadeh, R., Toker, N. K., & Ahmadi-adli, M. (2013). Water content controlled instead of suction controlled strength tests. *Life Science Journal*, 10(1), 2023-2030.
- Aitchison, G. D. (1960). Relationships of moisture stress and effective stress functions in unsaturated soils. *Conference on Pore Pressure and Suction in Soils*, (pp. 47-52).
- Alonso, E. E., Gens, A., & Josa, A. (1990). A constitutive model for partially saturated soils. *Geotechnique*, 40(3), 405-430.

- American Society for Testing and Materials (ASTM). (2010). *Standard Test Method for Measurement of Hydraulic Conductivity of Unsaturated Soils*. Designation ASTM D7664, D-18 Committee on Soils and Rock. doi:10.1520/D7664-10
- Arora, M. K., & Gupta, R. P. (2004). An artificial neural network approach for landslide hazard zonation in the Bhagirathi (Ganga) Valley, Himalayas. *Int J Remote Sens*, 25(3), 559-572.
- Arya, L. M., & Paris, J. F. (1981). A physicoemprical model to predict the soil moisture characteristic from particle-size distribution and bulk density data. *Soil Sci. Soc. Am. J.*, 45, 1023-1030.
- Askarinejad, A. (2013). Failure mechanism of unsaturated silty sand slopes triggered by rainfall. *PhD thesis*. ETH zurich.
- Askarinejad, A., Casinni, F., Bischof, P., Beck, A., & Springman, S. M. (2012). *Rainfall induced instabilities in a silty sand slope: a case history in northern Switzerland*. Retrieved from <http://www.cces.ethz.ch/projects/hazri/tramm>
- Averjanov, S. F. (1950). About permeability of subsurface soils in case of complete saturation. *English Collection*, 7, 19-21.
- Baum, R. L., Savage, W. Z., & Godt, J. W. (2008). *TRIGRS: A FORTRAN Program for Transient Rainfall Infiltration and Grid-Based Regional Slope-Stability Analysis, version 2.0*. U.S. Geological Survey Open-File Report 2008-1159.
- Berardi, R., Mercurio, G., Bartolini, P., & Cordano, E. (2005). Dynamics of saturation phenomena and landslide triggering by rain infiltration in a slope. In O. Hunger, R. Fell, R. Couture, & E. Eberhardt, *International conference on landslide risk management* (pp. 212-219). Vancouver: Taylor & Francis Ltd.
- Berardi, R., Mercurio, G., Bartolini, P., & Cordano, E. (2005). Dynamics of saturation phenomena and landslide triggering by rain infiltration in a slope. In O. Hungr, R. Fell, R. Couture, & E. Eberhardt (Ed.), *International conference on landslide risk management* (pp. 212-219). Vancouver: Taylor & Francis Ltd.
- Bishop, A. W. (1959). The principle of effective stress. *Teknisk Ukeblad*, 106(39), 859-863.

- Bogaard, T. A., Greco, R., Olivares, L., & Picarelli, L. (2014). The Round Robin test on landslide hydrological modeling at IWL2013. *Procedia Earth Planet Sci*, 9, 180-188.
- Brady, N. C., & Weil, R. R. (1999). *The Nature and Properties of Soils*. New Jersey: Prentice Hall.
- Briggs, L. J. (1897). *The Mechanics of Soil Moisture*. US Department of Agriculture, Division of Soils, Bulletin No.38.
- Brooks, R. H., & Coery, A. T. (1964). Hydraulic properties of porous medium. *Hydrology paper*(No 3).
- Caine, N. (1980). The rainfall intensity: duration control of shallow landslides and debris flows. *Phys Geog*, 23-27.
- Campbell, J. D. (1973). Pore pressures and volume changes in unsaturated soils. *Ph.D. Thesis, University of Illinois at Urbana-Champaign, IL*.
- Can, T., Duman, T. Y., Olgun, S., Corekcioglu, S., Gulmez, F. K., Elmaci, H., . . . Emre, O. (2013). Landslide database of Turkey. *Congress of Turkish geographic data systems* (pp. 1-6). Ankara: TMMBO.
- Can, T., Nefeslioglu, H., Gokceoglu, C., Sonmez, H., & Duman, T. (2005). Susceptibility assessments of shallow earthflows triggered by heavy rainfall at three catchments by logistic regression analyses. *Geomorphology*, 72, 250-271.
- Chen, Z., & Wang, J. (2007). Landslide hazard mapping using logistic regression model in Mackenzie Valley, Canada. *Natural Hazards*, 42(1), 75-89.
- Cheng, D. X., & Lau, C. K. (2008). *Slope stability analysis and stabilization: new methods and insight*. Routledge: Taylor & Francis.
- Coleman, J. D. (1962). Stress /strain relations for partly saturated soils. *Geotechnique*, 12(4), 348-350.
- Crosta, G. (1998). Regionalization of rainfall thresholds: an aid to landslide hazard evaluation. *Env. Geol.*, 35(2), 131-145.

- Crosta, G., & Frattini, P. (2003). Distributed modelling of shallow landslides triggered by intense rainfall. *Nat Hazards Earth Syst Sci*, 3, 81-93.
- Crozier, M. J. (1989). *Landslides: causes, consequences and environment*. Routledge: Taylor & Francis.
- Crozier, M. J. (1999). Prediction of rainfall-triggered landslides: a test of the antecedent water status model. *Earth Surf Proc Land*, 24(9), 825-833.
- Dai, F. C., & Lee, C. F. (2002). Landslide characteristics and slope instability modeling using GIS, Lantau Island, Hong Kong. *Geomorphology*, 213-228.
- Damiano, E. (2004). Mechanisms of triggering mudslides in pyroclastic soils. *PhD thesis*. Aversa: Second University of Napoli (in Italian).
- Damiano, E., & Olivares, L. (2012). The role of infiltration processes in steep slope stability of pyroclastic granular soils: laboratory and numerical investigation. *Nat Hazards*, 52, 329–350. doi:10.1007/s11069-009-9374-3
- Damiano, E., Olivares, L., & Picarelli, L. (2012). Steep-slope monitoring in unsaturated pyroclastic soils. *Eng Geol*, 137-138, 1-12.
- Daniel, D. E. (1982). Measurement of hydraulic conductivity of unsaturated soils with thermocouple psychrometers. *J. of Soil Science Society of America*, 20(6), 1125-1129.
- Davidson, J. M., Stone, L. R., Nielson, D. R., & Larue, M. E. (1969). Field measurement and use of soil-water properties. *Water Resources Research*, 5, 1312-1321.
- Dhakal, G., Yoneda, T., Kato, M., & Kaneko, K. (2002). Slake durability and mineralogical properties of some pyroclastic and sedimentary rocks. *Eng Geol*, 65(1), 31–45.
- Donald, I. B. (1960). "Discussion". *Proceedings of conference on pore pressure* , (p. p.69). Butterworths, London.
- Duman, T. Y., Can, T., Emre, O., Kecer, M., Dogan, A., Ates, S., & Durmaz, S. (2005). Landslide inventory of northwestern Anatolia, Turkey. *Engineering Geology*, 77, 99-114.

- Eckel, E. B. (1958). Introduction. In E. B. Eckel, *Landslides and Engineering Practice* (pp. 1-5). Washington D.C.: National Academy of Sciences, National Research Council.
- Eichenberger, J., Ferrari, A., & Laloui, L. (2013). Early warning thresholds for partially saturated slopes in volcanic ashes. *Computers and Geotechnics*, 49, 79-89.
- Escario, V., & Juca, J. F. (1989). Shear strength and deformation of partly saturated soils. *Proceedings of the 12th International Conference on Soil Mechanics and Foundation Engineering*, 2, pp. 43-46. Rio de Janeiro.
- Francois, B., & Laloui, L. (2008). ACMEG-TS: A constitutive model for unsaturated soils under non-isothermal conditions. *International journal for numerical and analytical methods in geomechanics*, 32(16), 1955-1988.
- Fredlund, D. G., & Rahardjo, H. (1993). *Soil mechanics for unsaturated soils*. New York: John Wiley and Sons Inc.
- Fredlund, D. G., & Xing, A. (1994). Equations for the soil-water characteristic curve. *Canadian Geotechnical Journal*, 31, 521-532.
- Fredlund, D. G., Xing, A., & Huang, S. (1994). Predicting the permeability function for unsaturated soils using the soil water characteristic curve. *Canadian Geotechnical Journal*, 31(3), 533-546.
- Fredlund, D. G., Xing, A., Fredlund, M. D., & Barbour, S. L. (1995). The relationship of the unsaturated soil shear strength to the soil-water characteristic curve. *Canadian Geotechnical Journal*, 33, 440-448.
- Fredlund, M. D. (2007). *Soilvision-A Knowledge-Based Database System for Soil Properties*. Saskatoon, Saskatchewan, Canada: SoilVision Systems Ltd.
- Fredlund, M. D., Fredlund, D. G., & Wilson, G. W. (1997). Prediction of the Soil Water Characteristic Curve from Grain-Size Distribution and Volume-Mass properties. *Proceeding of 3rd Brazilian Symposium on Unsaturated Soils*, (pp. 1-12). Rio de Janeiro.

- Fredlund, M. D., Wilson, G. W., & Fredlund, D. G. (2002). Use of the grain-size distribution for estimation of the soil water characteristic curve. *Can. Geotech. J.*, 39, 1103-1117. doi:10.1139/T02-049
- Gallage, C., Kodikara, J., & Uchimura, T. (2013). Laboratory measurement of hydraulic conductivity functions of. 53(3), 417-.
- Gan, K. J., & Fredlund, D. G. (1988). Multistage direct shear testing of unsaturated soils. *Geotechnical Testing Journal*, 11(2), 132-138.
- GDDA. (2008). *Report of disasters*. Ankara: Turkish Ministry of Public Works and Settlement.
- Glade, T. (1998). Establishing the frequency and magnitude of landslide-triggering rainstorm events in New Zealand. *Env. Geog*, 160-174.
- Glade, T., & Crozier, M. J. (2005). Landslide hazard and risk: issues, concepts, and approach. In T. Glade, M. Anderson, & M. J. Crozier, *Landslide hazard and risk* (pp. 43-74). New York: Wiley.
- Godt, J. W., Baum, R. L., & Chleborad, A. F. (2006). Rainfall characteristics for shallow landsliding in Seattle. *Earth Surf Proc Land*, 31(1), 97-110.
- Godt, J. W., Baum, R. L., & Lu, N. (2009). Landsliding in partially saturated materials. *Geophysical research letters*, 36(L02403), 1-5. doi:10.1029/2008GL035996
- Greco, R., Comegna, L., Damiano, E., Guida, A., Olivares, L., & Picarelli, L. (2013). Hydrological modelling of a slope covered with shallow pyroclastic deposits from field monitoring data. *Hydrol Earth Syst Sci*, 17, 4001-4013.
- Greco, R., Guida, A., Damiano, E., & Olivares, L. (2010). Soil water content and suction monitoring in model slopes for shallow flowslides early warning applications. *Physics and Chemistry of the Earth*, 35, 127-136. doi:10.1016/j.pce.2009.12.003
- Green, W. H., & Ampt, G. A. (1911). Studies on soil physics, Part I. The flow of air and water through soils. *Journal of Agricultural Science*, 4, 1-23.

- Gupta, S. C., & Larson, S. M. (1979). Estimating Soil Water Retention Characteristics from Particle Size Distribution, Organic Matter Percent and Bulk Density. *Water Resources Research*, 15(6), 325-339.
- Guzzetti, F., Carrara, A., Cardinali, M., & Reinchenbach, P. (1999). Landslide hazard evaluation: a review of current techniques and their application in a multi-scale study, Central Italy. *Geomorphology*, 31, 181-216.
- Guzzetti, F., Peruccacci, S., Rossi, M., & Stark, C. P. (2007). Rainfall thresholds for the initiation of landslides in central and southern Europe. *Meteorol Atmos Phys*, 98(3 & 4), 239-267.
- Harp, E. L., Wells, W. G., & Sarmiento, J. (1990). Pore pressure response during failure in soils. *Geological Society of America Bulletin*, 102, 428-438.
- Hong, Y., Adler, R., & Huffman, G. (2006). Evaluation of the potential of NASA multi-satellite precipitation analysis in global landslide hazard assessment. *Geophysical Research Letters*.
- Hong, Y., Adler, R., & Huffman, G. (2007). Use of satellite remote sensing data in the mapping of global landslide susceptibility. *Nat. Hazards*, 43, 245-256.
- Huang, C.-C., & Yuin, S.-C. (2010). Experimental investigation of rainfall criteria for shallow slope failures. *Geomorphology*, 120, 326-338.
- Huvaj, N., Toker, N. K., Egeli, I., Ahmadi-adli, M., & Sahin, Y. (2013). *Mechanism and modeling of rainfall triggered shallow landslides*. Ankara: TUBITAK.
- Ildir, B. (1995). Turkiyede heyelanlarin dagilimi ve afetler yasasi ile ilgili uygulamalar. *Proc. 2nd National Landslide Symposium of Turkey* (pp. 1-9). Sakarya: Sakarya University.
- Iverson, R. M., Reid, M. E., & LaHusen, R. G. (1997). Debris-flow mobilization from landslides. *Annu. Rev. Earth Planet. Sci.*, 25, 85-138.
- Jackson, C. R. (1992). Hillslope infiltration and lateral downslope unsaturated flow. *Water Resources Research*, 2533-2539.
- Jackson, C. R. (1993). Reply. *Water Resources Research*, 4169-4170.

- Karube, D., Kato, S., Hamada, K., & Honda, M. (1996). The relationship between the mechanical behavior and the state of pore water in soil. *Journal of JSCE*, 535, 83-92.
- Khalili, N., & Khabbaz, M. H. (1998). A unique relationship for the determination of the shear strength of unsaturated soils. *Geotechnique*, 48(5), 681-687.
- Kong, L. W., & Tan, L. R. (2000). A simple method of determining the soil-water characteristic curve indirectly. *Proceedings of Asian Conference on Unsaturated Soils*, (pp. 341-345). Singapore.
- Lagrega, M. D., Buckingham, P. L., & Evans, J. C. (2001). *Hazardous Waste Management* (2nd edition ed.). Boston: McGraw-Hill.
- Laplace, P. S. (1806). *Mecanique Celeste. Supplement to the Tenth Edition*.
- Lee, S., & Pardhan, B. (2006). Probabilistic landslide hazards and risk mapping on Penang Island, Malaysia. *J Earth Syst Sci*, 115(6), 661-672.
- Lee, S., Ryu, J.-H., & Kim, I.-S. (2007). Landslide susceptibility analysis and its verification using likelihood ratio, logistic regression, and artificial neural network models: case study of Youngin, Korea. *Landslides*, 4, 327-338.
- Leong, E. C., & Rahardjo, H. (1997). Permeability Functions for Unsaturated Soils. *Journal of Geotechnical and Geoenvironmental Engineering*, 123(12), 1118-1126.
- Leroueil, S. (2004). Geotechnics of slopes before failure. In W. Lacerda, M. Ehrlich, S. Fontoura, & A. Sayao, *Landslides: evaluation and stabilization. Ninth international symposium on landslides* (pp. 863–884). Leiden: A.A. Balkema Publishers.
- Lu, N., & Likos, W. J. (2004). *Unsaturated soil mechanics*. New Jersey: John Wiley & Sons Inc.
- Lu, N., Godt, J. W., & Wu, D. T. (2010). A closed-form equation for effective stress in unsaturated soil. *Water Resources Research*, 46(W05515).
doi:10.1029/2009WR008646

- Lu, N., Sener-Kaya, B., Wayllace, A., & Godt, J. W. (2012). Analysis of rainfall-induced slope instability using a field of local factor of safety. *Water Resources Research*, 48(W09524). doi:10.1029/2012WR011830
- Matsushi, Y., & Matsukura, Y. (2007). Rainfall thresholds for shallow landsliding derived from pressure-head monitoring: cases with permeable and impermeable bedrocks in Boso Peninsula. *Earth Surf Proc Land*, 32(9), 1308-1322.
- Matsushi, Y., & Matsukura, Y. (2007). Rainfall thresholds for shallow landsliding derived from pressure-head monitoring: cases with permeable and impermeable bedrocks in Boso Peninsula, Japan. *Earth Surf Proc Land*, 32(9), 1308–1322.
- Montgomery, D. R., Dietrich, W. E., & Torres, R. (1997). Hydrologic response of a steep, unchanneled valley to natural and applied rainfall. *Water Resources Research*, 33, 91–109.
- Montrasio, L., & Valentino, R. (2007). Experimental analysis and modelling of shallow landslides. *Landslides*, 1-6. doi:10.1007/s10346-007-0082-3
- Morgenstern, N. R., & de Matos, M. M. (1975). Stability of slopes in residual soils. *Proceedings of the 5th Panamerican Conference on Soil Mechanics and Foundation Engineering*, 3, pp. 367–383. Buenos Aires.
- Mualem, Y. (1978). Hydraulic conductivity of unsaturated porous media: Generalized macroscopic approach. *Water Resources Research*, 14(2), 325-334.
- Munoz, J. J., Gennare, V. D., & Delaure, E. (2008). Experimental determination of unsaturated hydraulic conductivity in compacted silt. In D. G. Toll, C. E. Augarde, D. Gallipoli, & S. J. Wheeler (Ed.), *Unsaturated soils-Advances in Geo-engineering* (pp. 123-127). London: Taylor & Francis.
- Nadim, F., Cepeda, F., Sandersen, F., Jaedicke, C., & Heyerdahl, H. (2009). Prediction of Rainfall-Induced Landslides through Empirical and Numerical Models. *Rainfall-induced landslides: mechanisms, monitoring techniques and nowcasting models for early-warning systems - First Italian Workshop on Landslides*, 1-10. Naples, Italy.

- Ng, C. W., & Shi, Q. (1998). A numerical investigation of the stability of unsaturated soil slopes subjected to transient seepage. *Computers and Geotechnics*, 22, 1-28.
- Nuth, M., & Laloui, L. (2008). Effective Stress Concept in Unsaturated Soils :Clarification and Validation of an Unified Framework. *Int. Journ. of Numerical and Analytical Methods in Geomechanics*, 32, 771-801.
- Oberg, A. L., & Salfors, G. (1995). A rational approach to the determination of the shear strength parameters of unsaturated soils. *Proceedings of First International conference on Unsaturated Soils*, 1, pp. 151-158. Paris.
- Oka, H. (1972). Impacts by the “artificial landslide”: re-examine the rage of nature (in Japanese). *Kagaku Asahi*, 32(1), 152-153.
- Okura, Y., Kitahara, H., Ochiai, H., Sammori, T., & Kawanami, A. (2002). Landslide fluidization process by flume experiments. *Engineering Geology*, 66, 65-78.
- Olivares, L., & Damiano, E. (2007). Postfailure Mechanics of Landslides: Laboratory Investigation of Flowslides in Pyroclastic Soils. *Journal of Geotechnical and Geoenvironmental Engineering*, 133(1), 51. doi:10.1061/(ASCE)1090-0241(2007)133:1-15
- Olivares, L., & Picarelli, L. (2003). Shallow flowslides triggered by intense rainfalls on natural slopes covered by loose unsaturated pyroclastic soils. *Geotechnique*, 53(2), 283-288.
- Olivares, L., Damiano, E., Greco, R., Zeni, L., Picarelli, L., Minardo, A., . . . Bernini, R. (2009). An Instrumented Flume to Investigate the Mechanics of Rainfall-Induced Landslides in Unsaturated Granular Soils. *Geotechnical Testing Journal*, 32(2), 1-11.
- Olivella, S., Gens, A., Carrera, J., & Alonso, E. E. (1996). Numerical formulation for a simulator (CODE_BRIGHT) for the coupled analysis of saline media. *Engineering computations*, 13(7), 87-112.

- Orense, R. P., Shimoma, S., Maeda, K., & Towhata, I. (2004). Instrumented Model Slope Failure due to Water Seepage. *Journal of Natural Disaster Science*, 26, 15-26.
- Pagano, L., Rianna, G., Zingariello, M., Urciuoli, G., & Vinale, F. (2008). An early warning system to predict flowslides in pyroclastic deposits. In Z. Chen, J.-M. Zhang, K. Ho, F.-Q. Wu, & Z.-K. Li (Ed.), *Landslides and engineered slopes: from the past to the future. Proceedings of the tenth international symposium on landslides and engineered slopes* (pp. 1259-1264). Xi'an: Taylor & Francis.
- Petley, D. (2012). Global patterns of loss of life from landslides. *Geology*, 40(10), 927-930.
- Petley, D. N., Bulmer, M. H., & Murphy, W. (2002). Patterns of movement in rotational and translational landslides. *Geology*, 30(8), 719.
- Petrucci, R. H. (n.d.). *General Chemistry: Principles and Modern Applications*. New York: Macmillan Publishing Co.
- Philip, J. R. (1993). Comment on "Hillslope infiltration and lateral downslope unsaturated flow" by C. R. Jackson. *Water Resources Research*, 29(12), 4167.
- Picarelli, L., Olivares, L., & Damiano, E. (2006). Discussion to "Evaluation of landslide triggering mechanisms in model fill slopes" by W.A. Take, M.D. Bolton, P.C.P. Wong, and F.J. Yeung [Landslides 1(3):173–184, October 2004] and "A fluidized landslide on a natural slope by artificial rainfall" by ... *Landslides*, 3, 269–272.
- Pockoski, M., & Duncan, J. M. (2000, December). Comparison of Computer Programs for Analysis of Reinforced Slopes. *Virginia Polytechnic Institute and State University*.
- Rahardjo, H., Ong, T. H., Rezaur, R. B., & Leong, E. C. (2007). Factors controlling instability of homogeneous soil slopes under rainfall. *J. Geotech. Geoenviron. Eng.*, 133(12), 1532-1543.

- Rahardjo, H., Ong, T. H., Rezaur, R. B., & Leong, E. C. (n.d.). Factors controlling instability of homogeneous soil slopes under rainfall. *Journal of Geotechnical and Geoenvironmental Engineering*, 133(12), 1532–1543.
- Rahimi, A., Rahardjo, H., & Leong, E.-C. (2011). Effect of Antecedent Rainfall Patterns on Rainfall-Induced Slope Failure. *Journal of Geotechnical and Geoenvironmental Engineering*, 137(5), 483-491.
- Rawls, W. J., & Brakensiek, D. L. (1985). Prediction of soil water properties for hydrologic modeling. In E. Jones, & T. J. Ward, *Watershed Management in the Eighties* (pp. 293-299). Denver: ASCE.
- Reichenbach, P., Cardinali, M., De Vita, P., & Guzzetti, F. (1998). Regional hydrological thresholds for landslides and floods in the Tiber River Basin (central Italy). *Env. Geol.*, 35(2 & 3), 146-159.
- Reid, M. E., LaHusen, R. G., & Iverson, R. M. (1997). Debris-flow initiation experiments using diverse hydrological triggers. In C. L. Chen, *Debris-Flow Hazards Mitigation: Mechanics, Prediction, and Assessment* (pp. 1-10). New York: American Society of Civil Engineers.
- Richards, L. A. (1931). Capillary conduction of liquids through porous medium. *Journal of physics*, 318-333.
- Rossi, M., Guzzetti, F., Reichenbach, P., Mondini, A. C., & Peruccacci, S. (2010). Optimal landslide susceptibility zonation based on multiple forecasts. *Geomorphology*, 114, 129-142.
- Rumpf, H. (1961). The strength of granules and agglomerates. *International Symposium on Agglomeration*, (pp. 379-418). Philadelphia.
- Santacana, N., Baeza, B., Corominas, J., De Paz, A., & Marturia, J. (2003). A GIS-based multivariate statistical analysis for shallow landslide susceptibility mapping in La Pobla de Lillet Area (Eastern Pyrenees, Spain). *Nat. Hazards*, 30, 281-295.
- Scheinost, A. C., Sinowski, W., & Auerswald, K. (1997). Regionalization of soil water retention curves in a highly variable soilscape, I. Developing a new pedotransfer function. *Geoderma*, 78, 129-143.

- Schnellmann, R., Busslinger, M., Schneider, H. R., & Rahardjo, H. (2010). Effect of rising water table in an unsaturated slope. *Engineering Geology*, 114, 71-83.
- Shoarian Sattari, A. (2014). Obtaining soil-water characteristic curves by numerical modeling of drainage in particulate media. *Thesis for Master of Science*. Ankara: Middle East Technical University.
- Sidle, R. C., & Ochiai, H. (2006). *Landslides: Processes, Prediction, and Land Use*. Washington, D.C.: American Geophysical Union Water Resources Monograph 18.
- Sjoblom, J. K. (2000). The mechanisms involved during the desaturation process of a porous matrix.
- Srivastava, R., & Yeh, T. J. (1991). Analytical solutions for one-dimensional, transient infiltration toward the water table in homogeneous and layered soils. *Water Resources Research*, 753-762.
- Suryo, E. A. (2013). Real - time prediction of rainfall induced instability of residual soil slopes associated with deep cracks. *PhD thesis*. Queensland University of Technology.
- Take, W. A., Bolton, M. D., Wong, P. C., & Yeung, F. J. (2004). Evaluation of landslide triggering mechanisms in model fill slopes. *Landslides*, 3(1), 173-184.
doi:10.1007/s10346-004-0025-1
- Terlien, M. T. (1998). The determination of statistical and deterministic hydrological landslide triggering thresholds. *Env Geol*, 124-130.
- Terranova, O., Antronico, L., & Gulla, G. (2007). Landslide triggering scenarios in homogeneous geological contexts: The area surrounding Acri (Calabria, Italy). *Geomorphology*, 87(4), 250-267.
- Terzaghi, K. (1925). *Erdbaumechanik auf bodenphysikalischer Grundlage*. F. Deuticke. Vienna.
- Terzaghi, K. (1943). *Theoretical Soil Mechanics*. New York: Wiley.

- Teysseire, P. (2005). *Geotechnische Eigenschaften von Moränen, Diss-Nr. 16322*. ETH Zurich, Zurich. Retrieved from (<http://dx.doi.org/10.3929/ethz-a-005166289>)
- Thiebes. (2012). *Landslide Analysis and Early Warning Systems. PhD thesis.*
- Tohari, A., Nishigaki, M., & Komatsu, M. (2007). Laboratory Rainfall-Induced Slope Failure with Moisture Content Measurement. *Journal of Geotechnical and Geoenvironmental Engineering*, 133(5), 575-587. doi:10.1061/(ASCE)1090-0241(2007)133:5(575)
- Toker, N. K. (2002). Improvements and reliability of the MIT tensiometer and studies on soil moisture characteristic curves. *Master of Science Dissertation in Civil and Environmental Engineering*. Cambridge: Massachusetts Institute of Technology.
- Toker, N. K. (2007). Modeling the relation between suction, effective stress and shear strength in partially saturated granular media. *PhD thesis*. Massachusetts Institute of Technology.
- Toker, N. K., Germaine, J. T., & Culligan, P. J. (2014). Effective Stress and Shear Strength of Moist Uniform Spheres. *Vadose zone journal*, 1-13.
- Toker, N. K., Germaine, J. T., Sjoblom, K. J., & Culligan, P. J. (2004). A new technique for rapid measurement of continuous SMC curves. *Geotechnique*, 54(3), 179-186.
- Toll, D. G., Lourenco, S. D., Mendes, J., Gallipoli, D., Evans, F. D., Augarde, C. E., . . . Tarantino, A. (2011). Soil suction monitoring for landslides and slopes. *Quarterly Journal of Engineering Geology and Hydrogeology*, 44(1), 23-33. doi:10.1144/1470-9236/09-010
- Torres, R., & Alexander, L. (2002). Intensity-duration effects on drainage: column experiments at near-zero pressure head. *Water Resources Research*, 38, 1240.
- van Genuchten, M. T. (1980). A closed-form equation for predicting the hydraulic conductivity of unsaturated soils. *Soil Sci. Soc. of Am. J.*, 44, 892-898.

- van Westen, C. J. (2007). Mapping landslides: recent developments in the use of digital information. *Proceedings of the first North American conference on landslides*, (pp. 221-238). Vail.
- Vanapalli, S. K., Fredlund, D. G., Pufahl, D. E., & Clifton, A. W. (1996). Model for the prediction of shear strength with respect to soil suction. *Canadian Geotechnical Journal*, 33, 379-392.
- Vereecken, H. J., Feyen, J., Maes, J., & Darius, P. (1989). Estimating the soil moisture retention characteristic from texture, bulk density, and carbon content. *Soil Science*, 148, 389-403.
- Wieczorek, G. F., & Glade, T. (2005). Climatic factors influencing occurrence of debris flows. In M. Jakob, & O. Hunger, *Debris-flow hazards and related phenomena* (pp. 325-362). Berlin: Springer.
- Wolle, C. M., & Hachich, W. (1989). Rain-induced landslides in southeastern Brazil. *Proceedings of the 12th International Conference on Soil Mechanics and Foundation Engineering*, (pp. 1639–1644). Rio de Janeiro.
- Yagi, N., Yatabe, R., & Enoki, A. (1985). Laboratory and field experiments on prediction method of occurring time of slope failure due to rainfall ([in Japanese]). *Landslides (Japanese Landslide Society)*, 22(2), 1-7.
- Yamaguchi, I., Nishio, K., Kawabe, H., Shibano, H., & Lida, C. (1989). Initiation and fluidization of an artificial landslide: field experiment in Yui, Shizuoka Prefecture, Japan ([in Japanese]). *Shinrin Kosoku (Areal Survey)*, 158, 3-9.
- Zehtab, K. H., Toker, N. K., & Ahmadi-adli, M. (2012). Comparison of formulae for shear strength of unsaturated soils. *Proc. of 3rd International Conference on New Developments in Soil Mechanics and Geotechnical Engineering* (pp. 795-802). Nicosia, North Cyprus: Near East University.
- Znidarcic, D., Illangasekare, T., & Manna, M. (1991). Laboratory testing and parameter estimation for two-phase flow problems. *Geotechnical Special Publication*(27), 1089-1099.

APPENDIX A

DETAIL OF EXPERIMENTS IN FLUME AND LAMINAR BOX TESTS

Flume test specifications, details of sample preparation and illustrations of test setup and soil samples during testing for all flume and laminar box tests are summarized in appendix A. Test time (initiation and termination), temperature, soil sample properties (slope inclination, water content, relative density) and applied rainfall intensity as test specifications are reported for each of the experiments. Photos from stages of sample preparation and some details about instrumentation placement are also shown. Consequence of rainfalling, observed failure surfaces, opened gaps/cracks due to slope instability and wetting front at the time of failure are shown for each test. Any specific phenomenon and non-routine incident throughout sample preparation and testing are also reported illustratively in this section.

FLM_00

Sample preparation on: 27 August 2013 (13:00-16:30)	Test performance on: 28 August 2014 (19:14-22:20)
Room temperature: 27°C	D _R after test: 50.1%
Trapezoidal slope angle: 15.5°	Rainfalling sys. adjust: 15/60 (10.6 mm/hr)
Flume base tilt angle: 27.5°	Time to failure: No failure
Initial water content: 1.5 %	
Intended D _R : 61%	

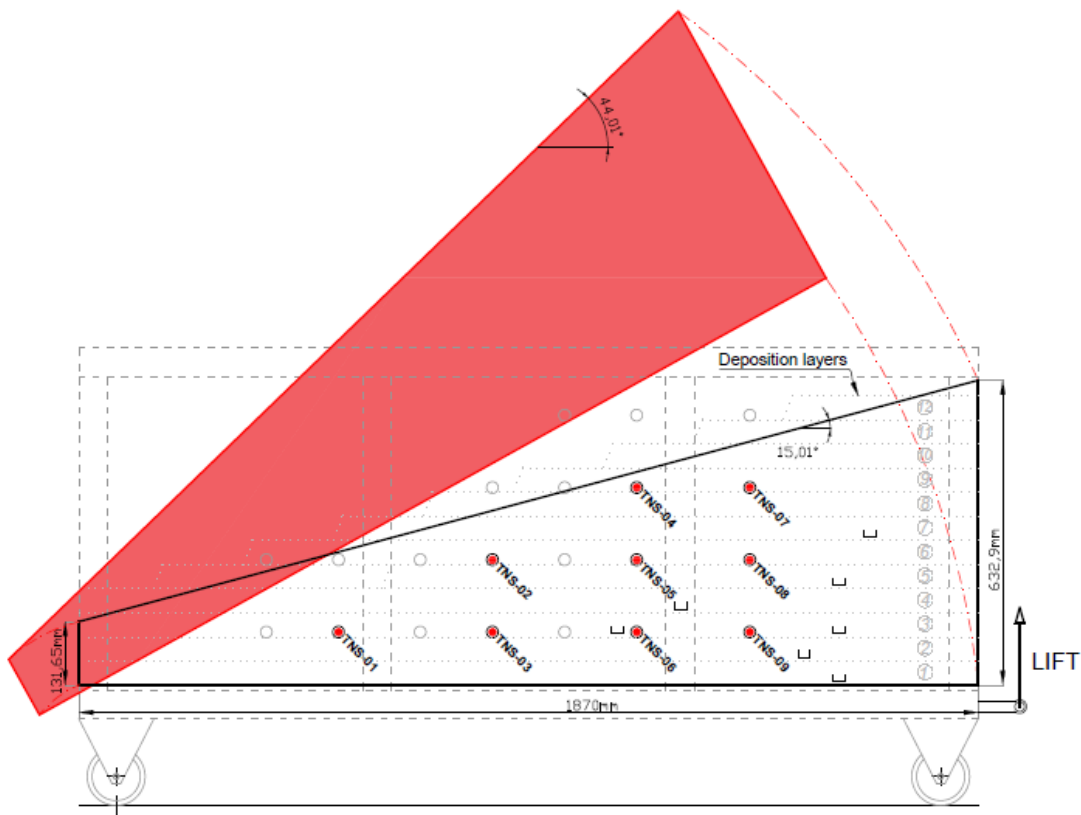


Fig. A.1. Deposition, instrumentation and positioning for FLM_00



Fig. A.2. (a) Sample placement in layers with no drain in slope toe, (b) soil layer placement, (c) placement of relative density checkup tares, (d) controlled compaction of soil layers, (e) placed instrumentation (tensiometers) and (f) trimmed soil slope for FLM_00

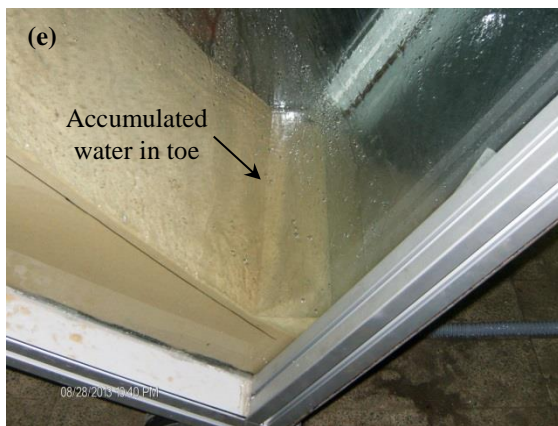


Fig. A.3. (a) positioned flume (slope), (b) rainfall spraying, (c) measurement of wetting front progress, (d) wetting front at the time of failure, (e) accumulation of water at toe of slope, (f) no failure in slope due to raining in FLM_00

FLM_01

Sample preparation on: 8 December 2013 (13:00-21:00)	Test performance on: 10 December 2013 (16:40-08:15 n.d.)
Room temperature: 21°C	D _R after test: 58.3%
Slope angles: 45° (left) & 50° (right)	Rainfalling sys. adjust: 5/60 (4.1 mm/hr) & 30/60 (24.8 mm/hr)
Initial water content: 1.5 %	Time to failure: No failure
Intended D _R : 61%	

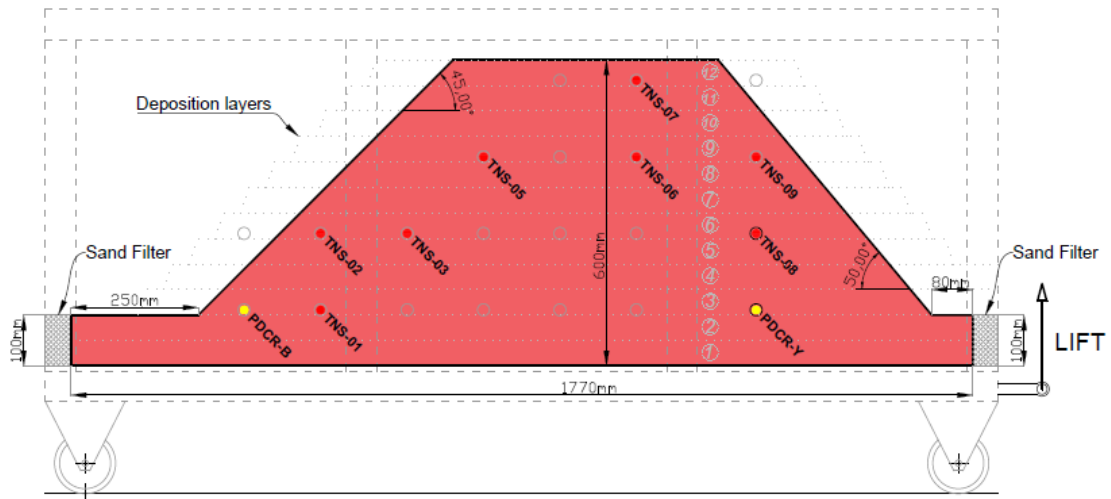


Fig. A.4. Deposition, instrumentation and positioning for FLM_01



Fig. A.5. (a) Constructed 2-sided slope subjected to rainfall for FLM_01, (b) covering flume box to have more controlled intensity for rainfall, (c) wetting front and locations of measurement, (d) instrumentations (pore pressure transducers and PCDR devices and (e) crest of the slope after raining, no failure crack (FLM_01).

FLM_02

Sample preparation on: 31 December 2013 (11:00-14:15)	Test performance on: 1 January 2014 (17:15-08:15 n.d.)
Room temperature: 21°C	D _R after test: 59.6%
Slope angles: 55° (left) & 60° (right)	Rainfalling sys. adjust: 15/60 (10.6 mm/hr)
Initial water content: 1.5 %	Time to failure: No failure
Intended D _R : 61%	

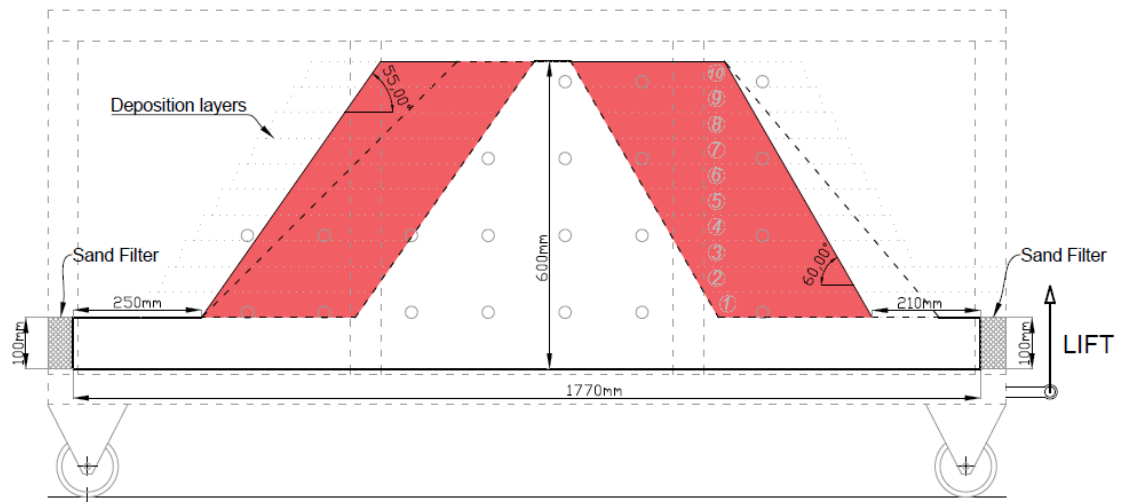


Fig. A.6. Deposition, instrumentation and positioning for FLM_02



Fig. A.7. (a) & (b) Right slope surface from FLM_01 which is trimmed in FLM_02, (c) & (d) controlled deposition of right and left slopes for FLM_02, (e) slope shape (covered till test date) and (f) slope subjected to rainfall for FLM_02

FLM_03

Sample preparation on: 8 April 2014 (15:45-21:00)	Test performance on: 12 April 2014 (12:06-13:00)
Room temperature: 19°C	D _R after test: 34.9%
Trapezoidal slope angle: 15.3°	Rainfalling sys. adjust: 55/60 (54.4 mm/hr)
Flume base tilt angle: 41.2°	Time to failure: 48 minutes
Initial water content: 1.5 %	
Intended D _R : 34%	

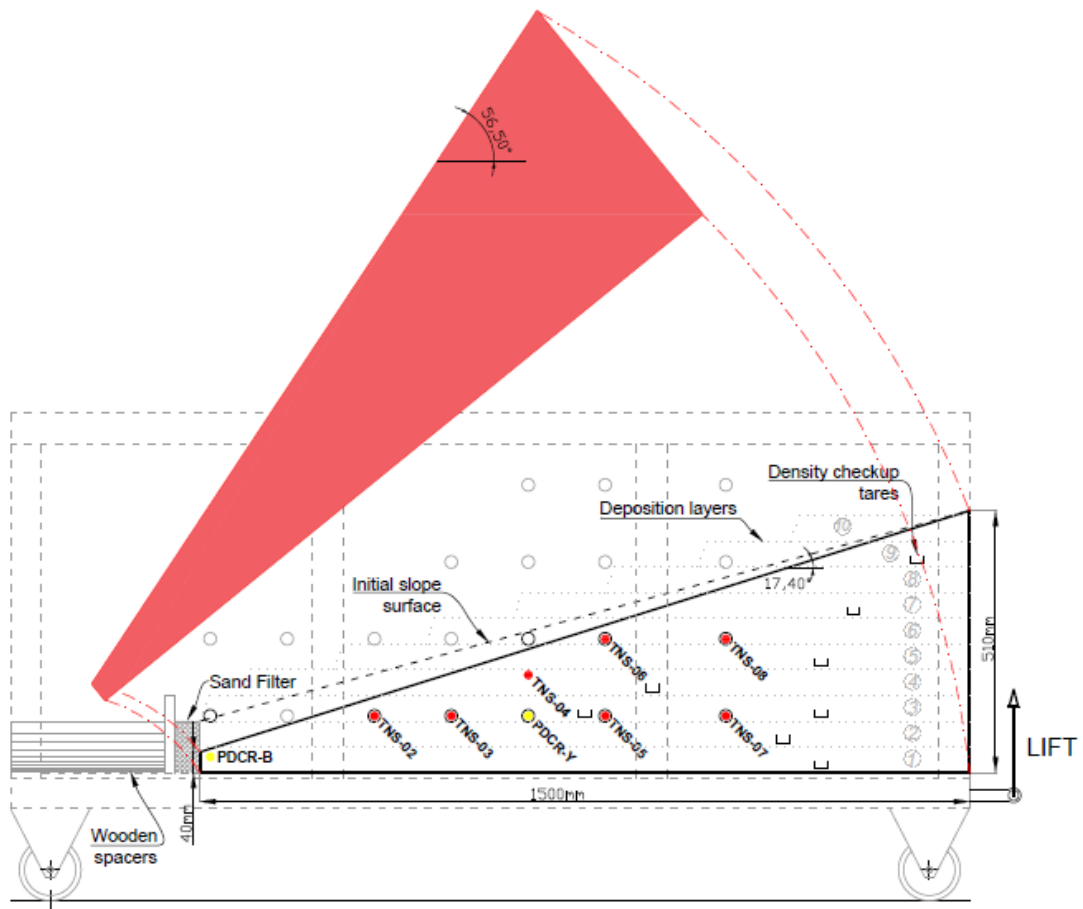


Fig. A.8. Deposition, instrumentation and positioning for FLM_03



Fig. A.9. (a) Geonet in the base of flume, (b) filter material and soil layer placement, (c) placement of tensiometers and dry density checkup tares, (d) fully placed sample, (e) trimmed soil sample and (f) tilted flume, covered surface and left for equalization in FLM_03



Fig. A.10. (a) & (b) desiccated soil surface, (c) wetting front at the time of failure, (d) slipped soil (top view), (e) slipped soil (side view), (f) & (g) disturbance in slipped mass in vicinity of tensiometers in FLM_03

FLM_04

Sample preparation on: 2 May 2014 (12:15-18:00)	Test performance on: 4 May 2014 (17:00-18:00)
Room temperature: 20°C	D_R after test: 36
Trapezoidal slope angle: 15.3°	Rainfalling sys. adjust: 43/60 (46.3 mm/hr)
Flume base tilt angle: 41.2°	Time to failure: 60 minutes
Initial water content: 1.5 %	
Intended D_R : 34	

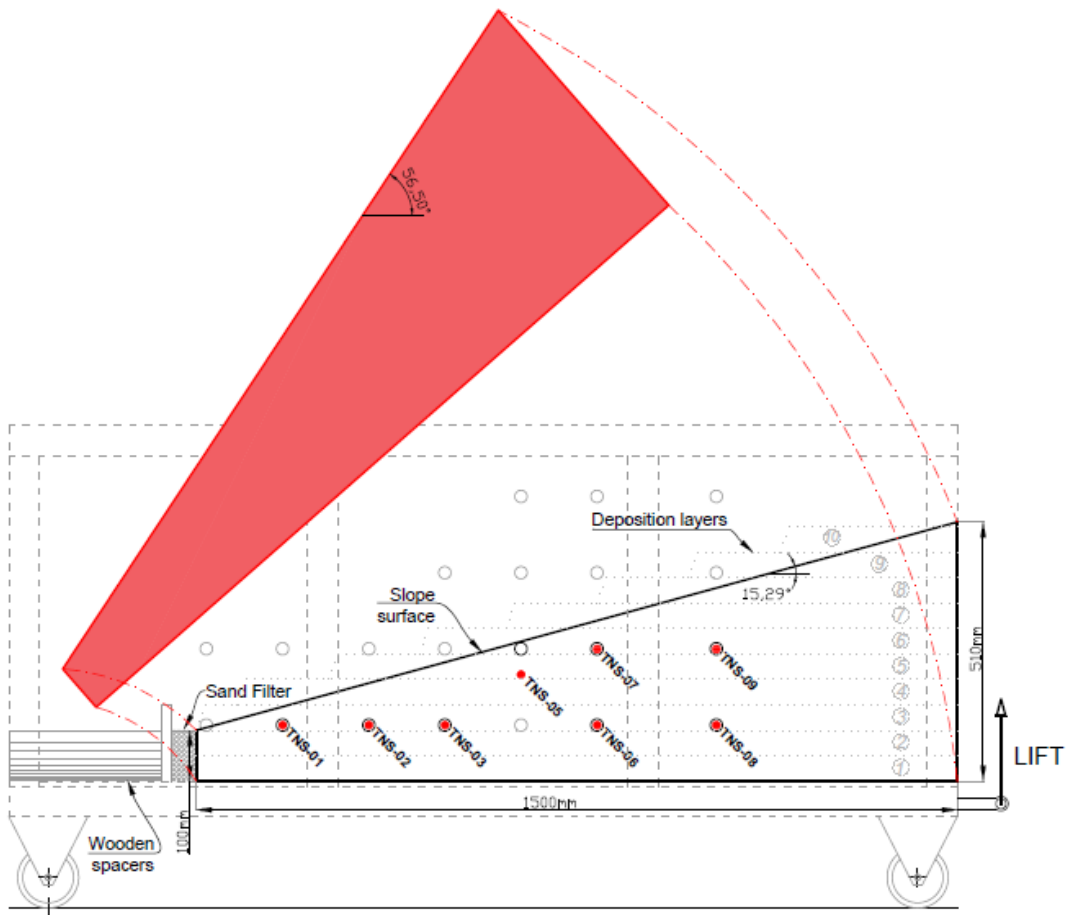


Fig. A.11. Deposition, instrumentation and positioning for FLM_04

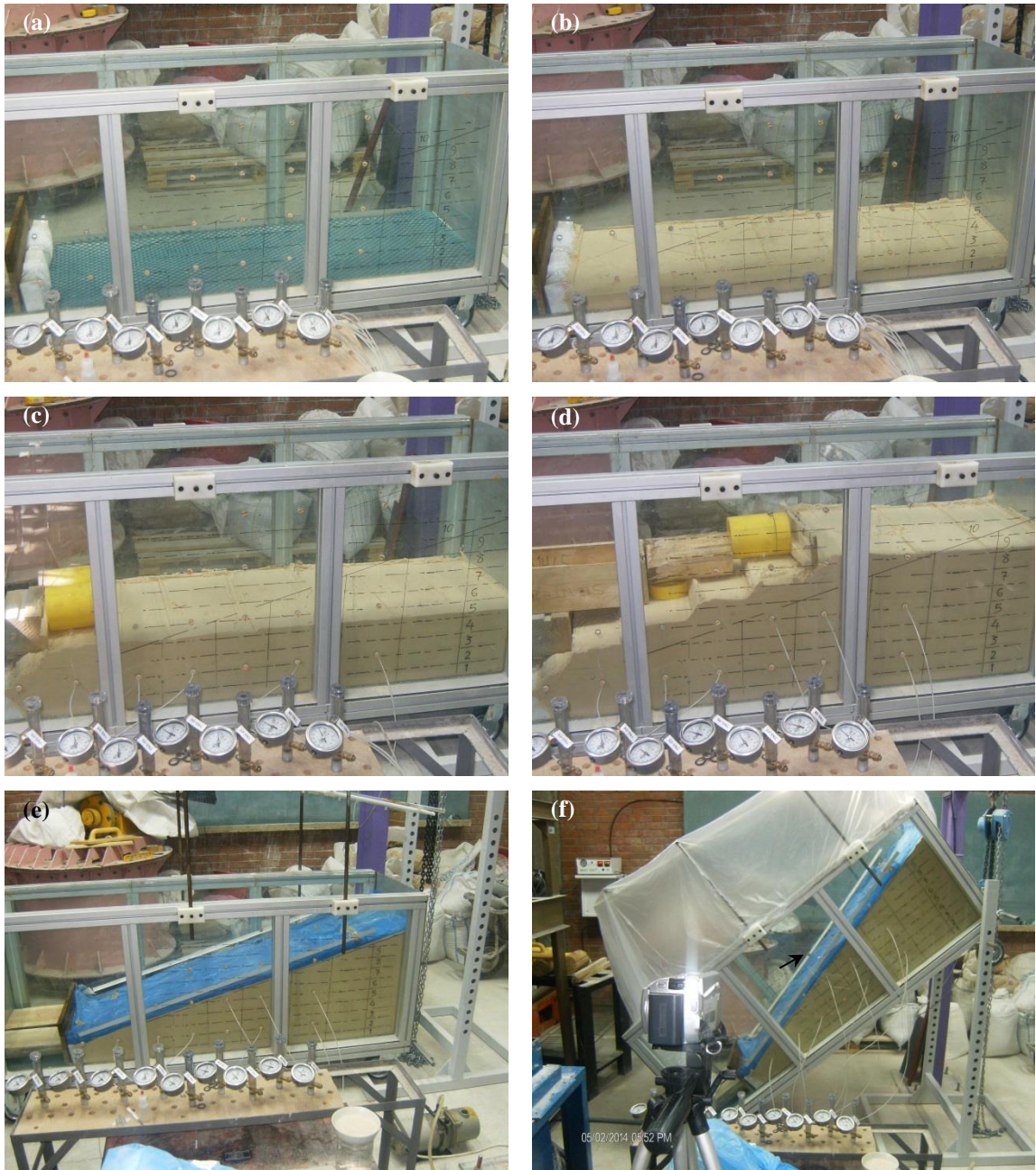


Fig. A.12. (a) Geonet in the base of flume and filter material boxes, (b) soil layer placement, (c) & (d) placement of tensiometers, (e) trimmed soil sample and (f) tilted flume, covered surface and left for equalization for FLM_04



Fig. A.13. (a) & (b) placement of intensity checkup tares on soil surface, (c) & (d) wetting front at the time of failure, (e) deformation in slope crest (top view), (f) slipped soil block in FLM_04

FLM_05

Sample preparation on: 10 May 2014 (21:00-04:00 n.d.)	Test performance on: 12 May 2014 (20:40-00:50 n.d.)
Room temperature: 21°C	D_R after test: 27
Trapezoidal slope angle: 15.3°	Rainfalling sys. adjust: 25/60 (28.3 mm/hr)
Flume base tilt angle: 41.2°	Time to failure: 69 minutes
Initial water content: 1.5 %	
Intended D_R : 34	

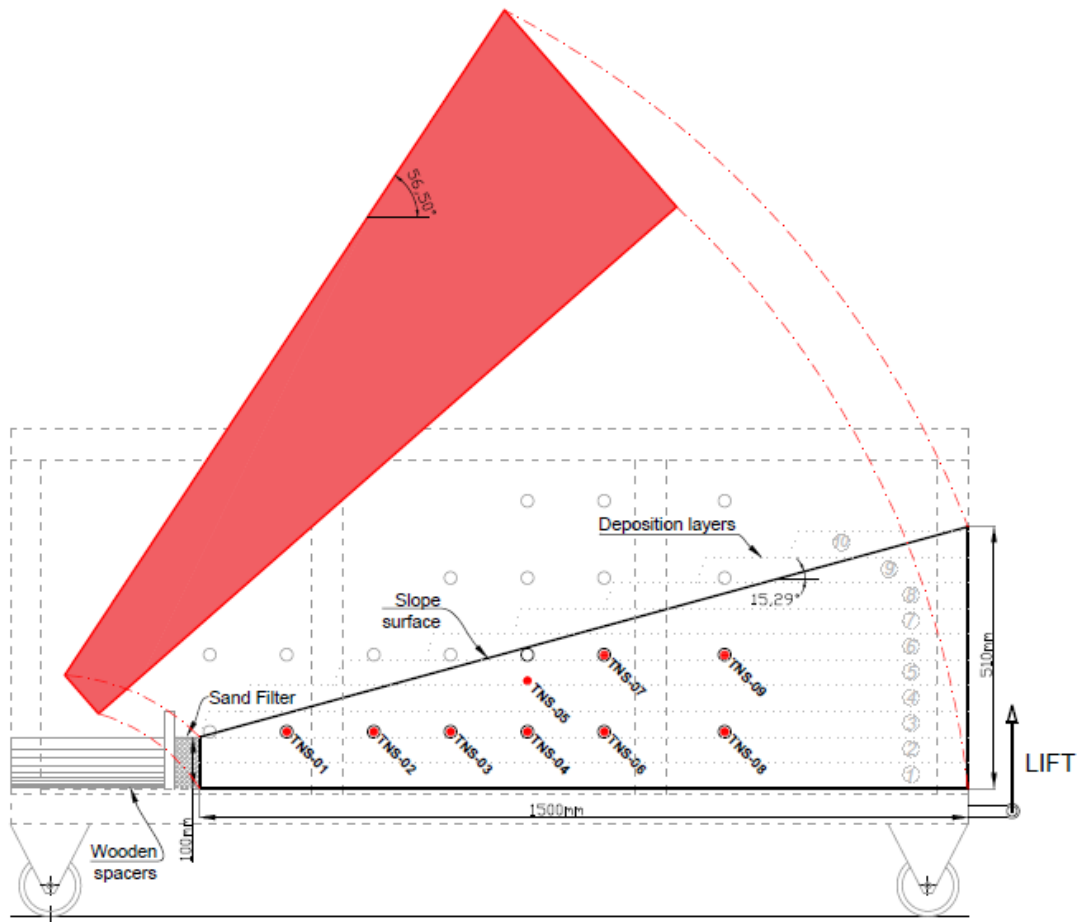


Fig. A.14. Deposition, instrumentation and positioning for FLM_05

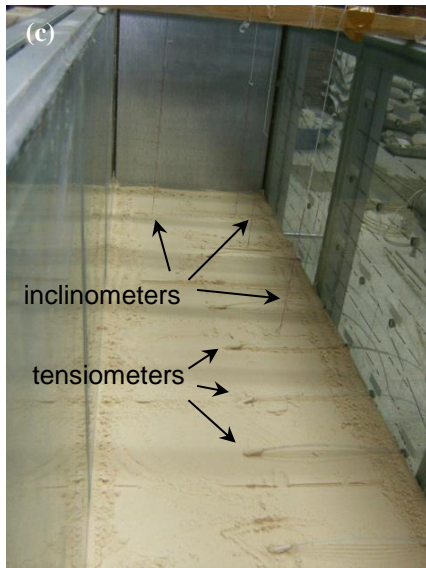
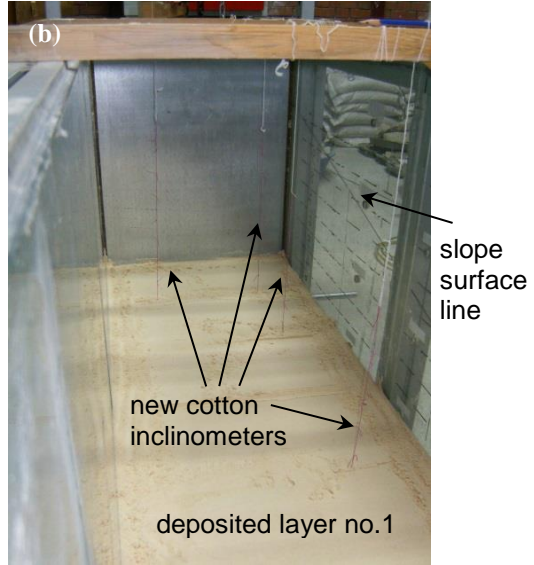


Fig. A.15. Geonet in the base of flume, (b) filter material and soil layer placement, (c) placement of tensiometers and dry density checkup tares, (d) fully placed sample, (e) trimmed soil sample and (f) tilted flume, covered surface and left for equalization in FLM_05

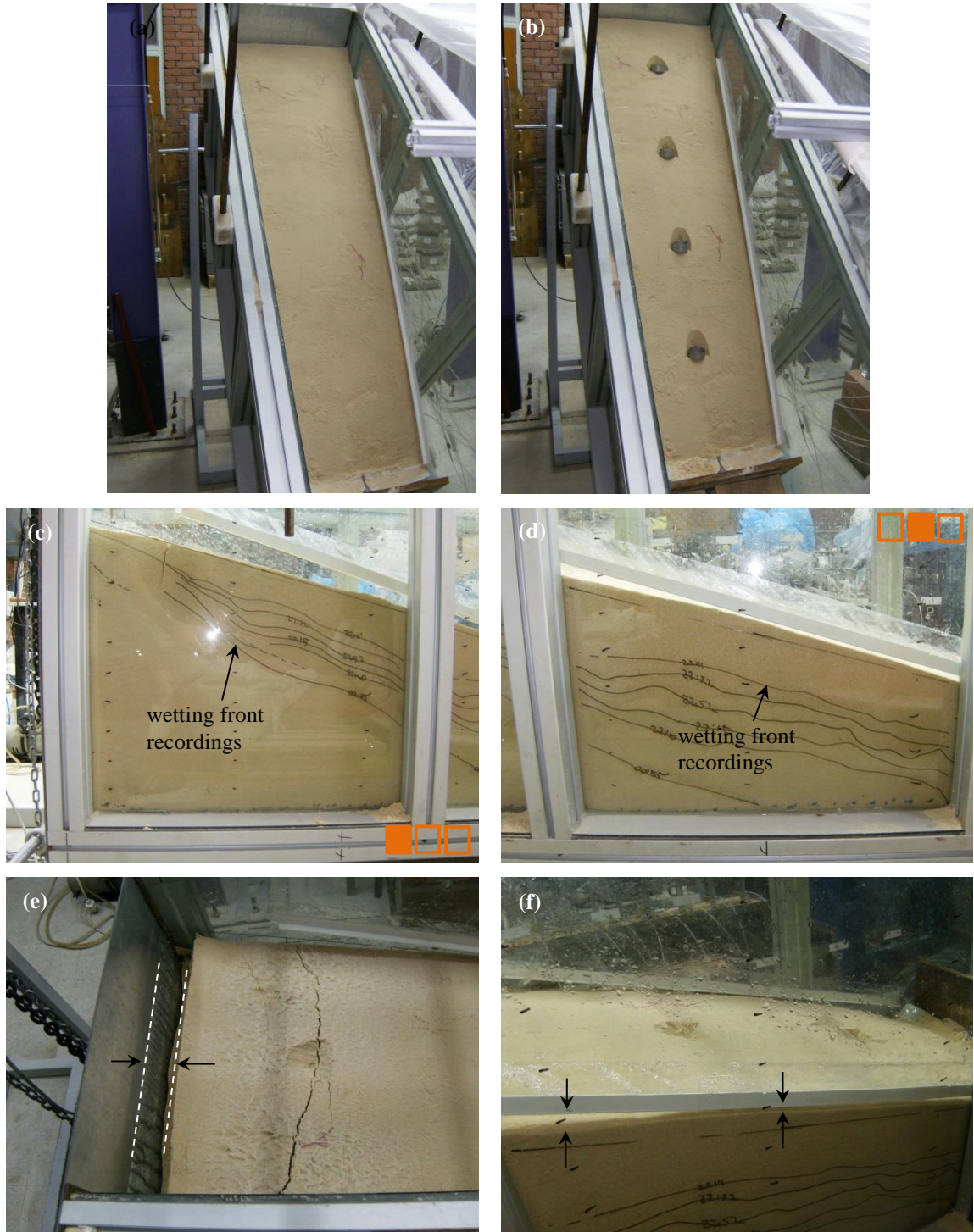


Fig. A.16. (a) & (b) placement of intensity checkup tares on soil surface, before and after, (c) & (d) wetting front recordings while testing, (e) slipped soil (top view) and (f) deformed soil surface for FLM_05

FLM_06

Sample preparation on: 23 May 2014 (14:00-13:00 n.d.)	Test performance on: 25 May 2014 (21:10-02:05 n.d.)
Room temperature: 21.7°C	D_R after test: 36.3
Trapezoidal slope angle: 15.3°	Rainfalling sys. adjust: 15/60 (15.6 mm/hr)
Flume base tilt angle: 41.2°	Time to failure: 295 minutes
Initial water content: 1.5 %	
Intended D_R : 34	

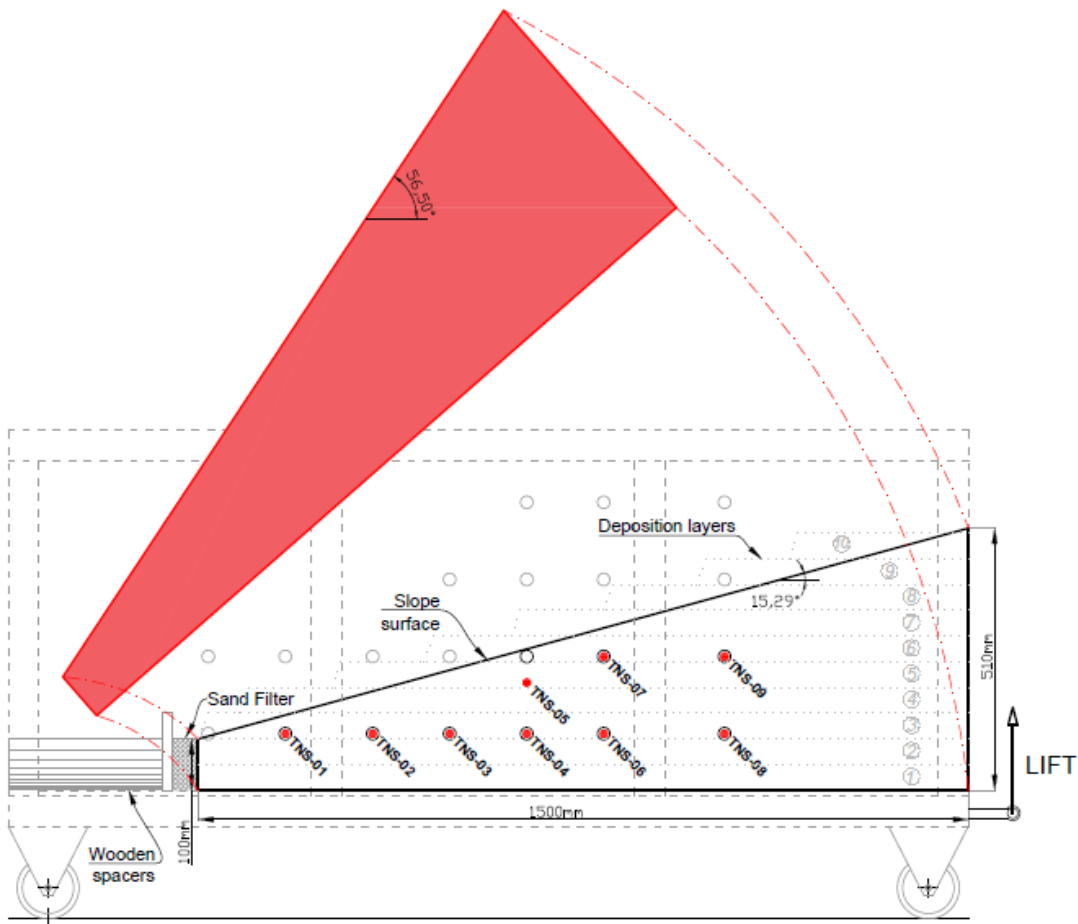


Fig. A.17. Deposition, instrumentation and positioning for FLM_06



Fig. A.18. (a), (b) & (c) mounted new inclinometers, placement of tensiometers and relative density checkup tares, (d) placed of soil layers, (e) & (f) fully placed sample for FLM_06



FLM_07

Sample preparation on: 30 May 2014 (18:00-23:00)	Test performance on: 30 May 2014 (23:15)
Room temperature: 21°C	D _R after test: 36.4
Trapezoidal slope angle: 15.3°	Rainfalling sys. adjust: 0/60
Flume base tilt angle: 42.7°	Time to failure: -
Initial water content: 1.5 %	
Intended D _R : 34	

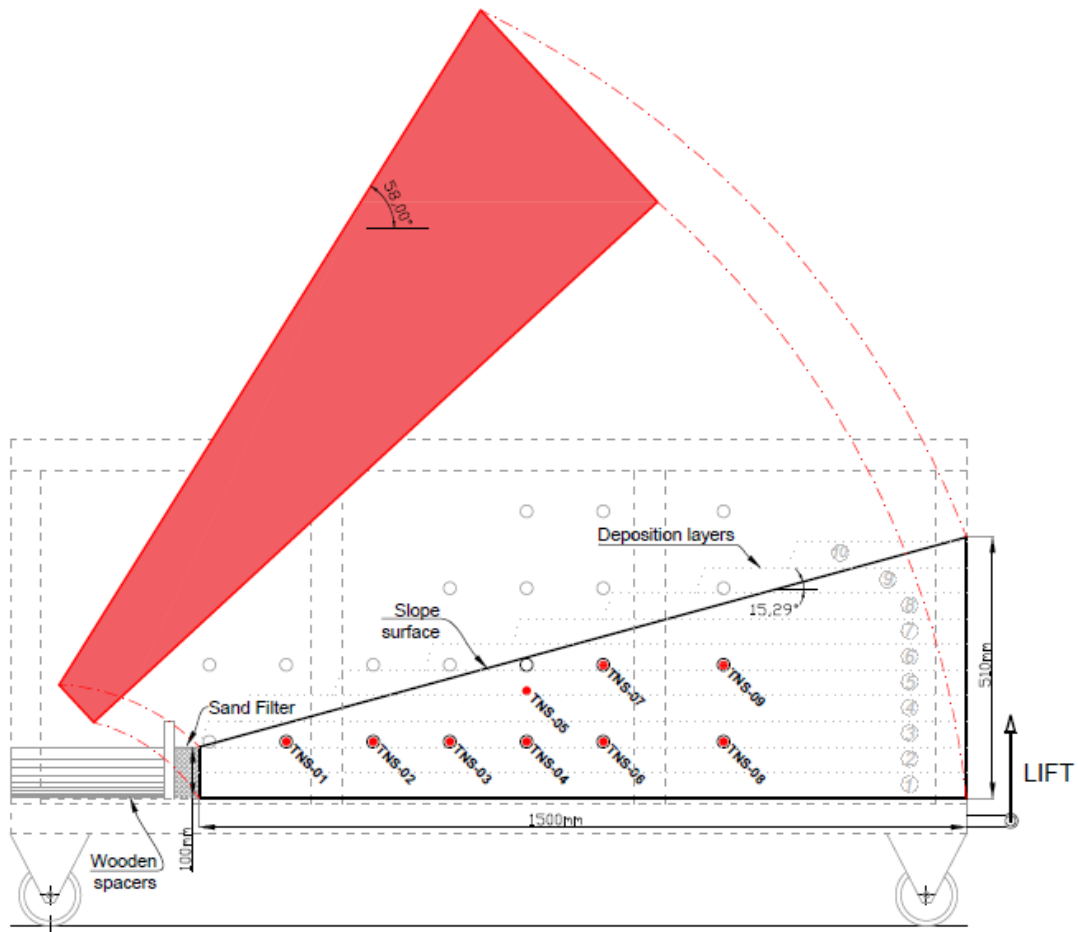


Fig. A.20. Deposition, instrumentation and positioning for FLM_07

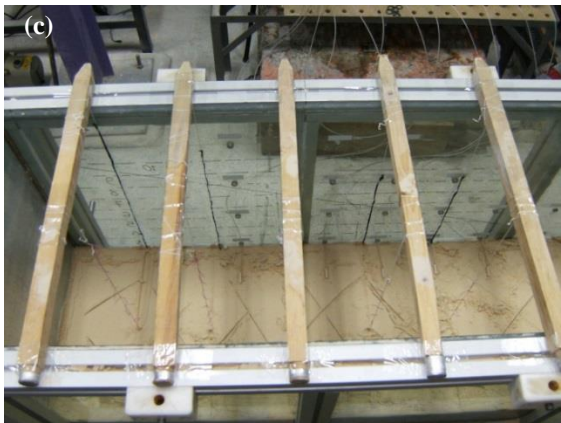
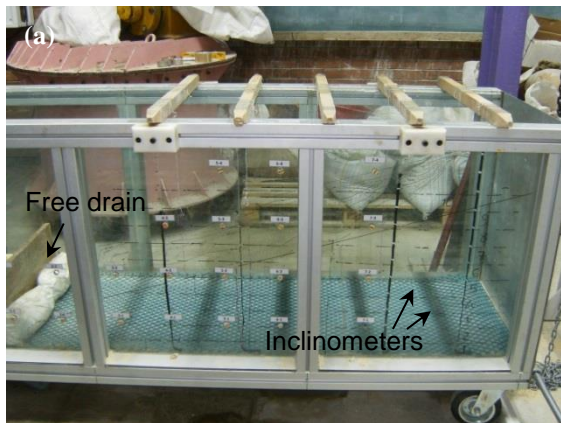


Fig. A.21. (a) wall inclinometers, (b) placement of tensiometers, (c), (d), (e) & (f) placement of soils for FLM_07

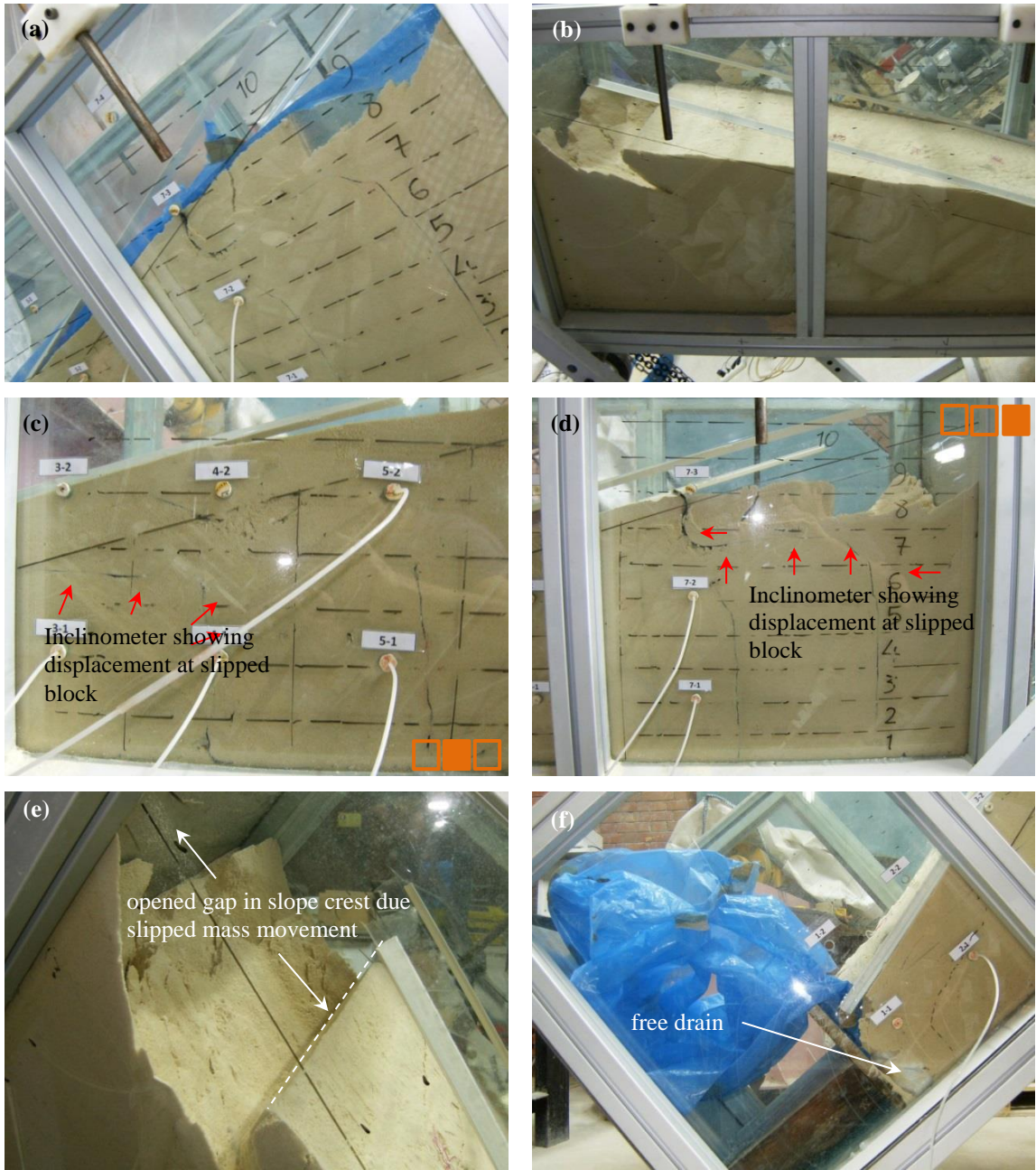


Fig. A.22. (a) rainfall intensity checkup tares, (b) slipped soil block, (c) & (d) inclinometers showing deformation at the time of failure, (e) opened gap in slope crest due slipped soil (top view), (f) override of slipped soil on free drain sacks for FLM_07

FLM_08

Sample preparation on: 16 June 2014 (17:00-22:30)	Test performance on: 18 June 2014 (15:00-16:15)
Room temperature: 21°C	D_R after test: 50.3
Trapezoidal slope angle: 15.3°	Rainfalling sys. adjust: 20/60 (21.6 mm/hr)
Flume base tilt angle: 41.2°	Time to failure: 73 minutes
Initial water content: 1.5 %	
Intended D_R : 48	

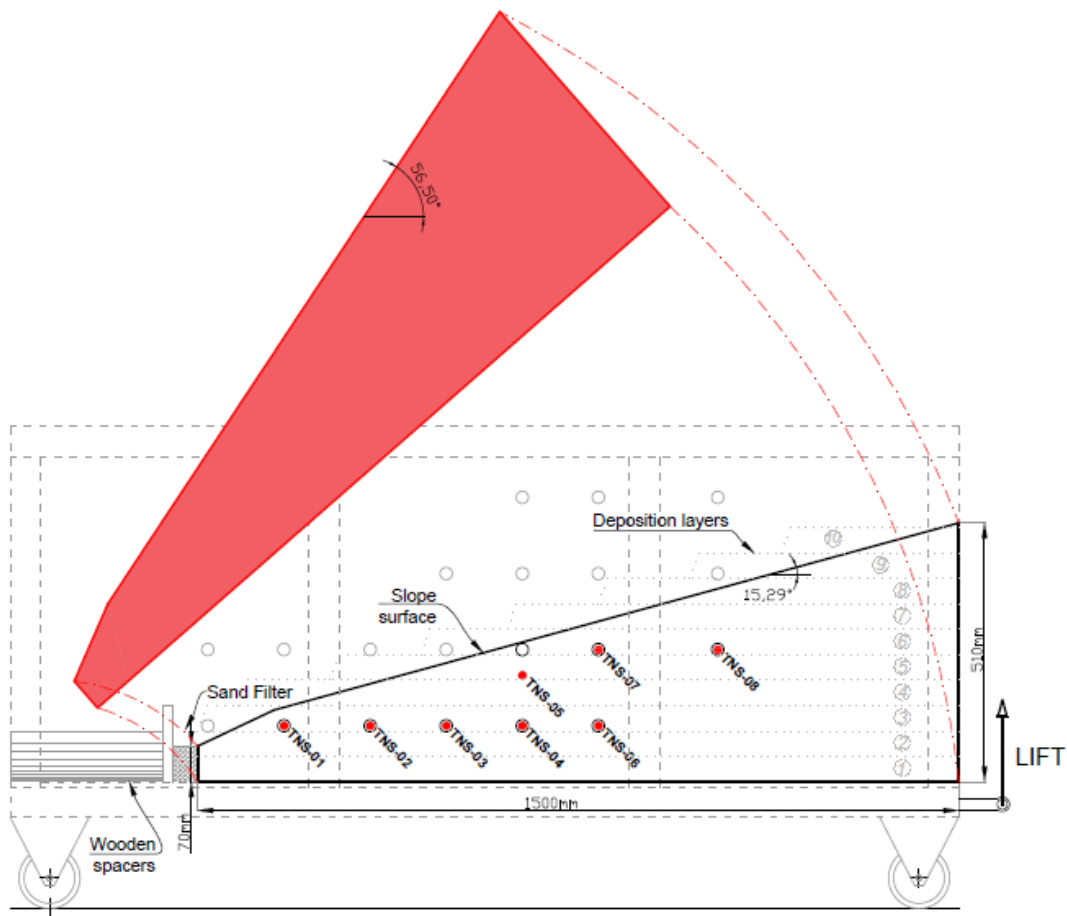


Fig. A.23. Deposition, instrumentation and positioning for FLM_08



Fig. A.24. (a) to (f) sample preparation for FLM_08

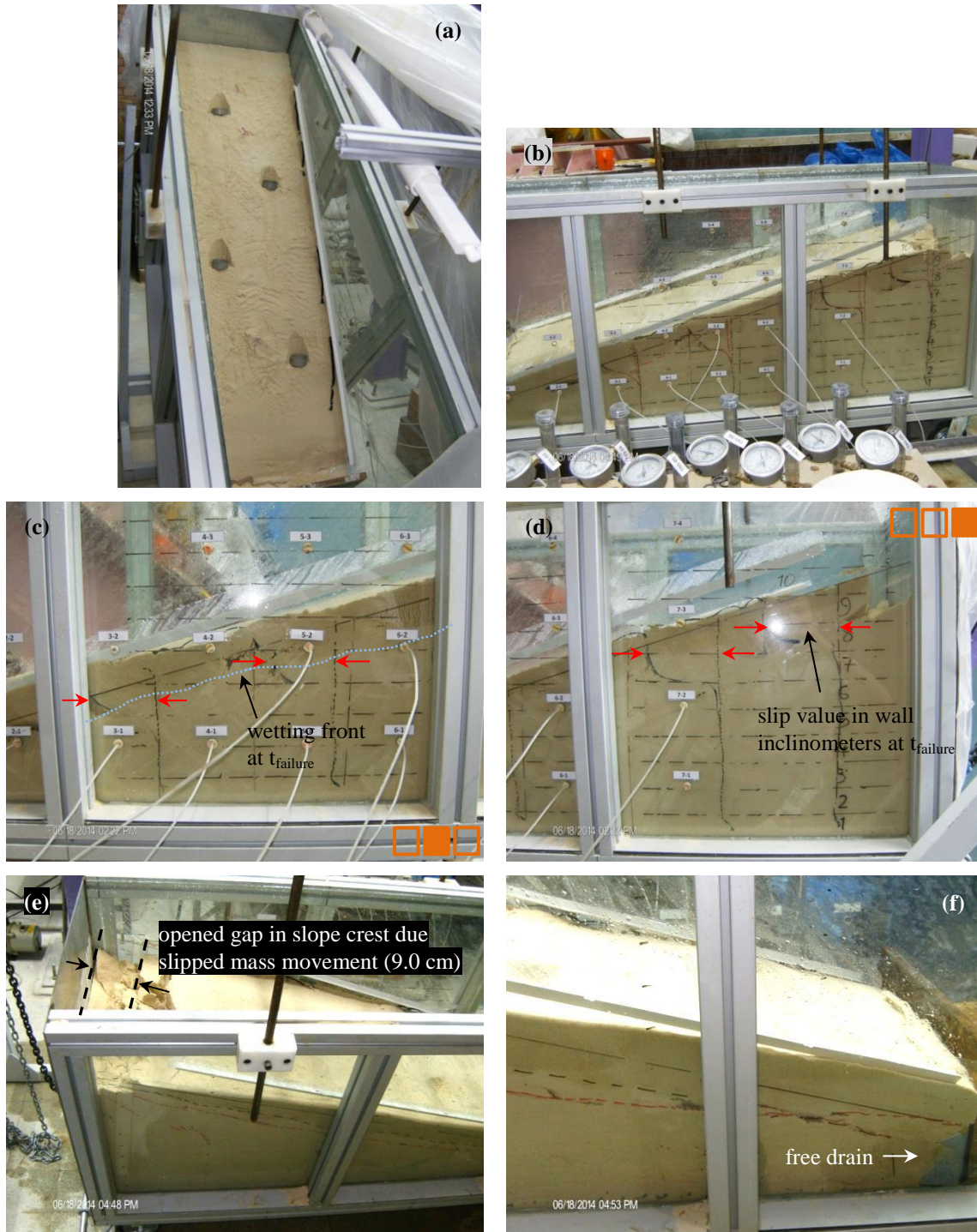


Fig. A.25. (a) rainfall intensity checkup tares, (b) slipped soil block, (c) & (d) inclinometers showing deformation at the time of failure, (e) opened gap in slope crest due to slipped soil (top view), (f) override of slipped soil on free drain sacks in FLM_08

FLM_09

Sample preparation on: 9 July 2014 (17:00-03:00 n.d.)	Test performance on: 13 July 2014 (15:40-17:48)
Room temperature: 19°C	D _R after test: 57
Trapezoidal slope angle: 15.3°	Rainfalling sys. adjust: 55/60 (59.6 mm/hr)
Flume base tilt angle: 42.8°	Time to failure: No failure
Initial water content: 1.5 %	
Intended D _R : 61	

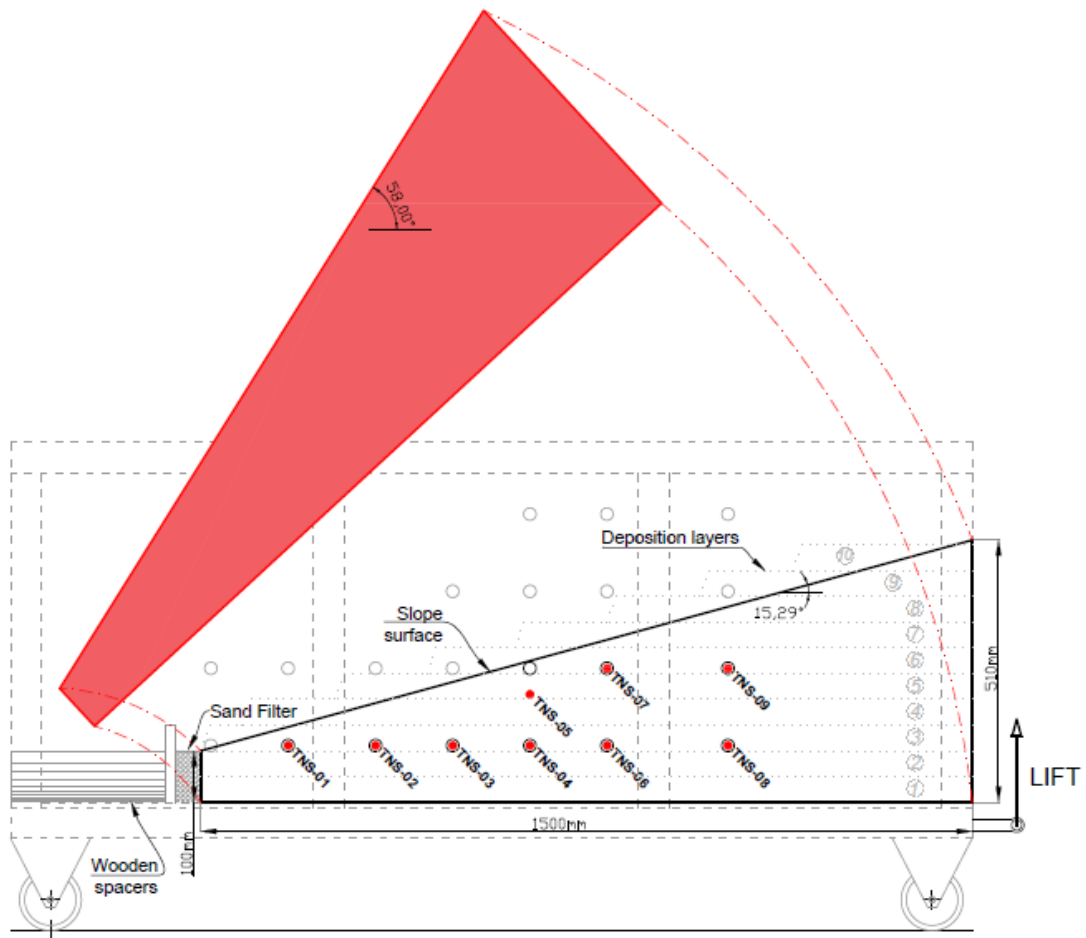


Fig. A.26. Deposition, instrumentation and positioning for FLM_09

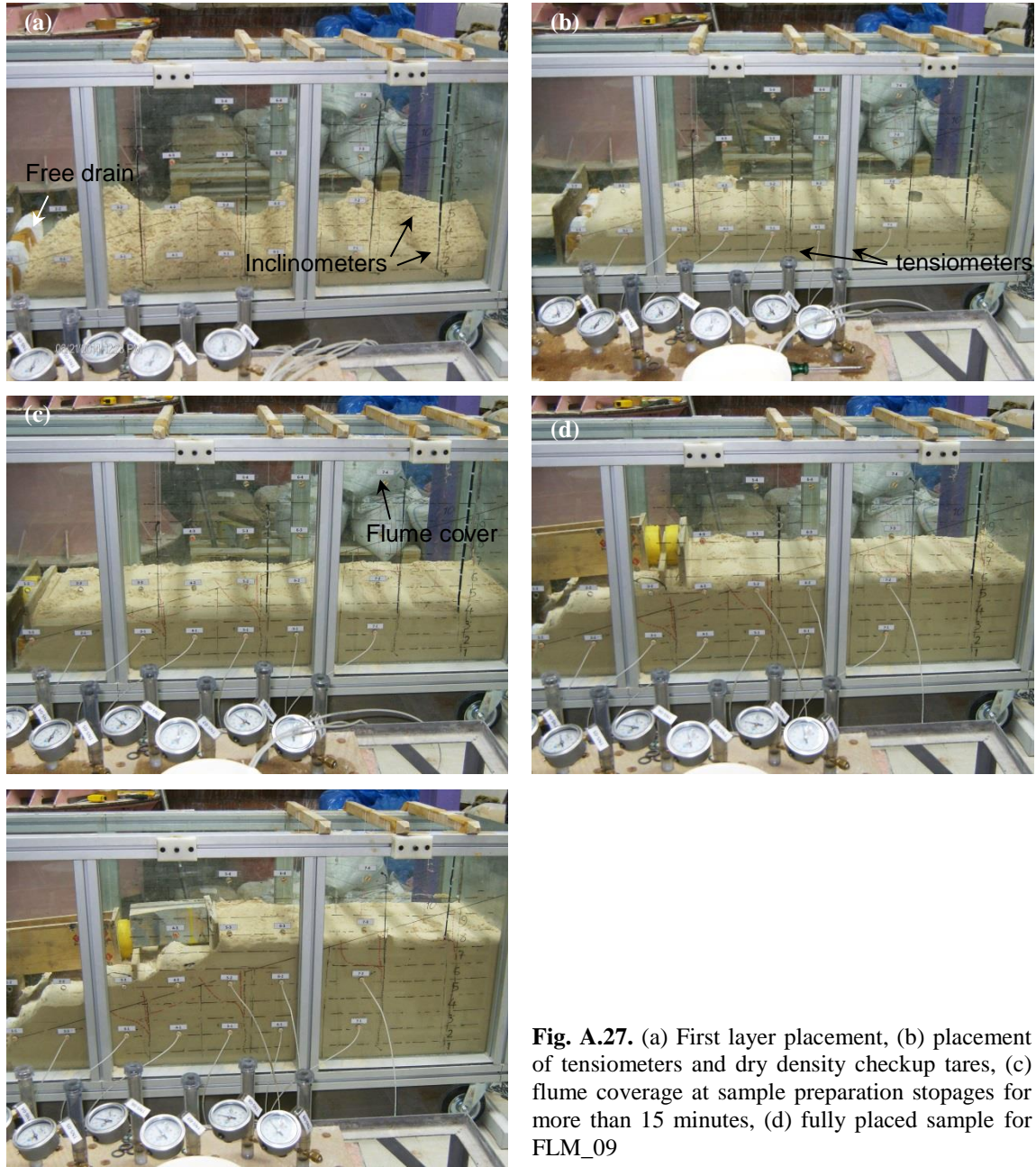


Fig. A.27. (a) First layer placement, (b) placement of tensiometers and dry density checkup tares, (c) flume coverage at sample preparation stoppages for more than 15 minutes, (d) fully placed sample for FLM_09



Fig. A.28. (a) high resolution filming from the opposite side, (b) wetting front at the opposite side (c) & (d) projectors and video camera, (e) wetting front after 130 minutes raining in FLM_09

FLM_10

Sample preparation on: 22 July 2014 (17:00-02:00 n.d.)	Test performance on: 28 July 2014 (20:20-22:45)
Room temperature: 23°C	D _R after test: 49.1
Trapezoidal slope angle: 15.3°	Rainfalling sys. adjust: 55/60 (63.0 mm/hr)
Flume base tilt angle: 41.2°	Time to failure: 103 minutes
Initial water content: 1.5 %	
Intended D _R : 48	

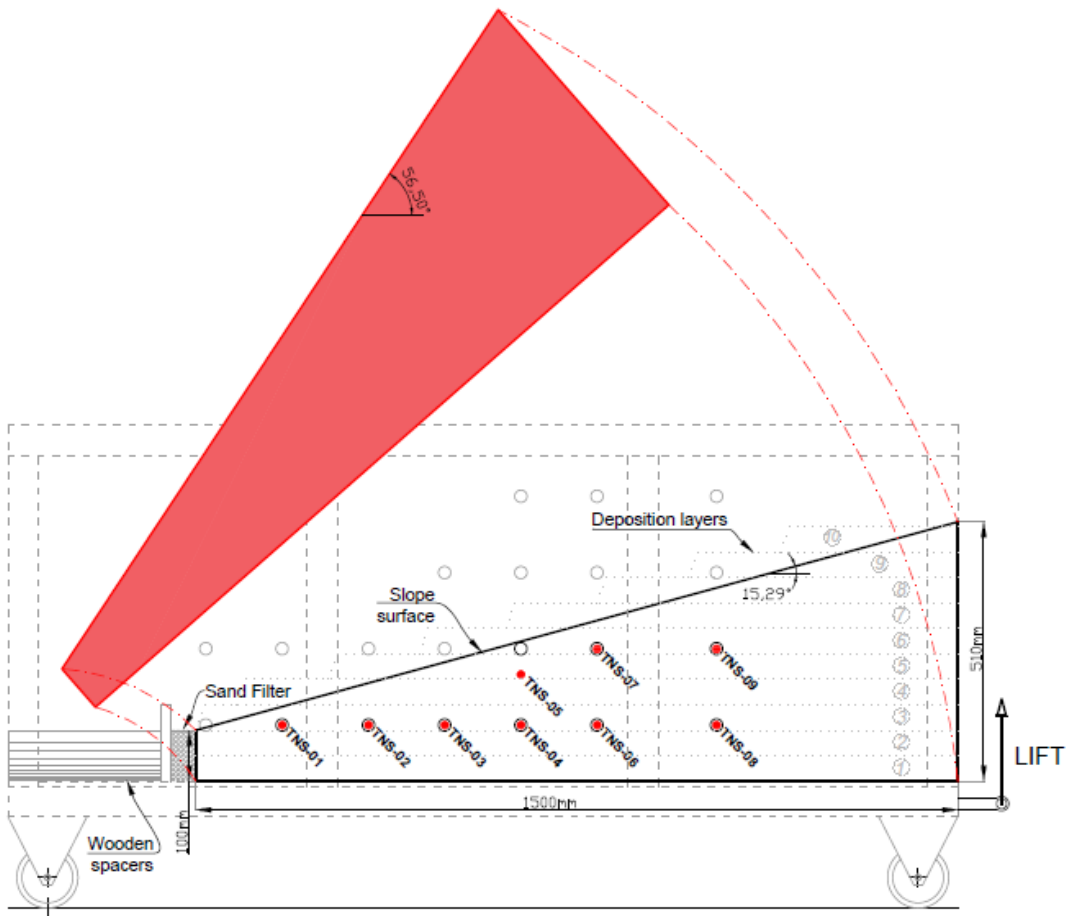


Fig. A.29. Deposition, instrumentation and positioning for FLM_10

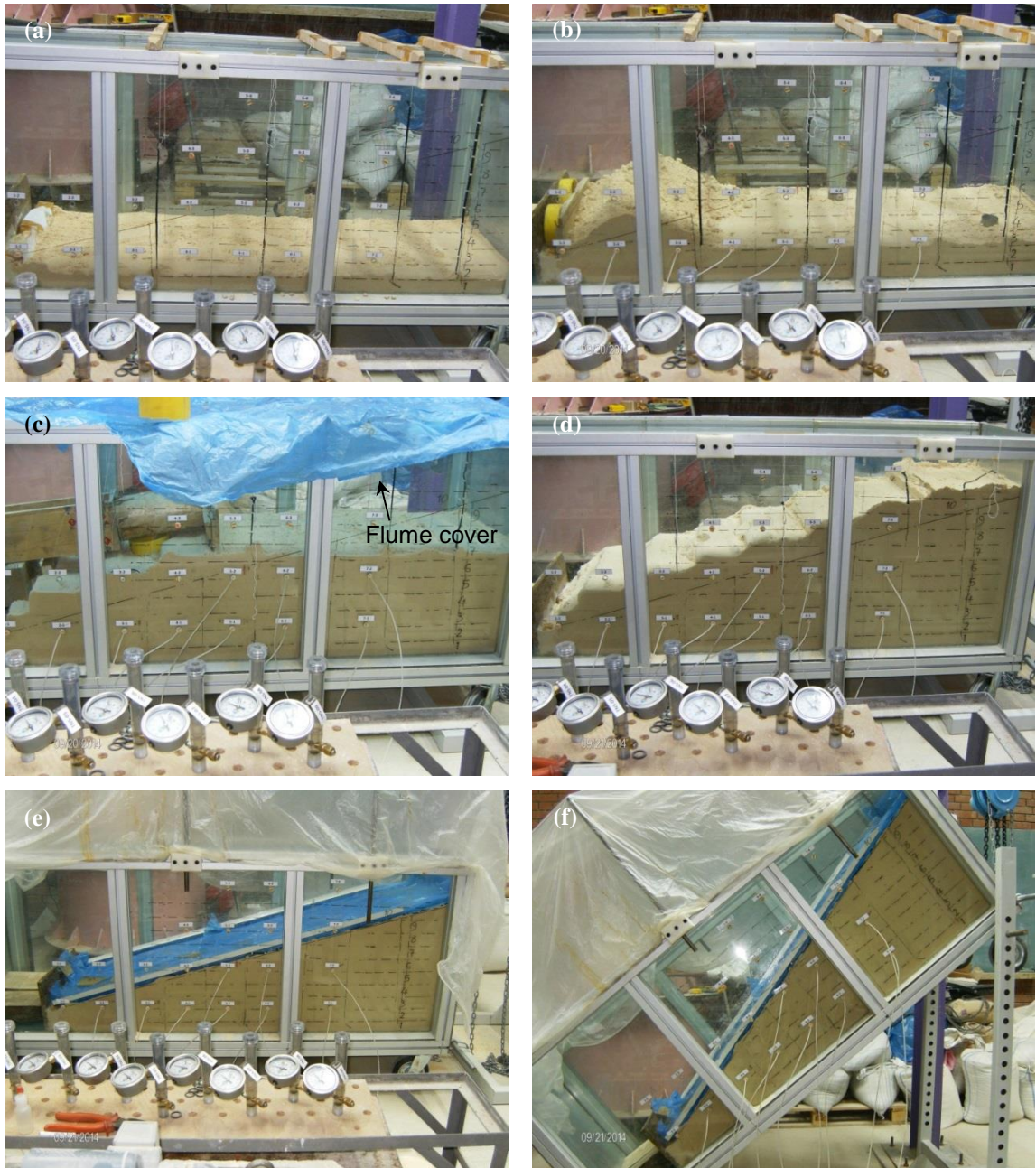


Fig. A.30. (a) First layer placement, (b) placement of tensiometers and dry density checkup tares, (c) flume coverage at sample preparation stoppage for more than 15 minutes, (d) fully placed sample, (e) trimmed and covered soil sample and (f) tilted flume, left for equalization for FLM_10

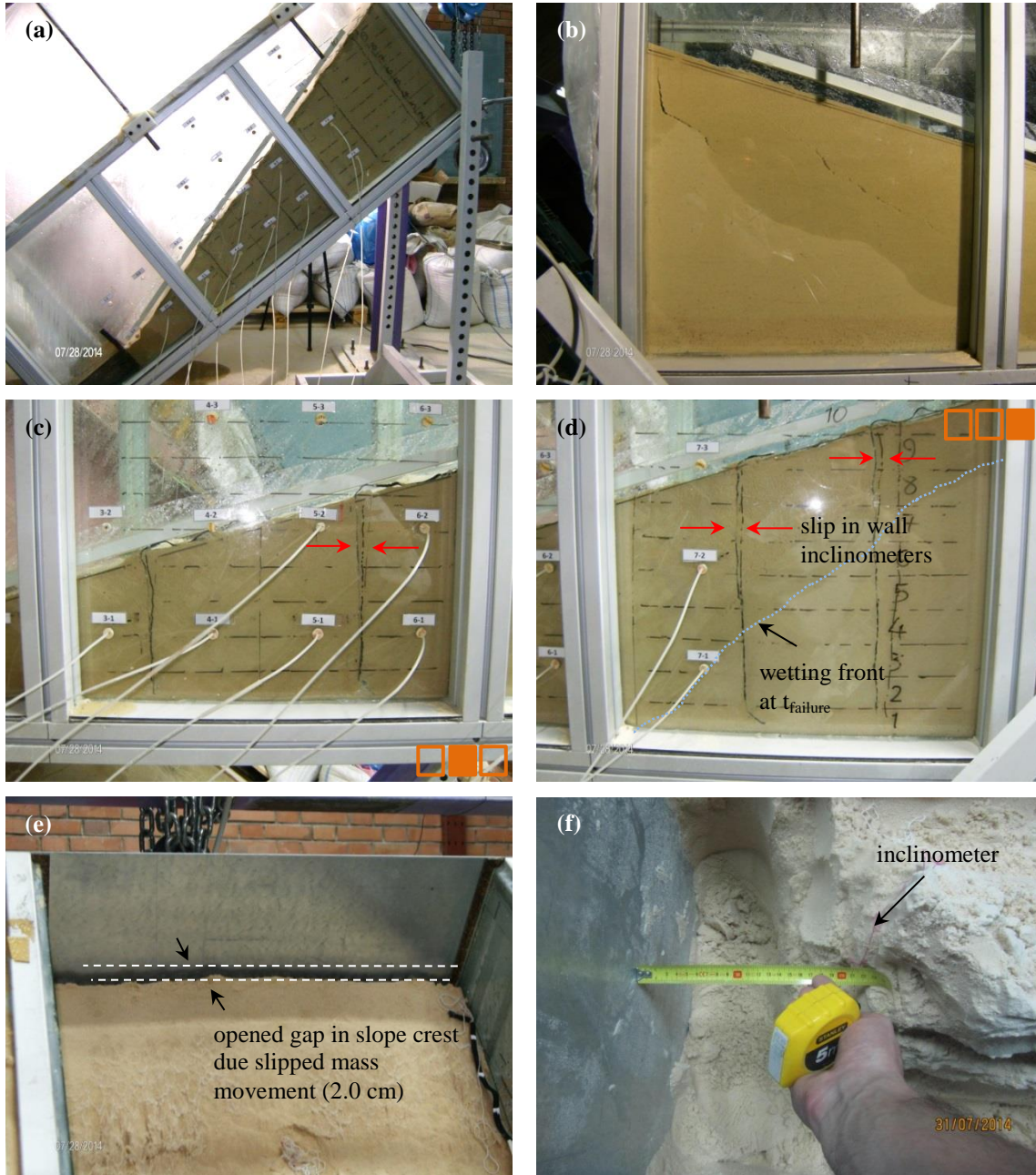


Fig. A.31. (a) high resolution filming from the opposite side, (b) wetting front and failure line at the opposite side (c) & (d) inclinometers showing deformation at the time of failure, (e) slipped soil (top view), (f) readings from inclinometer recordings in FLM_10

FLM_11

Sample preparation on: 10 August 2014 (16:00-21:30)	Test performance on: 13 August 2014 (18:10-23:30) & 16 August 2014 (12:30-15:00)
Room temperature: 28°C	D _R after test: 52.5
Trapezoidal slope angle: 15.3°	Rainfalling sys. adjust: 25/60 (28.9 mm/hr) & 55/60 (66.7 mm/hr)
Flume base tilt angle: 41.2°	Time to failure: No failure in low intensity rainfall
Initial water content: 1.5 %	
Intended D _R : 48	

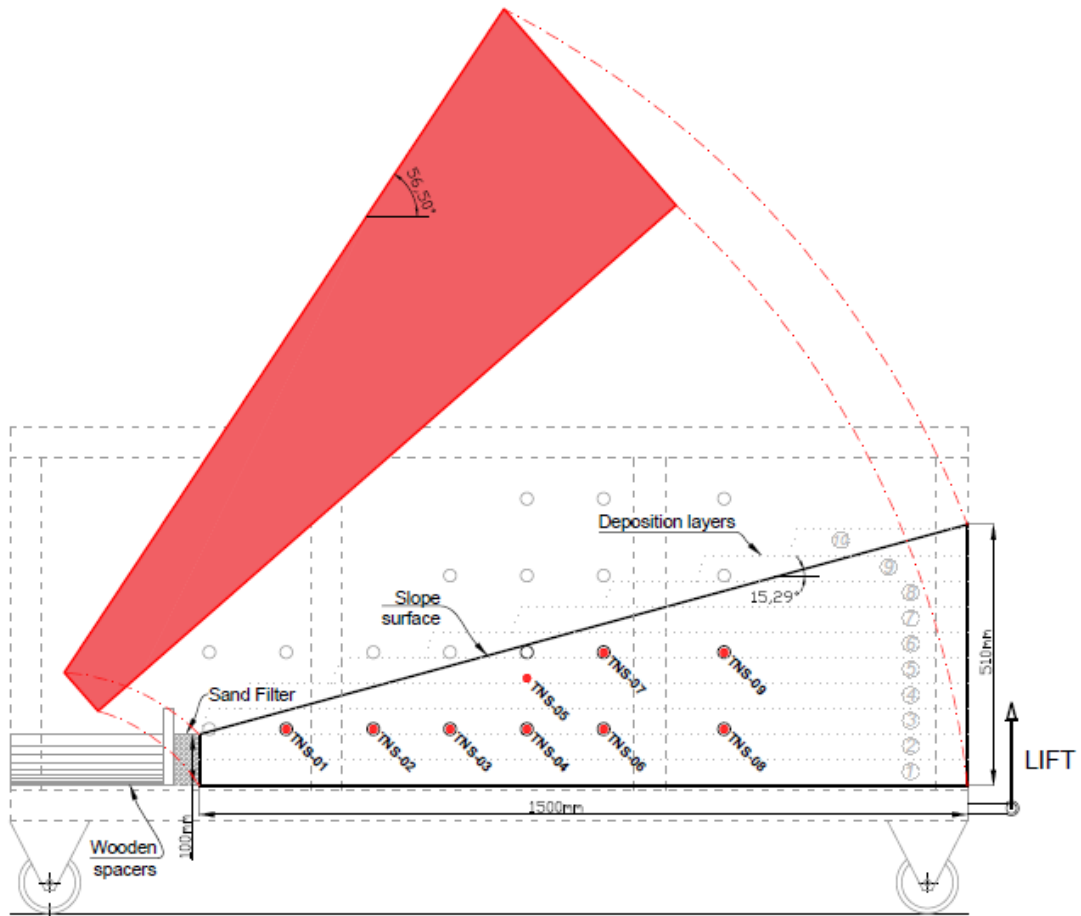


Fig. A.32. Deposition, instrumentation and positioning for FLM_11

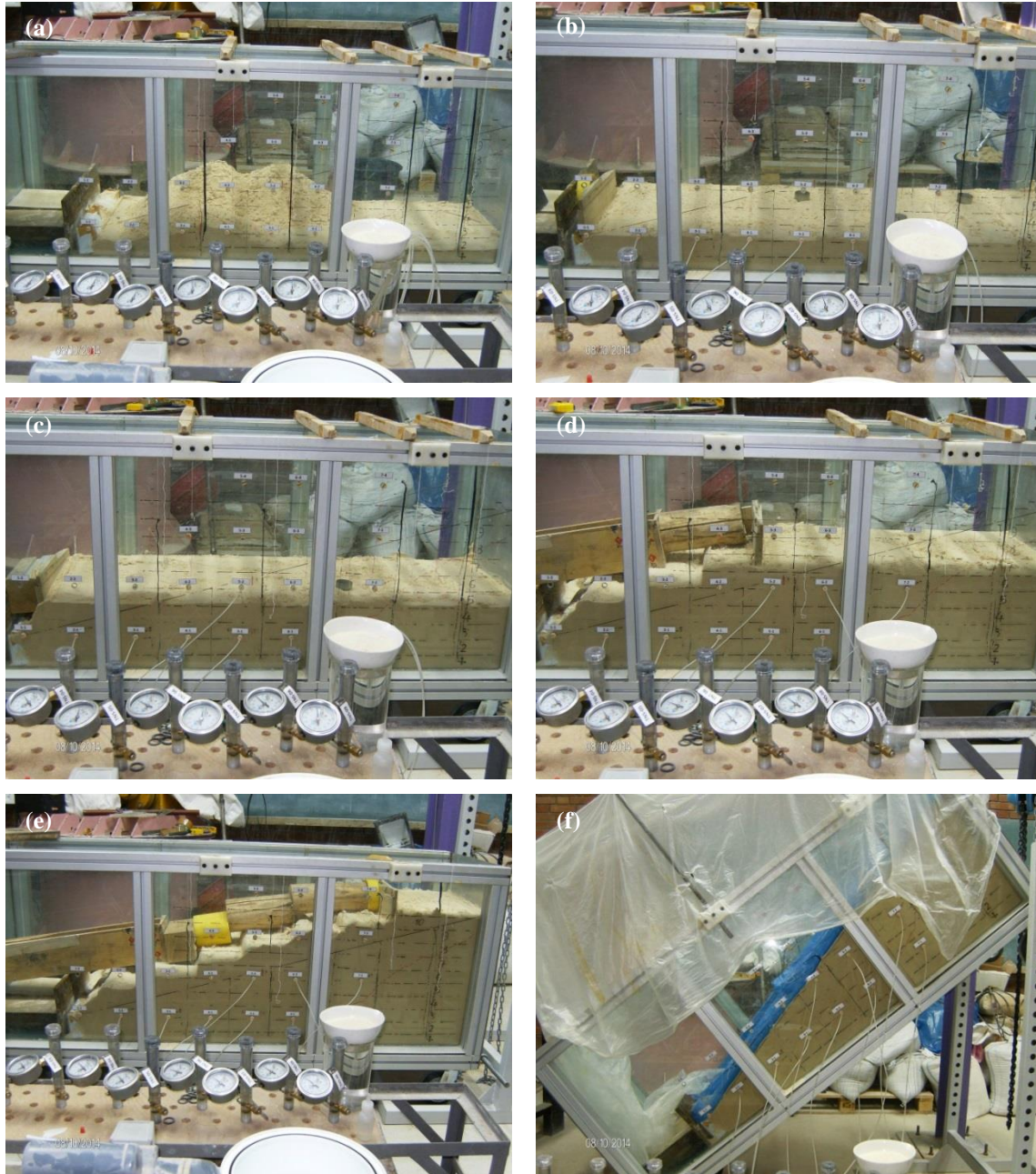


Fig. A.33. (a) to (f) sample preparation for FLM₁₁



Fig. A.34. (a) high resolution filming from the opposite side, (b), (c) & (d) no failure in the slope subjected to 28 mm/hr rainfall intensity, (e) & (f) failure after 66 mm/hr rainfall application in FLM_11

FLM_12

Sample preparation on: 20 August 2014 (10:00-16:30)	Test performance on: 22 August 2014 (15:30-17:44)
Room temperature: 25.4°C	D _R after test: 46
Trapezoidal slope angle: 15.3°	Rainfalling sys. adjust: 40/60 (48.8 mm/hr)
Flume base tilt angle: 41.2°	Time to failure: 134 minutes
Initial water content: 1.5 %	
Intended D _R : 48	

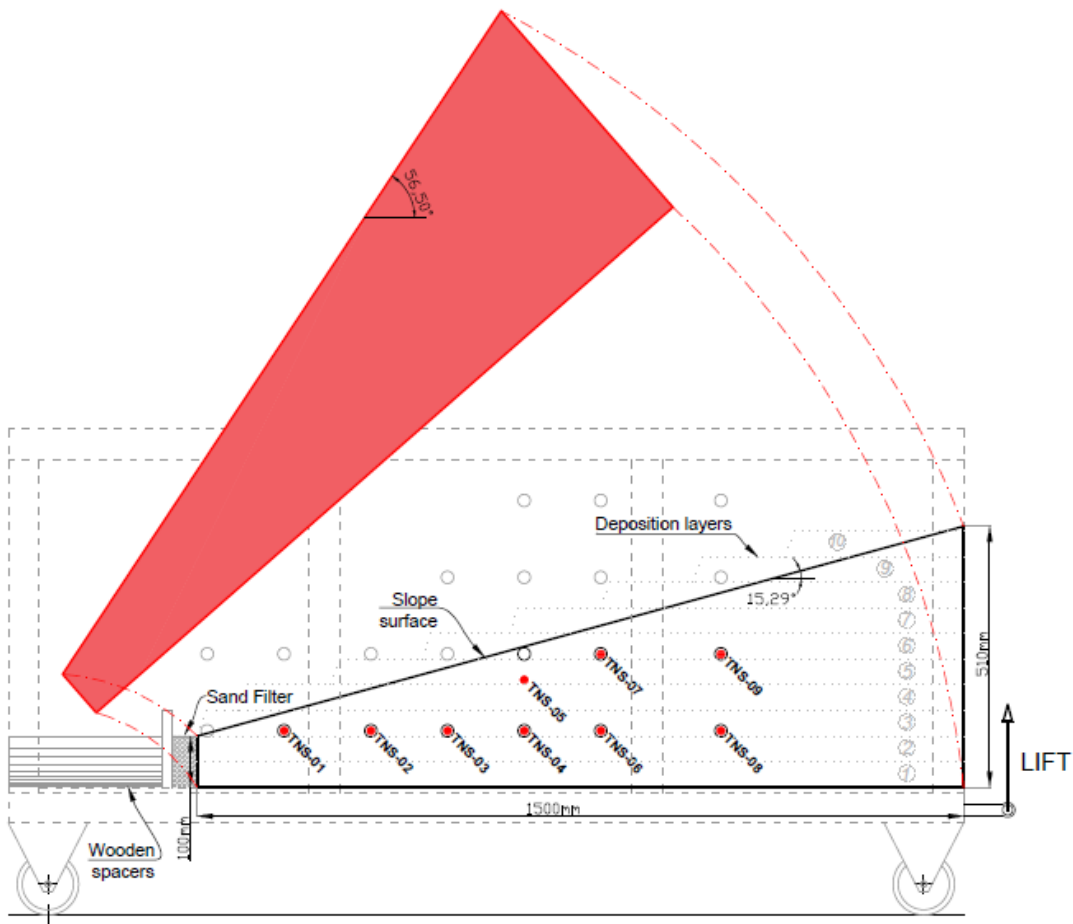


Fig. A.35. Deposition, instrumentation and positioning for FLM_12



Fig. A.36. (a) to (f) sample preparation for FLM_12

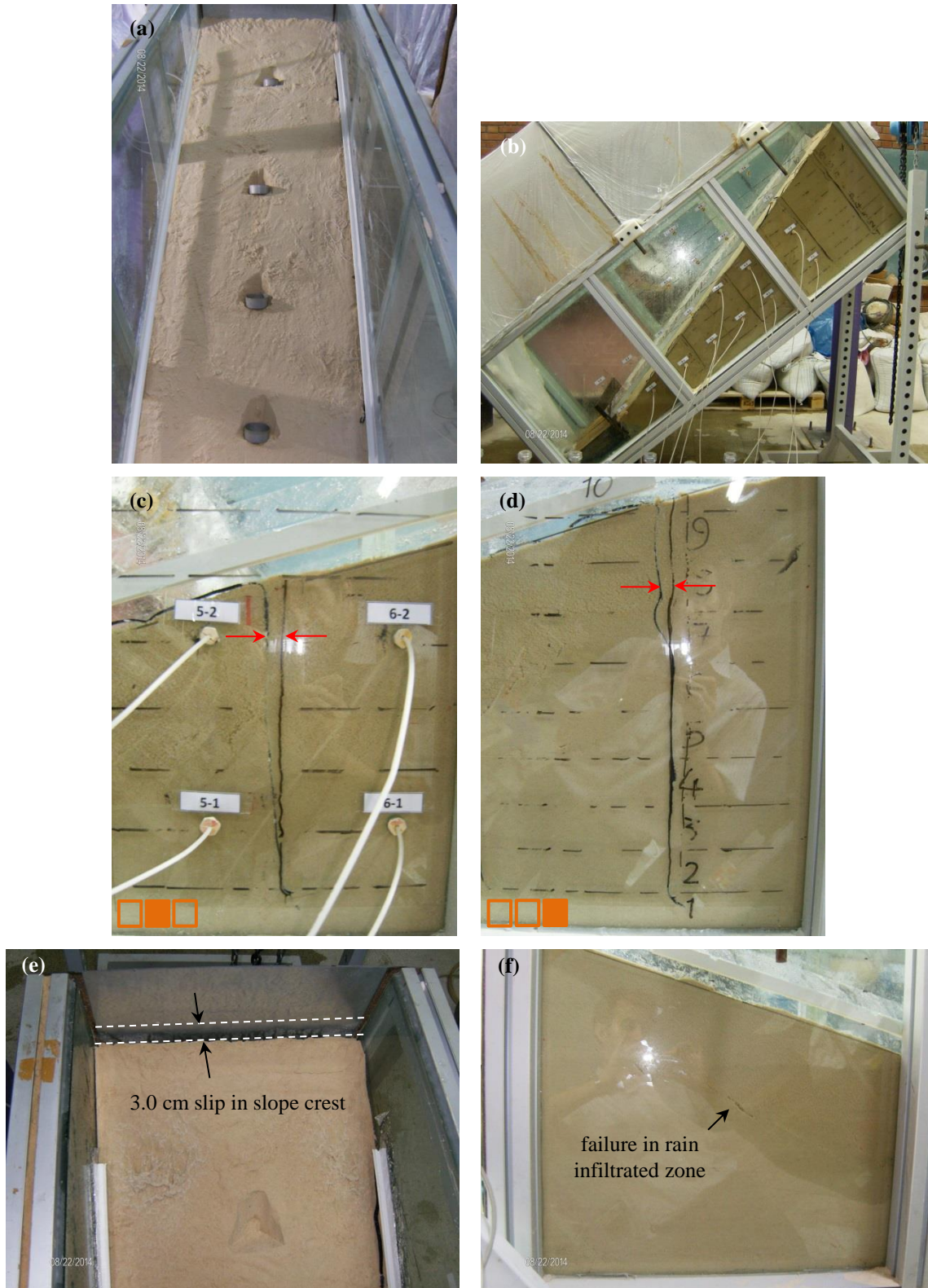


Fig. A.37. (a) rainfall intensity checkup tares, (b) slipped slope, (c) & (d) inclinometers showing deformation at the time of failure, (e) slipped soil (top view) and (f) evidences of failure in rain infiltrated soils in FLM_12

FLM_13

Sample preparation on: 25 August 2014 (21:30-03:30 n.d.)	Test performance on: 28 August 2014 (18:00-19:45)
Room temperature: 26.8°C	D _R after test: 38.5
Trapezoidal slope angle: 15.3°	Rainfalling sys. adjust: 22/60 (18 mm/hr)
Flume base tilt angle: 41.2°	Time to failure: 105 minutes
Initial water content: 1.5 %	
Intended D _R : 34	

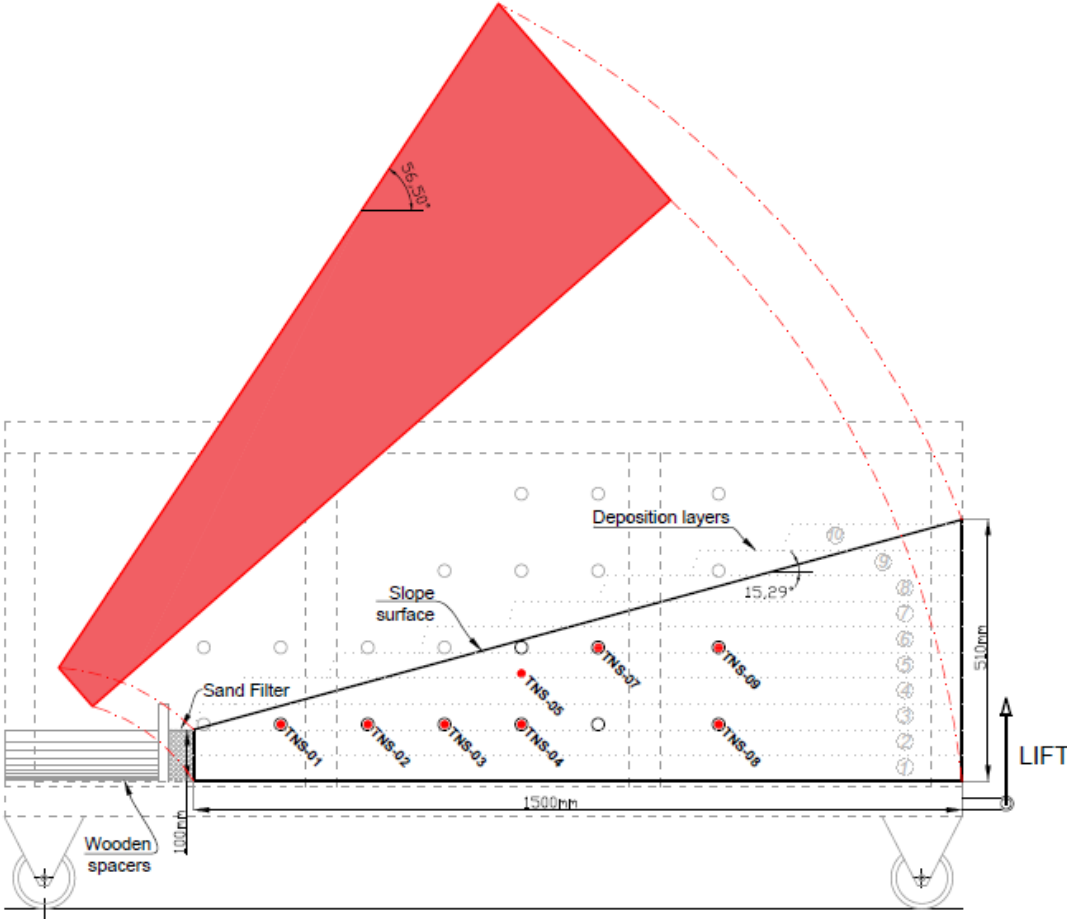


Fig. A.38. Deposition, instrumentation and positioning for FLM_13



Fig. A.39. (a) to (f) sample preparation for FLM_13



Fig. A.40. (a) high resolution filming from the opposite side, (b) slipped slope surface (c) inclinometers showing deformation at the time of failure, (d) slipped soil (top view), (e) wetting front and failure line at FLM_13

FLM_14

Sample preparation on: 1 September 2014 (08:30-15:30)	Test performance on: 2 September 2014 (17:00-23:59) 5 September 2014 (16:30-20:46) & (20:46-23:59)
Room temperature: 26.2°C	D_R after test: 46.1
Trapezoidal slope angle: 15.3°	Rainfalling sys. adjust: 22/60 (22 mm/hr)
Flume base tilt angle: 41.2°	40/60 (48.3 mm/hr) & 55/60 (62.6 mm/hr)
Initial water content: 1.5 %	
Intended D_R : 48	Time to failure: 205 minutes

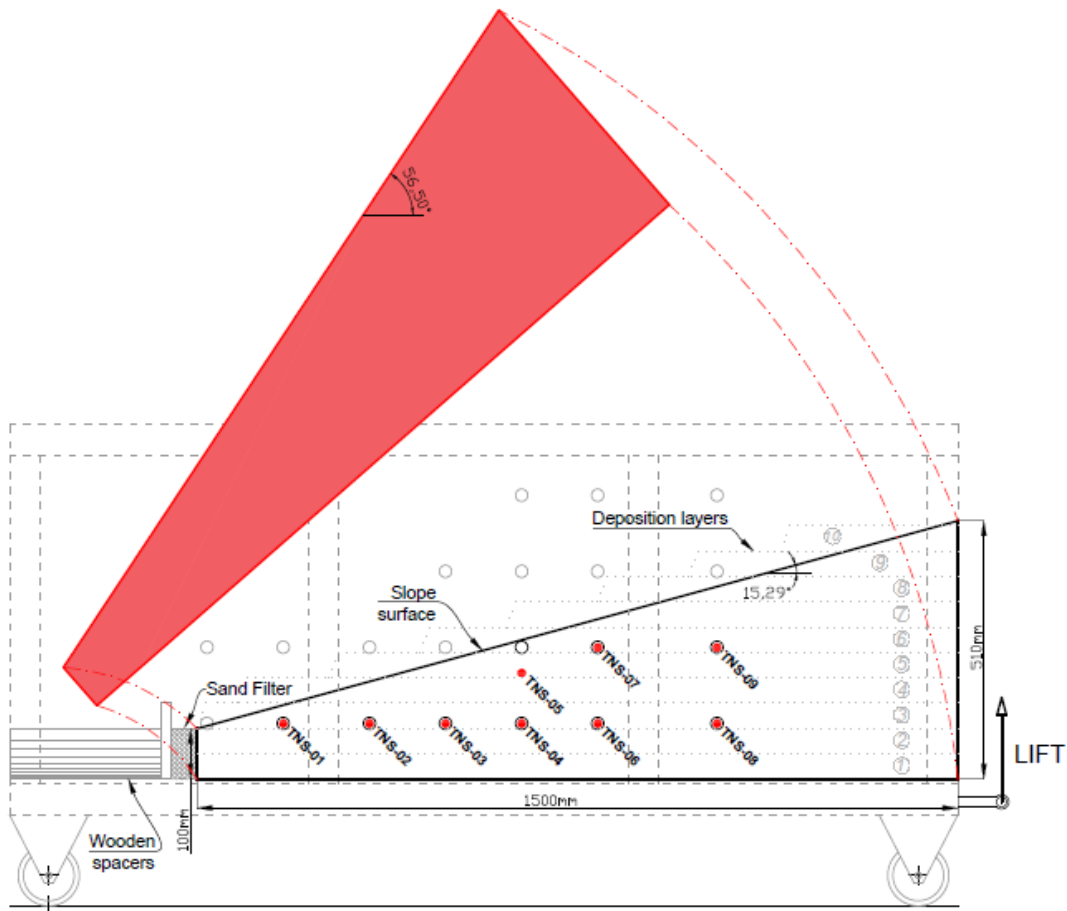


Fig. A.41. Deposition, instrumentation and positioning for FLM_14

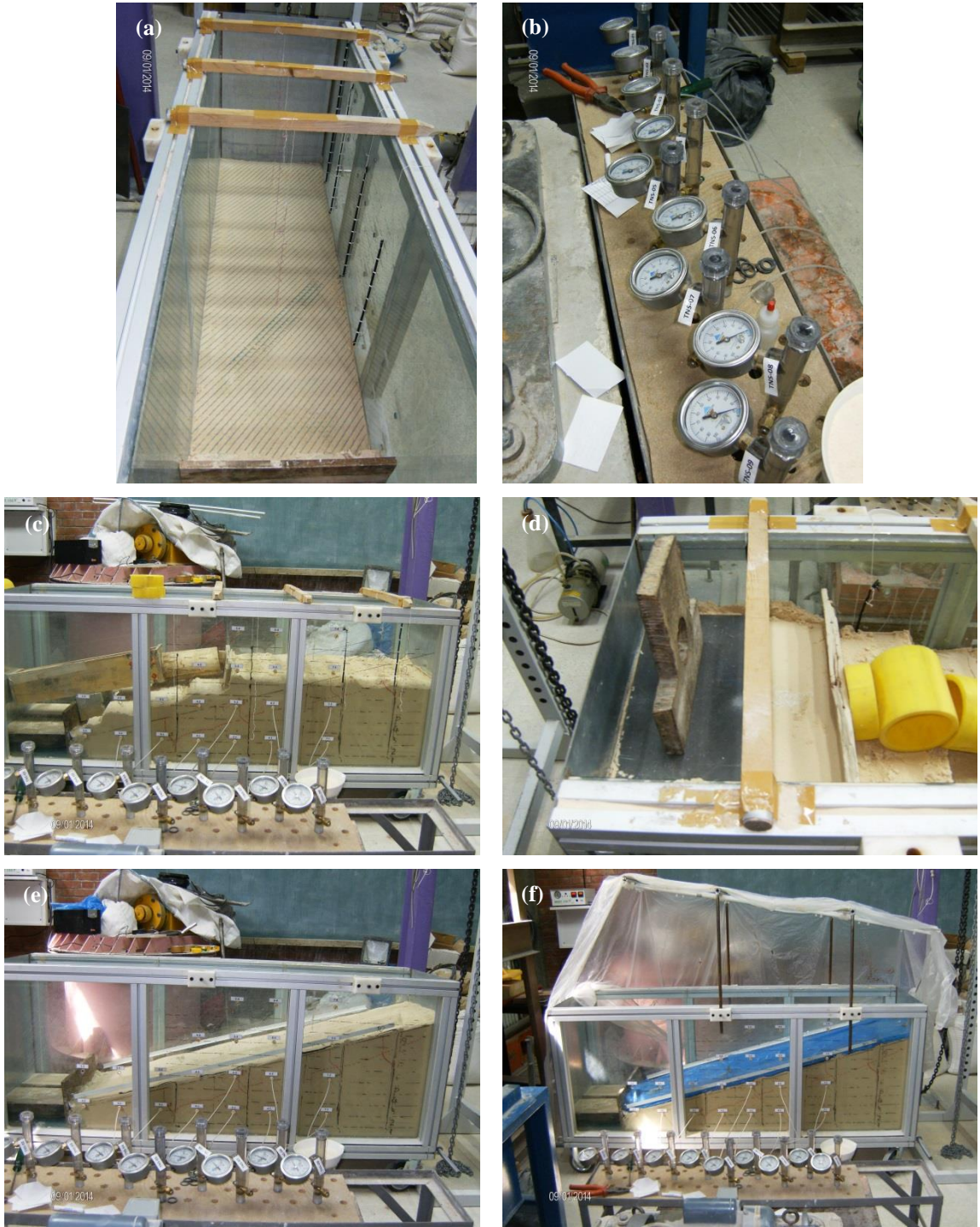


Fig. A.42. (a) to (f) sample preparation for FLM_14

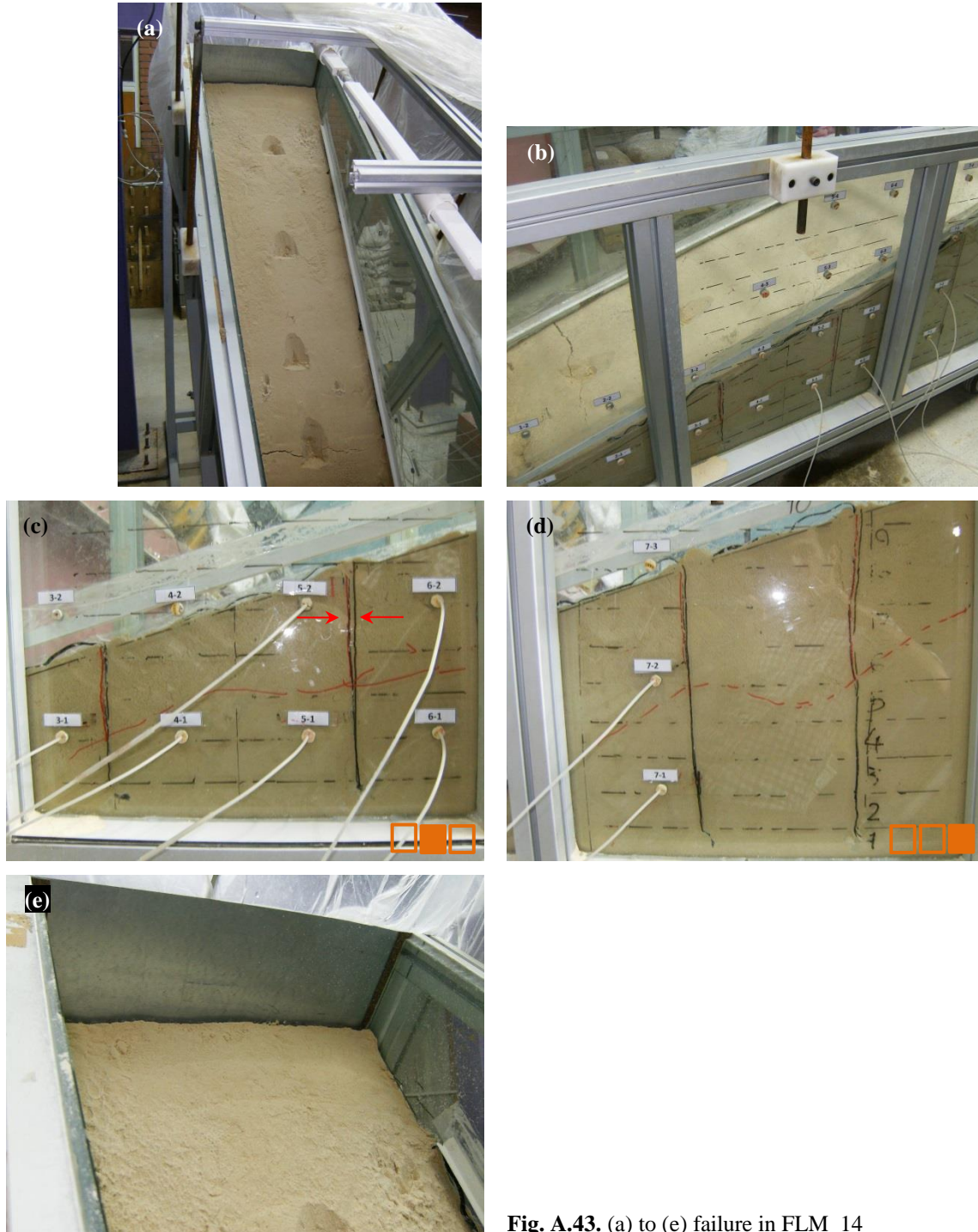


Fig. A.43. (a) to (e) failure in FLM₁₄

FLM_15

Sample preparation on: 6 November 2014 (18:00-10:00 n.d.)	Test performance on: 7 November 2014 (10:55-04:50 n.d.)
Room temperature: 27°C	D _R after test: -
Trapezoidal slope angle: 15.3°	Rainfalling sys. adjust: 18/60 (20.2 mm/hr)
Flume base tilt angle: 41.2°	Time to failure: No failure
Initial water content: 1.5 %	
Intended D _R : 48	

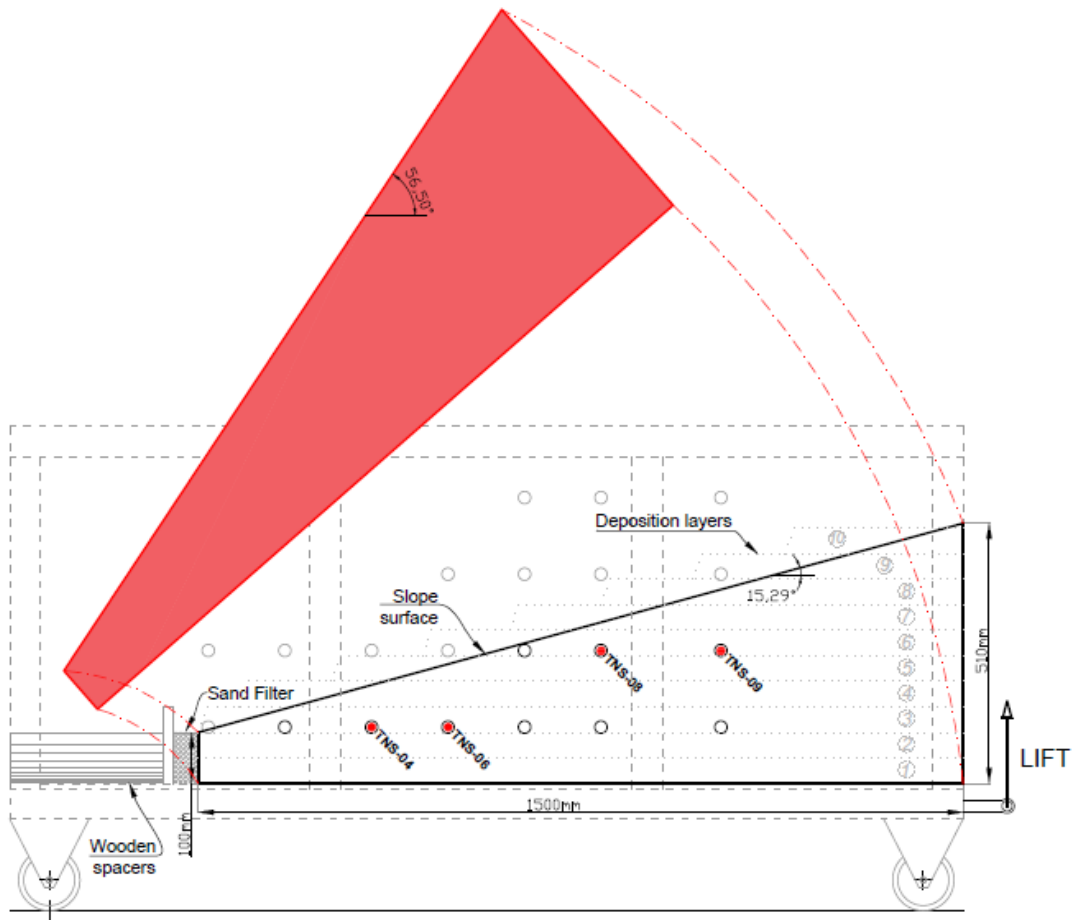


Fig. A.44. Deposition, instrumentation and positioning for FLM_15

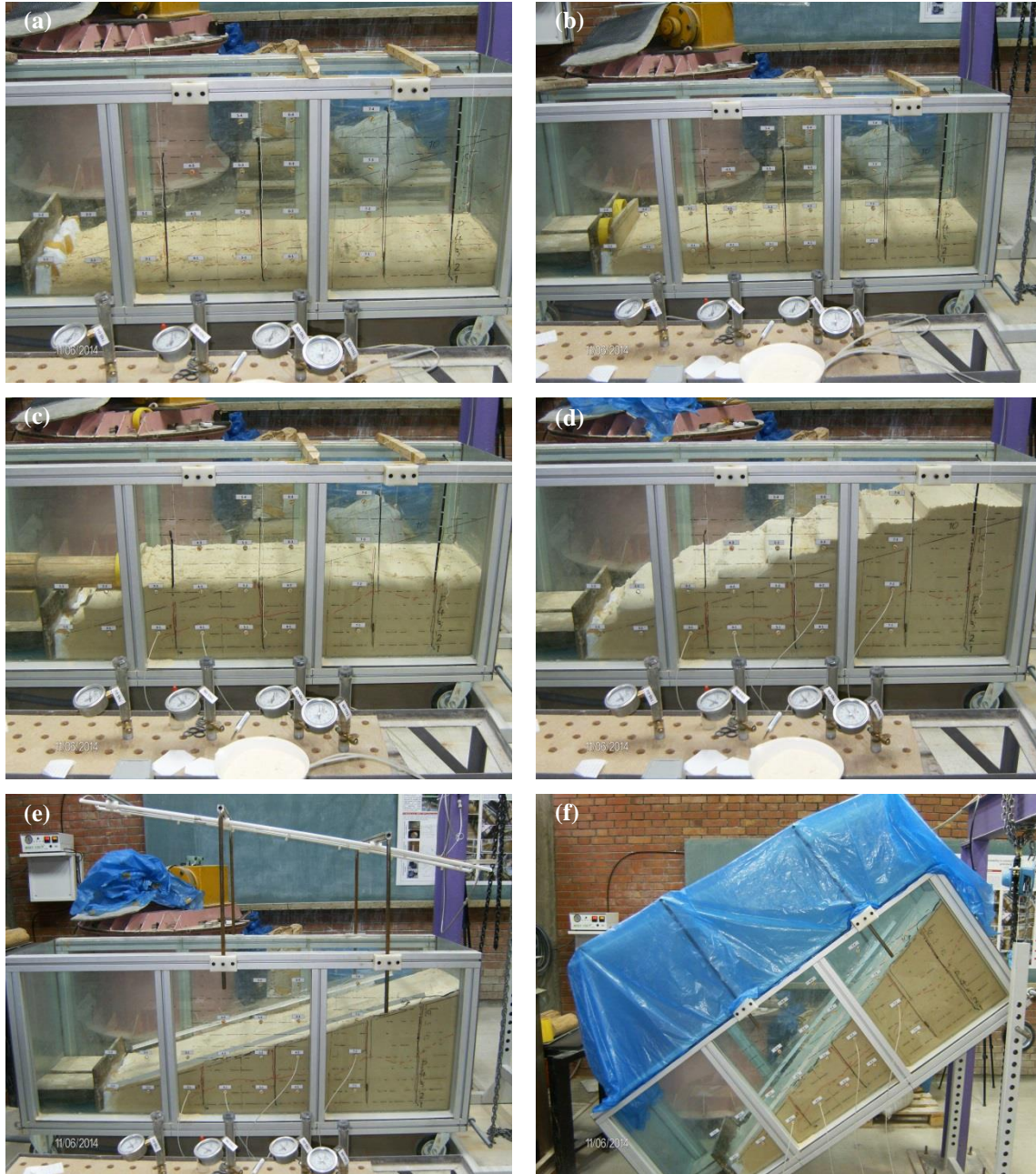


Fig. A.45. (a) to (f) sample preparation for FLM_15

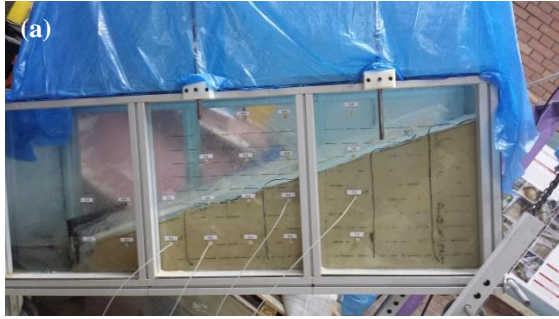


Fig. A.46. (a) & (b) no failure in FLM_15

LAM_0

Sample preparation on: 28 August 2013 (19:00-21:45)	Test performance on: 28 August 2014 (21:10)
Room temperature: 26°C	Intended D_R : 61%
Slope angle: starting 30°	D_R after test: 58%
Initial water content: 1%	Rainfalling sys. adjust: -

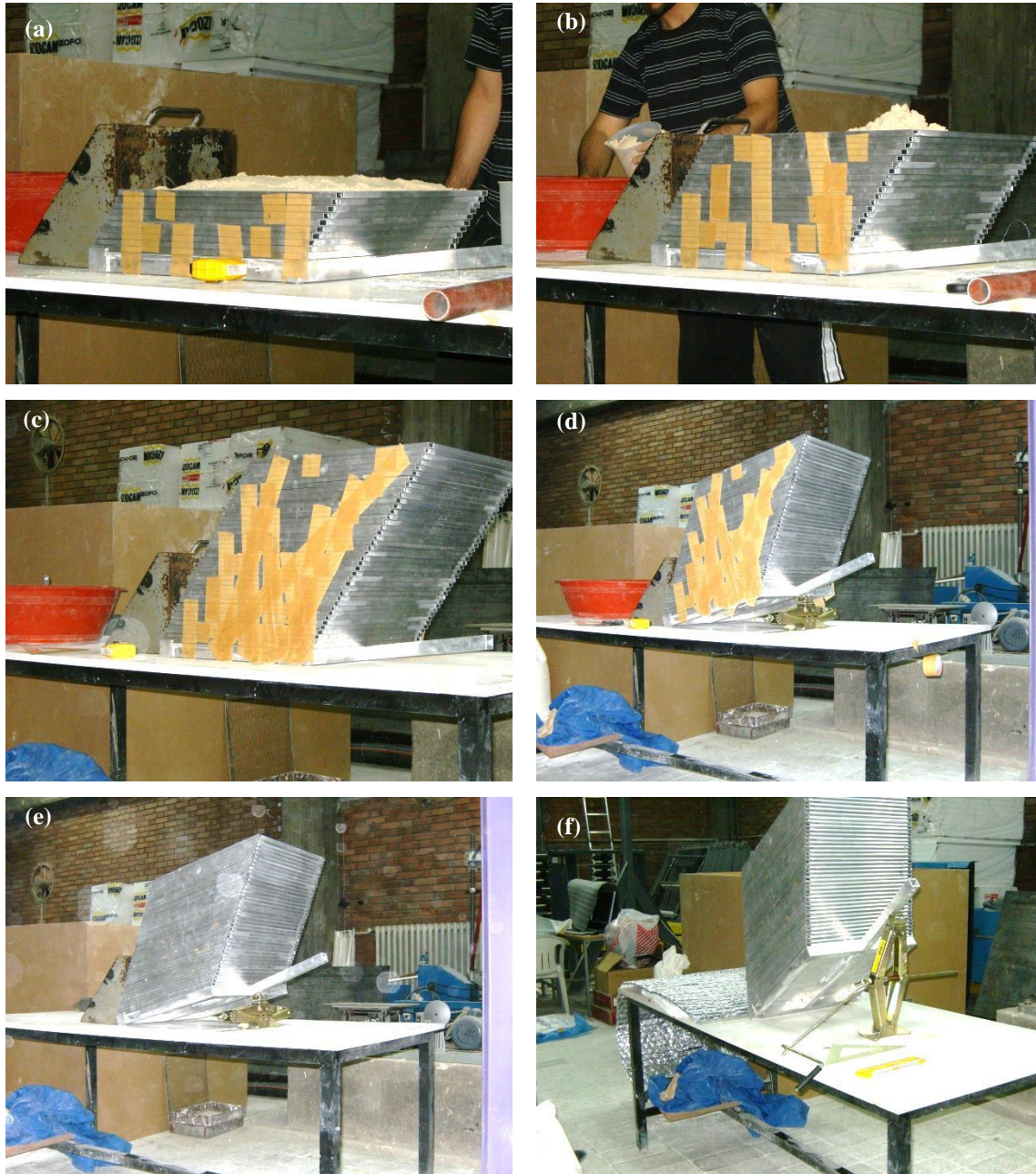


Fig. A.47. (a) to (f) sample placement in layers in laminar box for LAM_0

LAM_1

Sample preparation on: 08 September 2013 (14:00-18:00)	Test performance on: 10 September 2013 (17:40-19:55)
Slope angle: 30°	D_R after test: 56.5%
Initial water content: 1 %	Rainfalling sys. adjust: 15/60 (11.0 mm/hr)
Intended D_R : 61%	Time to failure: No failure



Fig. A.48. (a) & (b) soil sample placement in layers using clamping system for LAM_1, (c) & (d) laminar box positioned and (e) instrumented laminar box experiment.

LAM_2

Sample preparation on: 16 October 2013 (21:25-23:50)	Test performance on: 17 October 2013 (20:15-22:00)
Slope angle: starting 30°	D_R after test: 36.1%
Initial water content: 1 %	Rainfalling sys. adjust: 40/60 (48.8 mm/hr)
Intended D_R : 34%	Time to failure: No failure due rainfalling but due tilting to 42° after 105 minutes

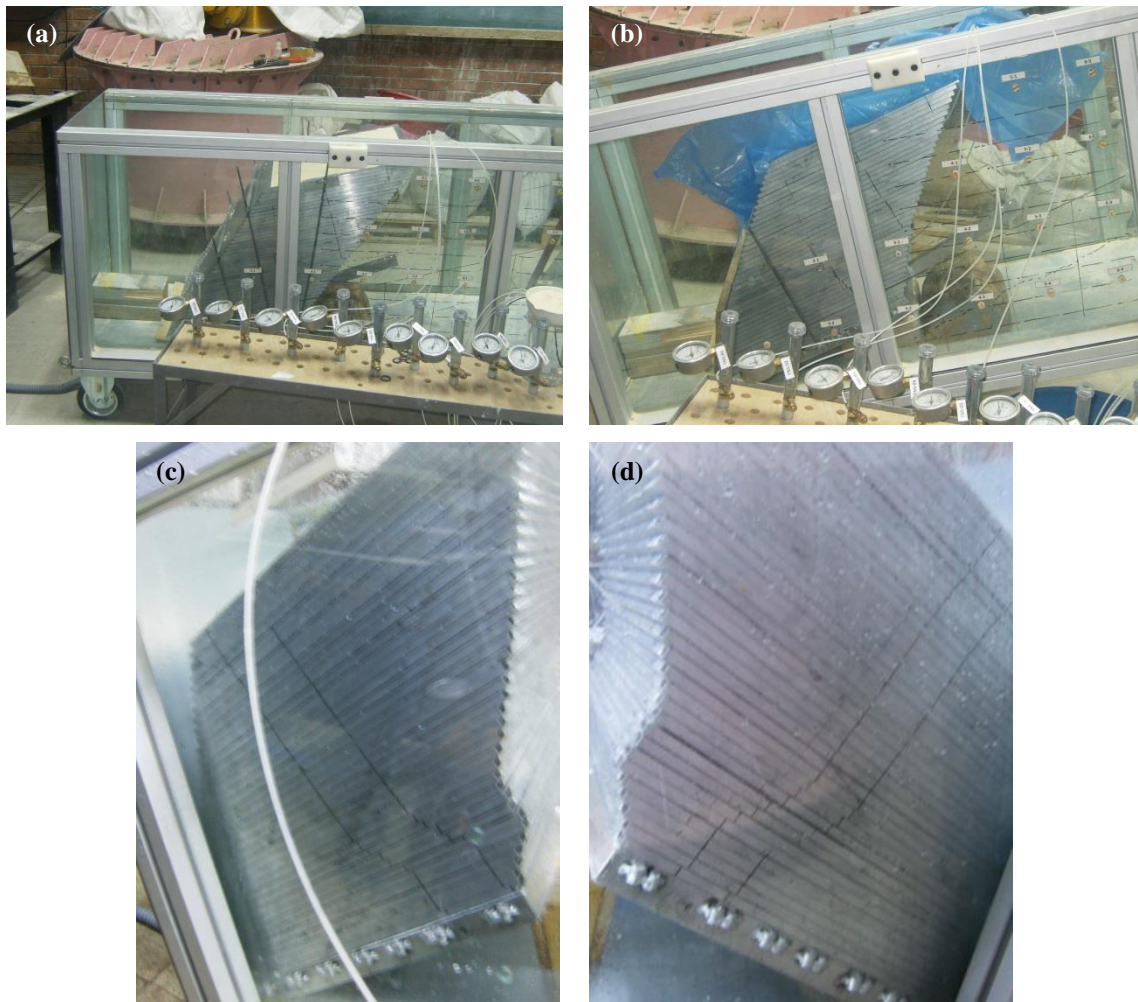


Fig. A.49. (a) & (b) sample preparation and (c) & (d) slip after 105 minutes rainfalling and then tilting to 42° in LAM_2

APPENDIX B

RESULTS OF FLUME EXPERIMENTS

Obtained (measured) pore water pressures, wetting front and displacements through laboratory experiments are summarized for all of the tests in Appendix B. In each figure all the suction recordings are plotted against time in accordance with rainfall intensity. Wetting front progress due to rainfall within slope experiment is also plotted in another graph for each of the experiments. In these figures deformation at the time of failure (if any) is also shown in the slope experiments.

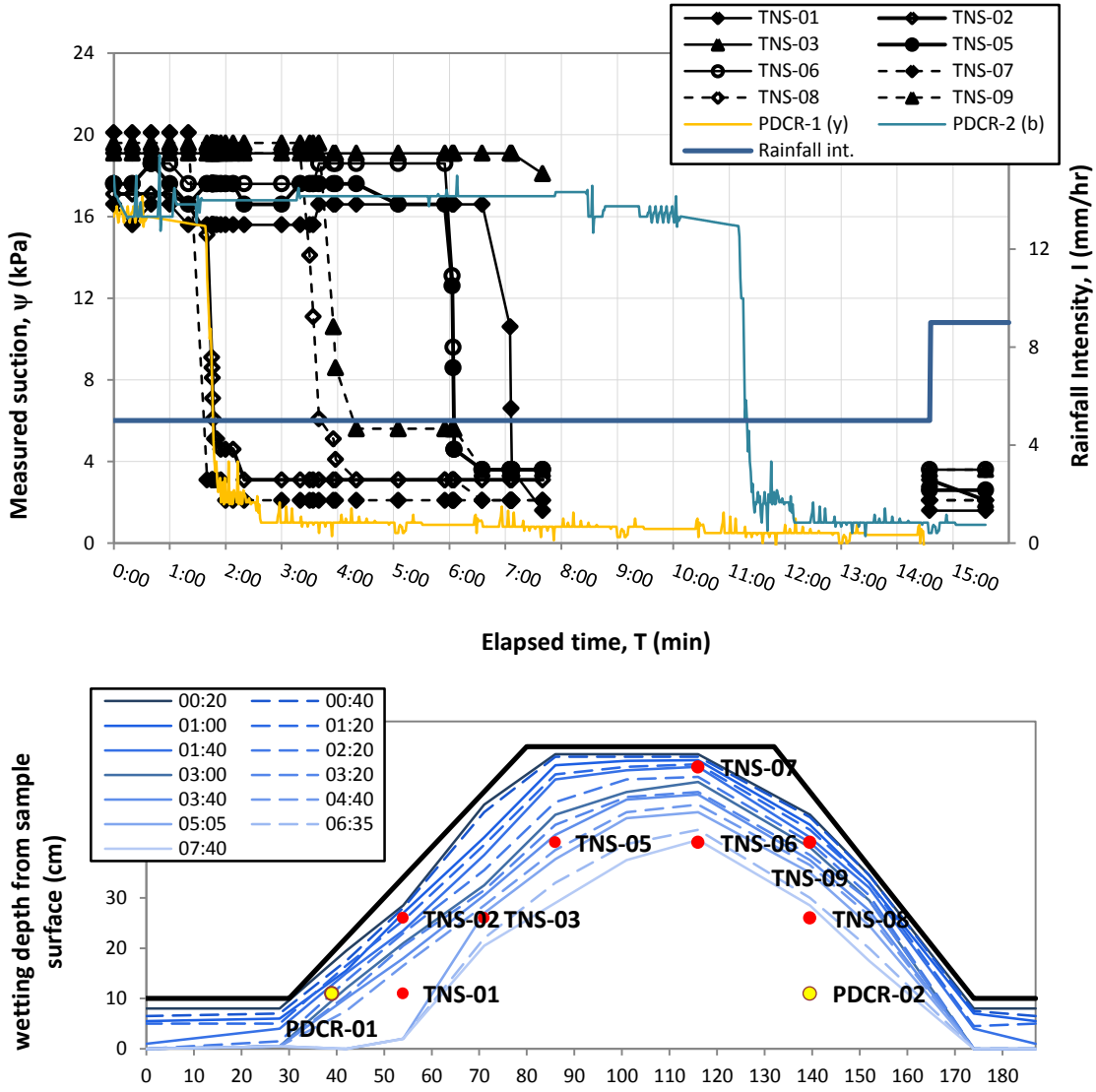


Fig. B.1. (a) Changes in pore pressure (suction) values throughout the test and (b) wetting front progress at different time steps and slip (failure) surface at the time of failure for FLM_01

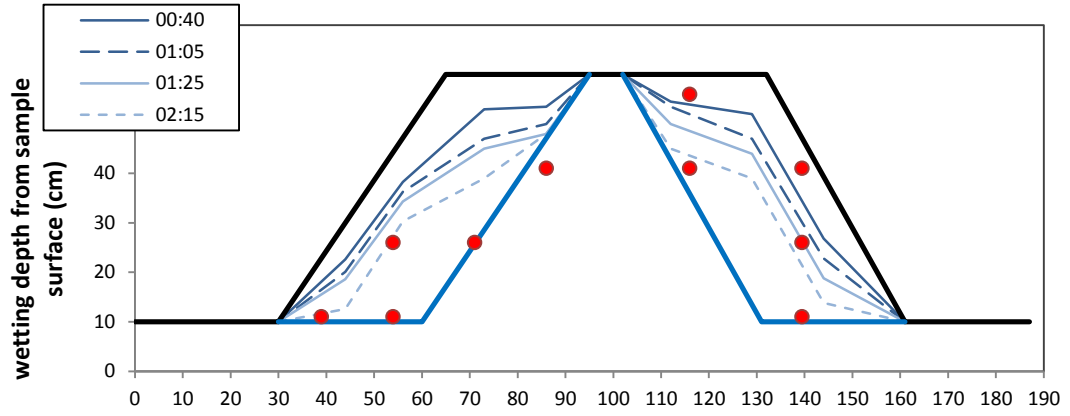


Fig. B.2. wetting front progress at different time steps for FLM_02

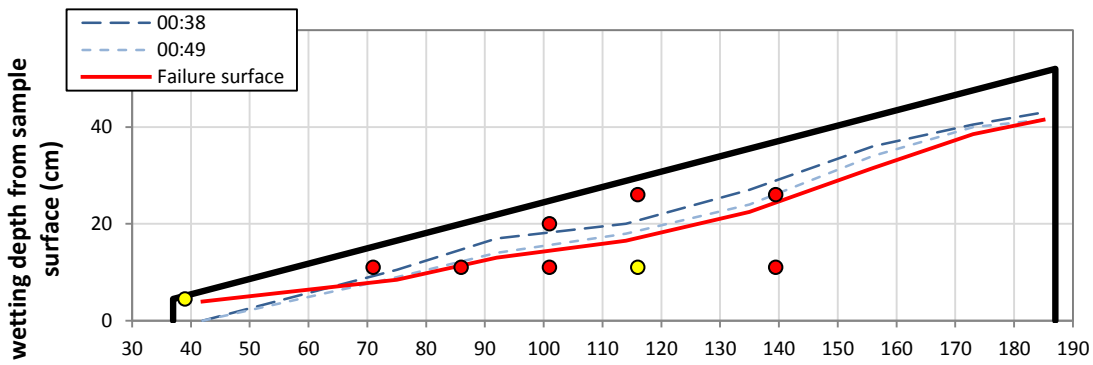
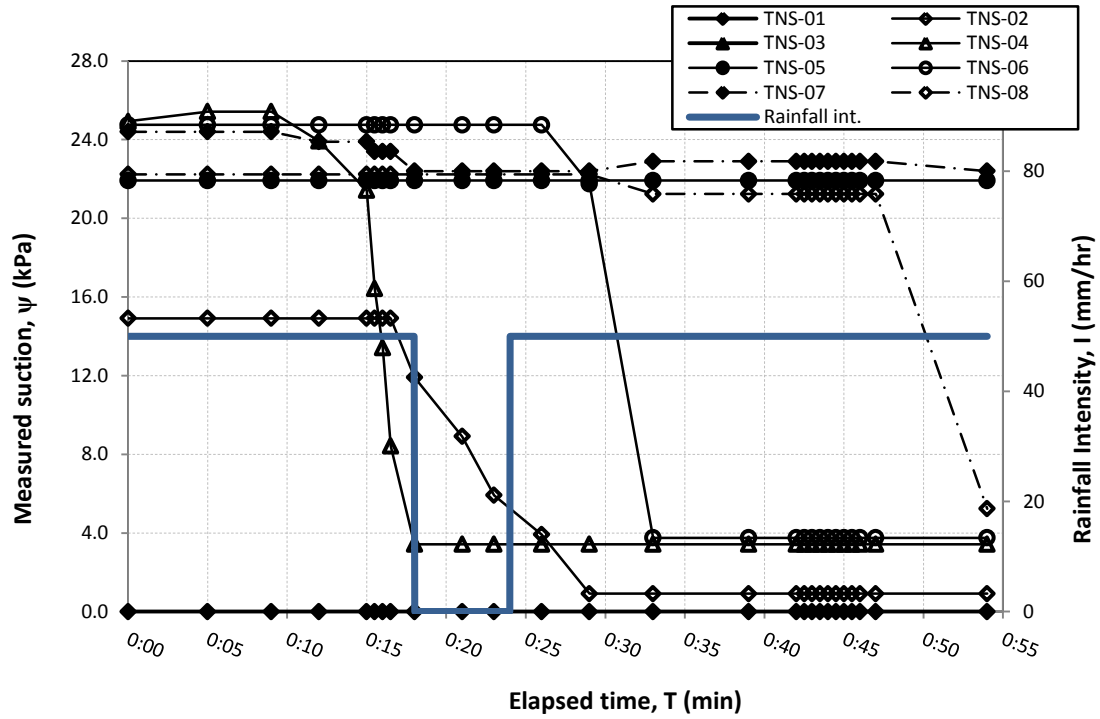


Fig. B.3. (a) Changes in pore pressure (suction) values throughout the test and (b) wetting front progress at different time steps and slip (failure) surface at the time of failure for FLM_03

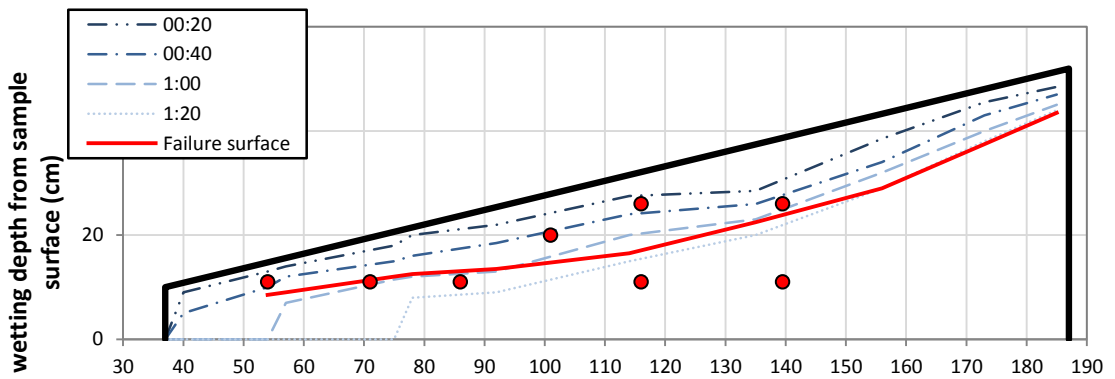
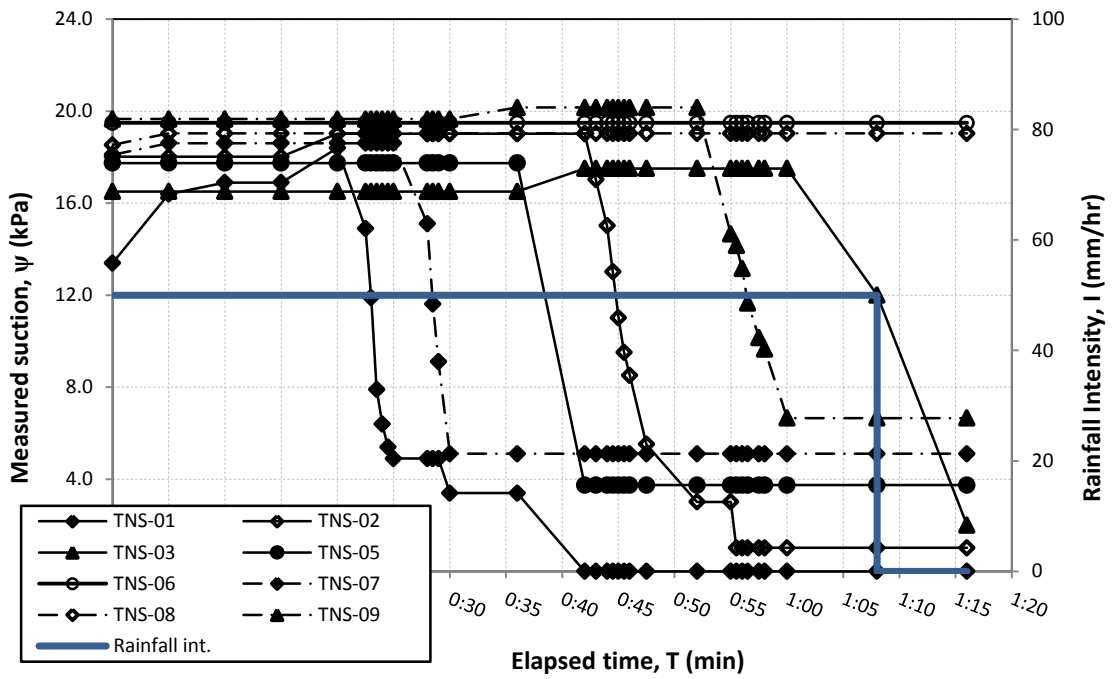


Fig. B.4. (a) Changes in pore pressure (suction) values throughout the test and (b) wetting front progress at different time steps and slip (failure) surface at the time of failure for FLM_04

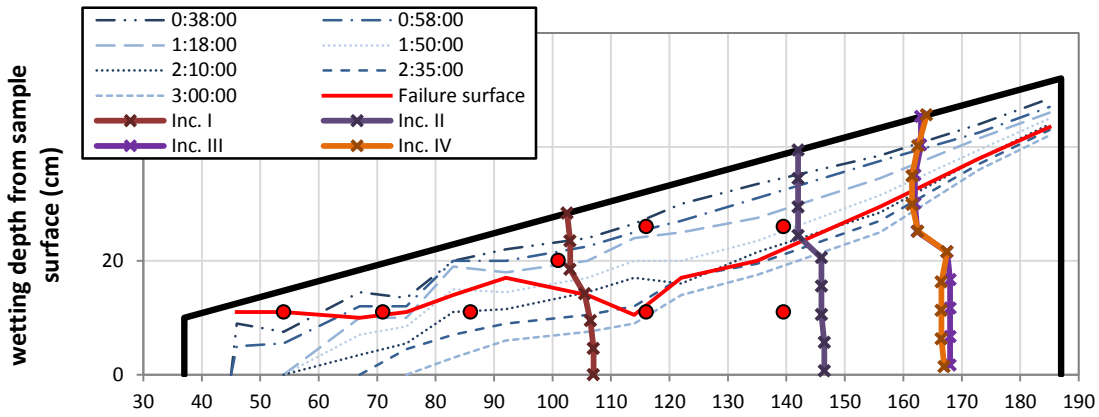
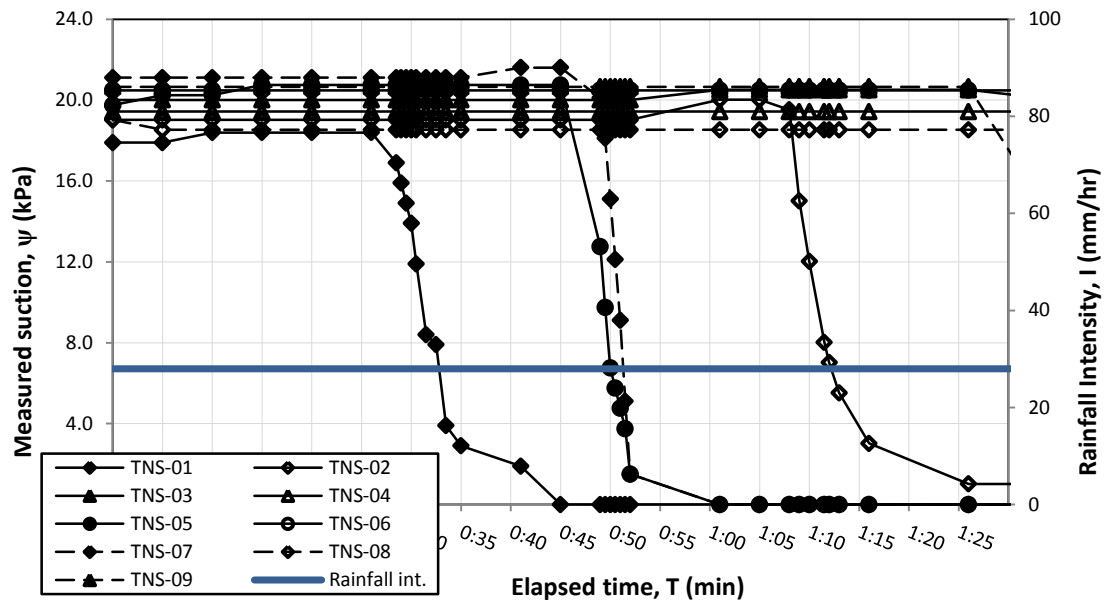


Fig. B.5. (a) Changes in pore pressure (suction) values throughout the test and (b) wetting front progress at different time steps and slip (failure) surface at the time of failure for FLM_05

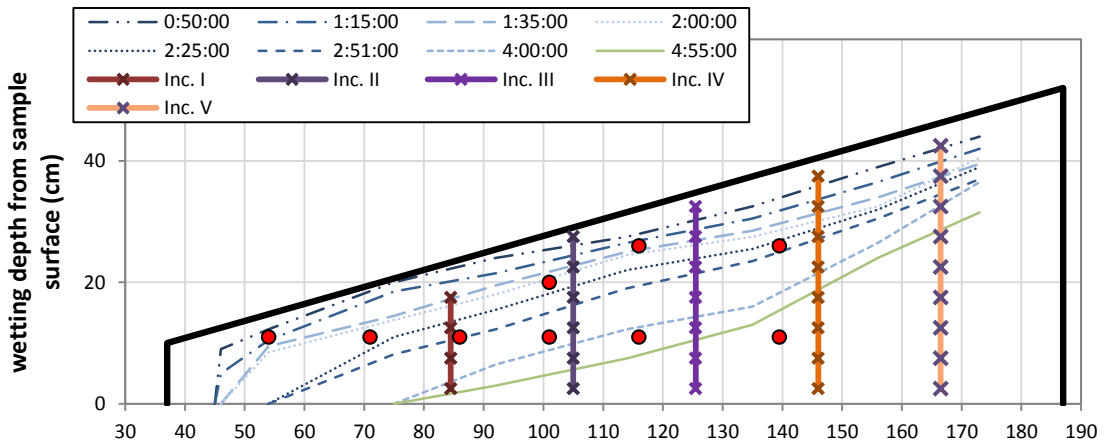
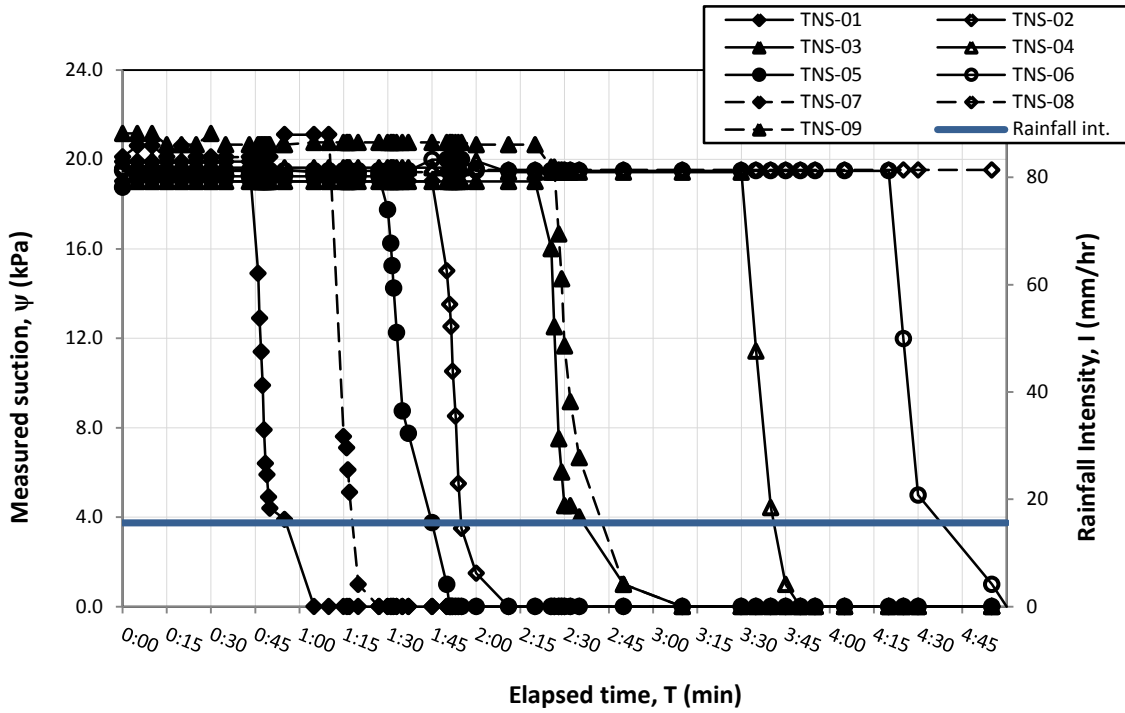


Fig. B.6. (a) Changes in pore pressure (suction) values throughout the test and (b) wetting front progress at different time steps for FLM_06

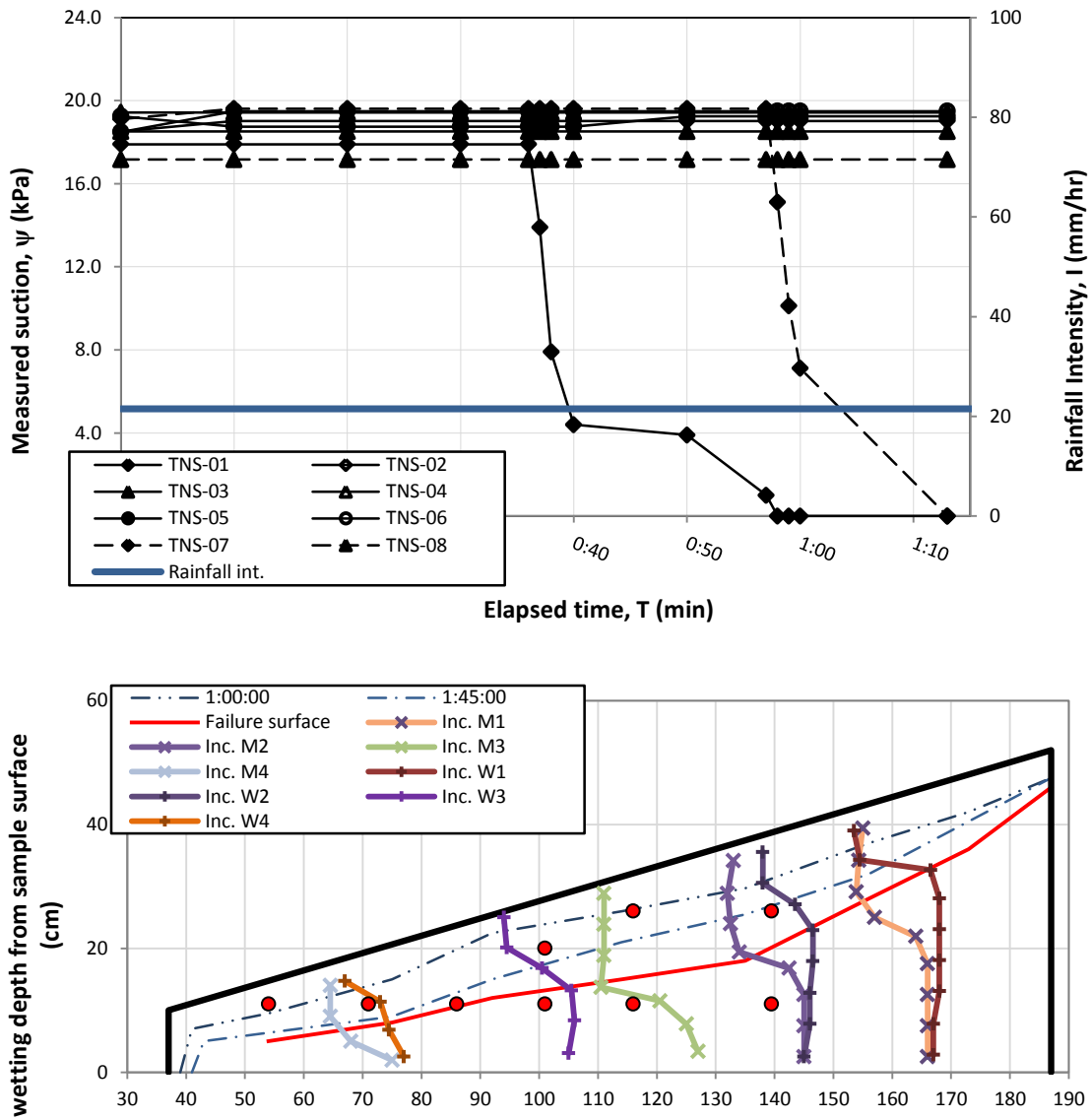


Fig. B.7. (a) Changes in pore pressure (suction) values throughout the test and (b) wetting front progress at different time steps and slip (failure) surface at the time of failure for FLM_08

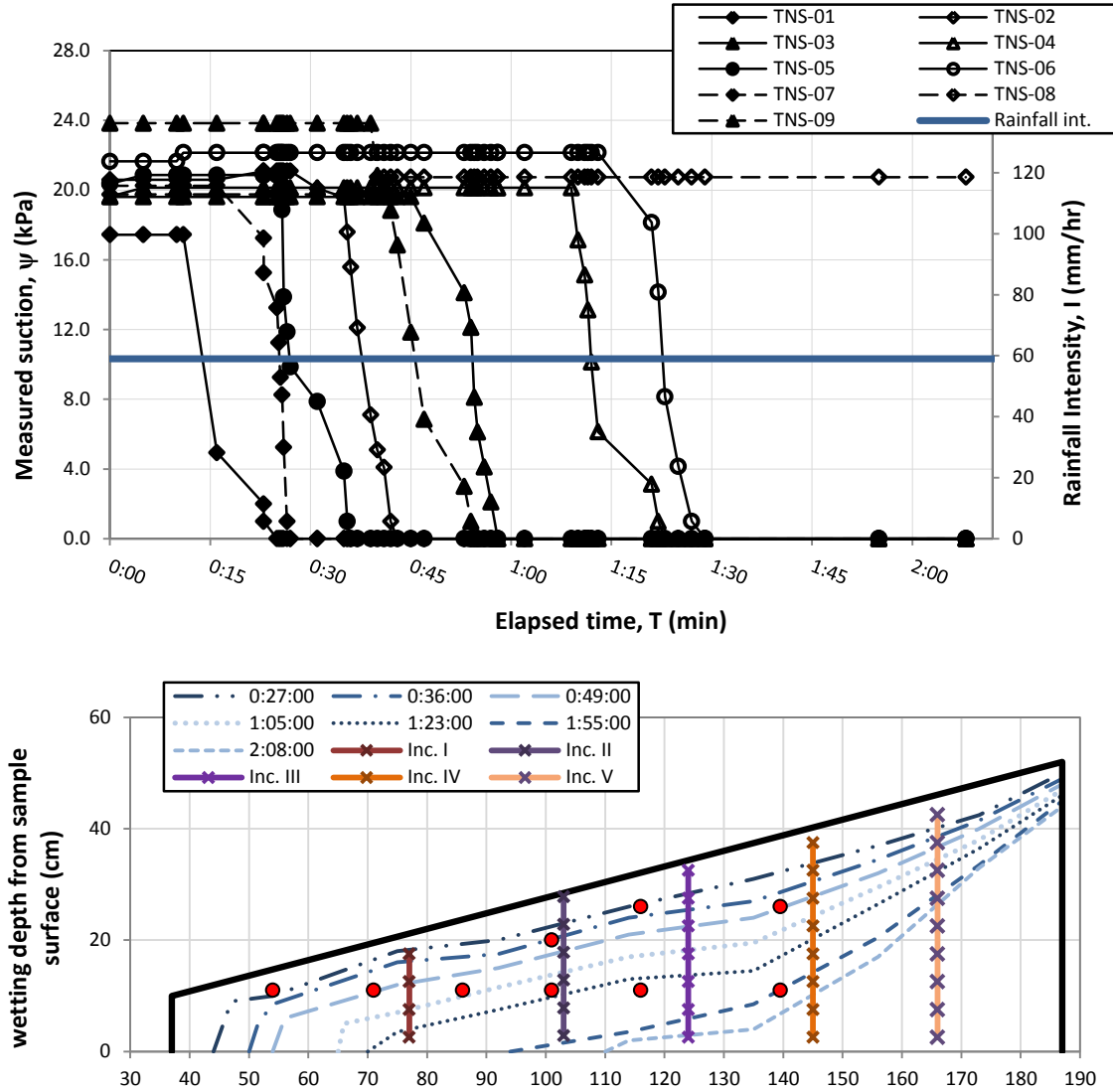


Fig. B.8. (a) Changes in pore pressure (suction) values throughout the test and (b) wetting front progress at different time steps for FLM_09

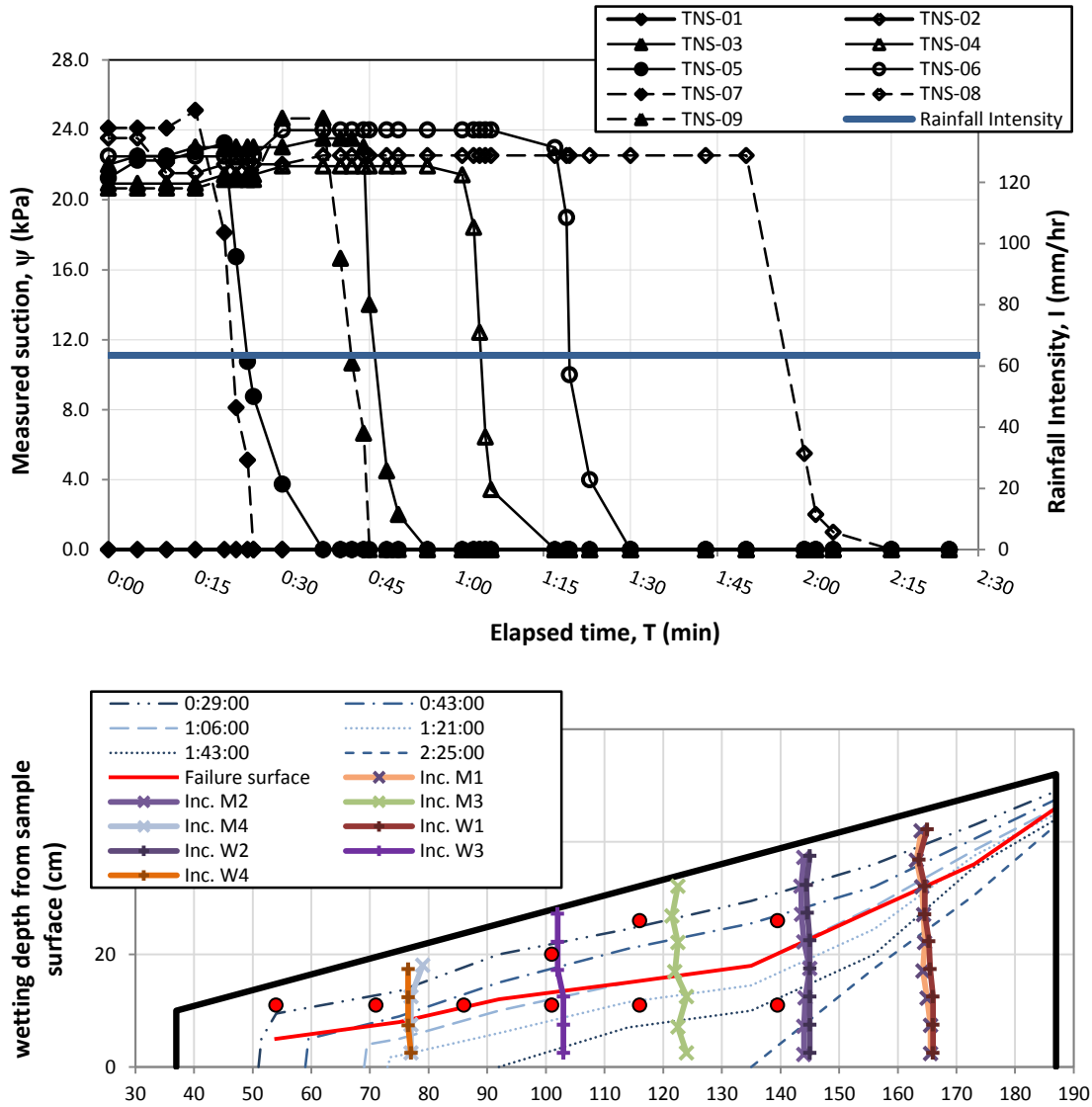


Fig. B.9. (a) Changes in pore pressure (suction) values throughout the test and (b) wetting front progress at different time steps and slip (failure) surface at the time of failure for FLM_10

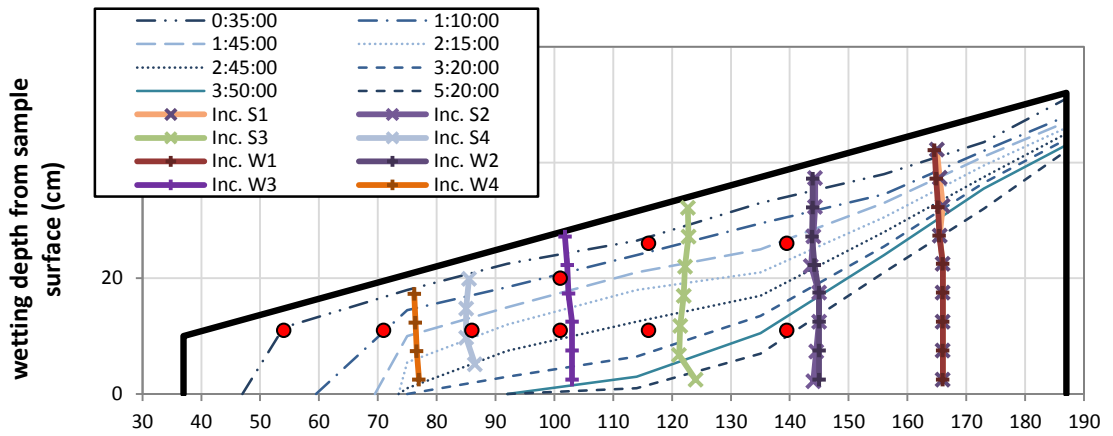
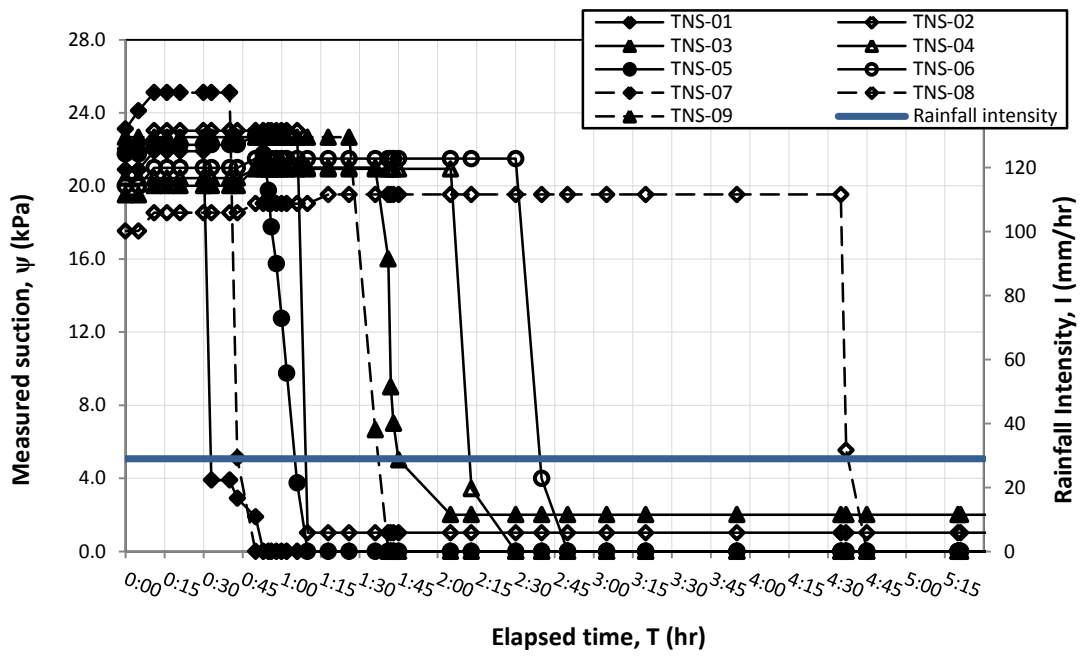


Fig. B.10. (a) Changes in pore pressure (suction) values throughout the test and (b) wetting front progress at different time steps for FLM_11

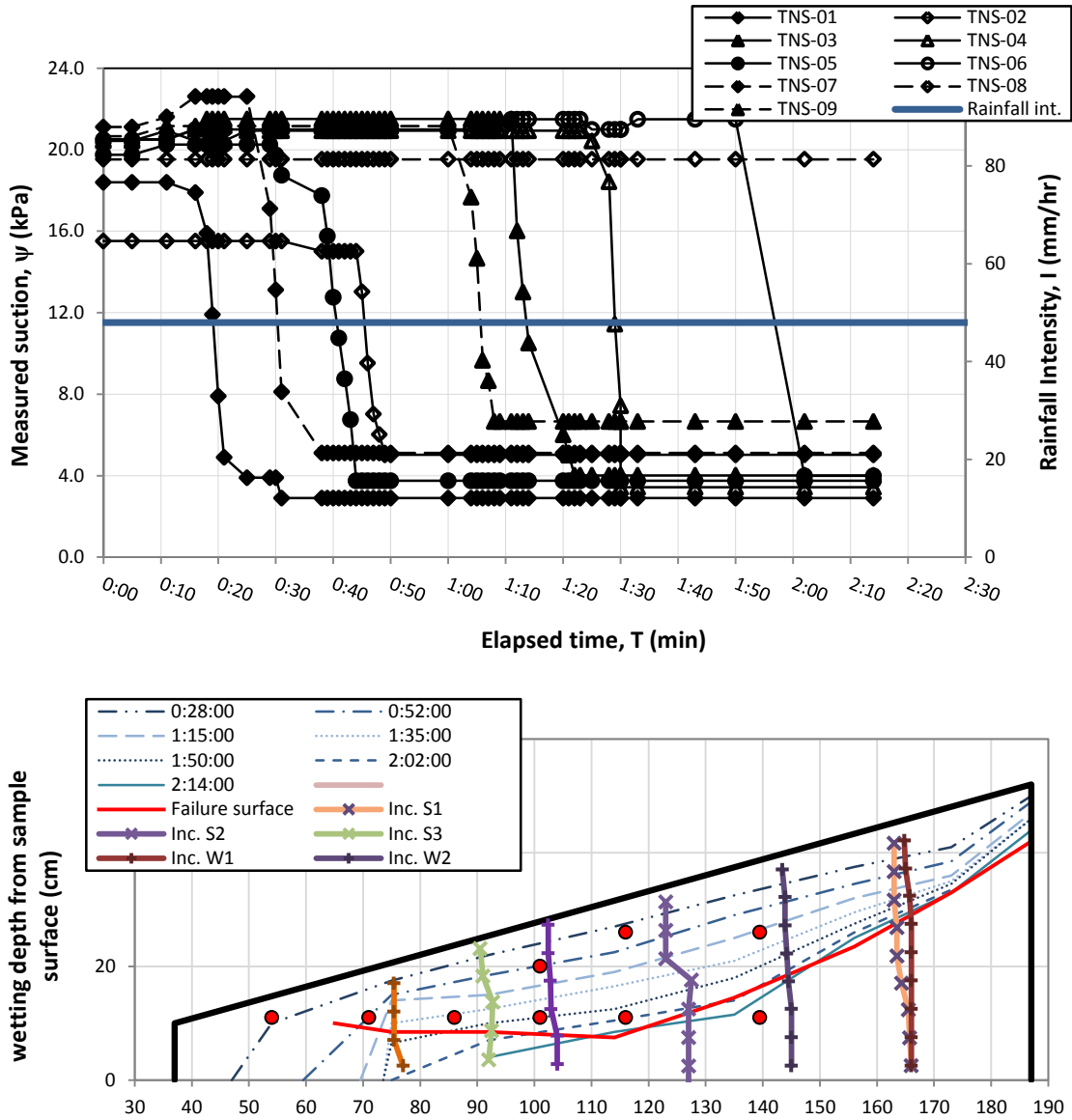


Fig. B.11. (a) Changes in pore pressure (suction) values throughout the test and (b) wetting front progress at different time steps and slip (failure) surface at the time of failure for FLM_12

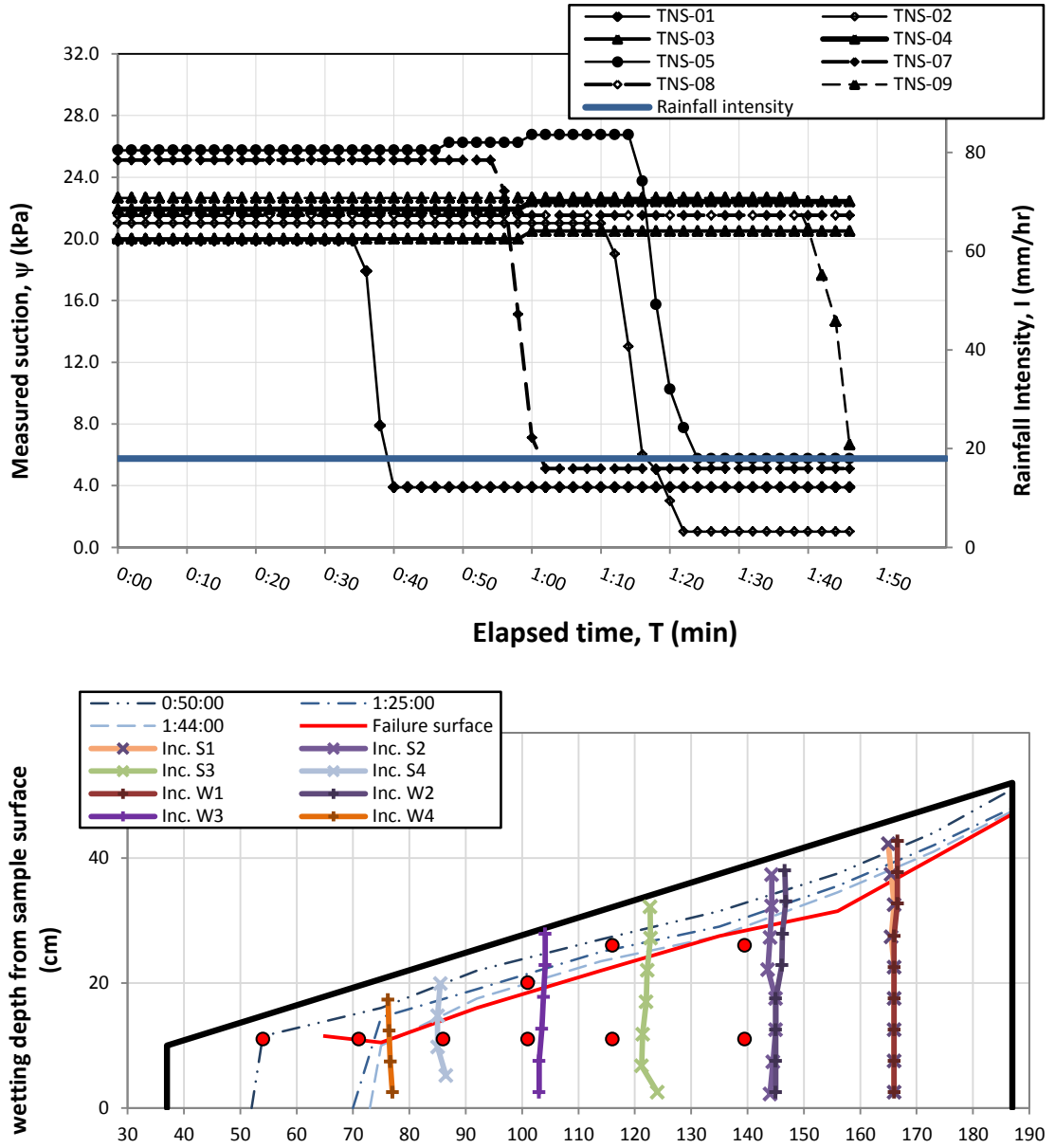


Fig. B.12. (a) Changes in pore pressure (suction) values throughout the test and (b) wetting front progress at different time steps and slip (failure) surface at the time of failure for FLM_13

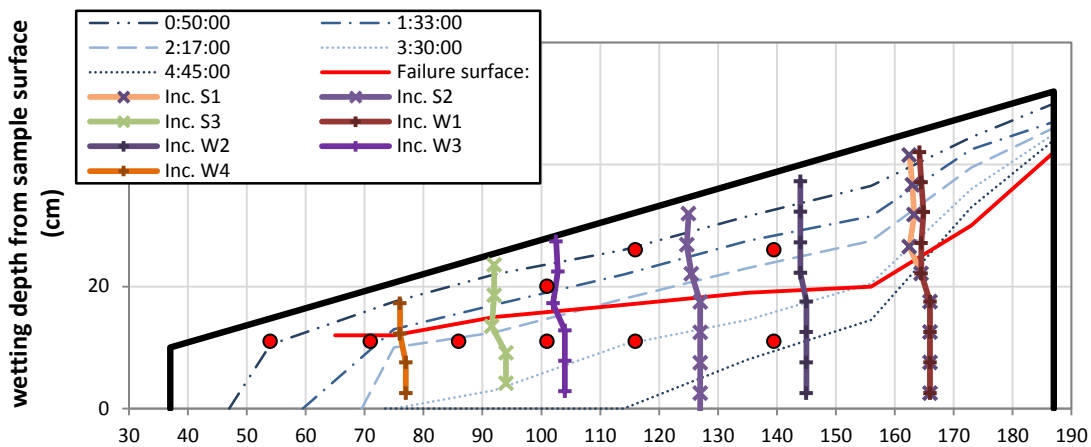
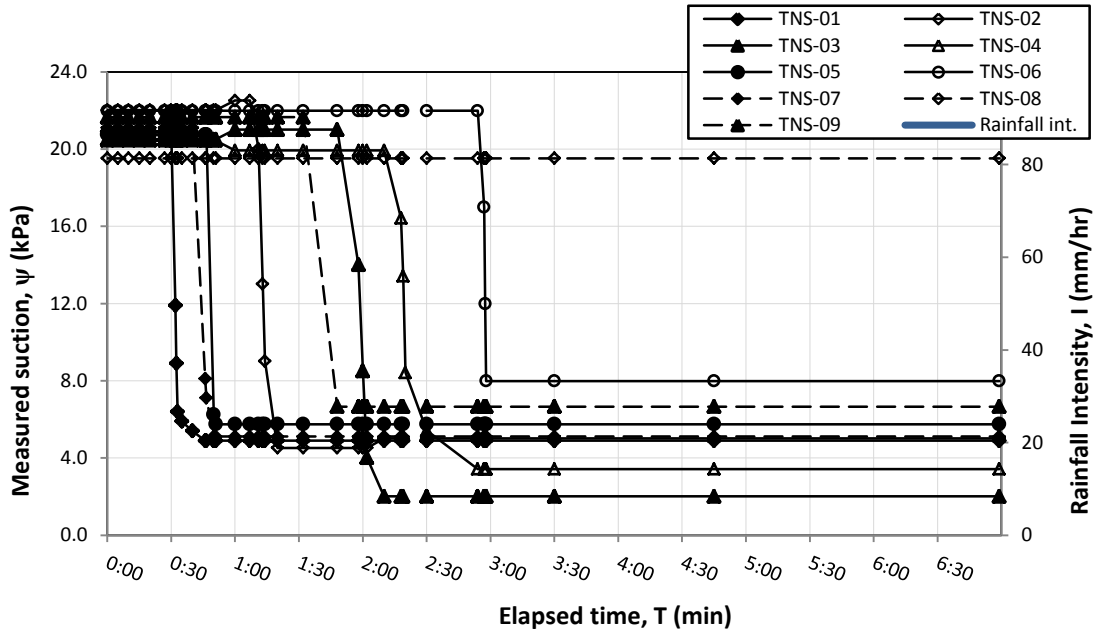


Fig. B.13. (a) Changes in pore pressure (suction) values throughout the test and (b) wetting front progress at different time steps and slip (failure) surface at the time of failure for FLM_14

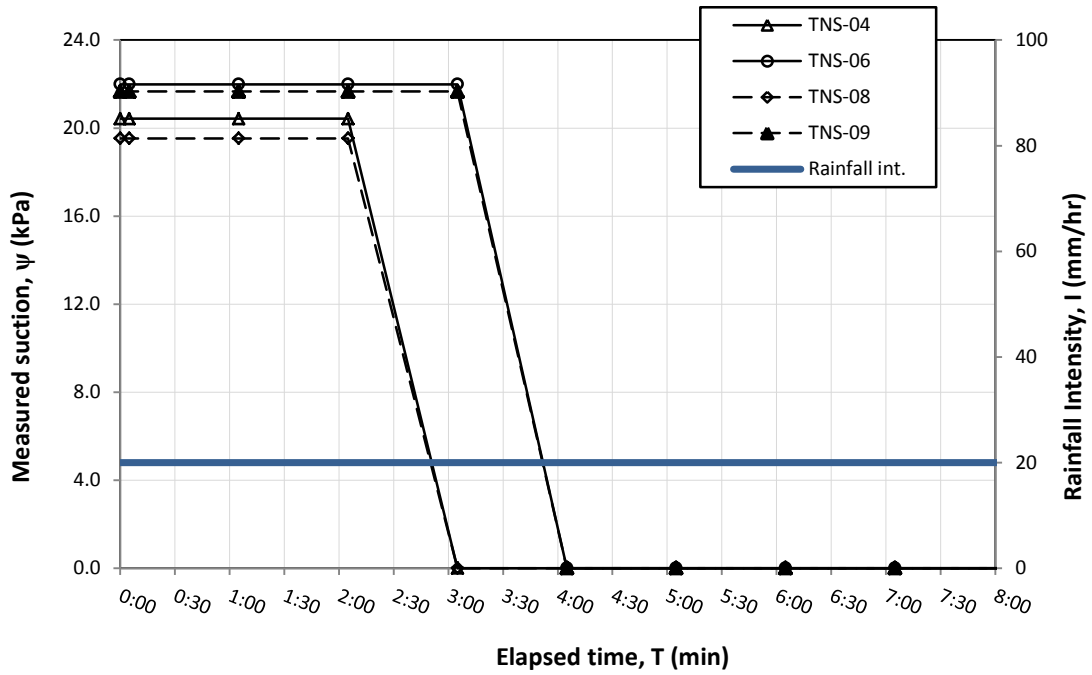


Fig. B.14. Changes in pore pressure (suction) values throughout the FLM_15; no wetting front recording has taken place in this test.

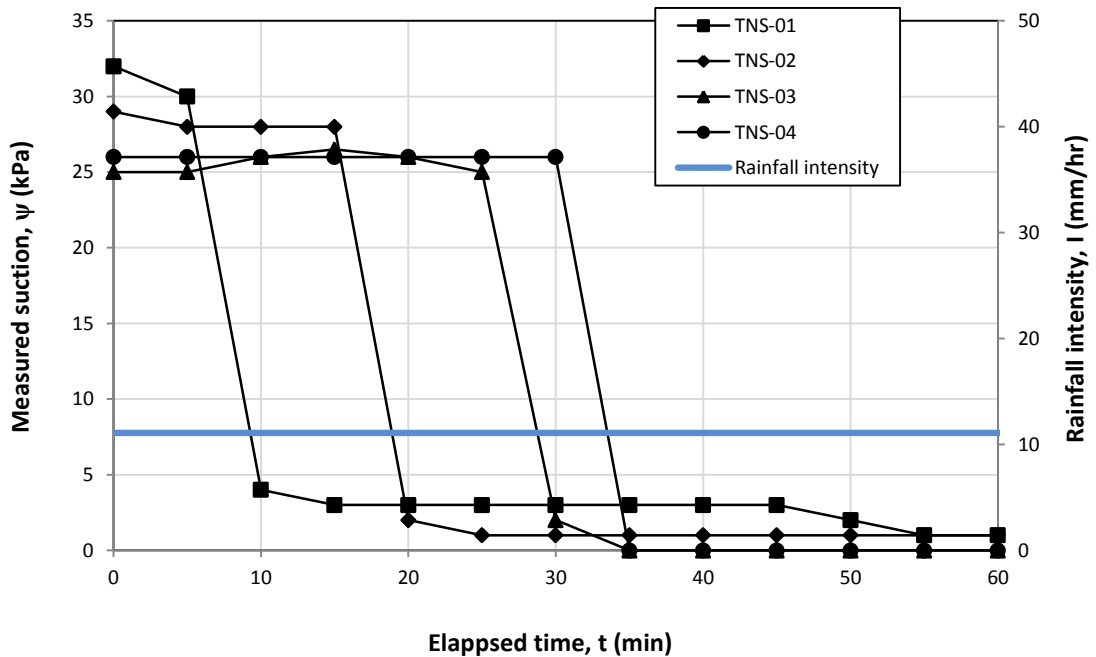


Fig. B.15. Changes in pore pressure (suction) values throughout the LAM_1.

APPENDIX C

RESULTS OF NUMERICAL SIMULATIONS

Simulated pore water pressures using SEEP/W 2012 for each of the flume experiments are presented in detail in Appendix C. In each figure all the suction recordings are plotted against time in accordance with rainfall intensity. Also, the results from slope stability analysis of each of flume experiments which are performed using SLOPE/W 2012 are presented here. Obtained results from this section are compared later with experimental results.

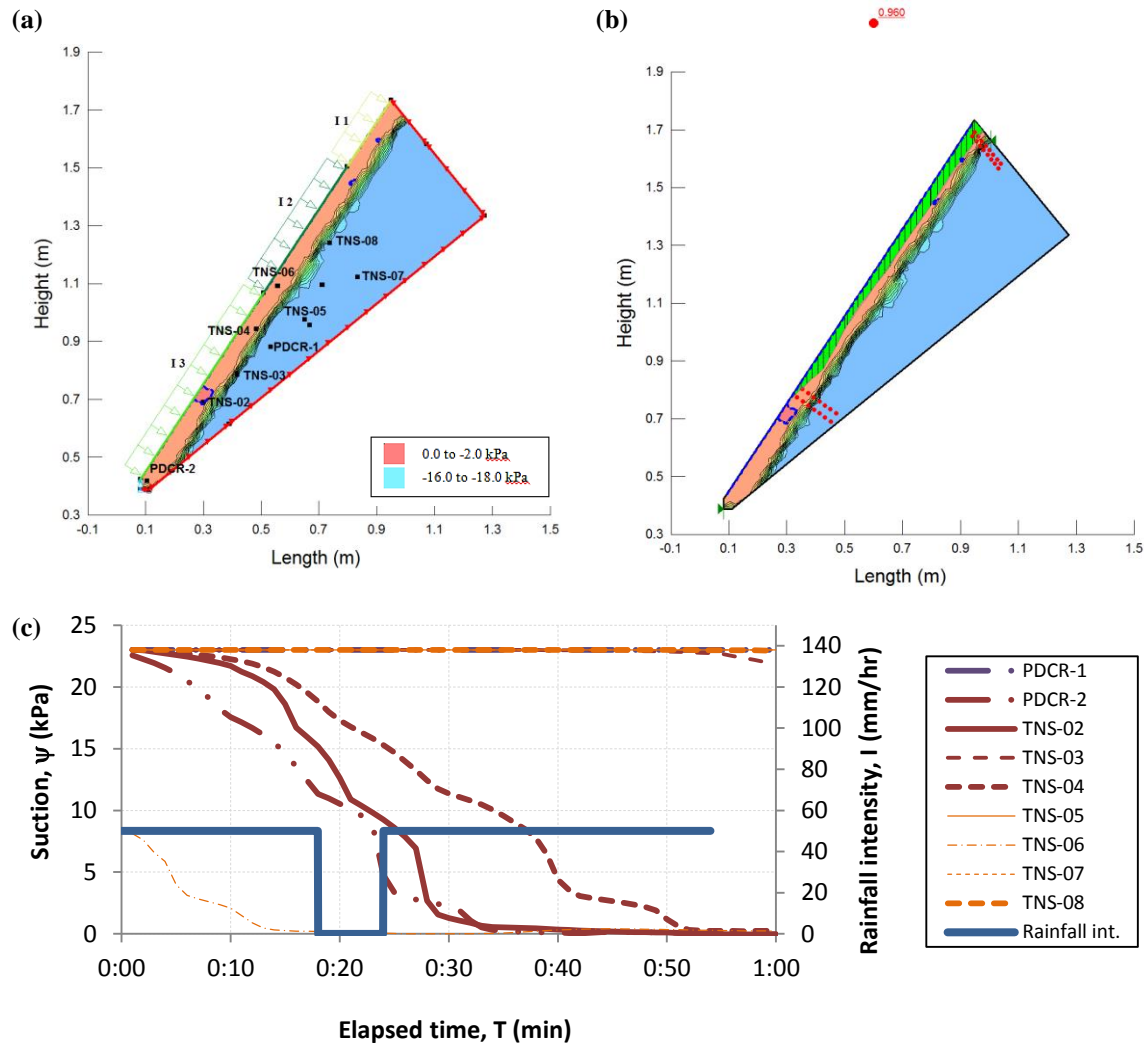


Fig. C.1. (a) Distribution of simulated pore water pressures (suction) within the slope at the time of failure (b) simulated slip surface and (c) simulated pore water pressure changes in the location of tensiometers

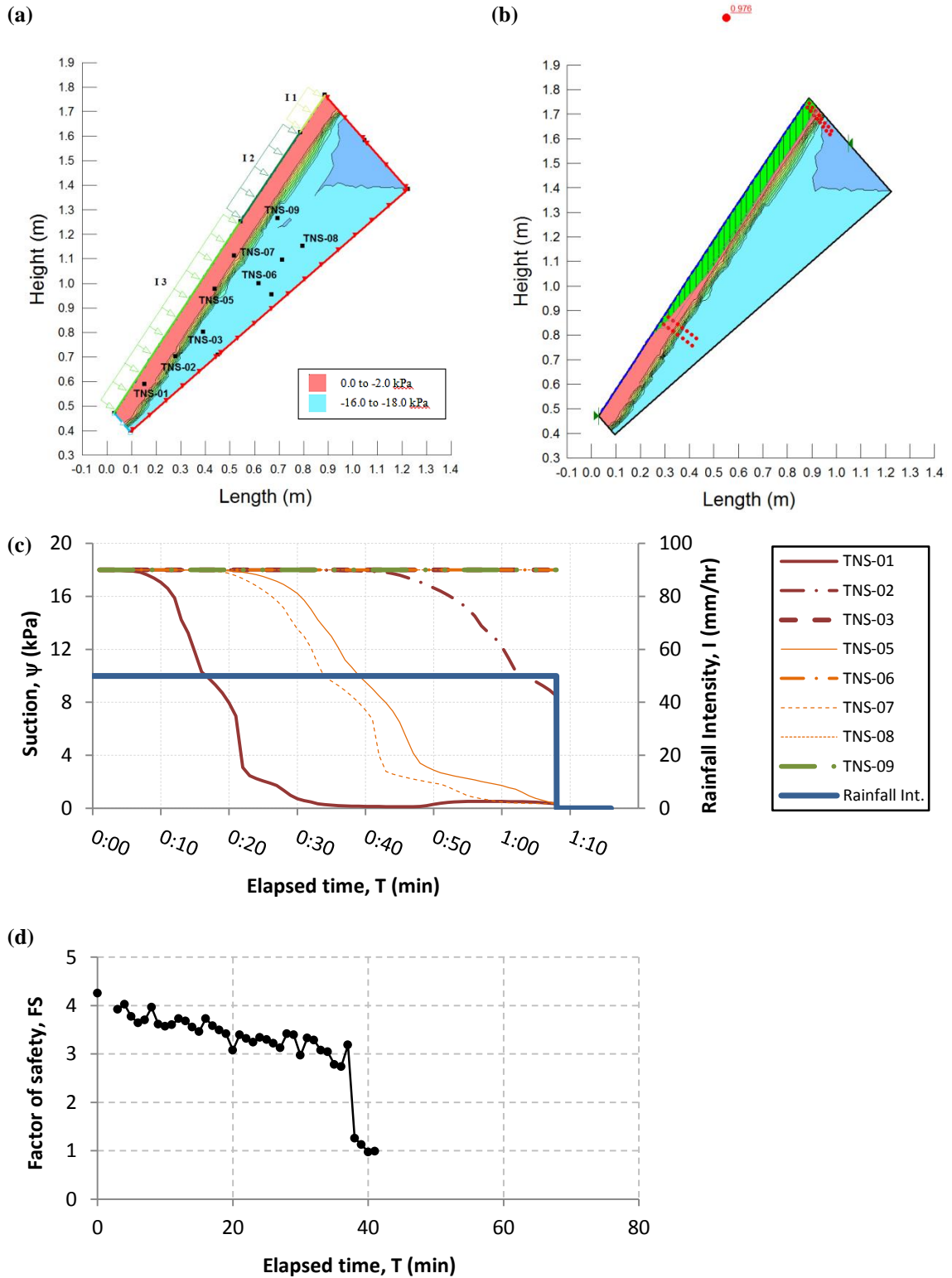


Fig. C.2. (a) Distribution of simulated pore water pressures (suction) within the slope at the time of failure (b) simulated slip surface, (c) simulated pore water pressure changes in the location of tensiometers and (d) FS versus time for FLM_04

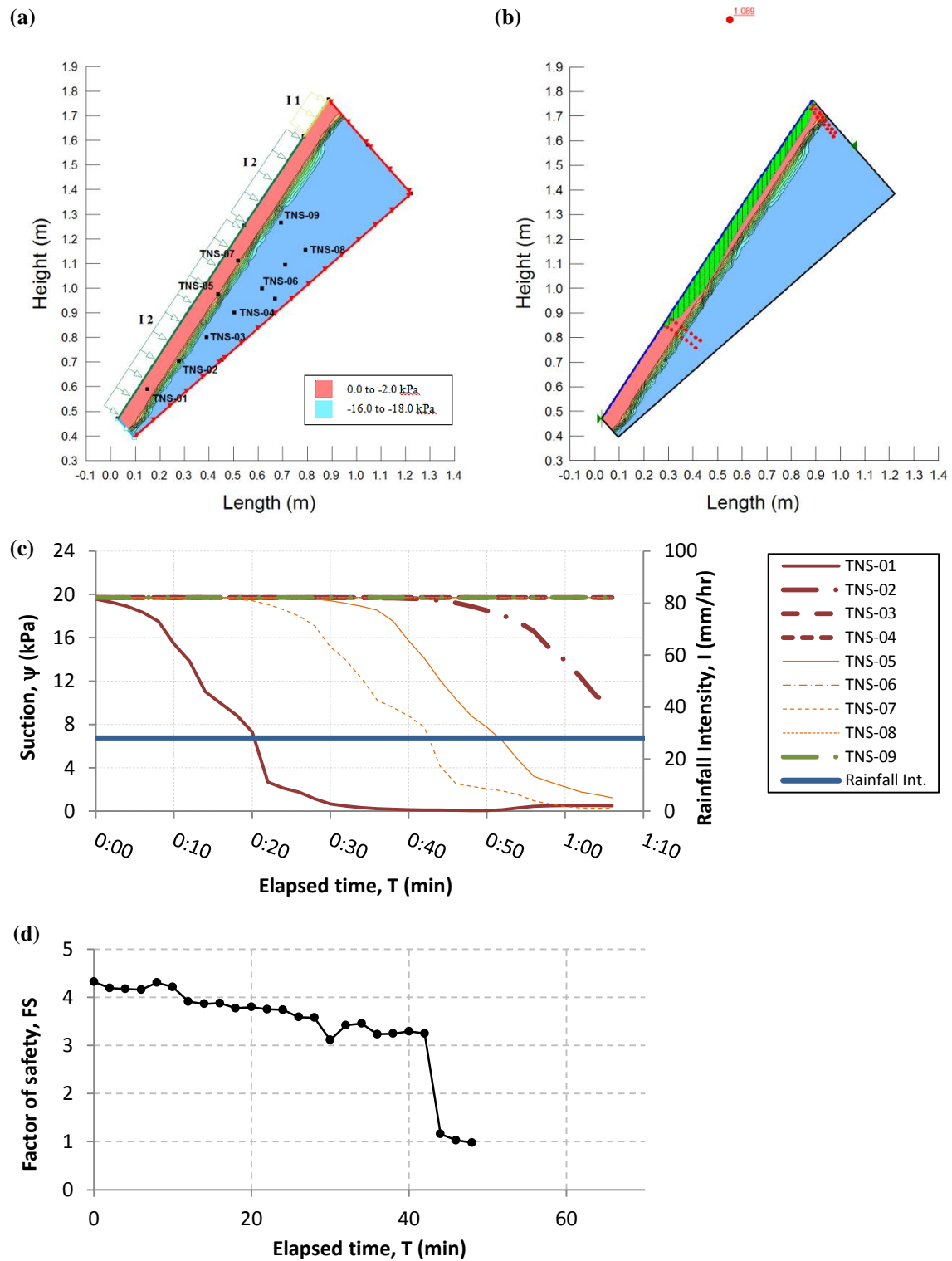


Fig. C.3. (a) Distribution of simulated pore water pressures (suction) within the slope at the time of failure (b) simulated slip surface, (c) simulated pore water pressure changes in the location of tensiometers and (d) FS versus time for FLM_05

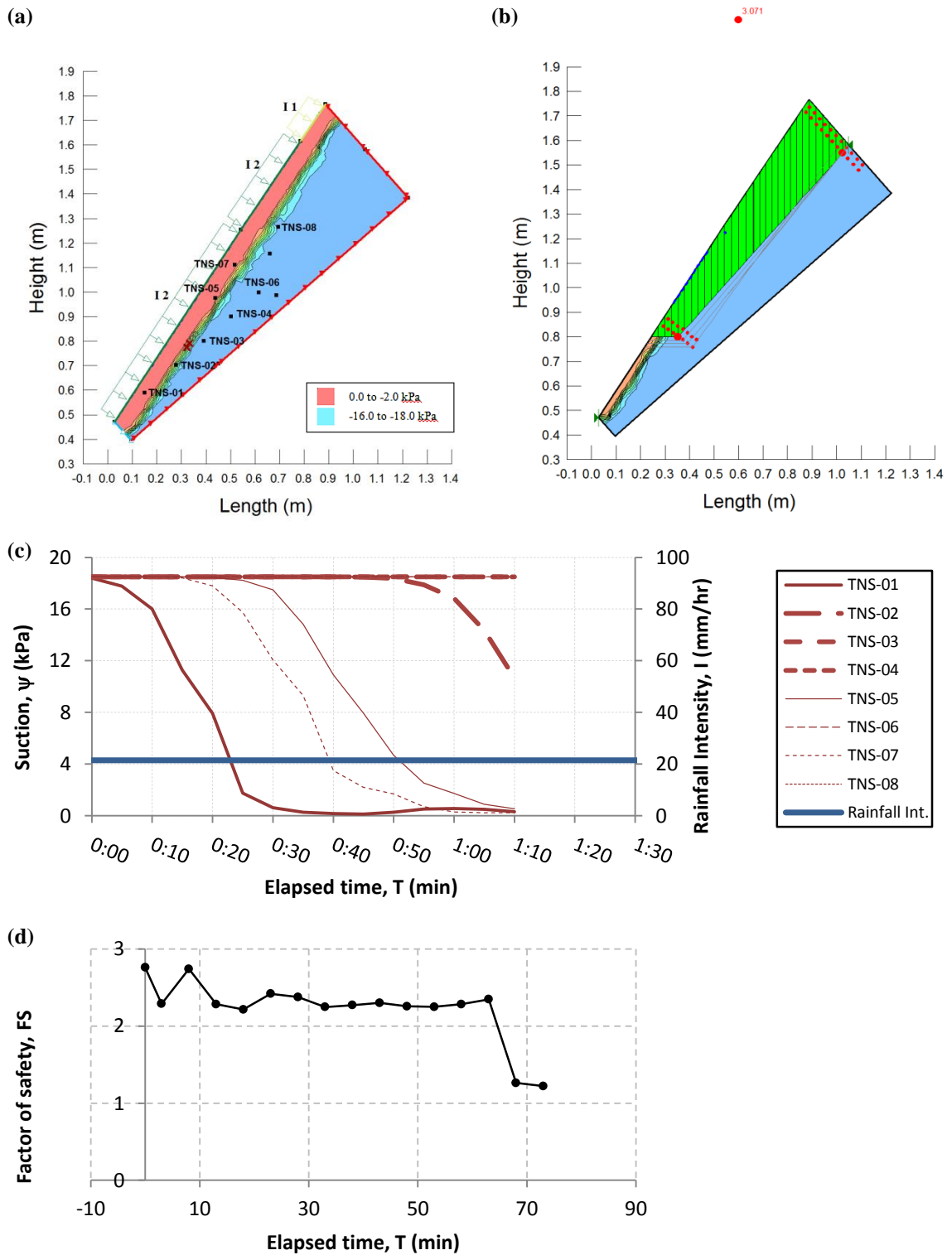


Fig. C.4. (a) Distribution of simulated pore water pressures (suction) within the slope at the end of test FLM_08 (end of raining), (b) simulated potential slip surface, (c) simulated pore water pressure changes at the location of tensiometers and (d) FS versus time

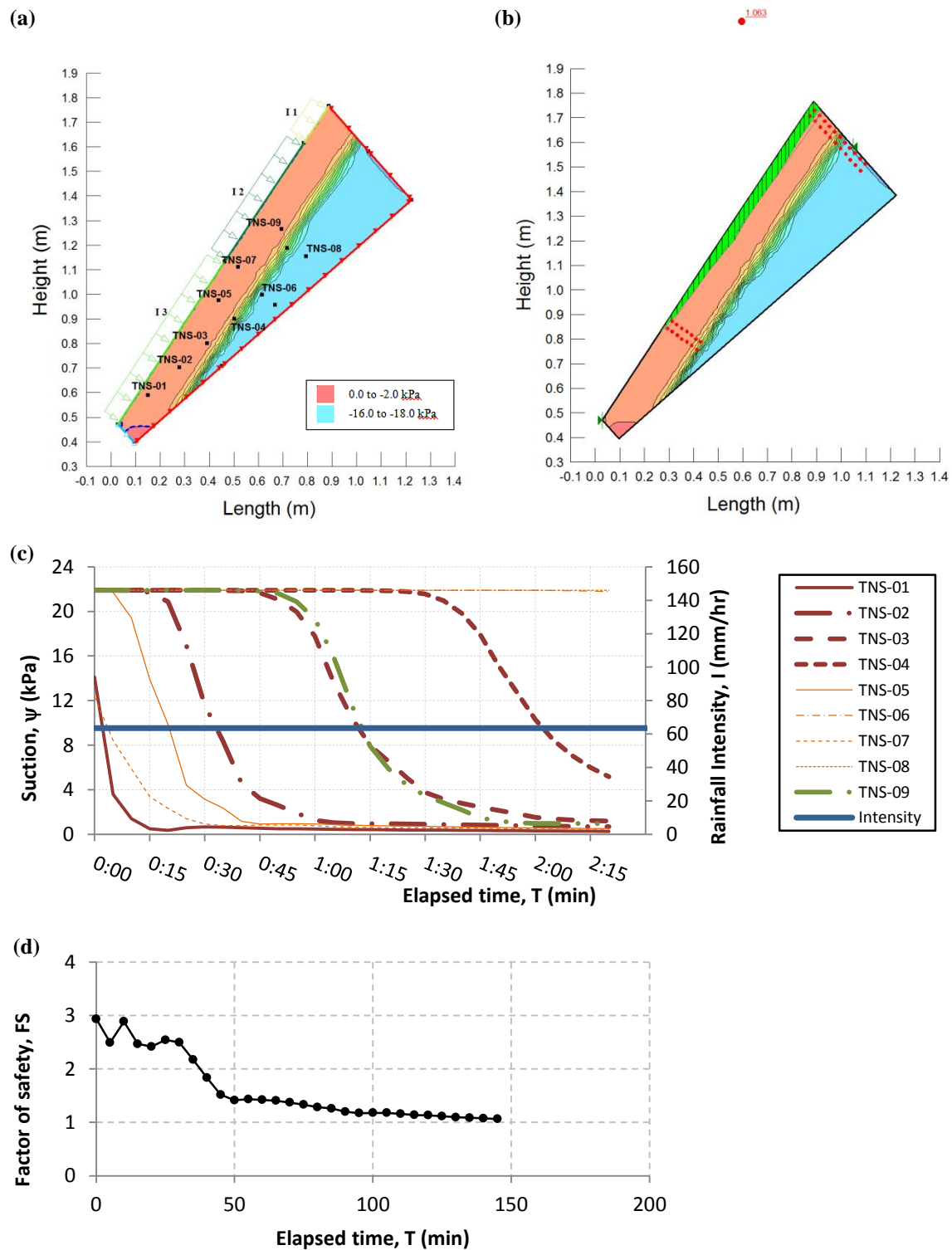


Fig. C.5. (a) Distribution of simulated pore water pressures (suction) within the slope at the end of FLM_10 (end of raining), (b) simulated potential slip surface and (c) simulated pore water pressure changes at the location of tensiometers and (d) FS versus time

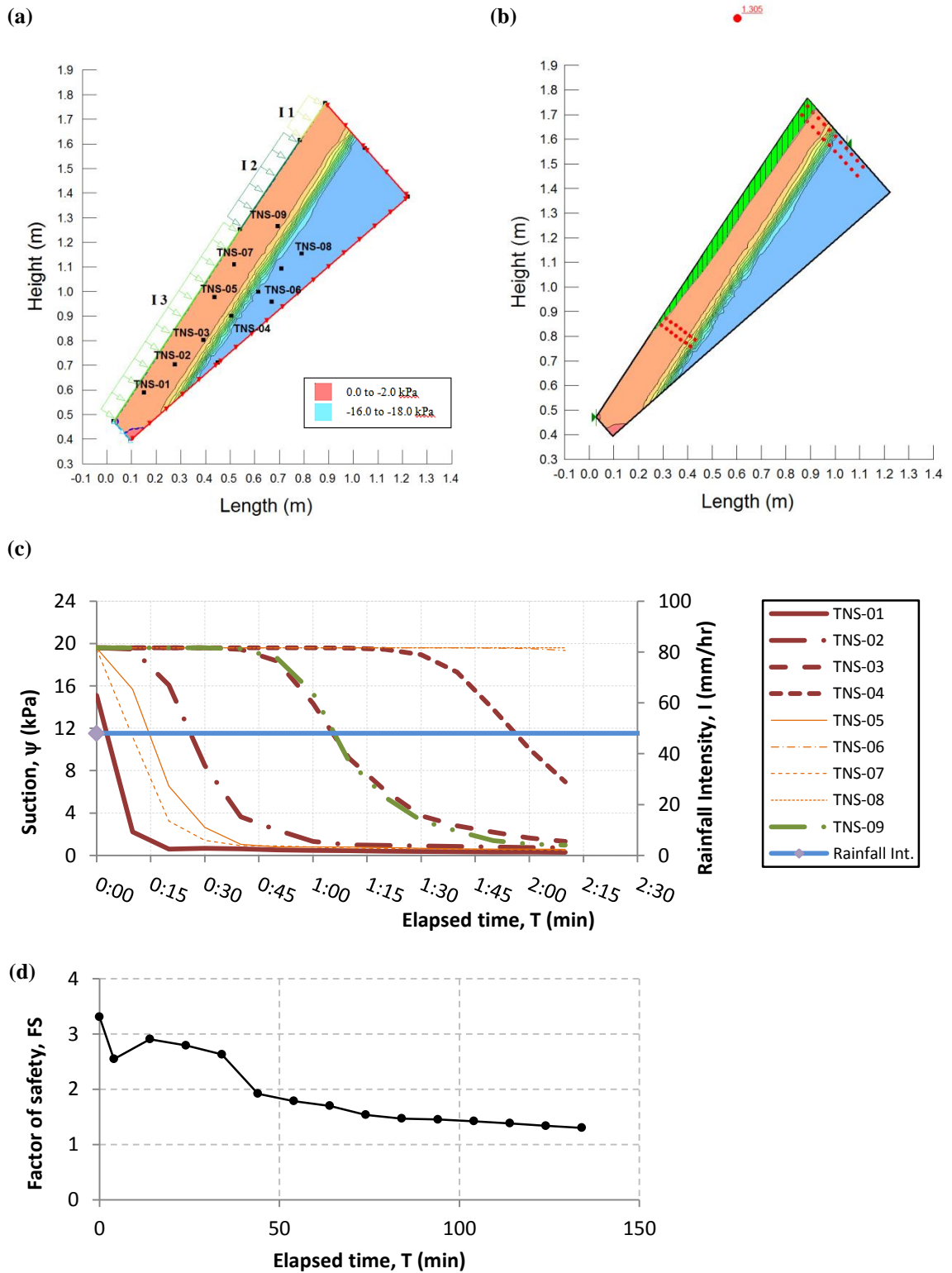


Fig. C.6. (a) Distribution of simulated pore water pressures (suction) within the slope at the end of test (end of raining), (b) simulated potential slip surface, (c) simulated pore water pressure changes in the location of tensiometers and (d) FS versus time for FLM_12

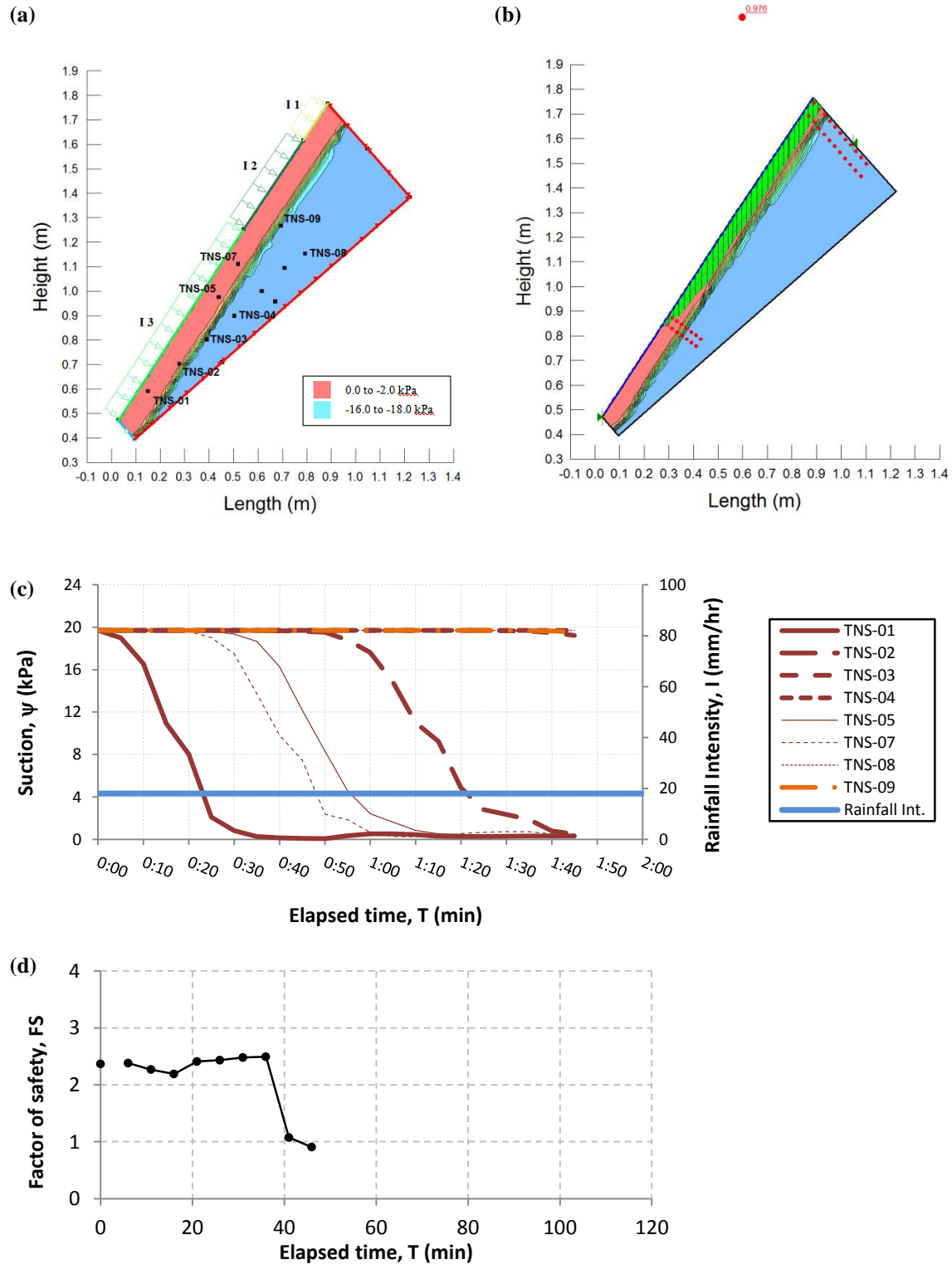


Fig. C.7. (a) Distribution of simulated pore water pressures (suction) within the slope at the end of test (end of raining), (b) simulated slip surface, (c) simulated pore water pressure changes in the location of tensiometers and (d) FS versus time for FLM_13

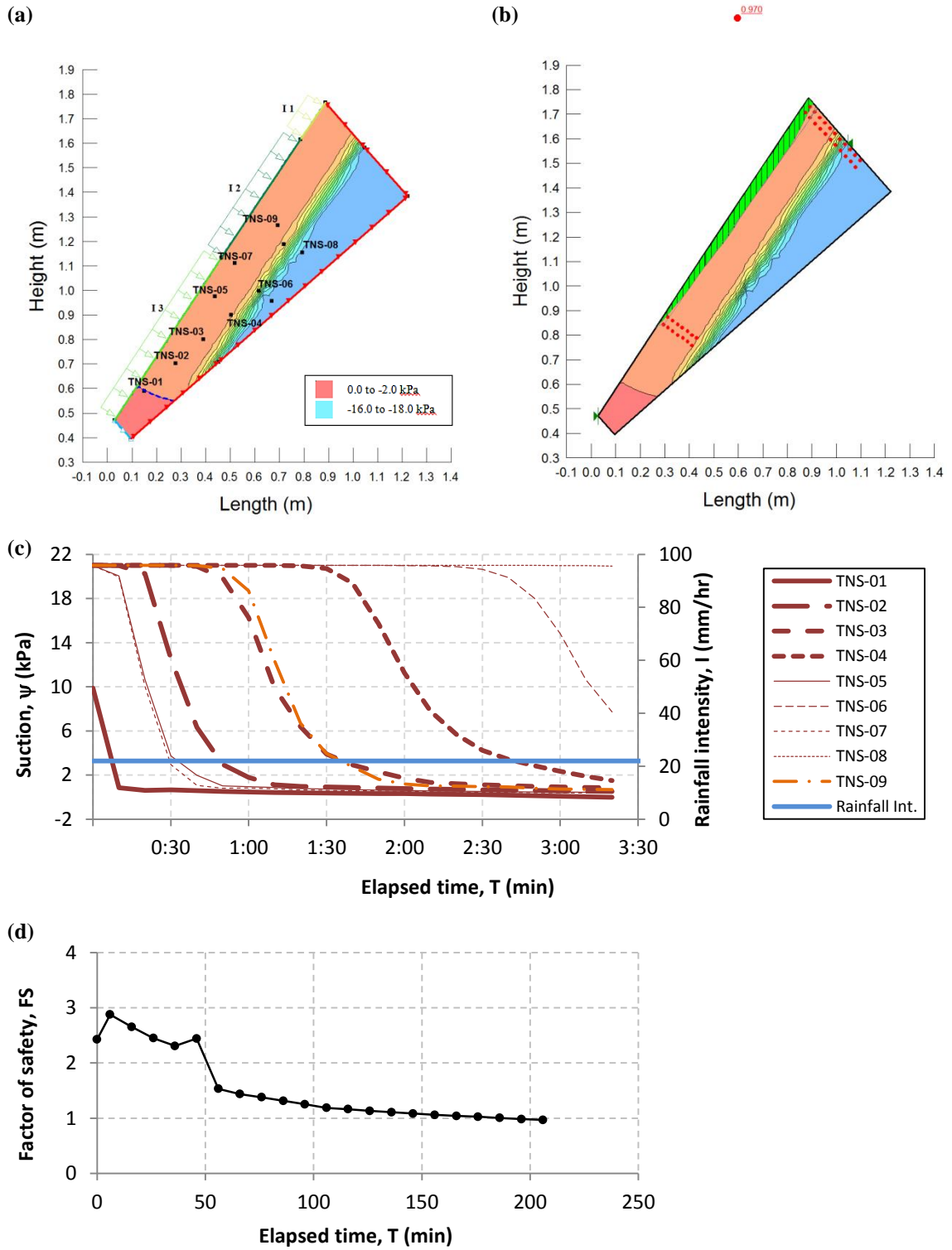


Fig. C.8. (a) Distribution of simulated pore water pressures (suction) within the slope at the time of failure (b) simulated slip surface, (c) simulated pore water pressure changes in the location of tensiometers and (d) FS versus time for FLM_14

APPENDIX D

COMPARISON OF TEST RESULTS AND NUMERICAL SIMULATIONS

Validity of numerical simulation of unsaturated seepage in flume tests is verified by monitoring pore water pressure (e.g. suction) changes in specific points (obtained from SEEP/W 2012) and recorded values using tensiometers and PDCR devices. In Appendix D, detail of the results for each at four representing monitoring points is reported for flume experiments. Also the detected failure surface using its projection on monitoring side wall and inclinometer data is presented with numerically simulated slip surface.

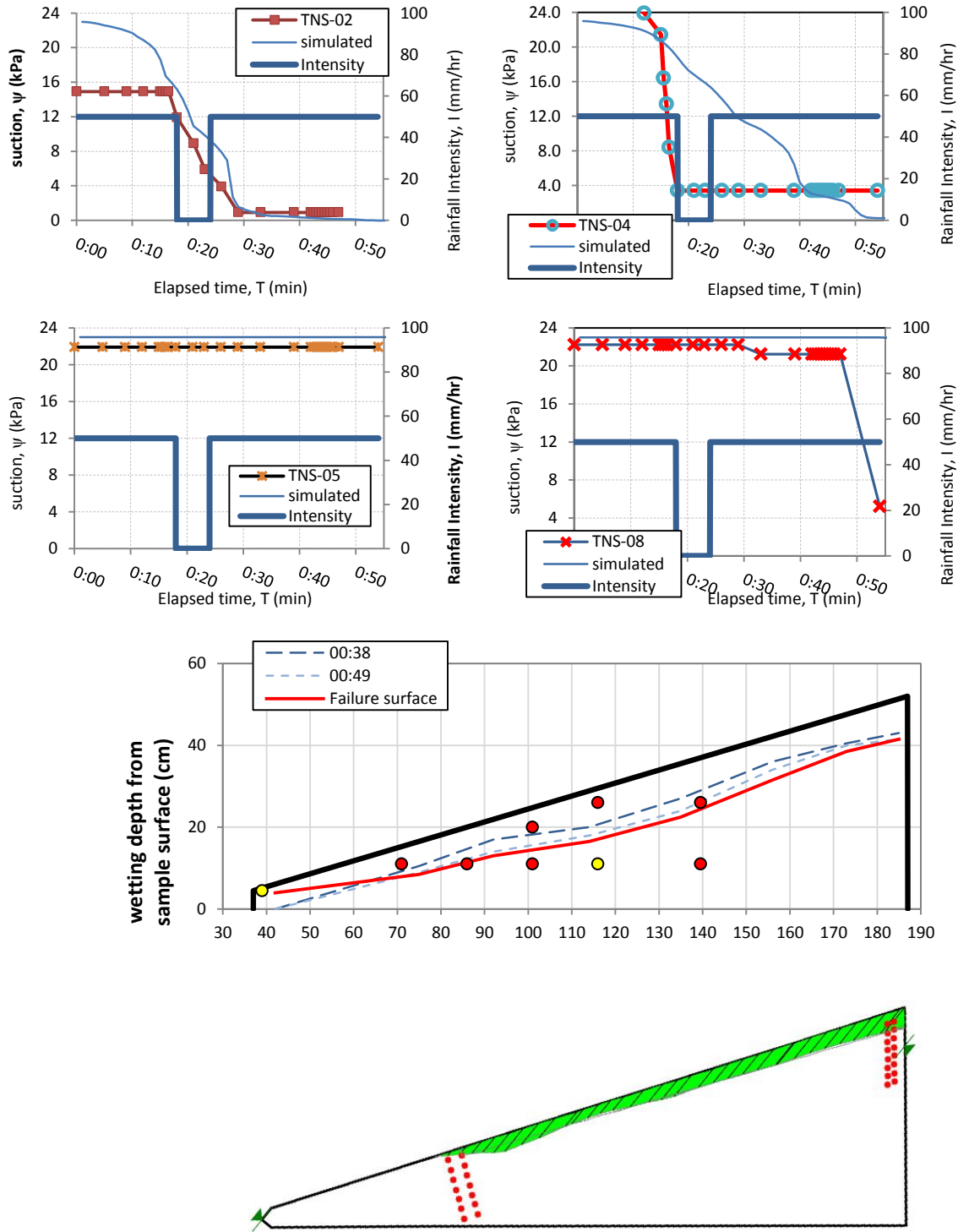


Fig. D.1. (a) Measured and simulated pore water pressure changes in the location of instrumentations for FLM_03, (b) observed and (c) simulated failure surfaces.

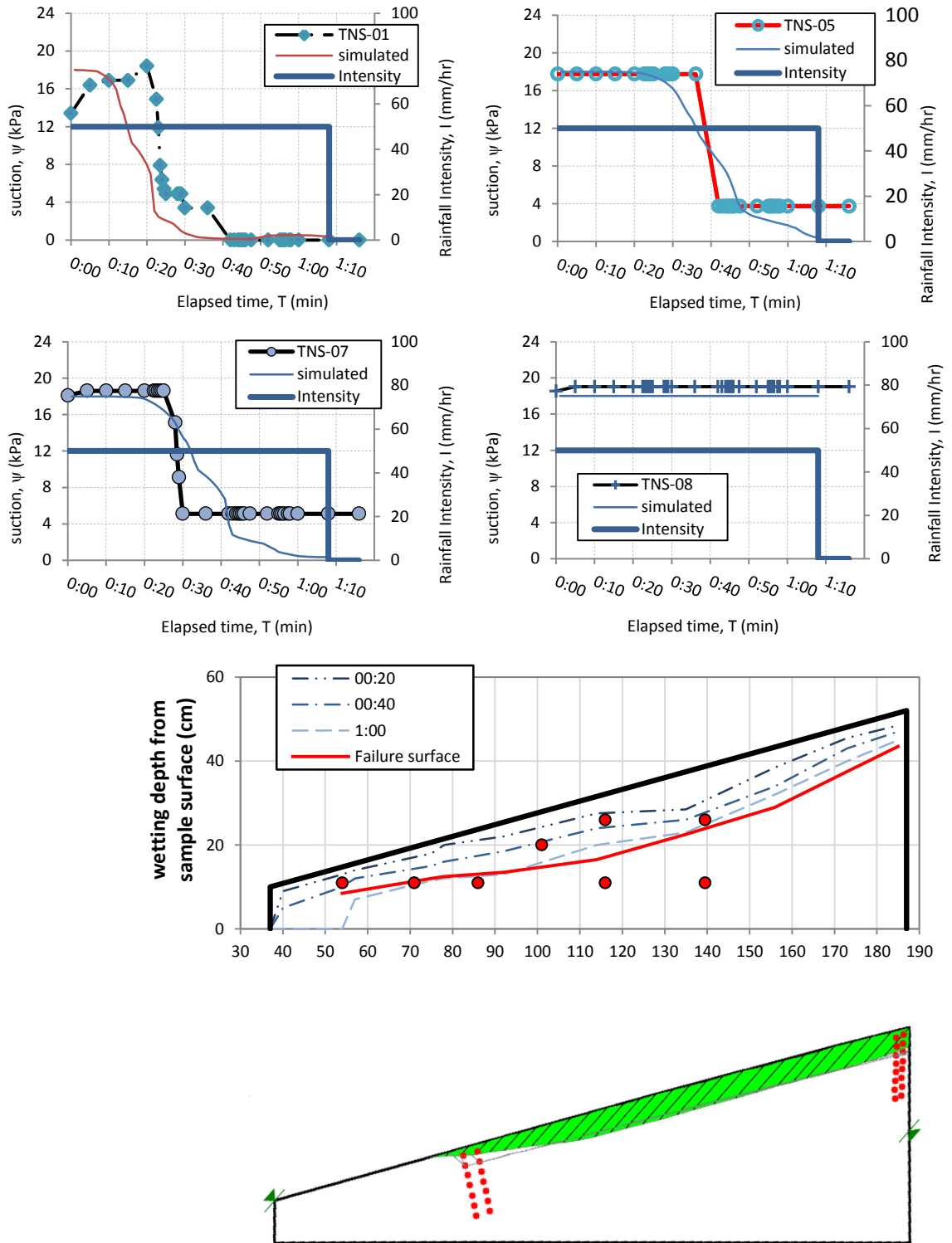


Fig. D.2. (a) Measured and simulated pore water pressure changes in the location of instrumentations for FLM_04, (b) observed and (c) simulated failure surfaces.

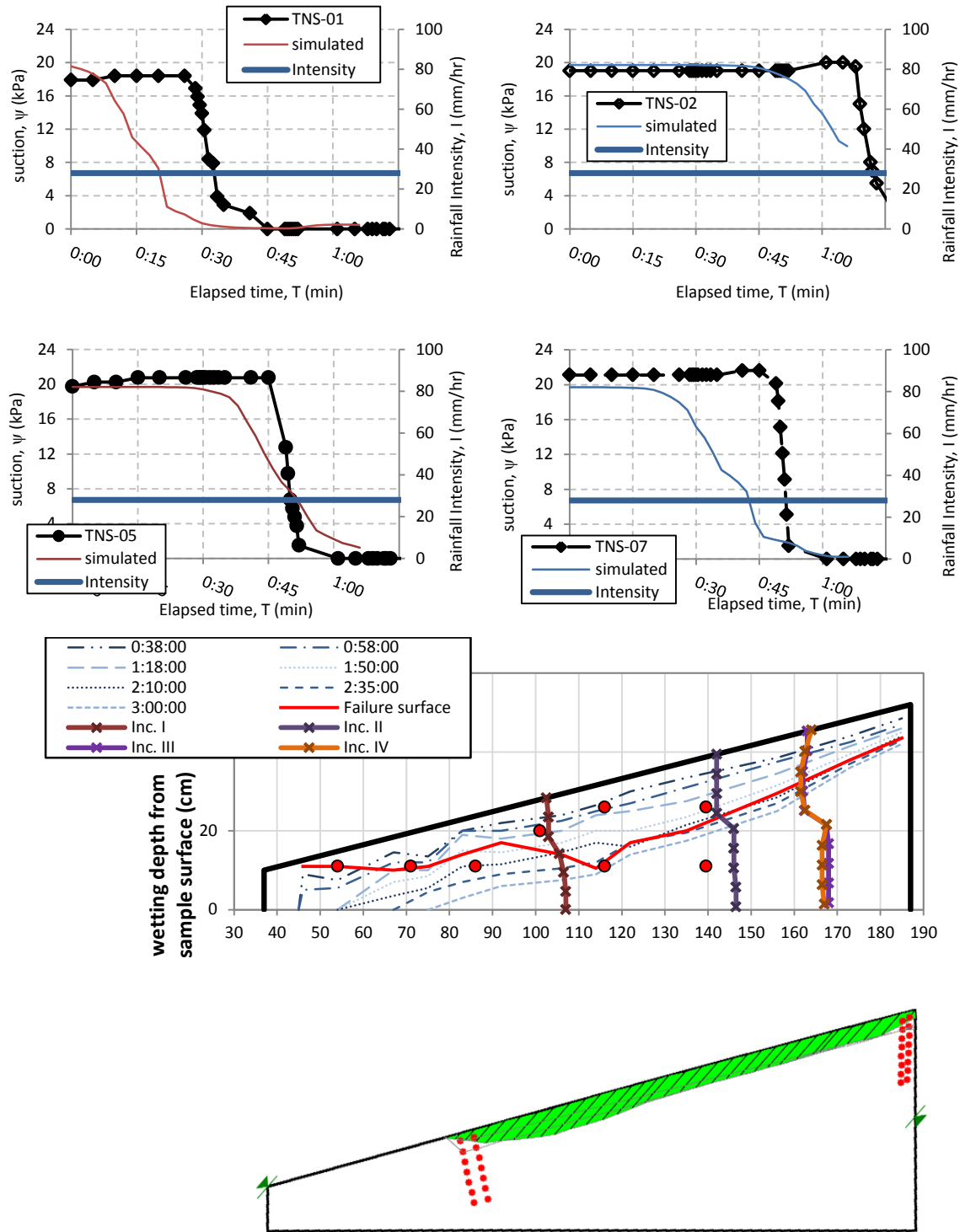


Fig. D.3. (a) Measured and simulated pore water pressure changes in the location of instrumentations for FLM_05, (b) observed and (c) simulated failure surfaces.

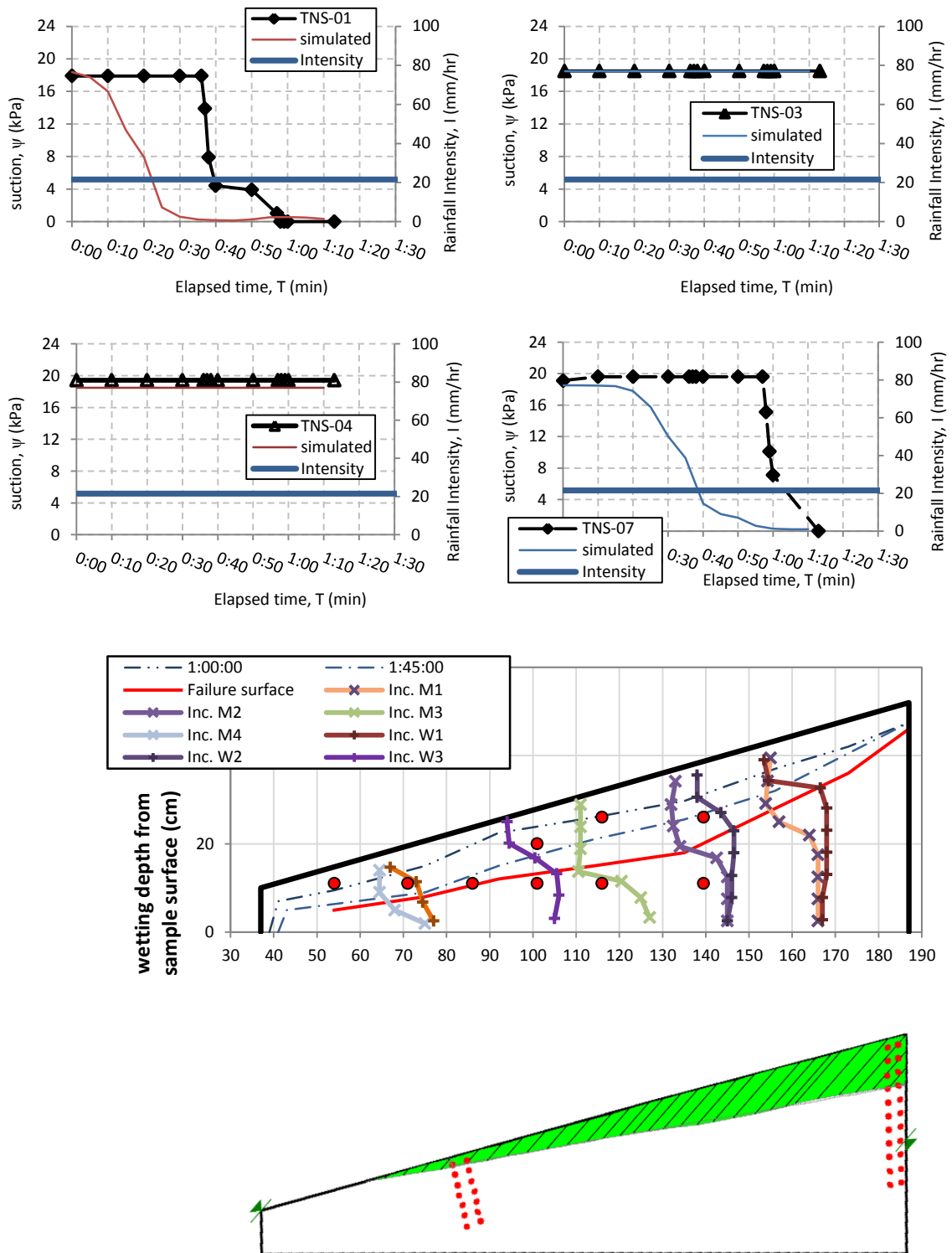


Fig. D.4. (a) Measured and simulated pore water pressure changes in the location of instrumentations for FLM_08, (b) observed and (c) simulated failure surfaces.

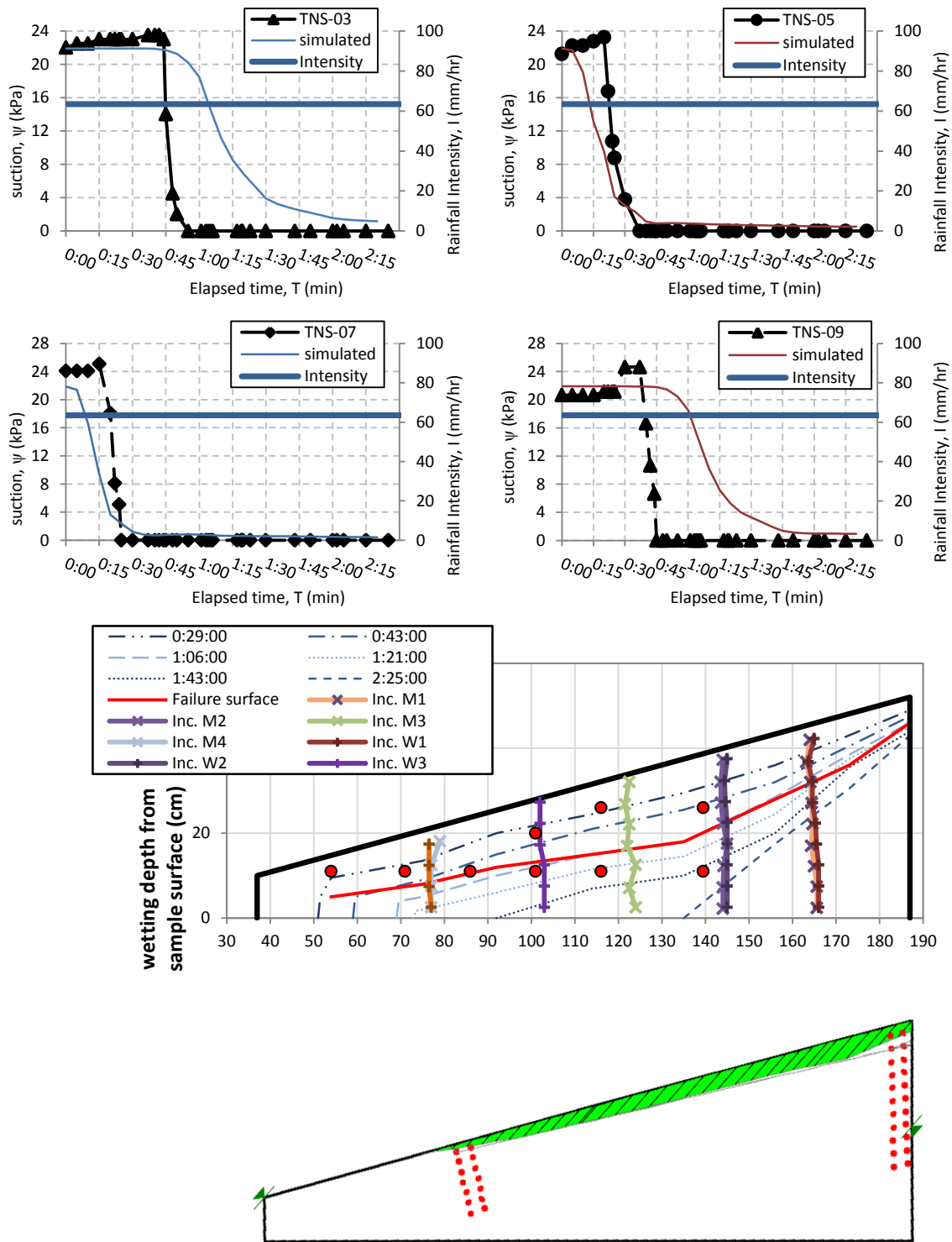


Fig. D.5. (a) Measured and simulated pore water pressure changes in the location of instrumentations for FLM₁₀, (b) observed and (c) simulated failure surfaces.

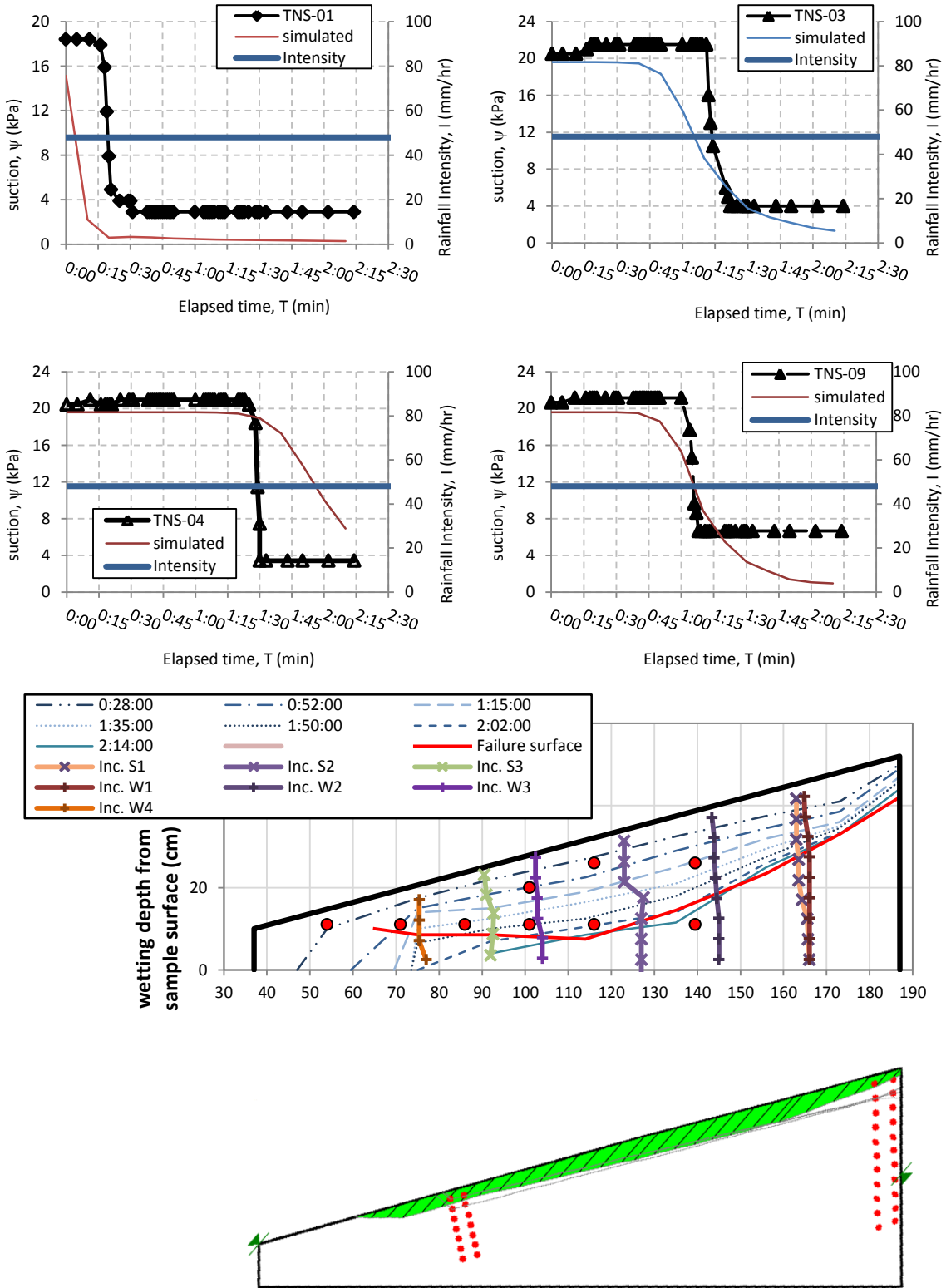


Fig. D.6. (a) Measured and simulated pore water pressure changes in the location of instrumentations for FLM₁₂, (b) observed and (c) simulated failure surfaces.

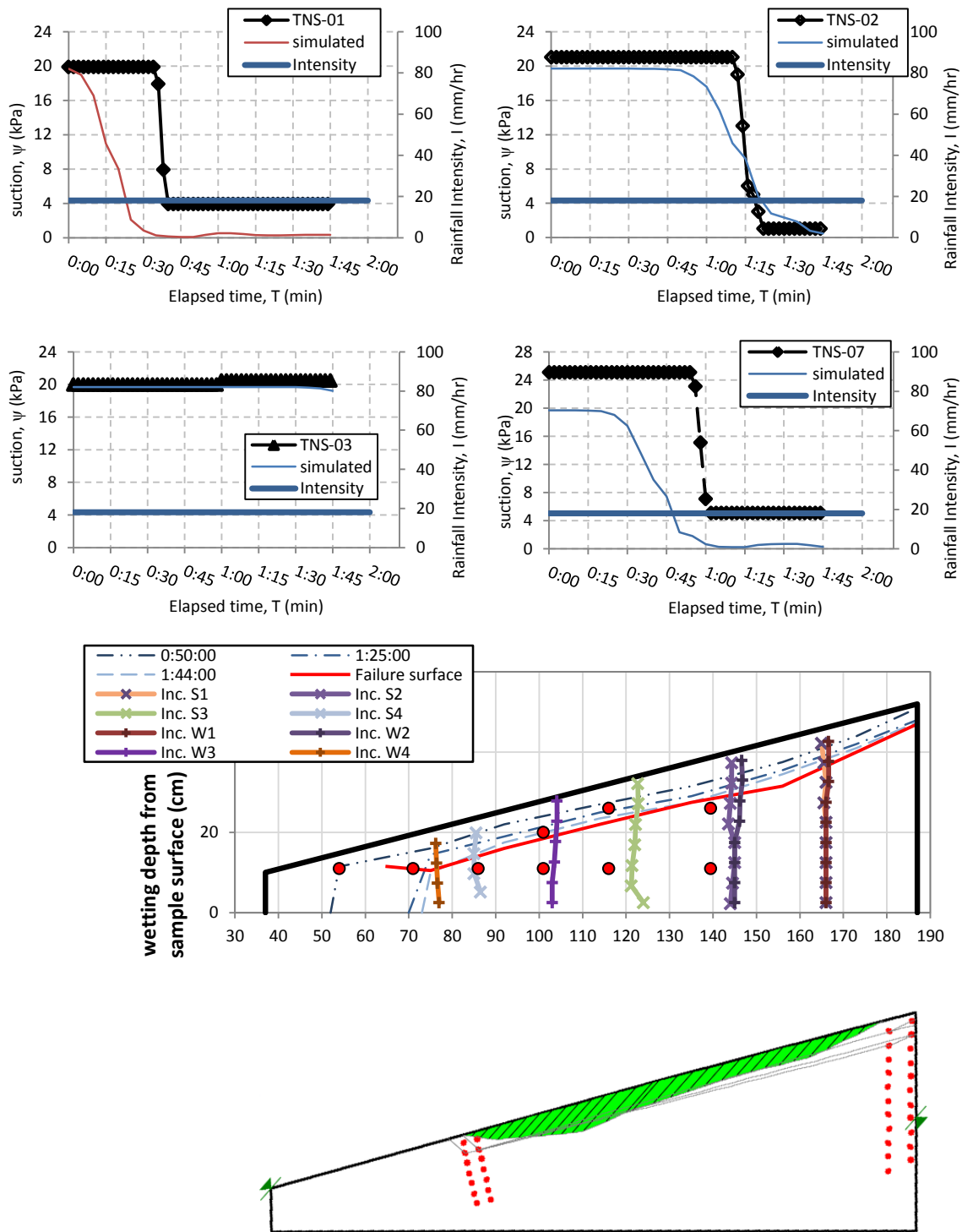


Fig. D.7. (a) Measured and simulated pore water pressure changes in the location of instrumentations for FLM_13, (b) observed and (c) simulated failure surfaces.

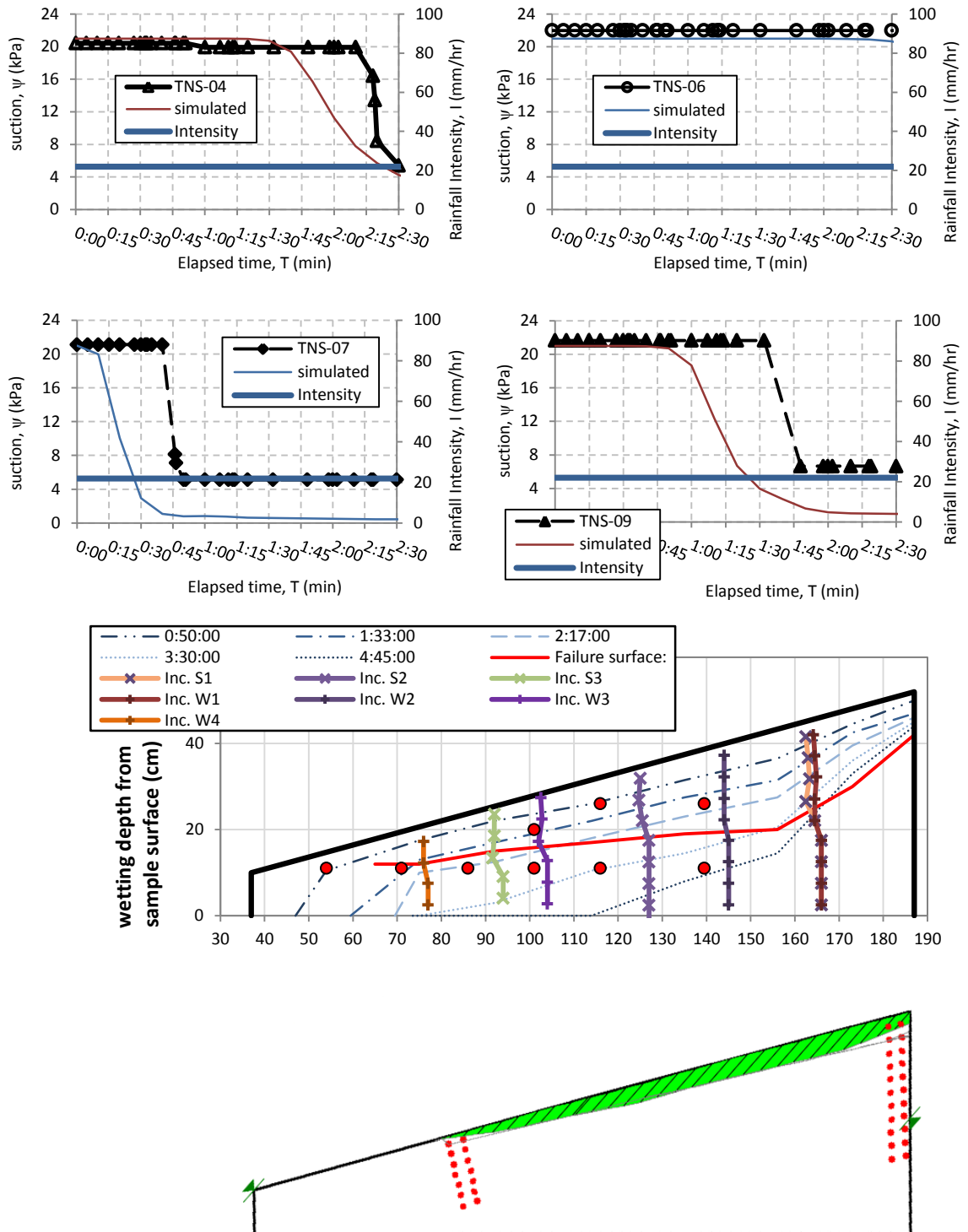


Fig. D.8. (a) Measured and simulated pore water pressure changes in the location of instrumentations for FLM_14, (b) observed and (c) simulated failure surfaces.

APPENDIX E

CODE FOR SEEPAGE AND STABILITY OF INFINITE SLOPE ELEMENT

In current appendix, a Matlab code prepared for unsaturated seepage and stability of an infinite slope element is presented. It can be used for modeling rainfall infiltration and stability in laminar box tests.

```

disp ('-----Model Specifications-----');

disp ('which HWCC model will be used');
disp ('1-) Brooks and Corey (BC) Model (1964)');
disp ('2-) van Genuchten (VG) Model (1980)');
disp ('3-) Fredlund and Xing (FX) Model (1994)');
hwcc= input('number of HWCC Model:');

disp ('which HCF model will be used');
disp ('1-) Leang and Rohardjo (1997)');
disp ('2-) Brooks and Corey (BC) Model (1964)');
disp ('3-) van Genuchten (VG) Model (1980)');
hcf= input('number of HCF Model:');

if hwcc==3 && hcf==1      % first if code

NI= input('number of laminates:');
deltaz= input('length(height) of the laminates (delta z):');
tse= input('duration of time steps at evaporation(sec):');
ne= input('requested analysis time in evaporation(min):');
Si= input('constant initial suction(kPa):');
alfa= input('angle:');
RI= input('Rainfall Int(m/s):');
BSI= input('Bot. Seep Int(m/s):');
deltat= input('delta t(sec):');
A= input('Area(m2):');
a= input('a:');
Ks= input('Ks:');
tetas= input('teta s:');
p= input('p:');

SAI=zeros((ne*60/tse),NI); % Defining matrix of matric suction
VWC=zeros((ne*60/tse),NI); % Defining matrix of Volumetric Water Content
UHC=zeros((ne*60/tse),NI); % Defining matrix of Unsaturated Hydraulic Conductivity
DIS=zeros((ne*60/tse),NI-1); % Defining matrix of Discharge from an element to another

    % to assign Si to first row of matrix of matric suction
i=1;
while i<=NI
    SAI(1,i)=Si;
    i=i+1;
end

    % to assign the first row of matrix of Volumetric Water Content
j=1;
while j<=NI
    VWC(1,j)=tetas*(1/(log((exp(1))+SAI(1,j)/a)));
    j=j+1;
end

    % to assign the first row of matrix of Unsaturated Hydraulic Conductivity
k=1;
while k<=NI
    UHC(1,k)=Ks*(VWC(1,k)/tetas)^p;
    k=k+1;
end

    % to assign the first row of matrix of Discharge from an element to another
l=1;
while l<=NI-1
    DIS(1,l)=((UHC(1,l)+UHC(1,l+1))/2)*(((SAI(1,l)-SAI(1,l+1))/9.807)+deltaz/(cos(pi*alfa/180)))/deltaz/(cos(pi*alfa/180))*A;
    l=l+1;
end

end

    % to assign the other rows of matrixs

```

```

f=2;
h=1;
n=1;
while f<=ne*60/tse

    WWC(f,1)=WWC(h,1)+((RI*deltat*A)-(DIS(h,1)*deltat))/(deltaz*A);    % to assign first column (except (1,1)) of Volumetric
Water Content
    x=2;
    while x<=NI-1
        WWC(f,x)=WWC(f-1,x)+(DIS(f-1,x-1)-DIS(f-1,x))*deltat/(deltaz*A);
        x=x+1;
    end
    WWC(f,NI)=WWC(f-1,NI)+((DIS(f-1,NI-1)*deltat)-(BSI*A*deltat))/(deltaz*A);

    b=1;
    while b<=NI
        SAI(f,b)=a*(exp(tetas/VWC(f,b))-exp(1));
        b=b+1;
    end

    m=1;
    while m<=NI
        UHC(f,m)=Ks*(VWC(f,m)/tetas)^p;
        m=m+1;
    end

    d=1;
    while d<=NI-1
        DIS(f,d)=((UHC(f,d)+UHC(f,d+1))/2)*((-SAI(f,d)-
SAI(f,d+1))/9.807)+deltaz/(cos(pi*alfa/180))/deltaz/(cos(pi*alfa/180))*A;
        d=d+1;
    end

    h=h+1;
    f=f+1;

end

elseif hwcc==1 && hcf==1    % second if code

NI= input('number of laminates:');
deltaz= input('length(height) of the laminates (delta z):');
tse= input('duration of time steps at evaporation(sec):');
ne= input('requested analysis time in evaporation(min):');
Si= input('constant initial suction(kPa):');
alfa= input('angle:');
RI= input('Rainfall Int(m/s):');
BSI= input('Bot. Seep Int(m/s):');
deltat= input('delta t(sec):');
A= input('Area(m2):');
Ks= input('Ks:');
suchb= input('suction b:');
tetas= input('teta s:');
tetar= input('teta r:');
lamda= input('lamda:');
p= input('p:');

SAI=zeros((ne*60/tse),NI);    % Defining matrix of matric suction
WWC=zeros((ne*60/tse),NI);    % Defining matrix of Volumetric Water Content
UHC=zeros((ne*60/tse),NI);    % Defining matrix of Unsaturated Hydraulic Conductivity
DIS=zeros((ne*60/tse),NI-1);    % Defining matrix of Discharge from an element to another

    % to assign Si to first row of matrix of matric suction

i=1;
while i<=NI
    SAI(1,i)=Si;
    i=i+1;
end
end

```

```

    % to assign the first row of matrix of Volumetric Water Content

j=1;
while j<=NI
    WWC(1,j)=tetar+(tetas-tetar)*(such/SAI(1,j))^lamda;
    j=j+1;
end

    % to assign the first row of matrix of Unsaturated Hydraulic Conductivity

k=1;
while k<=NI
    UHC(1,k)=Ks*(VWC(1,k)/tetas)^p;
    k=k+1;
end

    % to assign the first row of matrix of Discharge from an element to another

l=1;
while l<=NI-1
    DIS(1,l)=((UHC(1,l)+UHC(1,l+1))/2)*((-SAI(1,l)-SAI(1,l+1))/9.807)+deltaz/(cos(pi*alfa/180))/deltaz/(cos(pi*alfa/180))*A;
    l=l+1;
end

    % to assign the other rows of matrixs

f=2;
h=1;
n=1;
while f<=ne*60/tse

    WWC(f,1)=VWC(h,1)+((RI*deltat*A)-(DIS(h,1)*deltat))/(deltaz*A);    % to assign first column (except (1,1)) of Volumetric
Water Content
    x=2;
    while x<=NI-1
        WWC(f,x)=VWC(f-1,x)+(DIS(f-1,x-1)-DIS(f-1,x))*deltat/(deltaz*A);
        x=x+1;
    end
    WWC(f,NI)=VWC(f-1,NI)+((DIS(f-1,NI-1)*deltat)-(BSI*A*deltat))/(deltaz*A);

    b=1;
    while b<=NI
        SAI(f,b)=such/((VWC(f,b)-tetar)/(tetas-tetar));
        b=b+1;
    end

    m=1;
    while m<=NI
        UHC(f,m)=Ks*(VWC(f,m)/tetas)^p;
        m=m+1;
    end

    d=1;
    while d<=NI-1
        DIS(f,d)=((UHC(f,d)+UHC(f,d+1))/2)*((-SAI(f,d)-
SAI(f,d+1))/9.807)+deltaz/(cos(pi*alfa/180))/deltaz/(cos(pi*alfa/180))*A;
        d=d+1;
    end

    h=h+1;
    f=f+1;
end

elseif hwcc==2 && hcf==1    % third if code

NI= input('number of laminates:');

```

```

deltaz= input('length(height) of the laminates (delta z):');
tse= input('duration of time steps at evaporation(sec):');
ne= input('requested analysis time in evaporation(min):');
Si= input('constant initial suction(kPa):');
alfa= input('angle:');
RI= input('Rainfall Int(m/s):');
BSI= input('Bot. Seep Int(m/s):');
deltat= input('delta t(sec):');
A= input('Area(m2):');
Ks= input('Ks:');
tetas= input('teta s:');
a= input('a:');
em= input('m:');
en= input('n:');
p= input('p:');

SAI=zeros((ne*60/tse),NI); % Defining matrix of matric suction
VWC=zeros((ne*60/tse),NI); % Defining matrix of Volumetric Water Content
UHC=zeros((ne*60/tse),NI); % Defining matrix of Unsaturated Hydraulic Conductivity
DIS=zeros((ne*60/tse),NI-1); % Defining matrix of Discharge from an element to another

% to assign Si to first row of matrix of matric suction

i=1;
while i<=NI
    SAI(1,i)=Si;
    i=i+1;
end

% to assign the first row of matrix of Volumetric Water Content

j=1;
while j<=NI
    VWC(1,j)=tetas*(1/(1+(a*SAI(1,j))^en))^em;
    j=j+1;
end

% to assign the first row of matrix of Unsaturated Hydraulic Conductivity

k=1;
while k<=NI
    UHC(1,k)=Ks*(VWC(1,k)/tetas)^p;
    k=k+1;
end

% to assign the first row of matrix of Discharge from an element to another

l=1;
while l<=NI-1
    DIS(1,l)=((UHC(1,l)+UHC(1,l+1))/2)*(((SAI(1,l)-SAI(1,l+1))/9.807)+deltaz/(cos(pi*alfa/180)))/deltaz/(cos(pi*alfa/180))*A;
    l=l+1;
end

% to assign the other rows of matrixs

f=2;
h=1;
n=1;
while f<=ne*60/tse

    VWC(f,1)=VWC(h,1)+((RI*deltat*A)-(DIS(h,1)*deltat))/(deltaz*A); % to assign first column (except (1,1)) of Volumetric
    Water Content
    x=2;
    while x<=NI-1
        VWC(f,x)=VWC(f-1,x)+(DIS(f-1,x-1)-DIS(f-1,x))*deltat/(deltaz*A);
        x=x+1;
    end
    VWC(f,NI)=VWC(f-1,NI)+((DIS(f-1,NI-1)*deltat)-(BSI*A*deltat))/(deltaz*A);

    b=1;

```

```

while b<=NI
    SAI(f,b)=(1/(a*(VWC(f,b)/tetas)^(1/m))-1/a)^(1/n);
    b=b+1;
end

m=1;
while m<=NI
    UHC(f,m)=Ks*(VWC(f,m)/tetas)^p;
    m=m+1;
end

d=1;
while d<=NI-1
    DIS(f,d)=((UHC(f,d)+UHC(f,d+1))/2)*((-SAI(f,d)-
SAI(f,d+1))/9.807)+deltaz/(cos(pi*alfa/180))/deltaz/(cos(pi*alfa/180))*A;
    d=d+1;
end

h=h+1;
f=f+1;

end

elseif hwcc==1 && hcf==3 % fourth if code

NI= input('number of laminates:');
deltaz= input('length(height) of the laminates (delta z):');
tse= input('duration of time steps at evaporation(sec):');
ne= input('requested analysis time in evaporation(min):');
Si= input('constant initial suction(kPa):');
alfa= input('angle:');
RI= input('Rainfall Int(m/s):');
BSI= input('Bot. Seep Int(m/s):');
deltat= input('delta t(sec):');
A= input('Area(m2):');
suchb= input('suction b:');
tetas= input('teta s:');
tetar= input('teta r:');
lamda= input ('lamda:');
em= input ('m:');

SAI=zeros((ne*60/tse),NI); % Defining matrix of matric suction
VWC=zeros((ne*60/tse),NI); % Defining matrix of Volumetric Water Content
UHC=zeros((ne*60/tse),NI); % Defining matrix of Unsaturated Hydraulic Conductivity
DIS=zeros((ne*60/tse),NI-1); % Defining matrix of Discharge from an element to another

% to assign Si to first row of matrix of matric suction

i=1;
while i<=NI
    SAI(1,i)=Si;
    i=i+1;
end

% to assign the first row of matrix of Volumetric Water Content

j=1;
while j<=NI
    VWC(1,j)=tetar+(tetas-tetar)*(suchb/SAI(1,j))^lamda;
    j=j+1;
end

% to assign the first row of matrix of Unsaturated Hydraulic Conductivity

k=1;
while k<=NI
    UHC(1,k)=((VWC(1,k)/tetas)^(0.5))*(1-(1-(VWC(1,k)/tetas)^(1/em))^(em))^2;

```

```

k=k+1;
end

% to assign the first row of matrix of Discharge from an element to another
l=1;
while l<=NI-1
    DIS(1,l)=((UHC(1,l)+UHC(1,l+1))/2)*(((SAI(1,l)-SAI(1,l+1))/9.807)+deltaz/(cos(pi*alfa/180)))/deltaz/(cos(pi*alfa/180))*A;
    l=l+1;
end

% to assign the other rows of matrixs

f=2;
h=1;
n=1;
while f<=ne*60/tse

    VWC(f,1)=VWC(h,1)+((RI*deltat*A)-(DIS(h,1)*deltat))/(deltaz*A); % to assign first column (except (1,1)) of Volumetric
Water Content
    x=2;
    while x<=NI-1
        VWC(f,x)=VWC(f-1,x)+(DIS(f-1,x-1)-DIS(f-1,x))*deltat/(deltaz*A);
        x=x+1;
    end
    VWC(f,NI)=VWC(f-1,NI)+((DIS(f-1,NI-1)*deltat)-(BSI*A*deltat))/(deltaz*A);

    b=1;
    while b<=NI
        SAI(f,b)=suchb/((VWC(f,b)-tetar)/(tetas-tetar));
        b=b+1;
    end

    m=1;
    while m<=NI
        UHC(f,m)=((VWC(f,m)/tetas)^(0.5))*(1-(1-(VWC(f,m)/tetas)^(1/em))^(em))^2;
        m=m+1;
    end

    d=1;
    while d<=NI-1
        DIS(f,d)=((UHC(f,d)+UHC(f,d+1))/2)*(((SAI(f,d)-
SAI(f,d+1))/9.807)+deltaz/(cos(pi*alfa/180)))/deltaz/(cos(pi*alfa/180))*A;
        d=d+1;
    end

    h=h+1;
    f=f+1;

end

elseif hwcc==2 && hcf==3 % fifth if code

NI= input('number of laminates:');
deltaz= input('length(height) of the laminates (delta z):');
tse= input('duration of time steps at evaporation(sec):');
ne= input('requested analysis time in evaporation(min):');
Si= input('constant initial suction(kPa):');
alfa= input('angle:');
RI= input('Rainfall Int(m/s):');
BSI= input('Bot. Seep Int(m/s):');
deltat= input('delta t(sec):');
A= input('Area(m2):');
tetas= input('teta s:');
a= input('a:');

```

```

em= input('m:');
en= input('n:');

SAI=zeros(ne*60/tse,Nl); % Defining matrix of matric suction
VWC=zeros(ne*60/tse,Nl); % Defining matrix of Volumetric Water Content
UHC=zeros(ne*60/tse,Nl); % Defining matrix of Unsaturated Hydraulic Conductivity
DIS=zeros(ne*60/tse,Nl-1); % Defining matrix of Discharge from an element to another

% to assign Si to first row of matrix of matric suction

i=1;
while i<=Nl
    SAI(1,i)=Si;
    i=i+1;
end
% to assign the first row of matrix of Volumetric Water Content

j=1;
while j<=Nl
    VWC(1,j)=tetas*(1/(1+(a*SAI(1,j))^en))^em;
    j=j+1;
end
% to assign the first row of matrix of Unsaturated Hydraulic Conductivity

k=1;
while k<=Nl
    UHC(1,k)=((VWC(1,k)/tetas)^(0.5))*(1-(1-(VWC(1,k)/tetas)^(1/em))^(em))^2;
    k=k+1;
end
% to assign the first row of matrix of Discharge from an element to another
l=1;
while l<=Nl-1
    DIS(1,l)=((UHC(1,l)+UHC(1,l+1))/2)*(((SAI(1,l)-SAI(1,l+1))/9.807)+deltaz/(cos(pi*alfa/180)))/deltaz/(cos(pi*alfa/180))*A;
    l=l+1;
end

% to assign the other rows of matrixs

f=2;
h=1;
n=1;
while f<=ne*60/tse

    VWC(f,1)=VWC(h,1)+((RI*deltat*A)-(DIS(h,1)*deltat))/(deltaz*A); % to assign first column (except (1,1)) of Volumetric
Water Content
    x=2;
    while x<=Nl
        VWC(f,x)=VWC(f-1,x)+(DIS(f-1,x-1)-DIS(f-1,x))*deltat/(deltaz*A);
        x=x+1;
    end
    VWC(f,Nl)=VWC(f-1,Nl)+((DIS(f-1,Nl-1)*deltat)-(BSI*A*deltat))/(deltaz*A);

    b=1;
    while b<=Nl
        SAI(f,b)=(1/(a*(VWC(f,b)/tetas)^(1/m))-1/a)^(1/n);
        b=b+1;
    end

    m=1;
    while m<=Nl
        UHC(f,m)=((VWC(f,m)/tetas)^(0.5))*(1-(1-(VWC(f,m)/tetas)^(1/em))^(em))^2;
        m=m+1;
    end
end

```

```

d=1;
while d<=NI-1
    DIS(f,d)=((UHC(f,d)+UHC(f,d+1))/2)*((-SAI(f,d)-
SAI(f,d+1))/9.807)+deltaz/(cos(pi*alfa/180))/deltaz/(cos(pi*alfa/180))*A;
    d=d+1;
end

h=h+1;
f=f+1;

end

elseif hwcc==3 && hcf==3          % sixth if code

NI= input('number of laminates:');
deltaz= input('length(height) of the laminates (delta z):');
tse= input('duration of time steps at evaporation(sec):');
ne= input('requested analysis time in evaporation(min):');
Si= input('constant initial suction(kPa):');
alfa= input('angle:');
RI= input('Rainfall Int(m/s):');
BSI= input('Bot. Seep Int(m/s):');
deltat= input('delta t(sec):');
A= input('Area(m2):');
a= input('a:');
tetas= input('teta s:');
em= input('m:');

SAI=zeros((ne*60/tse),NI); % Defining matrix of matric suction
VWC=zeros((ne*60/tse),NI); % Defining matrix of Volumetric Water Content
UHC=zeros((ne*60/tse),NI); % Defining matrix of Unsaturated Hydraulic Conductivity
DIS=zeros((ne*60/tse),NI-1); % Defining matrix of Discharge from an element to another

    % to assign Si to first row of matrix of matric suction
i=1;
while i<=NI
    SAI(1,i)=Si;
    i=i+1;
end

    % to assign the first row of matrix of Volumetric Water Content
j=1;
while j<=NI
    VWC(1,j)=tetas*(1/(log((exp(1))+(SAI(1,j)/a))));
    j=j+1;
end

    % to assign the first row of matrix of Unsaturated Hydraulic Conductivity
k=1;
while k<=NI
    UHC(1,k)=((VWC(1,k)/tetas)^(0.5))*(1-(1-(VWC(1,k)/tetas)^(1/em))^(em))^2;
    k=k+1;
end

    % to assign the first row of matrix of Discharge from an element to another
l=1;
while l<=NI-1
    DIS(1,l)=((UHC(1,l)+UHC(1,l+1))/2)*((-SAI(1,l)-SAI(1,l+1))/9.807)+deltaz/(cos(pi*alfa/180))/deltaz/(cos(pi*alfa/180))*A;
    l=l+1;
end

end

    % to assign the other rows of matrixs

```

```

f=2;
h=1;
n=1;
while f<=ne*60/tse

    VWC(f,1)=VWC(h,1)+((RI*deltat*A)-(DIS(h,1)*deltat))/(deltaz*A);    % to assign first column (except (1,1)) of Volumetric
Water Content
    x=2;
    while x<=NI-1
        VWC(f,x)=VWC(f-1,x)+(DIS(f-1,x-1)-DIS(f-1,x))*deltat/(deltaz*A);
        x=x+1;
    end
    VWC(f,NI)=VWC(f-1,NI)+((DIS(f-1,NI-1)*deltat)-(BSI*A*deltat))/(deltaz*A);

    b=1;
    while b<=NI
        SAI(f,b)=a*(exp(tetas/VWC(f,b))-exp(1));
        b=b+1;
    end

    m=1;
    while m<=NI
        UHC(f,m)=((VWC(f,m)/tetas)^(0.5))*(1-(1-(VWC(f,m)/tetas)^(1/em))^(em))^2;
        m=m+1;
    end

    d=1;
    while d<=NI-1
        DIS(f,d)=((UHC(f,d)+UHC(f,d+1))/2)*((-SAI(f,d)-
SAI(f,d+1))/9.807+deltaz/(cos(pi*alfa/180)))/deltaz/(cos(pi*alfa/180))*A;
        d=d+1;
    end

    h=h+1;
    f=f+1;

end

elseif hwcc==1 && hcf==2    % seventh if code

NI= input('number of laminates:');
deltaz= input('length(height) of the laminates (delta z):');
tse= input('duration of time steps at evaporation(sec):');
ne= input('requested analysis time in evaporation(min):');
Si= input('constant initial suction(kPa):');
alfa= input('angle:');
RI= input('Rainfall Int(m/s):');
BSI= input('Bot. Seep Int(m/s):');
deltat= input('delta t(sec):');
A= input('Area(m2):');
sucb= input('suction b:');
tetas= input('teta s:');
tetar= input('teta r:');
Ks= input('Ks:');
lamda= input('lamda:');
eta=2+3*lamda;

SAI=zeros((ne*60/tse),NI); % Defining matrix of matric suction
VWC=zeros((ne*60/tse),NI); % Defining matrix of Volumetric Water Content
UHC=zeros((ne*60/tse),NI); % Defining matrix of Unsaturated Hydraulic Conductivity
DIS=zeros((ne*60/tse),NI-1); % Defining matrix of Discharge from an element to another

    % to assign Si to first row of matrix of matric suction

i=1;
while i<=NI
    SAI(1,i)=Si;

```

```

i=i+1;

end
% to assign the first row of matrix of Volumetric Water Content

j=1;
while j<=NI
    VWC(1,j)=tetar+(tetas-tetar)*(sucb/SAI(1,j))^lamda;
    j=j+1;
end

% to assign the first row of matrix of Unsaturated Hydraulic Conductivity

k=1;
while k<=NI

    if SAI(1,k)<=sucb
        UHC(1,k)=Ks;
    else SAI(1,k)>sucb
        UHC(1,k)=Ks*(sucb/(SAI(1,k)))^eta;
    end

    k=k+1;
end

% to assign the first row of matrix of Discharge from an element to another
l=1;
while l<=NI-1
    DIS(1,l)=(UHC(1,l)+UHC(1,l+1))/2*((-(SAI(1,l)-SAI(1,l+1))/9.807+deltaz/(cos(pi*alfa/180)))/deltaz/(cos(pi*alfa/180)))*A;
    l=l+1;
end

% to assign the other rows of matrixs

f=2;
h=1;
n=1;
while f<=ne*60/tse

    VWC(f,1)=VWC(h,1)+((RI*deltat*A)-(DIS(h,1)*deltat))/(deltaz*A); % to assign first column (except (1,1)) of Volumetric
    Water Content
    x=2;
    while x<=NI-1
        VWC(f,x)=VWC(f-1,x)+(DIS(f-1,x-1)-DIS(f-1,x))*deltat/(deltaz*A);
        x=x+1;
    end
    VWC(f,NI)=VWC(f-1,NI)+((DIS(f-1,NI-1)*deltat)-(BSI*A*deltat))/(deltaz*A);

    b=1;
    while b<=NI
        SAI(f,b)=sucb/((VWC(f,b)-tetar)/(tetas-tetar));
        b=b+1;
    end

    m=1;
    while m<=NI
        if SAI(f,m)<=sucb
            UHC(f,m)=Ks;
        else SAI(f,m)>sucb
            UHC(f,m)=Ks*(sucb/(SAI(f,m)))^eta;
        end
        m=m+1;
    end

    d=1;
    while d<=NI-1

```

```

        DIS(f,d)=((UHC(f,d)+UHC(f,d+1))/2)*((-SAI(f,d)-
SAI(f,d+1))/9.807)+deltaz/(cos(pi*alfa/180))/deltaz/(cos(pi*alfa/180))*A;
        d=d+1;
    end

    h=h+1;
    f=f+1;

    end

elseif hwcc==2 && hcf==2          % eighth if code

NI= input('number of laminates:');
deltaz= input('length(height) of the laminates (delta z):');
tse= input('duration of time steps at evaporation(sec):');
ne= input('requested analysis time in evaporation(min):');
Si= input('constant initial suction(kPa):');
alfa= input('angle:');
RI= input('Rainfall Int(m/s):');
BSI= input('Bot. Seep Int(m/s):');
deltat= input('delta t(sec):');
A= input('Area(m2):');
Ks= input('Ks:');
tetas= input('teta s:');
a= input('a:');
em= input('m:');
en= input('n:');
sucb= input('suction b:');
lamda= input('lamda:');
eta=2+3*lamda;

SAI=zeros((ne*60/tse),NI); % Defining matrix of matric suction
VWC=zeros((ne*60/tse),NI); % Defining matrix of Volumetric Water Content
UHC=zeros((ne*60/tse),NI); % Defining matrix of Unsaturated Hydraulic Conductivity
DIS=zeros((ne*60/tse),NI-1); % Defining matrix of Discharge from an element to another

    % to assign Si to first row of matrix of matric suction

i=1;
while i<=NI
    SAI(1,i)=Si;
    i=i+1;
end
    % to assign the first row of matrix of Volumetric Water Content

j=1;
while j<=NI
    VWC(1,j)=tetas*(1/(1+(a*SAI(1,j))^en))^em;
    j=j+1;
end
    % to assign the first row of matrix of Unsaturated Hydraulic Conductivity

k=1;
while k<=NI

    if SAI(1,k)<=sucb
        UHC(1,k)=Ks;
    else SAI(1,k)>sucb
        UHC(1,k)=Ks*(sucb/(SAI(1,k)))^eta;
    end

    k=k+1;
end
    % to assign the first row of matrix of Discharge from an element to another

```

```

l=1;
while l<=NI-1
    DIS(1,l)=(UHC(1,l)+UHC(1,l+1))/2*((-SAI(1,l)-SAI(1,l+1))/9.807)+deltaz/(cos(pi*alfa/180))/deltaz/(cos(pi*alfa/180))*A;
    l=l+1;

end

    % to assign the other rows of matrixs

f=2;
h=1;
n=1;
while f<=ne*60/tse

    VWC(f,1)=VWC(h,1)+((RI*deltat*A)-(DIS(h,1)*deltat))/(deltaz*A);    % to assign first column (except (1,1)) of Volumetric
Water Content
    x=2;
    while x<=NI-1
        VWC(f,x)=VWC(f-1,x)+(DIS(f-1,x-1)-DIS(f-1,x))*deltat/(deltaz*A);
        x=x+1;
    end
    VWC(f,NI)=VWC(f-1,NI)+((DIS(f-1,NI-1)*deltat)-(BSI*A*deltat))/(deltaz*A);

    b=1;
    while b<=NI
        SAI(f,b)=(1/(a*(VWC(f,b)/tetas)^(1/m))-1/a)^(1/n);
        b=b+1;
    end

    m=1;
    while m<=NI
        if SAI(f,m)<=suchb
            UHC(f,m)=Ks;
        else SAI(f,m)>suchb
            UHC(f,m)=Ks*(suchb/(SAI(f,m)))^etas;
        end
        m=m+1;
    end

    d=1;
    while d<=NI-1
        DIS(f,d)=(UHC(f,d)+UHC(f,d+1))/2*((-SAI(f,d)-
SAI(f,d+1))/9.807)+deltaz/(cos(pi*alfa/180))/deltaz/(cos(pi*alfa/180))*A;
        d=d+1;
    end

    h=h+1;
    f=f+1;

end

else hwcc==3 && hcf==2    % ninth if code

NI= input('number of laminates:');
deltaz= input('length(height) of the laminates (delta z):');
tse= input('duration of time steps at evaporation(sec):');
ne= input('requested analysis time in evaporation(min):');
Si= input('constant initial suction(kPa):');
alfa= input('angle:');
RI= input('Rainfall Int(m/s):');
BSI= input('Bot. Seep Int(m/s):');
deltat= input('delta t(sec):');
A= input('Area(m2):');
a= input('a:');
Ks= input('Ks:');
tetas= input('teta s:');
suchb= input('suction b:');
lamda= input('lamda:');

```

```

eta=2+3*lamda;

SAI=zeros((ne*60/tse),NI); % Defining matrix of matric suction
VWC=zeros((ne*60/tse),NI); % Defining matrix of Volumetric Water Content
UHC=zeros((ne*60/tse),NI); % Defining matrix of Unsaturated Hydraulic Conductivity
DIS=zeros((ne*60/tse),NI-1); % Defining matrix of Discharge from an element to another

% to assign Si to first row of matrix of matric suction
i=1;
while i<=NI
    SAI(1,i)=Si;
    i=i+1;
end

% to assign the first row of matrix of Volumetric Water Content
j=1;
while j<=NI
    VWC(1,j)=tetas*(1/(log((exp(1))+SAI(1,j)/a)));
    j=j+1;
end

% to assign the first row of matrix of Unsaturated Hydraulic Conductivity
k=1;
while k<=NI

    if SAI(1,k)<=suchb
        UHC(1,k)=Ks;
    else SAI(1,k)>suchb
        UHC(1,k)=Ks*(suchb/(SAI(1,k)))^eta;
    end

    k=k+1;
end

% to assign the first row of matrix of Discharge from an element to another
l=1;
while l<=NI-1
    DIS(1,l)=((UHC(1,l)+UHC(1,l+1))/2)*(((SAI(1,l)-SAI(1,l+1))/9.807)+deltaz/(cos(pi*alfa/180)))/deltaz/(cos(pi*alfa/180))*A;
    l=l+1;
end

% to assign the other rows of matrixs
f=2;
h=1;
n=1;
while f<=ne*60/tse

    VWC(f,1)=VWC(h,1)+((RI*deltat*A)-(DIS(h,1)*deltat))/(deltaz*A); % to assign first column (except (1,1)) of Volumetric
    Water Content
    x=2;
    while x<=NI-1
        VWC(f,x)=VWC(f-1,x)+(DIS(f-1,x-1)-DIS(f-1,x))*deltat/(deltaz*A);
        x=x+1;
    end
    VWC(f,NI)=VWC(f-1,NI)+((DIS(f-1,NI-1)*deltat)-(BSI*A*deltat))/(deltaz*A);

    b=1;
    while b<=NI
        SAI(f,b)=a*(exp(tetas/VWC(f,b))-exp(1));
        b=b+1;
    end

    m=1;
    while m<=NI
        if SAI(f,m)<=suchb
            UHC(f,m)=Ks;

```

```

        else SAI(f,m)>subc
            UHC(f,m)=Ks*(subc/(SAI(f,m)))^eta;
        end
        m=m+1;
    end

    d=1;
    while d<=NI-1
        DIS(f,d)=((UHC(f,d)+UHC(f,d+1))/2)*((-SAI(f,d)-
        SAI(f,d+1))/9.807)+deltaz/(cos(pi*alfa/180))/deltaz/(cos(pi*alfa/180))*A;
        d=d+1;
    end

    h=h+1;
    f=f+1;

    end

end

disp ('-----Slope Stability-----');

gamaw= 9.807;
gamad= input('specific weight of dry soil(kN/m3):');
ce= input('c:');
frang= input('friction angle:');
frangb= input('friction angle b:');
Alam= input('area of laminate:');

GAMAI=zeros((ne*60/tse),NI); % Defining matrix of specific weight of soil
WSOIL=zeros((ne*60/tse),NI); % Defining matrix of weight of soil
WLAM=zeros((ne*60/tse),NI); % Defining matrix of weight of laminate
S=zeros((ne*60/tse),NI-1); % Defining matrix of
FS=zeros((ne*60/tse),NI-1); % Defining matrix of factor of safety

q=1;
while q<=ne*60/tse
    w=1;
    while w<=NI
        GAMAI(q,w)=gamad*(1+VWC(q,w)/(gamad/gamaw));
        w=w+1;
    end
    q=q+1;
end

end

qw=1;
while qw<=ne*60/tse
    WSOIL(qw,1)=deltaz*A*GAMAI(qw,1);
    qwe=2;
    while qwe<=NI
        WSOIL(qw,qwe)=WSOIL(qw,qwe-1)+deltaz*A*GAMAI(qw,qwe);
        qwe=qwe+1;
    end
    qw=qw+1;
end

end

```

```
WL= [288.9 289.2 290.1 288.2 288.9 287.2 288.6 287.3 290.4 290.7 289.3 289.5 289.6 290.4 290.3 287.4 290.4 289.4 290.4 289.9
288 287.8 289.3 291.5 290.8 288.1 289.7 286.7 289.4 288.2 290.1 290.1 288.7 289.9 290.4 288 288.5 288.2 286.4 290.2 288.9 288.9
289.9 288.4 286.6 289.8 288.1 286.8 287.3 290.4 ];
```

```
aa=1;
while aa<=ne*60/tse
    WLAM(aa,1)=WL(1,1)*9.807/1000000;
    bb=2;
    while bb<=NI
        WLAM(aa,bb)=WLAM(aa,bb-1)+WL(1,bb)*9.807/1000000;
        bb=bb+1;
    end
    aa=aa+1;
end
```

```
FL= [23 13 26 24 18 20 21 21 19 21 21 24 20          16          17          18          19          19          18          14
      13          17          11          12          18          15          14          18          20          21          18
      19          22          16          16          22          20          20          18          22          16          26
      18          18          21          14          17          17          19];
```

```
cc=1;
while cc<=ne*60/tse
    dd=1;
    while dd<=NI-1
        S(cc,dd)=A*(ce+(WSOIL(cc,dd)*cos(pi*alfa/180)/A)*tan(pi*frang/180)+((SAI(cc,dd)+SAI(cc,dd+1))/2)*tan(pi*frang/180))+Ala
        m*((WLAM(cc,dd)*cos(pi*alfa/180)/Alam)*tan(pi*FL(1,dd)/180));
        dd=dd+1;
    end
    cc=cc+1;
end
```

```
ff=1;
while ff<=ne*60/tse
    ss=1;
    while ss<=NI-1
        FS(ff,ss)=S(ff,ss)/((WSOIL(ff,ss)*sin(pi*alfa/180)+(WLAM(ff,ss)*sin(pi*alfa/180)));
        ss=ss+1;
    end
    ff=ff+1;
end
```

```
Time=input('Corresponding t value(min):');
Time=Time*60/deltat;
Time=int8(Time);
TimeMat=SAI(Time,:);
Tras=TimeMat';
xlswrite('SutionValue.xlsx',Tras);
```

```
MinValue=min(FS,[],2);
Duration=zeros((ne*60/tse),1);
for i=1:(ne*60/tse)
    Duration(i)=i*deltat;
end
```

```
plot(Duration,MinValue);
xlabel('Time')
ylabel('Factor of Safety')
```

APPENDIX F

DIRECT SHEAR TEST RESULTS

Detail of water content controlled direct shear tests are presented in Appendix F. Shear stress in the sample and vertical displacement in sample loading cap are recorded with horizontal shearing displacement. The shear tests are performed under normal stresses of 5.1, 12.0, 24.5 and 37.1 kPa to assess shear strength parameters in the samples. Different water content values and dry densities are considered in direct shear tests.

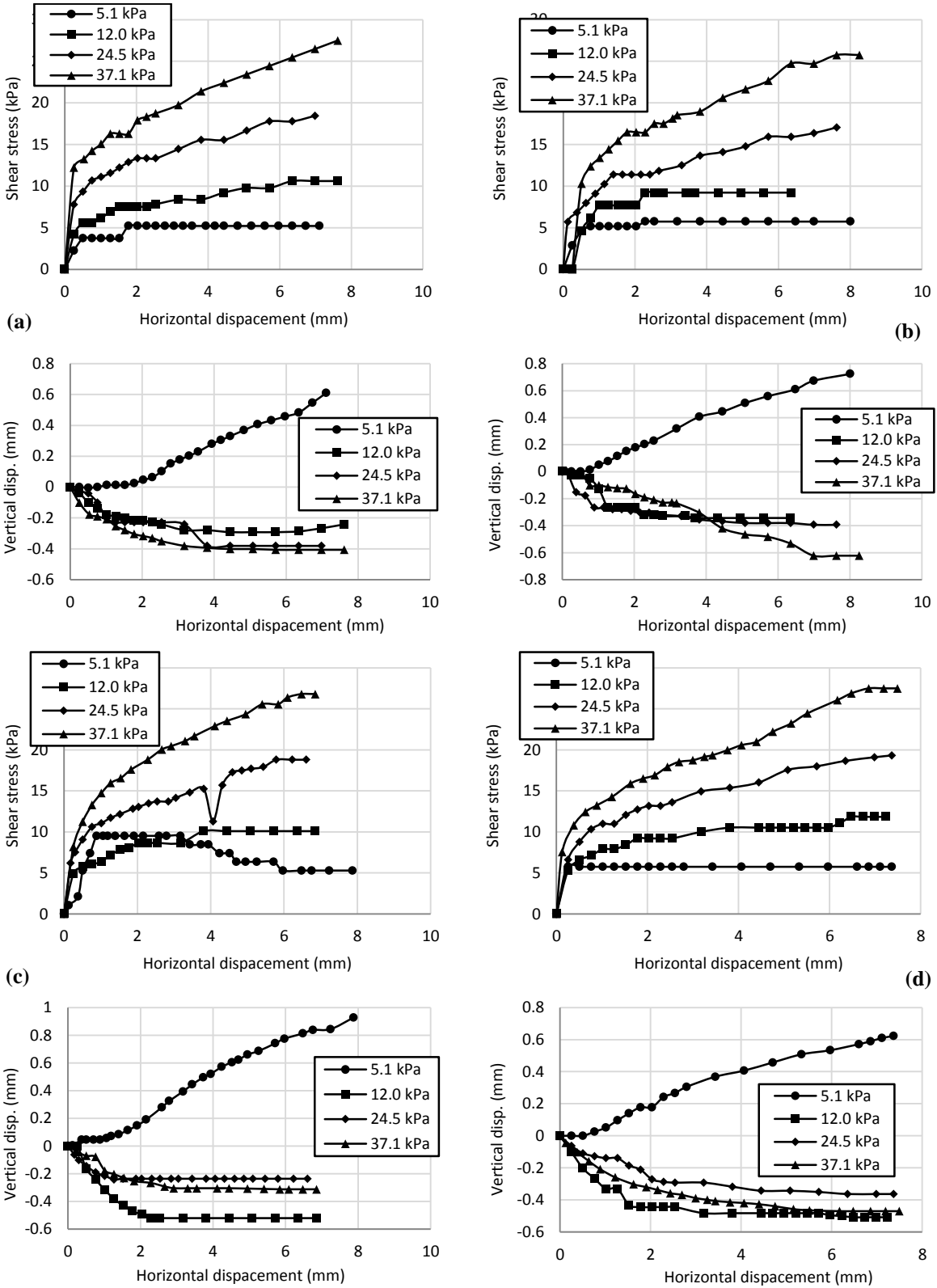


Fig. F.1. Shear stress and vertical settlement in water content controlled direct shear tests in samples with $\gamma_d=1.2 \text{ gr/cm}^3$ and (a) 1%, (b) 5%, (c) 10% and (d) 15% water content subjected to different normal stresses

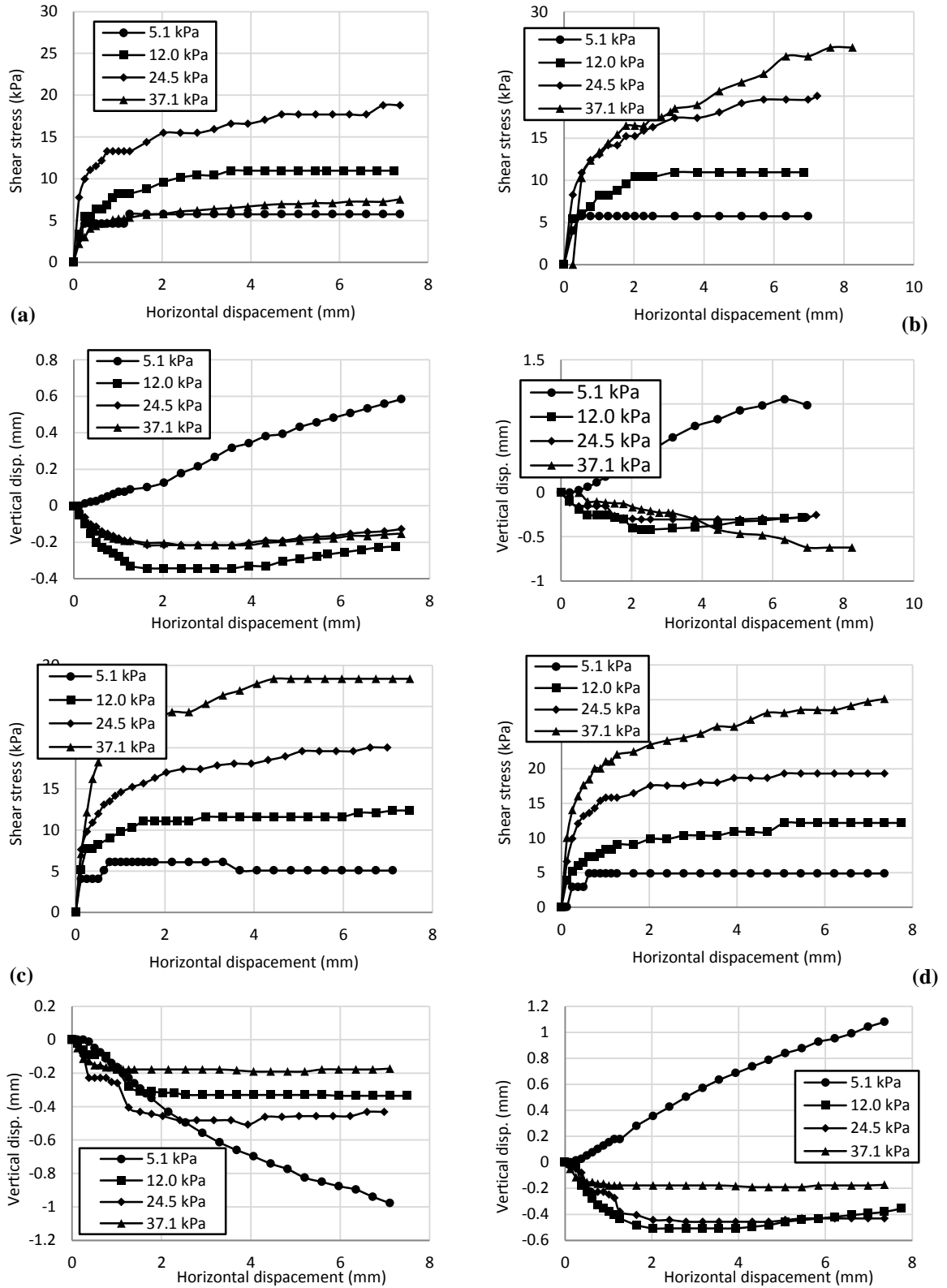


Fig. F.2. Shear stress and vertical settlement in water content controlled direct shear tests in samples with $\gamma_d=1.27 \text{ gr/cm}^3$ and (a) 1%, (b) 5%, (c) 10% and (d) 15% water content subjected to different normal stresses

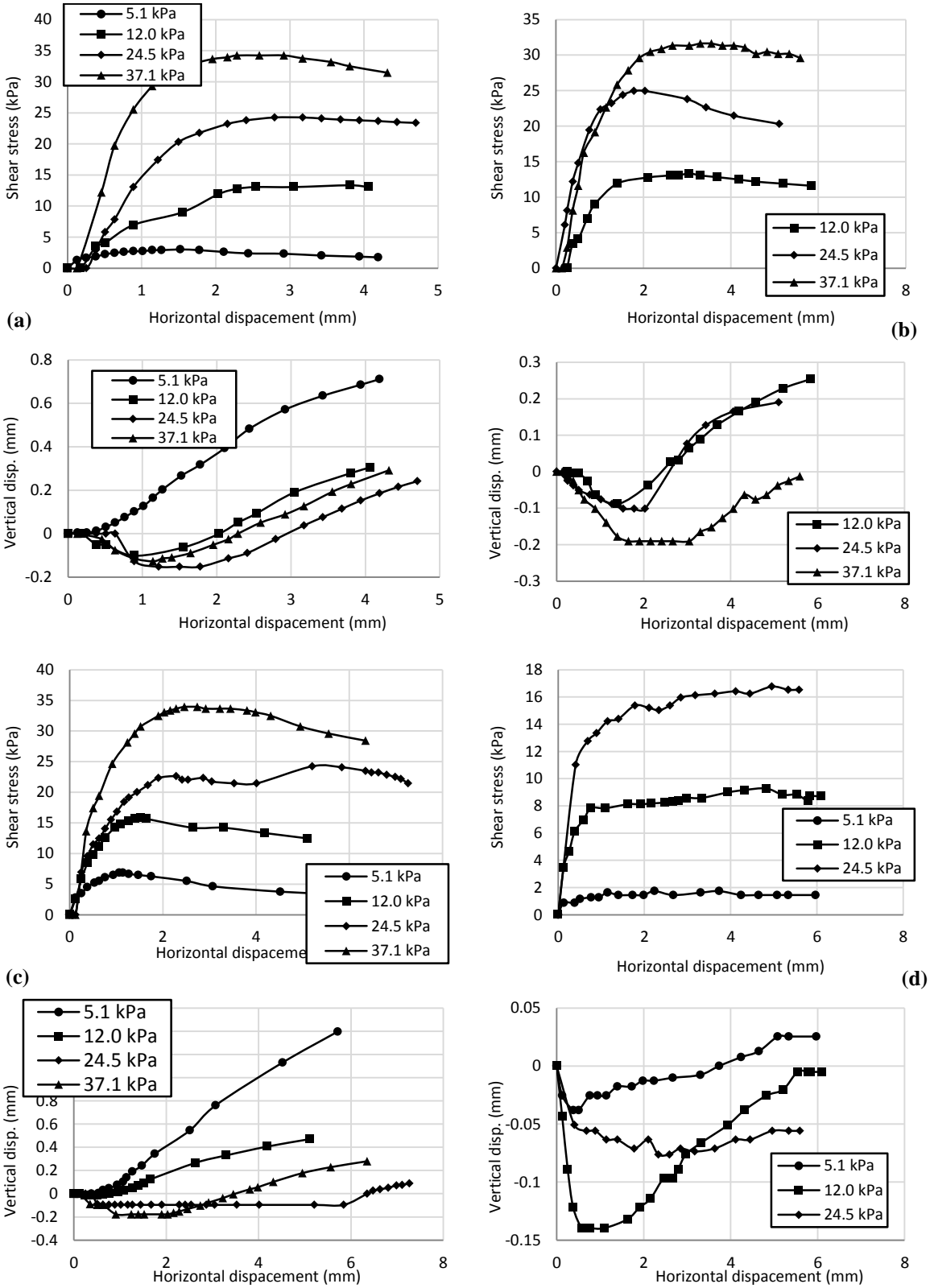


Fig. F.3. Shear stress and vertical settlement in water content controlled direct shear tests in samples with $\gamma_d=1.35 \text{ gr/cm}^3$ and (a) 1%, (b) 5%, (c) 10% and (d) saturated water content

CURRICULUM VITAE

PERSONAL INFORMATION

Surname, Name: Ahmadi Adli, Mohammad

Nationality: Iranian

Date and Place of Birth: 16 June 1982, Tabriz (Iran)

Phone (cell): +90 531 886 2000, +98 914 314 0831

Email: ahmadiadli@gmail.com

EDUCATION

2004 – 2006 University of Tabriz, Civil Engineering Department, MS (Geotechnics)

2000 – 2004 Tabriz Azad university, Civil Engineering Department, BS

WORK EXPERIENCE

2010 – 2013 METU, Department of Civil Engineering, RA

2005 – 2006 University of Tabriz, Department of Civil Engineering, RA/TA

PUBLICATIONS

Ahmadi-adli, M., Toker, N. K. & Huvaj, N. (2014) “Prediction of seepage and slope stability in a flume test and an experimental field case” , *Procedia Earth Planet Sci* 2014; 9:189-194.

Ahmadi-adli, M., Huvaj, N. & Toker, N. K. (2014) “Effects of the Size of Particles on Rainfall Induced Slope Instability in Granular Soils”, Proc. of *Geo-Congress 2014 (ASCE): Geo-Characterization and Modeling for sustainability II*, 23-26 Feb., Atlanta, Georgia, USA.

Ahmadi-adli, M., Huvaj, N. & Toker, N. K. (2014) “How changes in soil water characteristic function affects unsaturated slope instability”, Manuscript submitted to *Landslides*.

Ahmadi-Naghadeh, R., Toker, N. K. & **Ahmadi-adli, M.** (2013) “Water content controlled instead of suction controlled strength tests”, *Life Science Journal* 2013;10(1).

Ahmadi-adli, M., Huvaj, N. & Toker, N. K. (2012) “Rainfall Triggered Landslides in Unsaturated Soils: A numerical sensitivity analysis”, Proc. of *10th International Congress on Advances in Civil Engineering (doc. 1179)*, Middle East Technical University, Ankara, Turkey.

Ahmadi-Naghadeh, R., Toker, N. K. & **Ahmadi-adli, M.** (2012) “Water content variability of unsaturated soil specimens in conventional strength tests”, Proc. of *10th International Congress on Advances in Civil Engineering (doc. 1117)*, Middle East Technical University, Ankara, Turkey.

Ahmadi-adli, M., Huvaj, N., Toker, N. K. & Kurkcu, M. G. (2012) “Comparative study of Soil Water Characteristic Curve prediction methods”, Proc. of *3rd International Conference on New Developments in Soil Mechanics and Geotechnical Engineering*, Near East University, Nicosia, North Cyprus, pp. 559-567.

Hassan Zehtab, K., Toker, N. K. & **Ahmadi-adli, M.** (2012) “Comparison of formulae for shear strength of unsaturated soils”, Proc. of *3rd International Conference on New Developments in Soil Mechanics and Geotechnical Engineering*, Near East University, Nicosia, North Cyprus, pp. 795-802.

Ahmadi-adli, M., Huvaj, N. & Toker, N. K. (2012) “Rainfall triggered landslides in unsaturated soils: a numerical sensitivity analysis for rainfall threshold, presented”, *European Geosciences Union general assembly*, 22-27 April, Vienna, Austria.

Hajjalilue-Bonab, M., **Ahmadi-adli, M.**, Sabetamal, H. (2008) “The Effects of sample dimension and gradation on shear strength parameters of conditioned soils in EPBM”, Proc. of *6th International Symposium on Geotechnical Aspects of Underground Construction in soft Ground (IS-Shanghai 2008)*, Shanghai, China, vol.1, pp. 200-204.

Hajjalilue-Bonab, M., Sabetamal, H., **Ahmadi-adli, M.** & Katebi, H. (2008) “Experimental study on compressibility behavior of foamed sandy soil”, Proc. of *6th International Symposium on Geotechnical Aspects of Underground Construction in soft Ground (IS-Shanghai 2008)*, Shanghai, China, vol.1, pp. 205-211

Ahmadiadli, M., Sabetamal, H., Hajjalilue-Bonab, M. (2007) “An investigation on effects of fine content changes on shear strength parameters in conditioned soils by foam in EPBM tunneling”, Proc. of *3rd National Congress on Civil Engineering (3ncce)*, Tabriz, Iran, vol. 2, pp. 219.

Ahmadiadli, M., Hajjalilue-Bonab, M. (2008) “Effects of soil conditioning on improvement of mechanical properties of soils in mechanized tunneling in Tabriz”, Proc. of *4th National Congress on Civil Engineering (4ncce)*, Tehran, Iran, vol. 1, pp. 279.

Sabetamal, H., **Ahmadiadli, M.**, Hajjalilue-Bonab, M. (2007) “Study on compressibility and shear strength of conditioned granular soils for EPB excavations”, Proc. of *3rd National Congress on Civil Engineering (3ncce)*, Tabriz, Iran, vol. 2, pp. 230.

Ahmadiadli, M. (2006) “Investigation on Mechanical Properties of Conditioned Soils for EPB Mechanized Tunneling in Tabriz”, MS thesis, University of Tabriz, Tabriz, Iran.